
# DEVELOPMENT OF NEW SENSORS USING NANOMATERIALS AND MOLECULARLY IMPRINTED POLYMER MODIFIED ELECTRODES FOR DIAGNOSTIC AND FOOD SAFETY MONITORING

**WONGDUAN SROYSEE**

**A THESIS SUBMITTED IN PARTIAL FULFILLMENT OF THE REQUIREMENTS**
**FOR THE DEGREE OF DOCTOR OF PHILOSOPHY**
**MAJOR IN CHEMISTRY**
**FACULTY OF SCIENCE**
**UBON RATCHATHANI UNIVERSITY**
**ACADEMIC YEAR 2017**

# ACKNOWLWEGEMENTS

I would like to express my gratitude and appreciation to Asst. Prof. Dr. Maliwan Amatatongchai for supervising my PhD studies, continuous support, her constant advice, guidance, insight, and for sharing her extensive chemistry knowledge. I wish to thank Asst. Prof. Dr. Sanoe Chairam for helping me with the electrochemistry both experimentally and theoretically. I would like to thank Univ. Prof. Dr. Peter Lieberzeit for giving me the opportunity to do QCM experiment research at University of Vienna and for the supports during my stay in Austria. My sincere thanks go to Asst. Prof. Dr. Nathawut Choengchan for him advice and criticism as the external examiner. I also would like to thank Asst. Prof. Dr. Purim Jarujamrus and Dr. Suparb Tamuang for useful advice and guidance. Additionally, I appreciate all the people in the Analytical Group at Ubon Ratchathani University and University of Vienna that have been very friendly to me and providing a very productive and supportive environment for experiments and work.

The successful of this thesis cannot be achieved without funding. Therefore, I would like to thank the Science Achievement Scholarship of Thailand (SAST) and exchange scholarship of the University of Vienna, Faculty for Chemistry, Department of Physical Chemistry, Austria, for financial support. My gratitude is extended to Department of Chemistry, Faculty of Science, Ubon Ratchathani University for providing all laboratory facilities.

Above all, I would also like to express specially thank to my beloved parents in this acknowledgement, for their help and supporting both mentally and financially. I could not do this without them.

Wongduan Sroysee

Researcher

# บทคัดย่อ


เรื่อง : การพัฒนาเซนเซอร์ชนิดใหม่โดยใช้วัสดุขนาดนาโนและโพลิเมอร์ที่มีรอยประทับโมเลกุลดัดแปรขั้วไฟฟ้าสำหรับการตรวจวัดทางการแพทย์และความปลอดภัยทางอาหาร

ผู้วิจัย : วงเดือน สร้อยสี

ชื่อปริญญา : วิทยาศาสตรดุษฎีบัณฑิต

สาขาวิชา : เคมี

อาจารย์ที่ปรึกษา: ผู้ช่วยศาสตราจารย์ ดร. มะลิวรรณ อมตธงไชย

คำสำคัญ : วัสดุขนาดนาโน , อิเล็กโตรเคมิคัลเซนเซอร์ , คาร์บอนเพส , โพลิเมอร์ที่มีรอย - ประทับโมเลกุล, ควอตร์คริสตัลไมโครบาลานซ์

งานวิทยานิพนธ์นี้ได้พัฒนาเซนเซอร์ชนิดใหม่โดยอาศัยการตรวจวัดทางเคมีไฟฟ้าและ ควอตร์คริสตัลไมโครบาลานซ์ (quartz crystal microbalance; QCM) ในการตรวจวัดทางเคมีไฟฟ้าแบ่งออกเป็น 2 แบบคือการตรวจวัดด้วยเคมิคัลเซนเซอร์ (chemical sensor) และการตรวจวัดด้วยไบโอเซนเซอร์ (biosensor) สำหรับเคมิคัลเซนเซอร์จะใช้ในการตรวจวัดปริมาณโดพามีนและ กรดยูริคในตัวอย่างยาและปัสสาวะ โดยการดัดแปรขั้วไฟฟ้าคาร์บอนเพสด้วยเฟอร์โรซีนที่มี โพลิอะนิลีนและคาร์บอนนาโนทิวป์ (p(Fc-Ani)-CNTs/CPE) หลังจากนั้นนำขั้วไฟฟ้าที่ได้มาเคลือบด้วยแน ฟฟิออน (nafion; Nf) จะได้ขั้วไฟฟ้า Nf/p(Fc-Ani)-CNTs/CPE ตรวจวัดปฏิกิริยาออกซิเดชันของโดพามีนและกรดยูริค ด้วยเทคนิคดิฟเฟอ ร์เรนเชียลพัลส์โวลแทมเมตรี ผลการทดลองแสดงให้เห็นว่า ที่ศักย์ไฟฟ้า +0.3 โวลต์ และ +0.45 โวลต์ สำหรับโดพามีนและ กรดยูริค ตามลำดับ ในขณะที่ กรดออสคอบิคไม่ปรากฏ สัญญาณรบกวน ทางเคมีไฟฟ้า ขั้วไฟฟ้า Nf/p(Fc-Ani)-CNTs/CPE ที่พัฒนาขึ้น มีความจำเพาะเจาะจงสูงและมีความสามารถในการทำซ้ำ พีคออกซิเดชันจากเทคนิคดิฟเฟอ ร์เรนเชียลพัลส์โวลแทมโมแกรม มีการตอบสนองแบบเป็นเส้นตรง ในช่วง 1-150 และ 5-250 ไมโครโมลาร์ สำหรับโดพามีนและ กรดยูริค ตามลำดับ ขีดจำกัดต่ำสุดในการตรวจวัด ( 3S/N) เท่ากับ 0.21 และ 0.58 ไมโครโมลาร์ สำหรับโดพามีนและ กรดยูริค ตามลำดับ และสามารถ นำมาประยุกต์ใช้ในการตรวจวัดปริมาณของโดพามีนและกรดยูริคในตัวอย่างยาและตัวอย่างปัสสาวะได้อย่างมีประสิทธิภาพ

ไบโอเซนเซอร์จ ะใช้ตรวจวัด ปริมาณ ซัลไฟต์ในตัวอย่างไวน์และอาหารดอง โดยอาศัยการตรึงเอนไซม์ซัลไฟต์ออกซิเดส (SOx) ลงบนวัสดุขนาดนาโนชนิด $Fe_3O_4$@Au-Cys-FA ที่เตรียมจากการนำอนุภาค $Fe_3O_4$@Au มาเติมซิสเทอีน ที่มีหมู่ฟังก์ชันสองหมู่เป็นตัวเชื่อมประสาน สำหรับจับกับพื้นผิวของอนุภาคทองนาโนผ่านหมู่ไธออล จากนั้นหมู่อะมิโนที่ปลาย อีกข้างของซิสเทอีนจะจับกับ กรดโฟลิกโดยการสร้างพันธะผ่านหมู่เอไมด์จะได้นาโนคอมโพสิท $Fe_3O_4$@Au-Cys-FA สำหรับการสร้างขั้วไฟฟ้านั้นใช้สารผสมของโพลีไดเมทิลไซลอกเซน (PDMS) และ mineral oil เป็นตัวประสานเพื่อเพิ่มความเสถียรและความไวในการวิเคราะห์ ขั้วไฟฟ้า $Fe_3O_4$@Au-Cys-FA/CPE ที่พัฒนาขึ้นนี้ ได้ถูกนำมาศึกษาคุณสมบัติทางเคมีไฟฟ้าโดยใช้เทคนิคไซคลิกโวลแทมเมทรี และ นำมาประยุกต์ใช้ในการตรวจวัดซัลไฟต์แบบแอมเพอร์โรเมทรี ที่ศักย์ไฟฟ้า +0.35 โวลต์ ในระบบ เอฟไอเอ ช่วงการตอบสนอง

แบบเป็นเส้นตรง ของระบบที่พัฒนาขึ้น อยู่ในช่วง 0.1 ถึง 200 มิลลิกรัมต่อลิตร สมการเส้นตรงคือ y=1.086x-1.147 ($r^2$=0.998) เมื่อ y และ x คือพื้นที่ใต้พีคของสัญญาณกระแส ( ไมโครแอมแปร์) และความเข้มข้นซัลไฟต์ (มิลลิกรัมต่อลิตร) ขีดจำกัดต่ำสุดในการตรวจวัด (3$\sigma$ ) เท่ากับ 10 ไมโครกรัมต่อลิตร ค่ากระแสที่ได้จากการวัดความเที่ยง (%RSD) ของการวิเคราะห์ซัลไฟต์ความเข้มข้น 15 มิลลิกรัมต่อลิตรซ้ำ 20 ครั้ง มีค่าเท่ากับร้อยละ 3.1 และสามารถวิเคราะห์ได้รวดเร็วถึง 109 ตัวอย่างต่อชั่วโมง วิธีที่พัฒนาขึ้นนี้สามารถนำมาหาปริมาณของซัลไฟต์ในตัวอย่างไวน์และสารสกัดจากอาหารดองได้อย่างมีประสิทธิภาพและถูกต้องเทียบเท่าวิธีไอออโดเมทรีที่เป็นวิธีมาตรฐาน

การตรวจวัดด้วย เทคนิคควอตร์คริสตัลไมโครบาลานซ์ (QCM) จะใช้โพลิเมอร์ที่มีรอยประทับโมเลกุล (MIP) เพื่อเพิ่มความจำเพาะของเซนเซอร์ในการวิเคราะห์หาปริมาณสารกำจัดแมลงชนิดคาร์โบฟูแรน (carbofuran; CBF) และโปรเฟนโนฟอส (profenofos; PFF) โดยที่ CBF-MIP เตรียมโดยใช้กรดเมทาคริลิกเป็นมอนอเมอร์ เอทิลลีนไกลคอลไดเมทาคริเลตเป็นสารเชื่อมข้ามและใช้เอโซบีสไอโซบิวทิลโรไนไตร์ลเป็นตัวริเริ่ม สำหรับ PFF-MIP สังเคราะห์โดยใช้ โพลี -4-ไวนิลฟีนอล และไดฟีนิลมีเทน-4,4’-ได- ไอโซไซยาเนตเป็นมอนอเมอร์ ใช้ฟลอโรกลูซินอลเป็นสารเชื่อมข้าม และไดฟีนิลมีเทนเป็นสารที่ทำให้เกิดรูพรุน (porogen) โพลิเมอร์ที่ไม่มีรอยประทับโมเลกุล (NIP) ถูกสังเคราะห์ในสภาวะเดียวกันแต่ไม่ได้เติมสารแม่แบบยาฆ่าแมลง จากนั้นนำโพลิเมอร์ที่มีรอยประทับโมเลกุลและโพลิเมอร์ที่ไม่มีรอยประทับโมเลกุลที่เตรียมได้ไปเคลือบบนผิวหน้าทั้งสองด้านของขั้วไฟฟ้าโดยการเคลือบให้เป็นฟิล์มบางด้วยการปั่นเหวี่ยง ( spin coating) เมื่อนำไปตรวจวัดด้วยเทคนิค QCM พบว่าความถี่ของโพลิเมอร์ที่มีรอยประทับโมเลกุลที่เตรียมได้มีค่าสูงกว่าความถี่โพลิเมอร์ที่ไม่มีรอยประทับโมเลกุลเท่ากับ 10 เท่า และ 7 เท่าสำหรับ CBF และ PFF ตามลำดับ ได้ช่วงความเป็นเส้นตรงอยู่ในช่วง 0.5 – 1,000 ไมโครโมลาร์ สำหรับ CBF-MIP และ 10-1,000 ไมโครโมลาร์ สำหรับ PFF-MIP ตามลำดับ

# ABSTRACT

TITLE : DEVELOPMENT OF NEW SENSORS USING NANOMATERIALS AND MOLECULARLY IMPRINTED POLYMER MODIFIED ELECTRODES FOR DIAGNOSTIC AND FOOD SAFETY MONITORING
AUTHOR : WONGDUAN SROYSEE
DEGREE : DOCTOR OF PHILOSOPHY
MAJOR : CHEMISTRY
ADVISOR : ASST. PROF. MALIWAN AMATATONGCHAI, Ph. D.
KEYWORDS : NANOMATERIALS, ELECTROCHEMICAL SENSOR, CARBON PASTE, MOLECULARLY IMPRINTED POLYMER, QUARTZ CRYSTAL MICROBALANCE

In this work, the development of new sensors based on electrochemical sensors and quartz crystal microbalance (QCM) were investigated. The electrochemical sensors consist of 2 parts including chemical sensor and biosensor. The chemical sensor was developed for dopamine (DA) and uric acid (UA) determination in the pharmaceutical and urine samples. The development electrode was constructed based on ferrocence polyaniline and carbon nanotubes modified CPE (p(Fc-Ani)-CNTs/CPE). After that, Nafion (Nf) was coated onto p(Fc-Ani)-CNTs/CPE surface to obtain Nf/p(Fc-Ani)-CNTs/CPE. The oxidations of DA, UA and AA were measured by differential pulse voltammetry (DPV). The results revealed that the Nf/p(Fc-Ani)-CNTs/CPE exhibit the oxidation peaks at +0.3 and +0.45 V for the DA and UA, respectively, whereas the oxidation peak of AA does not appear. These results shows that the developed Nf/p(Fc-Ani)-CNTs/CPE provides high selectivity and good repeatability. The oxidation peaks current from DPV varied linearly with the concentrations of 1–150, and 5–250 μM for DA and UA, respectively. The estimated detection limit (3S/N) are 0.21 and 0.58 μM for DA and UA, respectively. The proposed electrode was successfully applied to determine DA and UA in pharmaceutical and urine samples with good performance.

Biosensor was developed for the determination of sulfite in wine and picked foods. The biosensor was constructed based on immobilized sulfite oxidase (SOx) enzyme onto $Fe_3O_4$@Au-Cys-FA nanocomposites which prepared using $Fe_3O_4$@Au core encased within a conjugated cysteine (Cys) as a bi-functional linker. The cysteine was attached to gold surface through thiol group. Then, amino-terminated from cysteine was conjugated to folic acid (FA) with an amide-linkage formation to obtain $Fe_3O_4$@Au-Cys-FA. The biosensor was fabricated using mixture of polydimethylsiloxane and mineral oil as binder to enhances the physical stability and sensitivity of the electrode. Cyclic voltammetry was used to investigate electrocatalytic behavior at the $Fe_3O_4$@Au-Cys-FA/CPE. The amperometric detection in FIA system was performed applying a potential at +0.35 V. Linear concentration dependence is observed in the range between 0.1 to 200 mg $L^{-1}$. The regression equation is given by y=1.086x-1.147 ($r^2$=0.998), when y and x are the area of peak current (µA) and sulfite concentration (mg $L^{-1}$). The detection limit ($3\sigma$) was 10 µg $L^{-1}$. The developed biosensor also provided good precision (RSD=3.1%) for sulfite signal (15 mg $L^{-1}$, n=20) with a rapid sample throughput (109 samples $h^{-1}$). The developed method was applied to the determination of sulfite content in wines and pickled food extracts with the high efficiency and accuracy with good agreement with the standard iodometric method.

The QCM sensor based on molecular imprinted polymer (MIP) to enhance the selectivity of the sensor for CBF and PFF determination pesticides. The CBF-MIP were prepared using methacrylic acid as a functional monomer, ethylene glycol dimethacrylate as a crosslinker, and azodiisobutyronitrile as an initiator. The PFF-MIP was synthesized using poly (4-vinylphenol) and diphenyl methane- 4, 4'-di-isocyanate as functional monomers, phloroglucinol as the cross-linker, and diphenylmethane as the porogen. The non-imprinted polymer (NIP) was synthesized using same condition but without the pesticides template. The obtained MIP and NIP were coated onto both side of electrode surface by spin coating. The frequency shifts of MIP exhibit higher than frequency shift of NIP about ten times and seven times for the CBF and the PFF, respectively. The linearity ranges were 0.5 - 1000 µM for CBF-MIP and 10-1,000 µM for PFF-MIP.

# CONTENTS

# CONTENTS (CONTINUED)

# LIST OF TABLE

# LIST OF FIGURE

# LIST OF FIGURE (CONTINUED)

# LIST OF FIGURE (CONTINUED)

# LIST OF FIGURE (CONTINUED)

# LIST OF FIGURE (CONTINUED)

# LIST OF FIGURE (CONTINUED)

# LIST OF FIGURE (CONTINUED)

# LIST OF ABBREVIATION

| ABBREVIATIONS | FULL WORD |
|---|---|
| CNTs | Carbon nanotubes |
| CBF | Carbofuran |
| PFF | Profenofos |
| CPE | Carbon paste electrode |
| QCM | Quartz crystal microbalance |
| P(FcAni) | Poly (*m*-ferrocenylaniline) |
| Nf | Nafion |
| DA | Dopamine |
| UA | Uric acid |
| AA | Ascorbic acid |
| SOx | Sulfite oxidase |
| MAA | Methacrylic acid |
| $Fe_3O_4$@Au | Magnetite coated gold nanoparticles |
| Cys | Cysteine |
| FA | Folic acid |
| CV | Cyclic voltammetry |
| DPV | Differential pulse voltammetry |
| FIA | Flow injection analysis |
| M | Molar |
| g | Gram |
| mL | Mililiter |
| mg | Miligram |
| min | Minute |
| s | Second |
| h | Hour |
| SD | Standard deviation |
| µL | Microliter |

# LIST OF ABBREVIATION (CONTINUED)

| ABBREVIATIONS | FULL WORD |
|---|---|
| LOD | Limit of detection |
| AIBN | 2, 2’-azobisisobutyronitrile |
| DPDI | Diphenyl methane 4, 4’-di-isocyanate |
| PG | Phloroglucinol |
| DPM | Diphenyl methane |
| EGDMA | Ethylene glycol dimethacrylate |

# CHAPTER 1
# INTRODUCTION

Fundamental and theories of dynamic electrochemistry, molecularly imprinted polymer (MIP), quartz crystal microbalance (QCM) relevant to the experiments presented in this thesis are discussed within this chapter.

## 1.1 Background significance

The quantitative measurements of small bio-molecules (uric acid; UA and dopamine; DA) in physiological processes of human metabolism as well as food analysis including food additives (sulfite) and quality control of pesticides (carbofuran; CBF and profenofos; PFF) are important in the various fields including pharmaceutical quality control, medical diagnostic and food safety. There are many developed analytical techniques that have been proposed for the detection based on spectrophotometry, chemiluminescence, fluorescence, electrochemistry, high performance liquid chromatography (HPLC), etc. However, enhancement of sensitivity and selectivity for the analysis is crucially important and challenge. Among the techniques, electrochemical sensors using nanomaterials and MIP offer several benefits over other methods, including greater sensitivity, selectivity and reliability, as well as the possibility of using in on-line applications. For these reasons, this thesis focuses on the development of sensors using carbon nanotubes (CNTs), conducting polymers, metal nanoparticles and MIP to enhance electrocatalytic activity and selectivity. Therefore, this thesis contains 2 main parts including 1) fabrication of sensitive and selective electrochemical sensors using carbon paste electrode (CPE) modified with nanomaterials and 2) development of MIP sensors based on QCM. The development of electrochemicals were concerned for 1.1 DA and UA detection in the presence ascorbic acid (AA) in pharmaceutical product and urine samples based on poly (*m*-ferrocenylaniline) (p(FcAni)) and CNTs modified electrode, and 1.2 the determination of sulfite in wines and pickled food extracts based on a gold-coated magnetite nanoparticle core, encased within a conjugated folic acid (FA) cysteine (Cys) shell immobilized with sulfite oxidase (SOx) enzyme electrode. Electrochemical

behavior of modified CPEs were studied by cyclic voltammetry (CV), differential pulse voltammetry (DPV) and amperometry. These modified CPE were used as the working electrode. In the second part, the synthesis of MIP based QCM sensor to detect CBF and PFF was studied. A CBF-MIP and PFF-MIP were synthesized using mathacrylic acid (MAA) and poly(4-vinylphenole) ( PVP) as the monomer and CBF and PFF as template, respectively. Then, these CBF-MIP and PFF-MIP were coated on surface quartz electrode to detect by QCM and used as the sensing for the analysis.

## 1.2 Fabrication of new electrochemical sensors using nanomaterials modified carbon paste electrode

### 1.2.1 Electrochemical sensors

Electrochemistry is a branch of chemistry, which is concerned with chemical reactions that occurs at the surface of a conductor (electrode), immersed in an electrolyte solution or the electron transfer between liquid/liquid interface. Electrochemical sensor can be widely divided into two classes including chemical sensor and biosensor. A biosensor is an analytical device capable of specific quantitative analytical signal using a biological element. A main biosensor consists of two parts including a bioreceptor and the transducer. A bioreceptor is immobilized biological elements (e.g. enzyme, nucleic acid, microorganism, etc) specifically bind to an analyte. The transducer is used to convert biochemical signal from the interaction of the analyte with bioreceptor into an electronic signal. The intensity signal is directly or inversely proportional to the analyte concentration [1-2]. In contrast with biosensors, chemical sensors contain non-biologically active elements, improving their sensitivity and selectivity in analyte detection. The basic design of an electrochemical sensor shown in Figure 1.1.

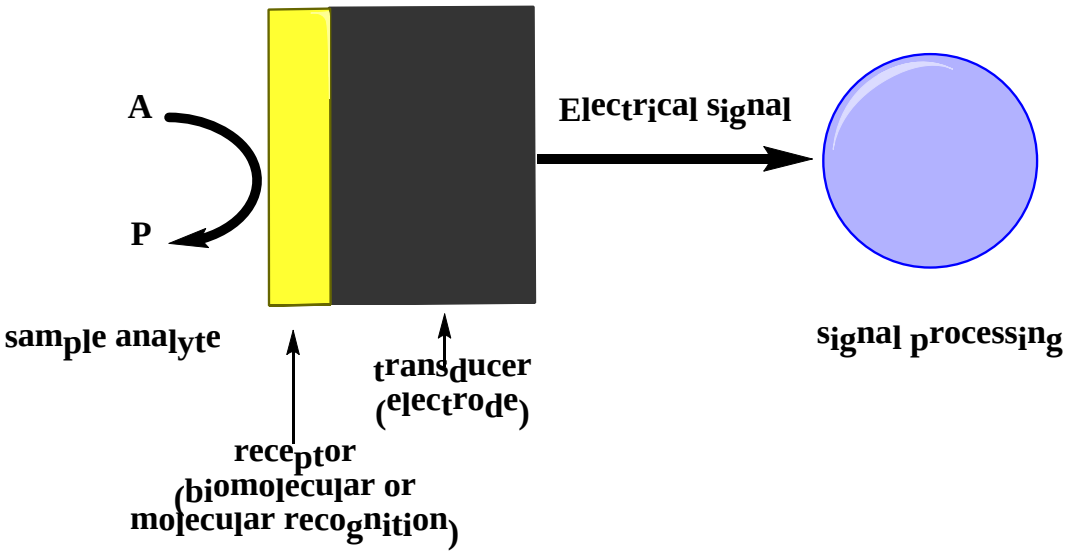


**Figure 1.1 Schematic of basic design of an electrochemical sensor**

The electrode was immobilized with materials to modify electrode surface with the recognition layer. When the analyte [A] interacts with the recognition. It catalyzes the substrate [A] of the reaction to product [P]. Then, the transducer converts biological or chemicals signals into another signals which is easily measured and quantified. The rapid growth of interest in the use of electrochemical sensor is due to the advantages; [3]:

(1) ability to measure non-polar molecules that cannot be estimated by other conventional devices

(2) excellent repeatability and accuracy

(3) can be specific to an analytes

(4) rapidity of response

(5) consume very less of reagents and standard solutions

(6) possible for miniaturized and automated devices

In this thesis, a novel electrochemical sensor was developed by incorporation of nanomaterials into the carbon paste electrode.

### 1.2.2 Carbon paste electrode (CPE)

CPE is the most popular type of carbon electrode which was initially reported in 1958 by Adams. [4]. CPE was widely used in electrochemical sensors because of low Ohmic resistance, low cost, wide potential window, easy of modification and suitable for a variety of sensing and detection applications [5]. CPE represents one of the most prevalent types of working electrodes in electrochemical investigation. CPE possesses many good features, such as ease of handling, cost effective and flexibility. Applications of CPEs are in the fields of analysis including clinical diagnostics, food quality control, security and environmental monitoring.

#### 1.2.2.1 CPE construction

The CPE composes of 2 parts which are the electrode body and carbon paste. The electrode body constructed from Teflon rod, a glass tube or a polyethylene syringe [6-8]. Then, a piece of copper wire was inserted into an electrode body which connected the carbon paste via the end of copper wire and allowed the other end of copper wire to communicate with potentiostat. The electrical contact was established via a copper wire. The carbon paste was prepared by thoroughly mixing appropriate ratio of graphite and binder (w/w) in a mortar and pestle until homogeneous. Generally, the organic liquid as a binder component of pastes is a non-conductive mineral oil, such as nujol, paraffin, or alike. Owing to its chemical inertness as well as good adhesive ability, this non-conductive viscous liquid is always being favored in the process of fabricating the traditional CPE. Then, the paste is filled into an electrode body by pressing the end into the paste composite to a depth of approximately 3 mm. Finally, the flat surface of CPE was manually smoothed using weighing paper [9]. The fabrication procedure of CPE is shown in Figure 1.2.

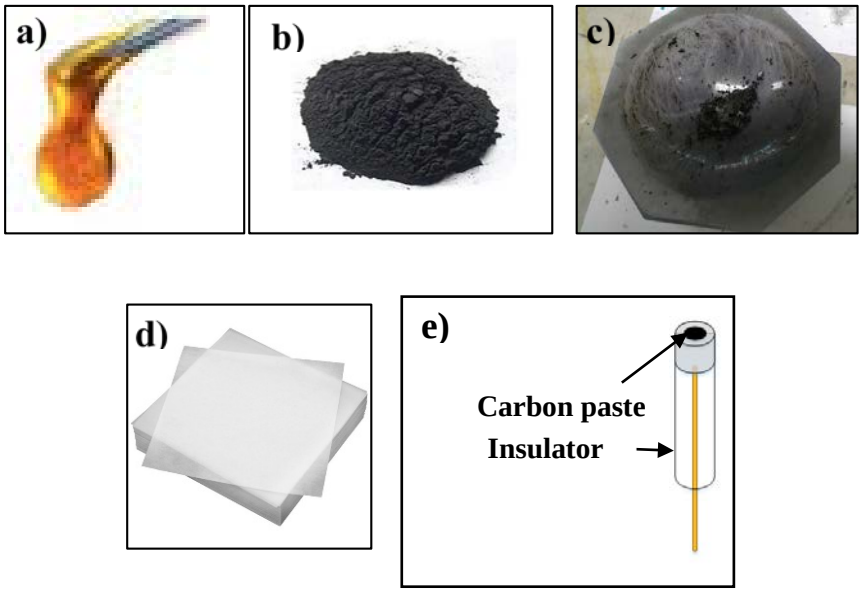


**Figure 1.2 Fabrication procedure of a carbon paste electrode: a) binder, b) graphite powder, c) homogenized carbon paste, d) weighing paper and e) example of carbon paste electrode [adopted from 9]**

The surface of the paste electrodes must be renewed after sometime run, else fouling of the electrode surface can cause considerable irreproducibility in the peak current. Which, to some extent, weakens the electrochemical response of CPE, and especially is disadvantageous to traces of detection [10]. Therefore, the use of a considerably unique properties chemicals to modify electrodes may be an alternative for improving of paste electrode.

### 1.2.3 Chemically modified electrodes

Electrochemical detection at bare electrode normally achieved at high potential. This high potential can produce large background current, resulting in inferior detection limits. Those drawbacks can be eliminated by modification of the electrode surface with conducting or large surface area materials. These modifications involve irreversible adsorption, self-assembled layers, covalent bonding, electropolymerization, and others. The important factors for the electrode surface modifications are in the following [11]:

(1) transfer of physicochemical properties of modified electrode

(2) enhanced electrocatalytic activity of electrode due to the use of materials with large surface area which in turn allows better sensitivity

(3) selectivity towards analyte due to the immobilized functional groups

(4) fast diffusion kinetics and conductivity in case of some materials

The materials for electrode modification can be classified into the following groups including metal nanoparticles (eg. Ag, Au, Cu, Pd, Pt), carbon based nanomaterials (e.g. SWCNTs, CNTs, graphene, graphene oxide), inorganic compounds ($Fe_3O_4$, $WO_3$, etc.), special dopant (complex ions, dyes, polyelectrolytes) and ternary system [12]. The concept for electrode surface modification is one of the exciting developments in the field of electroanalytical chemistry. In this thesis, attention focuses on materials-modified electrodes to detect DA, UA and sulfite.

1.2.3.1 Chemical sensor for DA and UA detection

DA, UA and AA are important biomolecules in body fluids in human body such as blood and urine. DA is an important neurotransmitter in the central nervous, renal, hormonal and cardiovascular system [13-14]. An abnormal concentration of DA is directly related to the motor functions of the central nervous system. Lower concentration of DA in human is related to several neurological diseases such as Parkinson's disease and hyperactivity [14]. On the other hand, higher level of DA leads to the mental disorder due to the abnormal brain function [15]. UA is the primary product of purine metabolism which is important for metabolic production in biological system mainly found at the human serum and urine. Abnormal concentration levels in urine and serum is related to several disease including hyperuricemia, gout, pneumonia, Lesch-Nyan Syndrome, cardiovascular and chronic renal disease [16].

1) Carbon nanotubes (CNTs)

CNTs, which were receiving more and more research interest, are receiving first discovery by Iijima [17]. There are two main structures of CNTs consisting of single-wall carbon nanotubes (SWCNTs) and multi-walled carbon nanotubes (CNTs). SWCNTs can be visualized as a rolled-up of grapheme sheet with an individual cylinder of 1-2 nm in diameter. CNTs comprise several to tens of concentric cylinders of rolled graphite sheet with an interlayer spacing of 0.34 nm and

diameters in the range of 2-100 nm [18, 19]. CNTs can display metallic, semiconducting and superconducting propeties. The electron transport properties are able to promote electron or proton transfer reaction and electrocatalysis processes. Their unique properties are due to high surface area, well chemical stability and significant mechanical strength [20, 21]. Moreover, they are friendly to the environment [22]. All these fascinating properties make CNTs as a suitable candidate for the modification of electrodes. Multi-walled carbon nanotubes are a collection of nested tubes of continuously increasing diameters as shown in Figure 1.3. The functionalized CNTs reveal distinctive properties which could enable diverse clinical, pharmaceutical and medical applications. The chemical functionalities can easily be conjugated and tuned for the modification of these tubular structures.

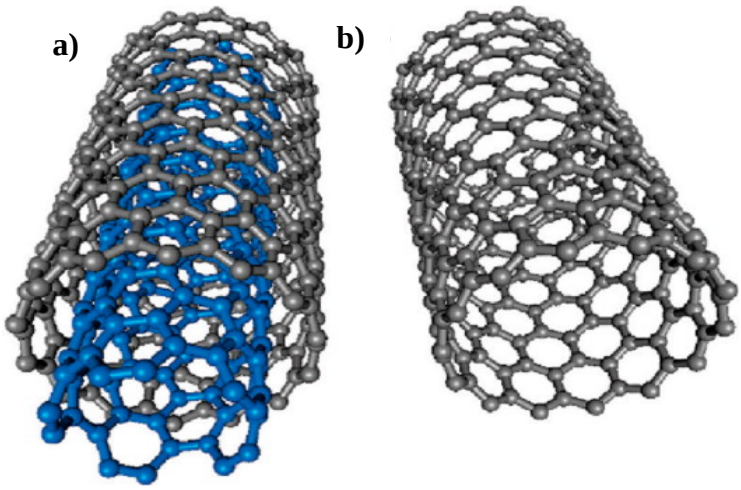


**Figure 1.3 Structure representation of a) CNTs and b) SWCNTs [23]**

Moreover, redox mediators are widely used to improve sensitivity, selectivity, and detection limits of electrochemical sensors and biosensors.

2) Ferrocence (Fc)

Redox mediators are widely used in electrochemical sensor because of its well electrochemical properties. Fc is one of the most interesting choice as mediators because it has a lower oxidation potential to lose an electron and can exist in two redox [24]. Fc can effectively catalyzed both the oxidation and reduction of various electroactive compound [25, 26]. Moreover, Fc and derivatives show the advantage properties to be applied in electrochemical application including good

stability in solution, rapid response to many electroactive substances, independent pH, un-reactivity with oxygen, regeneration at low potential and having fast electron transfer [27]. Fc is well suited to modify the electrode surface due to its excellent electron transfer properties during redox reactions. The reversible oxidation reaction of Fc shown in Figure 1.4. However, their limitation in electrode modification are because of Fc weakly adsorbed on the electrode surface due to its neutral charge. Therefore, Fc molecules were improved by substituting the Fc rings with the high molecular weight compounds or conducting polymer to resolve this problem.

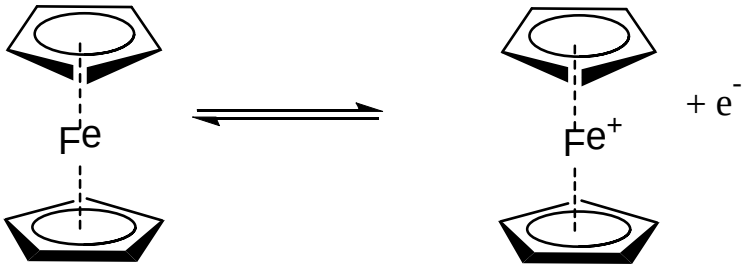


**Figure 1.4 Reversible oxidation reaction of Ferrocenc (Fc) [28]**

1.2.3.2 Biosensor for sulfite detection

Sulfite is widely used as a food additive due to its anti-septic, anti-bacterial and bleaching properties [29]. Sulfiting agents exist in various forms such as sulfite, sulfur dioxide, hydrogen sulfite, meta-bisulfite, they were used as preservatives in foods, beverages and several food products such as dried fruits and vegetables [30]. However, sulfite causes some adverse health effect in hypersensitive people such as symptoms from hives, nausea and diarrhea, asthmatic attacks and respiratory failure. [31]. The level of sulfite in food has been the subject of legislation since it was discovered that certain concentration level causes allergic reactions in some individuals. Therefore, a correct analytical sulfite determination in food industry in order to control product quality is very important. Since 1986, the United States Food and Drug Administration (FDA) have required labeling of products containing more than 10 mg $L^{-1}$ of sulfite in food or beverages [32].

1) Magnetite ($Fe_3O_4$) nanoparticles

$Fe_3O_4$ nanoparticles have useful physical and chemical properties including super paramagnetic property, a large surface area, strong adsorption characteristics, good mechanical stability and electrical conductivity, and superb electrocatalytic activity [33]. The $Fe_3O_4$ synthesis strategies compose of co-precipitation, thermal decomposition, and hydrothermal synthesis. The most popular method for synthesis of $Fe_3O_4$ is co-precipitation because of the ease of procedure [34].

2) Sulfite oxidase (SOx)

The SOx is a complex metalloprotein containing the molybdenum cofactor (Moco) and a cytochrome b5-type heme in two different domains of the protein, which are connected by a flexible loop region for catalyst of the oxidation of sulfite to sulfate [35]. SOx can be utilized with cytochrome c (Cyt c) which is electron acceptors for enhancing selectivity of redox reactions at lower potentials in a sulfite biosensor. The molecular structure of cytochrome c contains one iron-containing heme group buried within the molecule. Cyt c has been used extensively as a direct electron transfer (DET) of redox proteins and communication in a protein matrix [36].

### 1.2.4 Detection

#### 1.2.4.1 DA and UA detection

DA can be electrochemically oxidized to form dopamine –quinone (DAQ) at the electrode surface. When a potential is applied on the electrode, an interchange of 2 electrons and 2 protons occurs in the DA molecules and is oxidized to DAQ. In the same way, UA can be electrochemically oxidized to form uric acid 4, 5-diol. The mechanism of DA and UA shown in Equation 1.1 and 1.2, respectively. Therefore, current signals are produced when the electrode received the electrons [37].

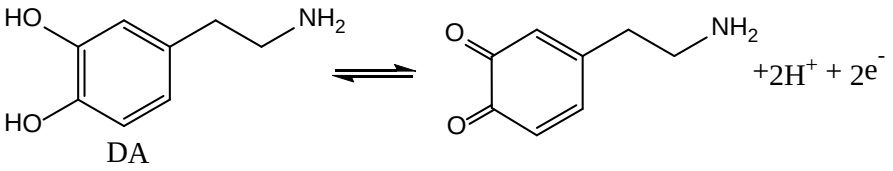


DA (1.1)

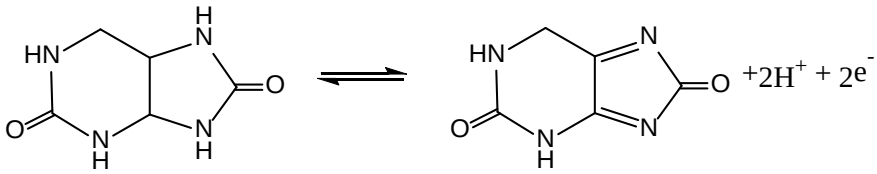


UA (1.2)

1.2.4.2 Sulfite detection

For the reaction of sulfite, SOx catalyses the oxidation of sulfite to sulfate and $H_2O_2$. There are several recent reports of amperometric sulfite-biosensors using SOx immobilized on various electrodes [35–36]. The mechanism is shown in Equation 1.3

$$SO_3^{2-} + H_2O + O_2 + 2(\text{Cyt c})_{ox} \xrightarrow{SOx} SO_4^{2-} + 2(\text{Cyt c})_{red} + H_2O_2 \quad (1.3)$$

From the reaction above, operation of the sulfite biosensor can be schematically shown in Figure 1.5. At the initiation step, the enzyme (SOx) catalytic oxidizes sulfite to sulfate, and simultaneously undergoes reduction at the active sites containing Cyt c-cofactor. The reduced form of SOx then reacts with the oxidized form of Cyt c. This process produces the oxidized form of the enzyme and simultaneously generates the reduced form of Cyt c. The reduced form of Cyt c is re-oxidised at the developed electrode which generates the analytical signal.

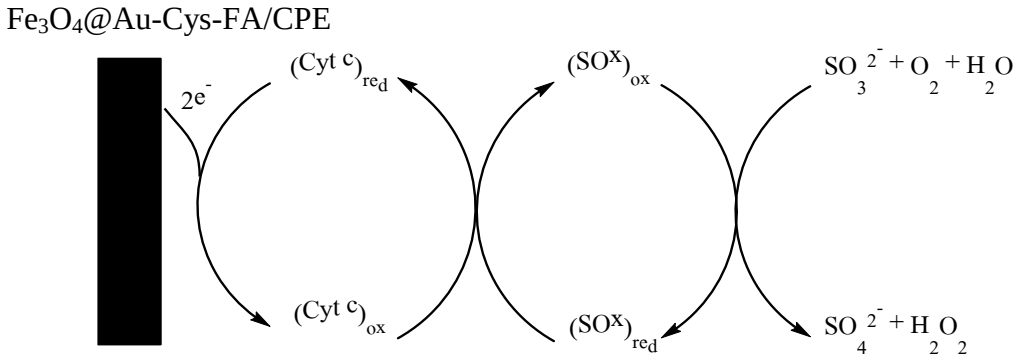


**Figure 1.5 Schematic diagram showing the various reactions occur during operation of the sulfite biosensor**

### 1.2.5 Electrochemical sensor method

Current response from the proposed methods were measured by electrochemical techniques including voltammetric (cyclic voltammetry (CV), diferential pulse voltammetry (DPV) and amperometry. The principles behind each approach are outlined below.

1.2.5.1 Cyclic voltammetry (CV)

CV is widely used as the most versatile electroanalytical technique for the qualitative study of the stability and homogeneous reactions of species. The CV consists of scanning linearly the potential of a stationary working electrode using a triangular potential wave form, which is shown in Figure 1.6a. During the potential sweep, the potentiostat measures the current resulting from the applied potential. The resulting plot of current (vertical axis) versus potential (horizontal axis) was called cyclic voltammogram as shown in Figure 1.6b. Typical voltamogram (Figure 1.6b) represented the reversible reaction and introducing the main measuring parameters for the CV technique: $E_{p,c}$ is the potential cathode peak, $E_{p,a}$ is the potential anodic peak, $I_{p,c}$ is the cathodic current and $I_{p,a}$ is the anodic current. $\Delta E$ is the difference between the reaction and oxidation potential peaks as shown in Equation 1.4.

$$\Delta E = E_{p,a} - E_{p,c} \quad (1.4)$$

Analysis of the position and shape of the peaks gives important information about the nature of the electrochemical process taking place and about the chemical species themselves [38].

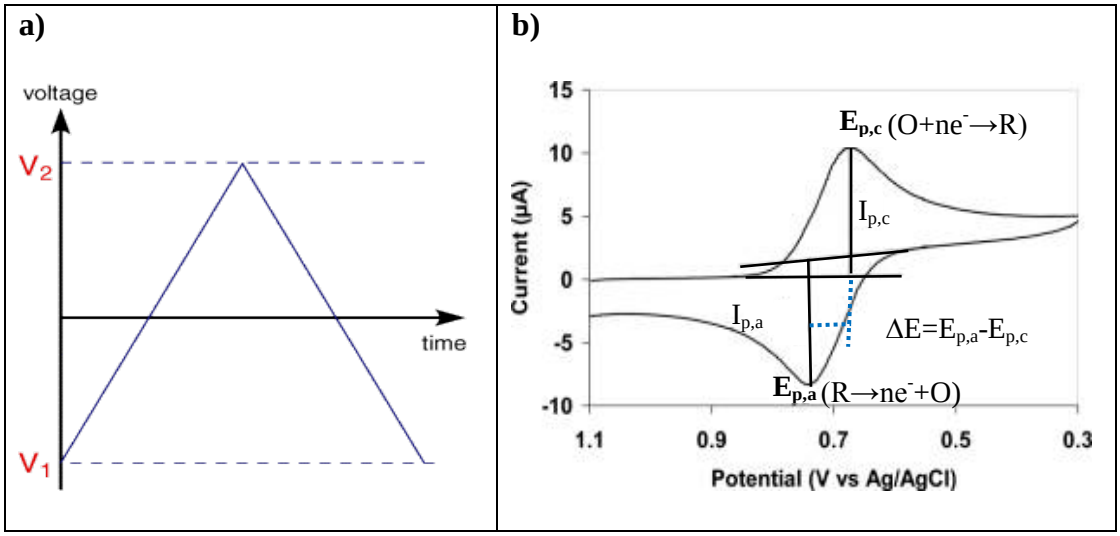


**Figure 1.6 a) Waveform of cyclic voltammetry and b) typical cyclic voltammogram. $E_{pc}$ ($E_{pa}$) and $i_{pc}$ ($i_{pa}$) are the potential and current at cathodic (anodic) peak, respectively [adopted 38].**

1.2.5.2 Diferential pulse voltammetry (DPV)

The DPV uses a small pulse (10–100 mV) of constant amplitude which are superimposed on a linear potential ramp applied to the working electrode as shown in Figure 1.7a. Current is measured at two point for each pulse of duration T, the first point just before the application of the pulse ($t_1$) and the second at the end of the pulse ($t_2$). These sampling points are selected to allow the decay of the nonfaradaric (charging) current [39]. The difference between current measurements at these points for each pulse is determined and plotted against the base potential as shown in Figure 1.7b, which is called a differential pulse voltamogram.

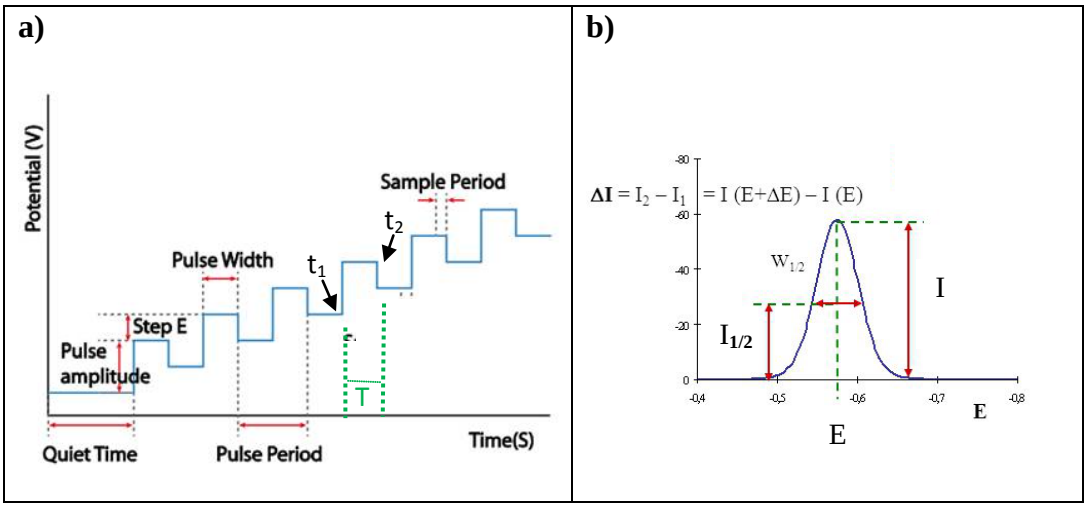


**Figure 1.7 a) Wave form of differential pulse voltammetry and b) a typical of differential pulse voltammogram [adopted 39-40]**

1.2.5.3 Amperometry

Amperometric detection is the most widely used and extensively reported electrochemical technique in flow injection analysis (FIA). In this technique, a constant potential is applied to the working electrode and the current is measured as a function of time. The redox reactions of the analytes at the working electrode surface are expedited by the applied potential, while the output current is proportional to the concentration of the analytes. The waveform incorporates the amperometric measurement with a potentiostatic is shown in Figure 1.8a. The first pulse is at a potential where the electrocatalytic reaction takes place. Since this step passivates the electrode, the next pulse is at a more positive voltage. This results in the oxidative removal of passivating species. Concomitant with this is the formation of a surface oxide layer. The electrode is reactivated by removal of the oxide layer using a negative potential. The electrode is now ready for the next detection step [41]. This gives the FIA gram as shown in Figure 1.8b.

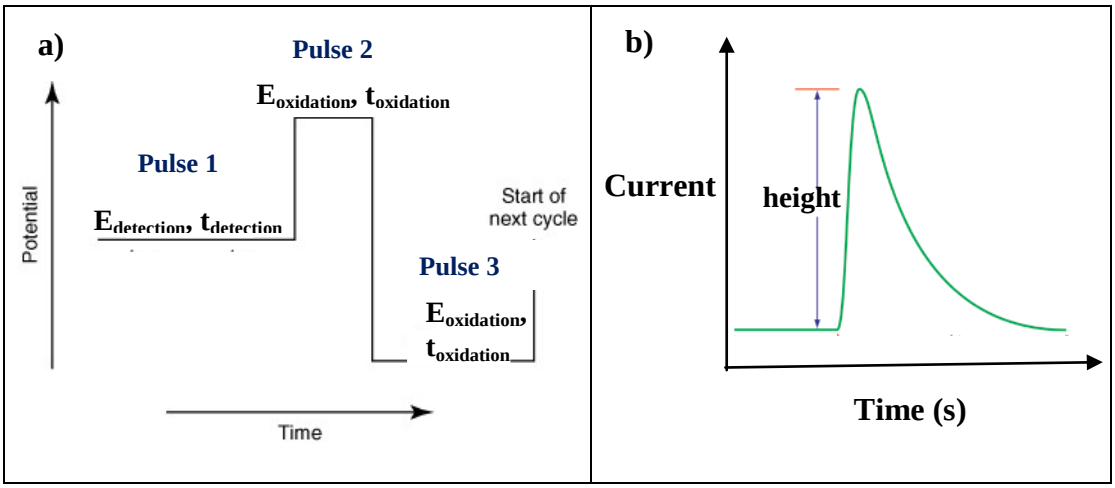


**Figure 1.8 a) Three-step potential waveform for the pulsed amperometric detection and b) a typical of FIA gram [adopted 41]**

The general batch setup for electrochemical detection consists of an electrolyte and an electrode. In this case, an aqueous solution consisting of analyte acts as the electrolyte. The cell potential is measured at the interface of the electrode and electrolyte solution. The half reaction of interest is at the working electrode (WE). The other electrode with respect to which the cell potential is measured in termed as reference electrode (RE). The current is usually passed between the WE and the counter electrode (CE). A general electrochemical experiment uses an external power supply to provide an excitation signal and measure the response function in the chemical solution considering various system variables to be kept constant.

The amperometry method has many advantages such as short operating time, high selectivity, high sensitivity and low limit of detection. Moreover, the amperometry was used with the flow injection system.

1) Amperometric flow-through detection

The amperometric flow-through detection is carried out based on a single-line configuration. A flow cell is very important in flow system because it is a place to hold the electrodes. An electrochemical reaction takes place inside the flow cell, and then the current flowing through the working electrode is the measured. The output current is proportional to the concentration of the analytes. FIA systems offer excellent advantages, such as the reproducibility of sample processing and transport to the detector (convective mass transport), leading to reproducible

measurements, high sampling rates, simple and low cost manifolds, reagent and waste economy, and the possibility of automation [42].

## 1.3 MIP modified QCM sensor for pesticides detection.

### 1.3.1 Molecularly imprinted polymer (MIP)

MIP technique is applied to fabricate recognition sites in order to exhibits affinity for the target or template molecule. MIP is prepared by forming a complex of template molecules and functional monomer and subsequent copolymerization with cross-linking monomer such as on polyurethane, polystyrene or polymethacrylate. Next, template molecules were leaved binding sites [43-44]. The MIPs possess impress upon simple, cheap, selectivity, excellent mechanical strength, and durability to heat, acid and base condition. Therefore, the MIPs extensively employed for various applications. The synthesis process of MIP is represented in the Figure 1.9.

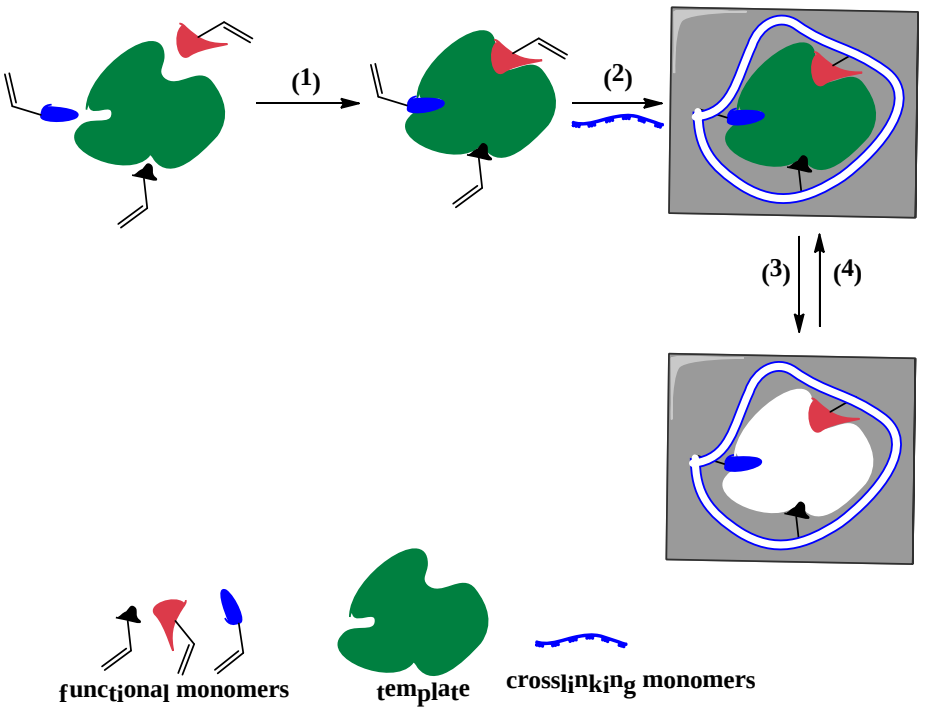


**Figure 1.9 Schematic representation of the fundamental steps for MIP formation: (1) interaction of the template (green) and functional monomers to form a template-monomer complex; (2) reaction of template momomer complex and crosslinking monomer to form a cross-linked polymer containing a template specific binding site; (3) removal of the template; (4) rebinding of the template**

MIPs are typically manufactured in a Four process

(1) Formation of the template-monomer complex

The template molecule and the functional monomer are added to the solvent (or porogen) at ratios that are designed. The interaction between the two species lead to the formation of the template-monomer complex in a noncovalent way such as via coulombic interactions, π-π stacking, hydrophobic and weak hydrogen bonding, van der Waals forces or by reversible formation of covalent bond [45].

(2) Polymerization

This step involved addition of crosslinking monomer in the template-monomer complex. This step is carried out in order to “lock” the template within a porous, polymeric materials. The complex is polymerized through thermal or photo-initiation in the presence of cross-linker, producing a tri-dimensional structure.

(3) Extraction of the template

This involves breaking the bond between the functionally polymer and template by removing the template from the polymer structure leading to the creation of specific binding site “cavity”.

(4) Rebinding of the template

The template rebinding with the polymer using the empty imprinted site or cavities. This step can be applied for generation of the signal in QCM or electrochemical measurement.

1.3.1.1 Optimizing the performance of molecularly imprinted polymer

In a molecular imprinting process, the choice of chemical reagents is primary importance. The factors involving functional monomer, cross-linker, initiator and solvent were considered for MIP synthesized.

1) Template

In the molecular imprinting processes, the template is an important in that it designs directly the interaction between the functional monomer and the template. The main choice of template is its stability, the ability to establish hydrogen bonding and the absence of polymerizable groups to avoid reaction with the newly free radicals. The questions to ask of a template are following: (1) Does the template bear any polymerisable groups, (2) Does the functional group template can be related a free radical polymerisation, and (3) Will the template be stable at moderately elevated temperatures (e.g. at or around 60 °C if AIBN is being used as the chemical initiator) or upon exposure to UV irradiation.

2) The functional monomer

The functional monomer is largely responsible for the formation of template specific binding sites within the polymer matrix. The monomers can be broken down into the following general groups: acidic, basic, neutral and electrostatic charge. An example of each type of monomer are presented in Table 1.1.

**Table 1.1 Examples of functional monomer structure**

| Monomer | structure | Functionality |
|---|---|---|
| Methacrylic acid (MAA) | 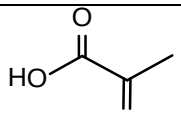 | Acidic |
| 4-vinyl pyridine (4-VP) | 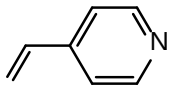 | Basic |
| 2-Hydroxyethyl methacrylate (HEMA) | 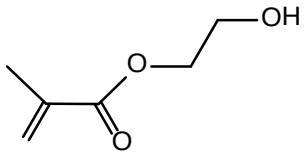 | Neutral |
| 2-acrylamido-2-methylpropane sulfonic acid (AMPSA) | 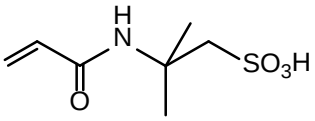 | Charged |

MAA is the most widely used choice of the monomer due to its capability to act both as hydrogen bond and proton donor and as hydrogen bond acceptor. Moreover, more strong functional monomers were developed via metal coordination interactions to bind specific amino acid sequences.

3) Cross-linker

In an imprinted polymer the cross-linker fulfils three major functions. First of all, the cross-linker is important in controlling the morphology of the polymer matrix, whether it be gel-type, macroporous or a microgel powder. Secondly, it serves to stabilize the imprinted binding site. Finally, it is parts mechanical stability to the polymer matrix. The cross-linker has a major impact on the physical characteristics of the polymers and much less effect on the specific interactions between the template and functional monomers. Different cross-linkers have been widely used are listed in Table 1.2.

**Table 1.2 Examples of cross-linker widely used in MIP synthesis**

| Cross-linked | structure |
|---|---|
| Ethylene glycol dimethacrylate (EGDMA) | 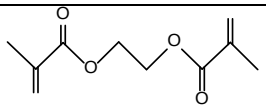 |
| Divinylbezene (DVB) | 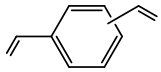 |
| phloroglucinol | 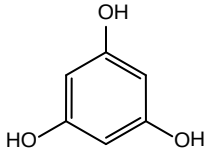 |
| Trimethylolpropane trimethacrylate (TRIM) | 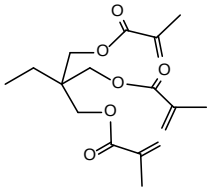 |
| Methylene-bis-acrylamide | 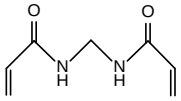 |

4) Initiator

Many chemical initiators with different chemical properties can be used as the radical source in free radical polymerization. Normally they are used at low levels compared to the monomer, e.g. 1 wt.%, or 1 mol.% with respect to the total number of moles of polymer sable double bonds. The rate and mode of decomposition of an initiator to radicals can be triggered and controlled in a number of ways, including heat, light and by chemical/electrochemical means, depending upon its chemical nature. An example of initiator presented in Table 1.3.

**Table 1.3 Examples of chemical structure and their selected initiator**

| Initiator | structure |
|---|---|
| Azobisisobutyronitrile (AIBN) | 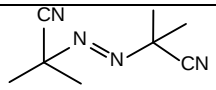 |
| diphenylmethane-4,4’-diisocyanate (DPDI) | 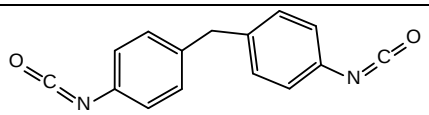 |
| 2, 2’-azobis(2-amidinopropane) hydrochloride (ABAH) | 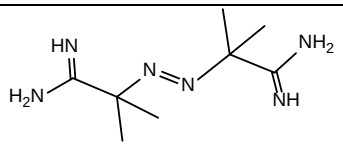 |
| Azobisdimethylvaleronitrile (ABDV) | 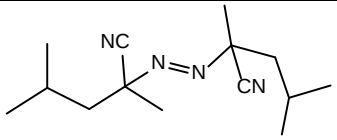 |

5) Solvent

Solvent plays an important role in the formation of the porous structure of MIPs in the polymerization of template, functional monomer(s), cross-linker and initiator into one phase. A polar and non-polar solvents were considered in MIP synthesis. The most common solvents used for MIPs synthesis are toluene, chloroform, dichloromethane, benzene or acetonitrile. Less polar solvents will increase complex formation which can be reacted by non-covalent interactions such as hydrogen bonding or bridging of ionic salts. However, more polar solvents tend to dissociate the non-covalent interactions in the pre-polymer complex because of a high degree of disruption to hydrogen bonds. [46].

The fabrication of MIP films to detect certain compounds via a quartz crystal microbalance (QCM) transducer has been accomplished in the recent years. The use of the target selective MIP as a sensing element for the highly sensitive gravimetric sensor.

### 1.3.2 Quartz crystal microbalance (QCM)

The QCM is a gravimetric sensor based on measurement the mass change caused by adsorption/re-adsorption at the specific binding site or the rigid film attached on the quartz crystal. Quartz is widely utilized material for the development of instruments containing oscillators because the first crystals were harvested naturally and synthetically grown nowadays. There are many ways to cut quartz crystals ( AT and BT cut) and each cut has a different vibrational mode upon application of a potential. The AT-cut has gained the most use in QCM applications due to its low temperature coefficient at room temperature. This means that small changes in temperature only result in small changes in frequency [47]. It has a vibrational mode of thickness shear deformation as shown below in Figure 1.10.

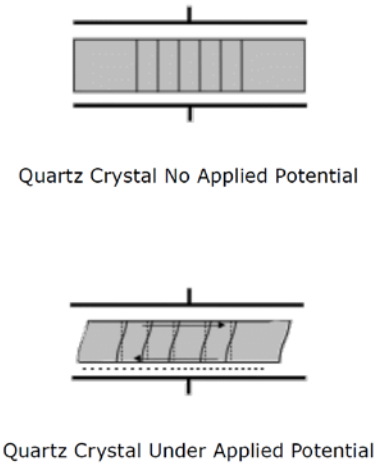


**Figure 1.10 Graphical representation of thickness shear deformation [48]**

The application of an alternating potential (a sine wave in nearly all cases) to the crystal faces causes the crystal to oscillate. The resonant frequency of such devices does not only depend on the thickness of the quartz plate, but also on the mass loading on the electrodes. The response from the device is then based on a decrease in the resonance frequency, once a mass is attached to the device or the recognition element as shown in Figure 1.11.

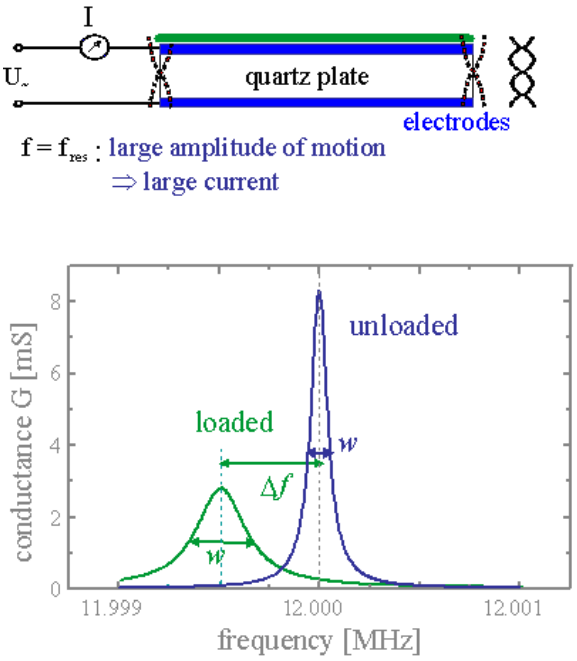


**Figure 1.11 The resonance frequency and load impedance which conductance curve such as resistance inverse as a function of the quartz vibration frequency [49]**

The resonance frequency changes of the quartz crystal related to the mass change as show in the well-known Sauerbrey equation below [50]:

$$\Delta f=-2f^{0}2/(\rho\mu)1/2\ \Delta m \qquad (1.5)$$

where Δf is the frequency shift produced as a consequence of a mass alteration per unit active area Δm; $f^0$ the fundamental resonance frequency with no attached mass; ρ the quartz density (2648 g $cm^{-3}$); and μ the quartz shear modulus. Sauerbrey equation is valid for elastic subjects such as metallic coatings, metal oxides, thin adsorbed layers, which don't dissipate any energy during oscillation. QCM sensor is suited as transducer elements for chemical sensor to produce sensitive, rapid and stable signal. There have some reports on the applications of molecularly imprinted piezoelectric sensors to pesticides.

## 1.4 Objectives

**Part I: Fabrication of new electrochemical sensors using nanomaterials modified carbon paste electrode**

1.4.1 To synthesize the new nanocomposites and investigate the possibility of using the nanocomposites for sensing materials in CPE.

1.4.1.1 poly (*m*-ferrocenylaniline) p(FcAni) and CNTs modified CPE (p(FcAni)-CNTs/CPE) for DA and UA detection in urine and pharmaceutical products.

1.4.1.2 $Fe_3O_4$@Au-Cys-FA immobilized SOx modified CPEs for sulfite detection in wines and pickled food extracts.

1.4.2 Parameters affecting the sensitivity of the developed CPE were studied and optimized using DPV for p(FcAni)-CNTs/CPE and amperometry in a flow injection analysis (FIA) for $Fe_3O_4$@Au-Cys-FA/CPE.

1.4.3 The developed CPEs was tested for the analytical efficiency and validated for the assigned samples.

**Part II: MIP modified QCM sensor for pesticides detection**.

1.4.4 To synthesize the CBF-MIP using mathacrylic acid (MAA) as a monomer and PFF-MIP using poly(4-vinylphenole) (PVP) as the monomer for QCM detection.

1.4.5 To construct high selectively QCM sensors based on MIP-modified electrodes for CBF and PFF detection.

1.4.6 Parameters affecting the selectivity of the developed MIP modified quartz electrode were studied and optimized by QCM technique.

1.4.7 The developed MIP-QCMs were tested for their analytical efficiency.

# CHAPTER 2
# LITERATURE REVIEWS

This chapter reviews about the role of nanomaterials in sensing applications, advantages and disadvantages of the design of catalytical chemical sensor, biosensors and molecularly imprinted polymer based sensors.

## 2.1 Fabrication of new electrochemical sensors using nanomaterials modified carbon-paste electrodes

### 2.1.1 Chemical sensor for DA and UA detection

In 1996, Britto, PJ. and co-worker [51] reported the use of carbon nanotubes electrode for DA detection. Carbon nanotubes electrode were constructed by mixing 10 mg of CNTs and 10 µL of bromoform as binder. This paste was packed inside a glass tube (diameter, 1.5 mm; length, 8 cm) to the height about 3-5 mm. A platinum or copper wire was inserted into the tube as a working electrode. The cyclic voltammetry (CV) was used to studied oxidative behavior of DA in phosphate buffer pH 7.4. The cyclic voltammogram of 5 mM dopamine was shown in Figure 2.1. The results illustrate the anodic peak due to dopamine oxidation at 0.22 V. The obtained anodic peak current, was linearly dependent on DA concentrations in the range of 2–1,000 µM. Moreover, this electrode was used to detect AA which it produces a quasi-reversible peak at 0.31 V. The potential peak of AA was appeared very closed to DA.

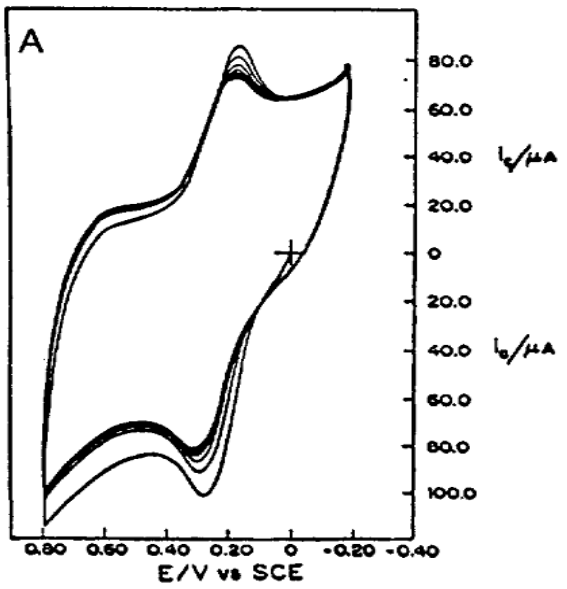


**Figure 2.1 Cyclic voltammogram of dopamine in PBS (pH 7.4) at carbon nanotube electrode** [51]

Development of inexpensive, simple, and rapid methods in routine analysis of simultaneous DA and UA detection in the presence of ascorbic acid (AA) was great interested. However, three major problems will be encountered at the bare solid electrode. Firstly, the concentration of DA is much less than that of UA in biological samples. Secondly, the sensitivities to DA and UA are low. Thirdly, DA and UA often coexist with AA in real biological samples and all of them are electrically active substances. Moreover, DA and AA exhibit nearly identical redox peaks. Therefore, it is difficult to achieve the simultaneous detection of DA and UA on the bare electrode. In order to tackle this issue, the polymeric film such as Nafion (Nf) was used for modified electrode.

In 2006, Wang, HS. et al [52] presented DA detection in the presence AA using Nf-SWCNTs coated poly (3-methylthiophen) (P3MT). The surface of the GCE was coated with hybrid film by electrodeposition in a solution containing 0.1 M of 3-methylthiophene and 0.1 M $NaClO_4$ dissolved in acetonitrile. CV was carried out to grow the film using potential between 0.0 V and +1.7 V at a scan rate of 20 mV $s^{-1}$. In this step, the P3MT/GCE (denoted as P/GCE) was obtained. Then, 5.0 µL of SWNTs-Nf dispersion were dropped onto the surfaces of P3MT/GCE and bare GCE.

After evaporation of the solvent in air for 5 min, the Nf/SWCNTs/P3MT/GCE (denoted as N/S/P/GCE) and Nf/SWCNTs/GCE (denoted as N/S/GCE) were achieved. The cyclic voltamogram of each electrode were shown in Figure 2.2. The N/S/P/GCE (curve d) demonstrated the highest peak current. The experimental results suggest that the hybrid film present the combining advantages of P3MT and Nf-SWCNTs and exhibiting dramatic electrocatalytic effect on the oxidation of DA. Moreover, the Nf/SWCNTs/P3MT/GCE was tested with the interference of AA and UA at the higher than mole ration with respect to DA concentration. The interferences from AA and UA are effectively diminished. This results may be attributed the negatively charged Nf/SWCNTs/P3MT hybrid film repels AA and UA anions and provides a transport channel only for DA cations, since in pH 7.0 PBS, DA (pKa =8.87) exits as cations, while AA (pKa =4.17), UA (pKa = 3.70) exits as anions. This hybrid film modified electrode can be applied to the determination of DA contents in dopamine hydrochloride injection and human serum. From these results, the Nf-coated chemically-modified successfully detects DA in the presence AA.

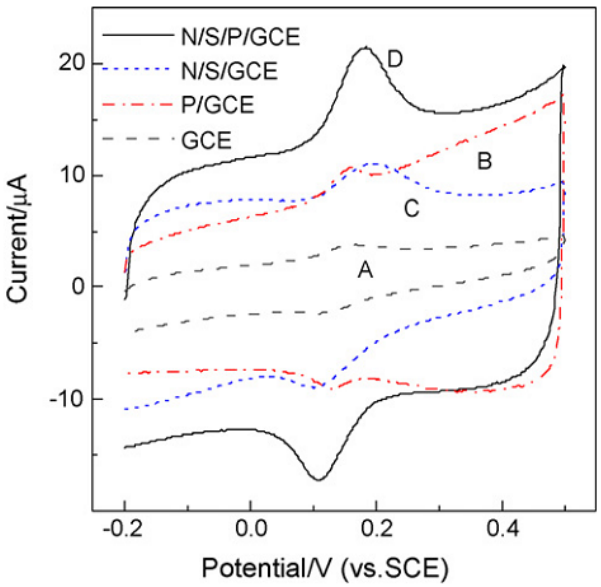


**Figure 2.2 CVs of 10.0 M of DA at A) the bare GCE, B) P/GCE, C) N/S/GCE and D) N/S/P/GCE in 0.1 M PBS with a scan rate of 100 mV $s^{-1}$** [53]

In 2008, Beitollahi, H. et al [53] constructed double-wall carbon nanotube paste electrode (DWCNTs/CPE) modified with [1,2-ethanediyl bis (nitrile-ethylidyne)]-bis-hydroquinone (EBNBH) for simultaneous epinephrine (EP), UA and folic acid (FA) detection. The EBNBH/DWCNTs/CPE was prepared by mixing 0.01 g of EBNBH, 0.89 g of graphite powder, 0.1 g of DWCNTs and oil in a mortar and pestle until a uniformly wetted paste was obtained. The paste was then packed into the end of a glass tube (ca. 2 mm i.d. and 10 cm long). Electrical contact was made by inserting a copper wire into the glass tube at the back of the mixture. finally, the electrode surface was polished on a weighing paper. This modified electrode exhibited potent and persistent electron mediating behavior followed by well separated oxidation peaks towards EP, UA and FA with activation over potential. Potential differences of 215, 560 and 345 mV between EP-UA, EP-FA and UA-FA were obtained, respectively. The obtained catalytic peak current, was linearly dependent on the EP, UA and FA concentrations in the range of 0.7–1200 µM, 25–750 µM and 15–800 µM and the detection limits for EP, UA and FA were 0.216±0.004, 8.8±0.2 and 11.0±0.3 µM, respectively. The proposed EBNBH/DWCNTs/CPE were successfully applied to voltametric measurements of various biological species.

It is well known that electrochemically well-behaved Fc and its derivatives are widely used in electrochemistry because of their good stability in solution and rapid response to many electroactive substances. However, it is difficult to adsorb Fc and their derivatives strongly to the electrode surface, so a few methods have been developed to synthesize a few Fc derivatives with specific functional groups.

In 2006, Savage, D. et al [54] synthesized a novel N-*m*-ferrocenyl benzoyl dipeptide esters. N-*m*-ferrocenyl benzoic acid was prepared by reacting N-Boc protected glycine with the amino acid ethyl ester hydrochloride salts of glycine, L-alanine, L-leucine and L-phenylalanine under alkaline condition in the presence of dicyclohexylcarbodiimide (DCC), catalytic of dicyclohexybenotriazole (HOBt) in dichromethan (DCM) at 0°C. Then, the N-*m*-ferrocenyl benzoyl dipeptide esters was synthesized by dipeptides (GlyGly(OEt), GlyAla(OEt), GlyLeu(OEt) and GlyPhe(OEt)) coupling *m*-ferrocenyl benzoic acid using DCC and catalytic amounts of HOBt. The synthesis step shown in Figure 2.3. The synthesized compounds were characterized by a combination of $^{1}$H-NMR, $^{13}$C-NMR, DEPT-135 and $^{1}$H-$^{13}$C COSY

(HMQC) spectroscopy, matrix assisted laser desorption ionization (MALDI) and electrospray ionization mass spectrometry (ESI). This compound was good yielded using standard organic peptide synthetic protocol.

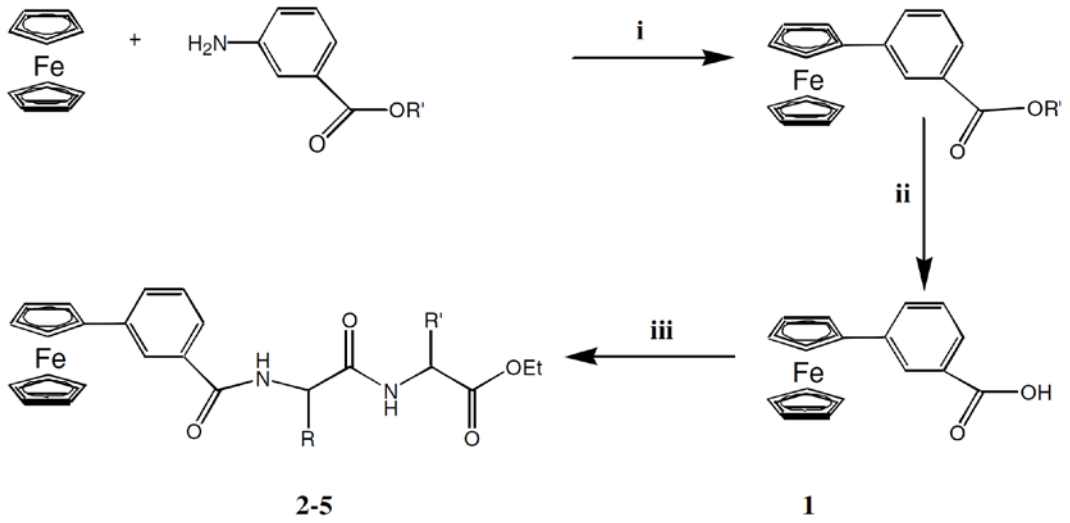


**Figure 2.3 Synthesis of the N-*m*-ferrocenyl benzoyl dipeptide esters (2–5): GlyGly (OEt) (2), GlyAla(OEt) (3), GlyLeu(OEt) (4) and GlyPhe(OEt) (5). (i) $NaNO_2$, HCl, 5 °C, (ii) NaOH/MeOH, $H_2O$, (iii) DCC, HOBt, $Et_3N$, dipeptide ethyl ester** [54]

In 2013, Chaicharoenwimolkul, L. and co-worker [55] studied the effect of Fc substituents and ferricinium additive on a polyaniline derivatives and catalytic activity of palladium-doped poly(*m*-ferrocenylaniline) (*m*-FcAni). A palladium-doped *m*-FcAni was synthesized with Suzuki-Miyara cross-coupling reactions. Firstly, the poly(aniline-co-*m*-FcAni) was synthesized by reduction reaction of *m*-ferrocenyl-nitrobenzene with Sn/HCl. Then, an ammonium peroxydisulfate was added to the mixture solution of aniline and *m*-FcAni. These solution was stirred under room temperature for 24 h. The product was filtered, washed with DI water and dried at 80°C for 24 h. Secondly, the ferricinium-doped polyaniline was prepared by slowly adding aniline in 1 M $H_2SO_4$ into ammonium peroxydisulfate. Then, the ferricinium was added into the mixture solution. The mixture solution was stirred under room temperature for 24 h. The ferricinium-doped polyaniline was obtained. Third, the

aniline and *m*-ferrocenylaniline was dissolved in 1 M $H_2SO_4$. Ammonium peroxydisulfate was dropped into the mixture solution. Follow by the ferricinium was added and the final solution was stood for 24 h. In this step, the ferricinium doped poly(aniline-co-*m*-FcAni) was obtained. Finally, palladium(II) acetate with polyaniline or poly(aniline-co-*m*-FcAni) was dissolved with toluene. The solution was kept under stirring for 24 h. The palladium-doped p(*m*-FcAni) was obtained. The synthesized ferricinium-doped poly(aniline-co-*m*-FcAni) was shown in Figure 2.4. This product was characterized by spectroscopy and quantitative analyzer. The results from Suzuki-Miyara cross-coupling reaction was confirmed the formation of this product.

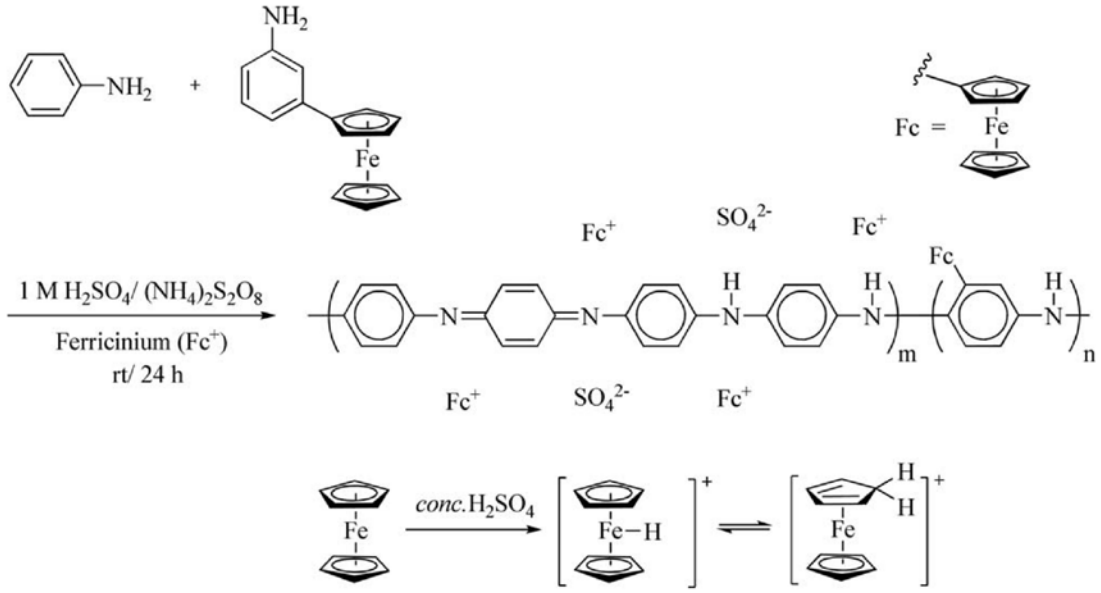


**Figure 2.4 The preparation of ferricinium-doped poly(aniline-co-*m*-FcAni)** [55]

### 2.1.2 Biosensor for sulfite detection

In 2015, Amatatongchai, M. et al [ 56] proposed method for sulfite detection using flow injection technique by CNTs-poly(diallyldimethylammonium chloride) (PDDA)-gold nanoparticles (AuNPs) modified GCE as shown in Figure 2.5. The CNTs-PDDA-AuNPs was prepared by dispersing 10 mg CNTs into 0.25% PDDA solution containing 0.5 M NaCl under stirring 30 min. Then, the resulting CNTs-PDDA composites were obtained. Then, CNTs-PDDA was mixed with 0.25% AuNPs solution for 15 min. The CNTs-PDDA-AuNPs were obtained. Finally, the CNTs-

PDDA-AuNPs re-dispersed and dropped on surface of GCE. The GCE, CNTs/GCE, CNTs–PDDA/GCE and CNTs–PDDA–AuNPs/GCE electrodes were used to investigate electrochemical behavior of sulfite using CV. The results shown in Figure 2.6A. It was found that the CNTs–PDDA–AuNPs/GCE shows the higher electrocatalytic activity of CNTs–PDDA–AuNPs/GCE than other electrodes. Results from FIA gram (Figure 2.6B) showed linearity ranged from 2-200 mg $L^{-1}$ at potential +0.4 V vs. Ag/AgCl. The proposed method was successfully applied to the determination of sulfite in fruit juices and wine samples.

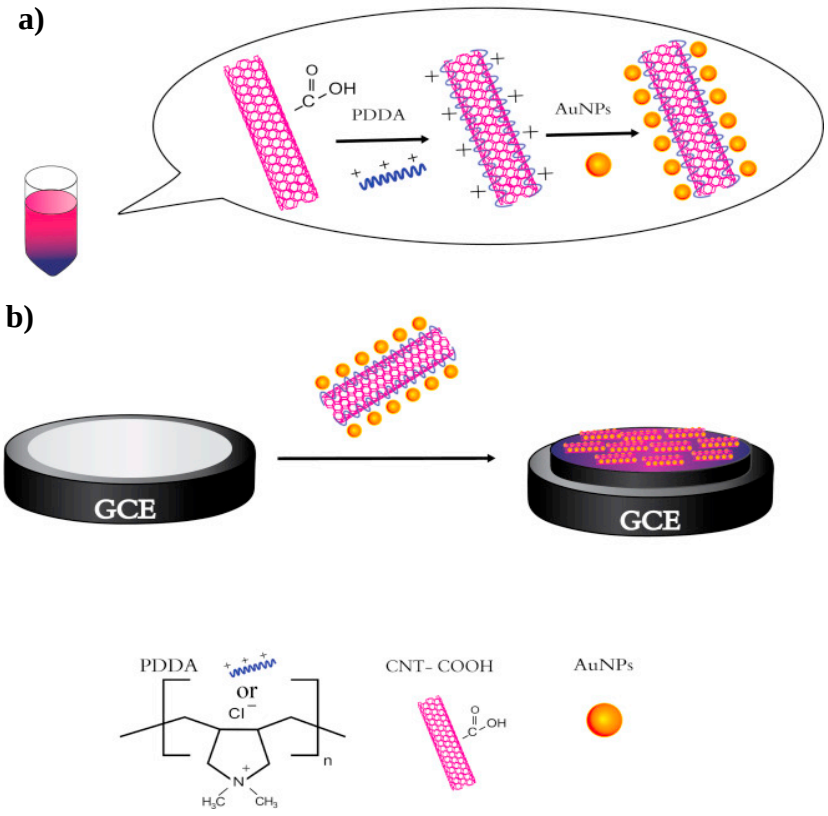


**Figure 2.5 Preparation of the sulfite sensor based on the CNTs–PDDA–AuNPs/ GCE electrode: (a) preparation of CNTs–PDDA–AuNPs dispersion and (b) drop-coating method of CNTs–PDDA–AuNPs dispersion on to GCE electrode** [56]

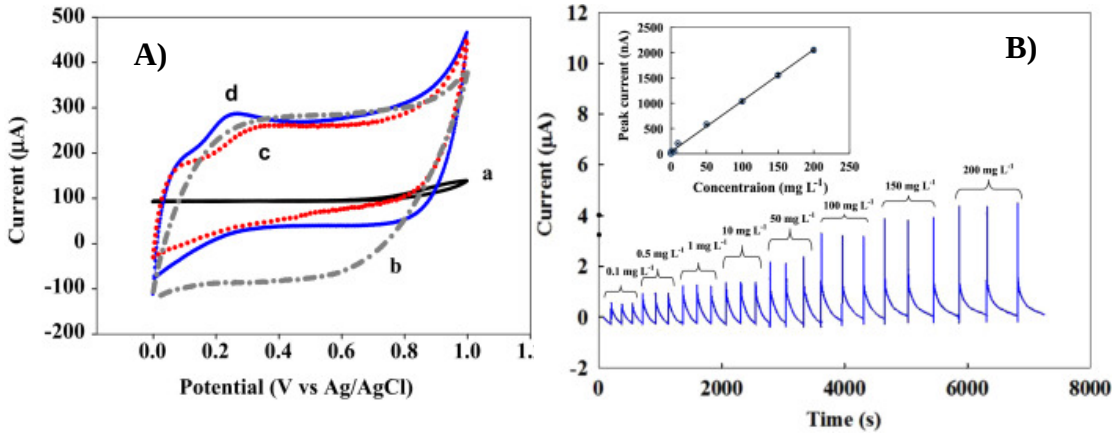


**Figure 2.6 A) Cyclic voltammograms of 4 mM sulfite in 0.1 M phosphate buffer pH 7.0 on (a) GCE, (b) CNTs/GCE, (c) CNTs–PDDA/GCE and (d) CNTs–PDDA–AuNPs/GCE and B) FIA gram obtained for injections of sulfite standards. The inset shows the linear relationship between the signal of sulfite and concentration** [56]

Fabrication of non- enzymatic modified electrodes allows electrocatalysis of sulfite oxidation reactions and reduction of the sulfite oxidation potential, although this report shows satisfactorily selectivity, sensitivity, and reliability. However, to enhance more selectivity, the use of enzymatic sensor was considered.

In 2011, Rawal, R. et al [57] developed the amperometric sulfite biosensor based on a AuNPs/chitosan (CHIT)/CNTs/Polyaniline (PANi) modified gold electrode (Au). The CNTs suspension was prepared by dispersing 1 g of CNTs in 1 mL of $H_2SO_4$:$HNO_3$ 3:1 and ultra- sonicating for 24 h. Then, 50 mL of PANi was added to 10 mL of 1 M HCl and mixed with 1 mL of CNTs suspension. This solution was called CNTs/PANi. Then the CNTs/PANi was electrodeposited onto the Au electrode through CV at 0-1.5 V by immersing the electrode into a solution (20 mL) containing 15 mL of electrolyte (0.1 M KCl) and 5 mL of 0.1 M tris-HCl buffer (pH 8.5). After that, the modified electrode was washed thoroughly with distilled water. 2 mL of AuNPs were dissolved into 2 mL of 0.5% CHIT solution. Next, the AuNPs/CHIT solution prepared by dissolving 2 mL of AuNPs into 2 mL of 0.5% CHIT was adsorbed onto the electrode surface by dipping the electrode into the solution for 3 h. The electrodes were dried in air. Finally, the 100 mL of SOx was immobilized onto the modified electrode at 4 ºC overnight and the electrode was washed with distilled

water. The fabrication of SOx/AuNPs/CHIT/CNTs/PANI/Au was summarized in Figure 2.7. Then, the SOx/AuNPs/CHIT/CNTs/PANI/Au was dried and stored in refrigerator at 4 ºC when not in use. Then the modified electrode was characterized by CV. The sensor produced response within 3 s when operated at 50 mV $S^{-1}$ in 0.1 M PBS (pH 7.0). The linear range and LOD of the sensor were 0.75-400 µM and 0.5 µM (S/N = 3).

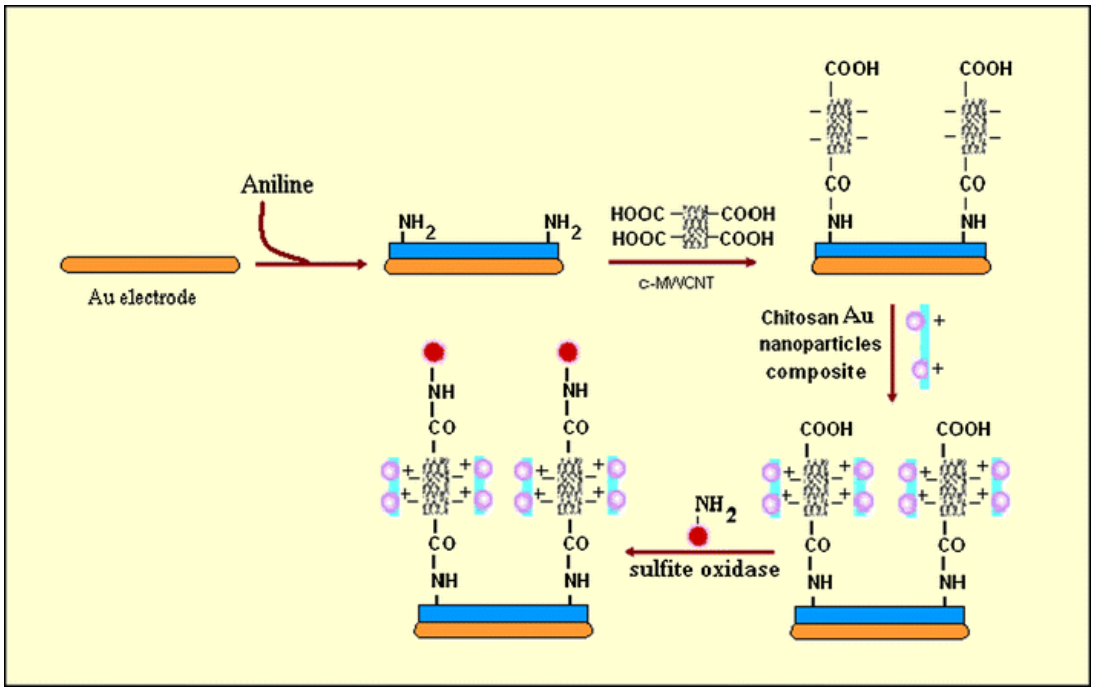


**Figure 2.7 The electropolymerization of SOx/AuNPs/CHIT/CNTs/PANI onto an Au electrode, and the chemical reaction for the immobilization of sulfite oxidase (SOx) on the modified electrode** [57]

Therefore, modified biosensing electrode by using biocompatible materials with good conductivity could be improved by the electrode sensitivity. The sensitivity of sulfite biosensor depends on the activity of enzyme and the efficiency of electron transfer between enzyme and electrode. Metal nanoparticles including gold and magnetite nanoparticles were considered as the efficient material for modified electrode.

In 2001, Kim, DK. et al [58] presented a controlled coprecipitation method of $Fe_3O_4$. The $Fe_3O_4$ was synthesized using stock solution containing 1:2 (molar

ration) of ferrous ($FeCl_3$) to ferric ($Fe_3Cl$) species in NaOH, under vigorous stirring and nitrogen atmosphere. Then, $Fe_3O_4$ was removed from solution through external magnetic field. The powder was rinsed with DI water and separated via centrifugation. This powder was rinsed to neutralize powder. The reaction mechanism can be described below. XRD analysis demonstrated the average particles diameter of 6 nm.

$$2Fe^{3+} + Fe^{2+} + 8OH^- \rightarrow Fe_3O_4 + 4H_2O \quad (2.1)$$

The obtained $Fe_3O_4$ were analyzed by X-ray powder diffraction (XRD) and zero-field-cooled (XFC) as shown in Figure 2.8 and 2.9, respectively. Figure 2.8 shows the XRD patterns for the as-precipitated powders of sample S1-S6 which were the concentration of NaOH and the pH were varied. From the results, sample S6 shown the most intense peak which corresponded the reflection in $Fe_3O_4$. Therefore, the condition according to sample S6, 1.5 M NaOH pH 11.54 was used to synthesize $Fe_3O_4$. Moreover, The DC magnetic properties were carried out using a Quantum Design $MPMS_2$ SQUID magnetometer as shown in Figure 2.9. This results show that the superparamagnetic behavior is observed showing almost immeasurable coercively and reminisce above the blocking temperature.

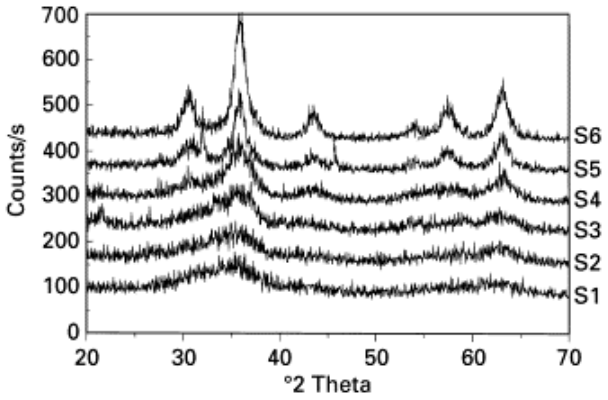


**Figure 2.8 X-ray powder diffraction pattern for the as-precipitated nanoparticles under different pH and NaOH concentration condition** [58]

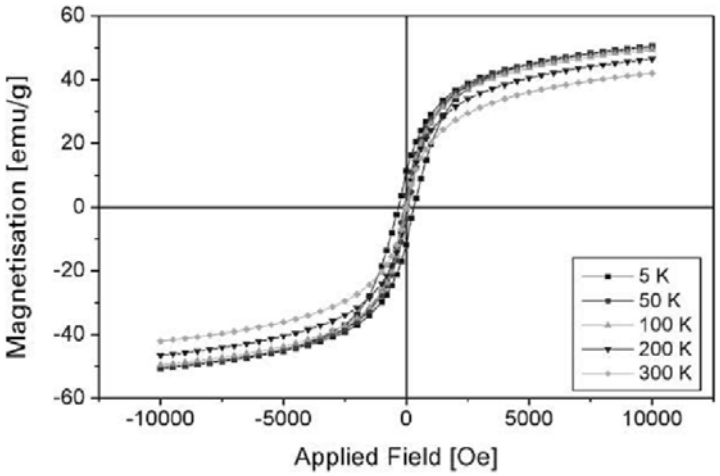


**Figure 2.9 Magnetization vs. applied magnetics field for nanoparticle (S6)** [58]

However, $Fe_3O_4$ are prone to oxidization, tend to aggregate, and lack of activating group, which result in weak magnetism, poor dispersibility and limitation of their further applications. To overcome these drawbacks, $Fe_3O_4$ are often coated with a polymers and surfactant stabilizers, precious metals or silica, and other. Core-shell iron oxide magnetic nanoparticles can thus show enhanced properties and functionalities that promote biocompatibility. There are many approaches available for the functionalization or modification of $Fe_3O_4$ surfaces for biomedical applications. One of the most promising modifications is gold-coated magnetite ($Fe_3O_4$@Au). This material is simple to prepare, offers the possibility of bio-conjugation, and has good biocompatibility for drug delivery applications [33, 59].

The core-shell $Fe_3O_4$@Au for the sulfite detection was reported on some published works.

In 2012, Rawal, R. and et al [ 60] presented an electrochemical sulfite biosensor based on $Fe_3O_4$@Au nanoparticles. Firstly, $Fe_3O_4$@Au was synthesized by dissolving $FeCl_3 \cdot 6H_2O$ and $FeCl_2 \cdot 4H_2O$ in 38 mL of 0.4 M HCl. Then, 0.7 M of ammonia solution was added quickly in the mixture solution for 30 min under stirring at room temperature. The precipitates were washed through DI water, $Fe_3O_4$ was obtained. The $Fe_3O_4$ was dispersed with $HAuCl_4$ solution containing ethanol and stood for 15 min at room temperature. Finally, the $Fe_3O_4$@Au was separated, washed with DI water. The biosensor electrode (SOx/$Fe_3O_4$@Au/Au electrode) was modified by immobilized SOx onto carboxylated $Fe_3O_4$@Au/Au electrode by electrodeposition of

$Fe_3O_4$@Au solution on Au electrode with CV at -0.4 to +0.6 V (vs. Ag/AgCl) at a scan rate 50 mV $s^{-1}$. The $Fe_3O_4$@Au/Au electrode was dipped in phosphate buffer containing N-ethyl-N'-(3-dimethylaminopropyl) carbodiimide (EDC)-N-hydroxy succinimide (NHS) solution for 6 h. Then, $Fe_3O_4$@Au/Au electrode was immersed into enzyme solution and kept overnight at 4°C. The $SO_X/Fe_3O_4$@Au/Au electrode was fabricated in Figure 2.10. The SOx/$Fe_3O_4$@Au/Au electrode was obtained. The biosensor showed response at 0.2 V (Figure 2.11c) in 0.1 M Tris-HCl buffer pH 8.5 at 35°C. The linear range and limit of detection were 0.50-1000 µM and 0.15 µM (S/N=3), respectively. These materials for modified Au electrode have resulted excellent towards sulfite.

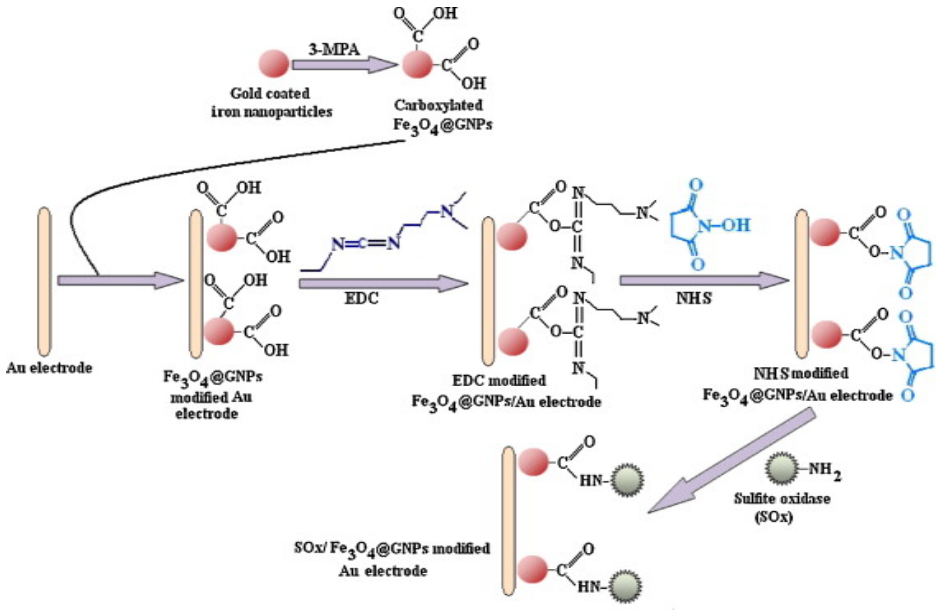


**Figure 2.10 Schematic representation of chemical reactions involved in fabrication of $SO_X/Fe_3O_4$@Au/Au electrode** [60]

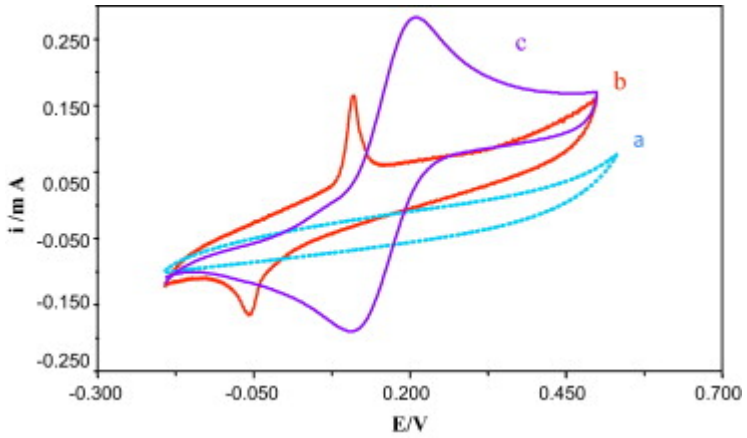


**Figure 2.11 CV of a) bare Au, b) $Fe_3O_4$@Au/Au electrode and c) SOx/$Fe_3O_4$@ Au/Au electrode** [60]

In 2009, Qiu, J-D. and co-worker [61] improved surface of $Fe_3O_4$@Au with 6-ferrocenylhexanethion ($HS(CH_2)_6Fc$) (Fc-$Fe_3O_4$@Au). The Fc- $Fe_3O_4$@Au was synthesized by mixing 0.5 mg $mL^{-1}$ $Fe_3O_4$@Au (1.5 mL) with 5.0 mM $HS(CH_2)_6Fc$ (0.5 mL) and shaking for 48 h under nitrogen atmosphere. The product was rinsed and dried. The preparation procedure shown in Figure 2.12A. Then 5 µL of Fc-$Fe_3O_4$@Au were spread evenly onto CPE surface. Transmission electron microscopy (TEM), UV–vis, and FT-IR spectroscopy were used to characterize the properties of the Fc-$Fe_3O_4$@Au nanocomposite. The CV was used for electrochemical behavior study as shown in Figure 2.12B. It was found that no redox peak at the $Fe_3O_4$@Au/CPE (curve a) was observed (curve a). On the other hand, a pair of well-defined peaks at +353 mV and +388 mV was appeared at Fc-$Fe_3O_4$@Au/CPE (curve b), which is attributed to the redox of Fc group in the Fc-$Fe_3O_4$@Au conjugate. With an increasing scan rate, the CV peak currents of the Fc-$Fe_3O_4$@Au/CPE increased (Figure 2.12B). Inset of Figure 2.12B shows that the cathodic and anodic peak currents increased linearly with the increase of the square root of scan rates, suggesting that the electrochemical reaction of Fc-$Fe_3O_4$@Au/CPE is a non-surface controlled electrode process.

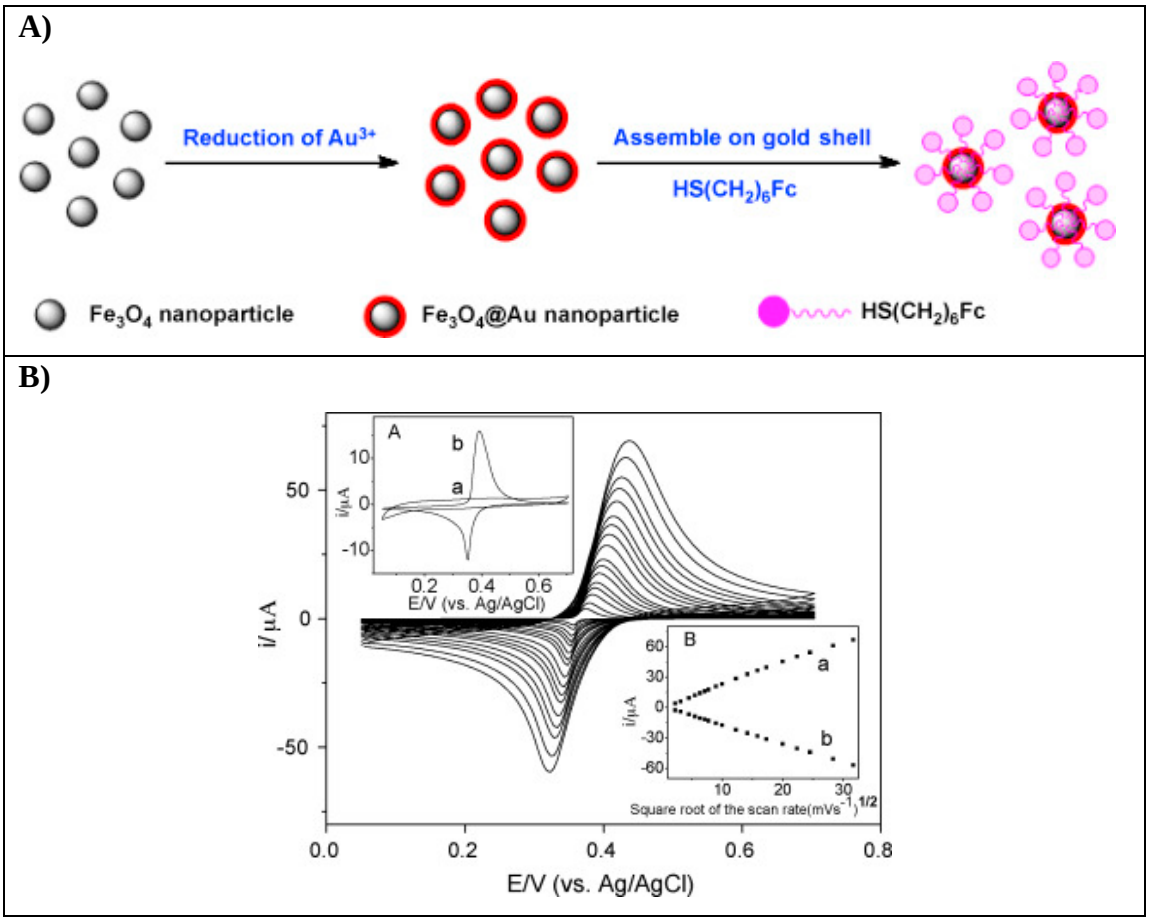


**Figure 2.12 A) Schematic illustration of the preparing procedures of the Fc-$Fe_3O_4$@Au and B) CVs of Fc-$Fe_3O_4$@Au/CPE in PBS at scan rates of 5–1000 mV $s^{-1}$ (from internal to external). Inset: (A) CVs of $Fe_3O_4$@Au/CPE (a) and Fc-$Fe_3O_4$@Au/CPE (b) in PBS at 50 mV $s^{-1}$ and (B) Plot of anodic peak current (a) and cathodic peak current (b) vs. $v^{1/2}$** [61]

In 2015, Karamipour, Sh. et al [62] synthesized folic acid (FA)-conjugated $Fe_3O_4$@Au for drug delivery application target. $Fe_3O_4$@Au core-shell was produced by reduction of $Au^{3+}$ with citrate ions in the presence $Fe_3O_4$. L-cysteine (Cys) as a bi-functional linker for attachment to gold surface through thiol group and connection to FA with an amide-linkage. For synthesis of $Fe_3O_4$@Au@Cys-FA, the $Fe(NO_3)_3 \cdot 9H_2O$ and $FeSO_4 \cdot 7H_2O$ were dissolved in NaOH solution under vigorous stirring at 70°C for 2 h. Then, 0.1% $HAuCl_4$ was added onto the $Fe_3O_4$ solution. Reduction of $Au^{3+}$ to $Au^0$ was rapidly achieved by 1% tri-sodium citrate under stirring

results in the color change from brown to reddish. Then, the pH solution was adjusted to 10 with 1% $NH_3$ solution and continuously stirred overnight at room temperature. Finally, the FA modified $Fe_3O_4$@Au@Cys nanoparticles were synthesized using N,N'-dicyclohexylcarbodiimide (DCC) for activation the carboxylic group to form FA for bond with $NH_2$ group of Cys. The FA solution containing DCC was mixed with $Fe_3O_4$@Au@Cys and stirred for overnight at room temperature. The solution was separated with external magnetic field. The $Fe_3O_4$@Au@Cys-FA was obtained as shown in Figure 2.13. This material was characterized with XRD, FT-IR, UV-visible spectroscopy, TEM, field emission scanning electron microscopy (FESEM), dispersive analysis of X-ray and vibrating sample magnetometer (VSM) analysis. This results successfully were synthesized.

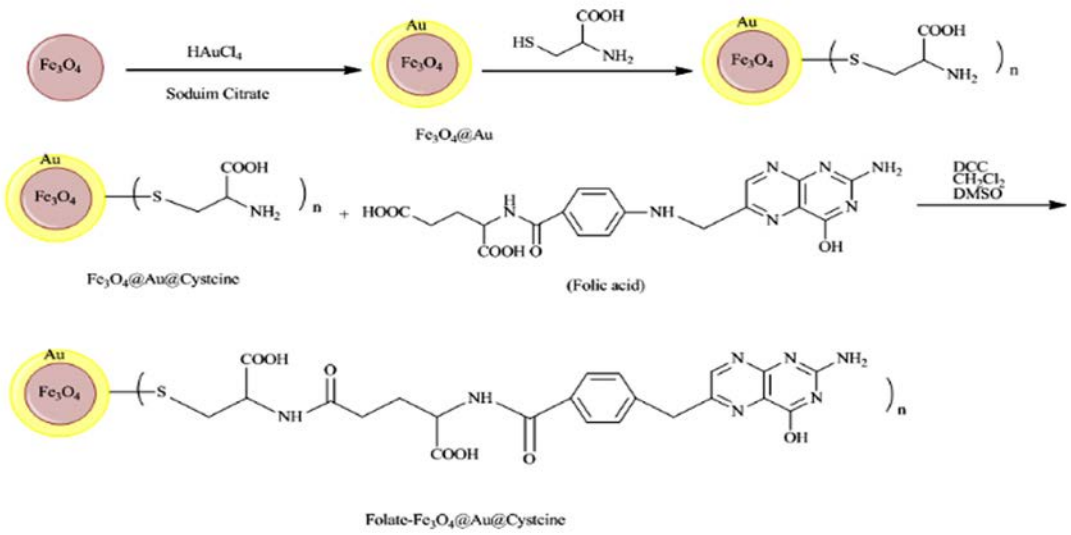


**Figure 2.13 Scheme for the synthesis procedure of $Fe_3O_4$@Au@Cys-FA** [62]

Moreover, a biosensor was constructed by the biocomposite-modified CPE for on-line amperometric detection in a flow injection (FIA) system.

In 2017, Amatatongchai, M. et al [63] reported FIA analysis of glucose using glucose oxidase (GOx) immobilized on CNTs-PDDA-platinum nanoparticles (PtNPs) modified CPE. The CPE was prepared by mixing 0.750 g of graphite powder, 0.007 g of PDMS, 0.0125 g of CNTs–PDDA, and 37.5 µL of PtNPs using a mortar and pestle until homogeneous. The composite material was then heated to 60 °C for 30 min. The 40 µL of GOx solution and 30 µL of mineral oil were carried out onto the

composite. This composite material was added to form a carbon paste electrode. The surface of the electrode was finally covered with 10 µL of Nf by drop casting onto the well-polished electrode surface. The synthesized glucose biosensor was shown in Figure 2.14. The detection potential was 0.5 V for the FIA experiments. The results from FIA (Figure 2.16) shows the linearity range between 0.1 – 100 mM. The system provides good precision of 2.8% R.S.D with a calculated detection limit (3 S/N) of 15 µM. The proposed method was successfully applied to determination of glucose in food and pharmaceutical samples with throughput of 200 samples $h^{-1}$. This results shows that this system has interested for usage in the electrochemical technique.

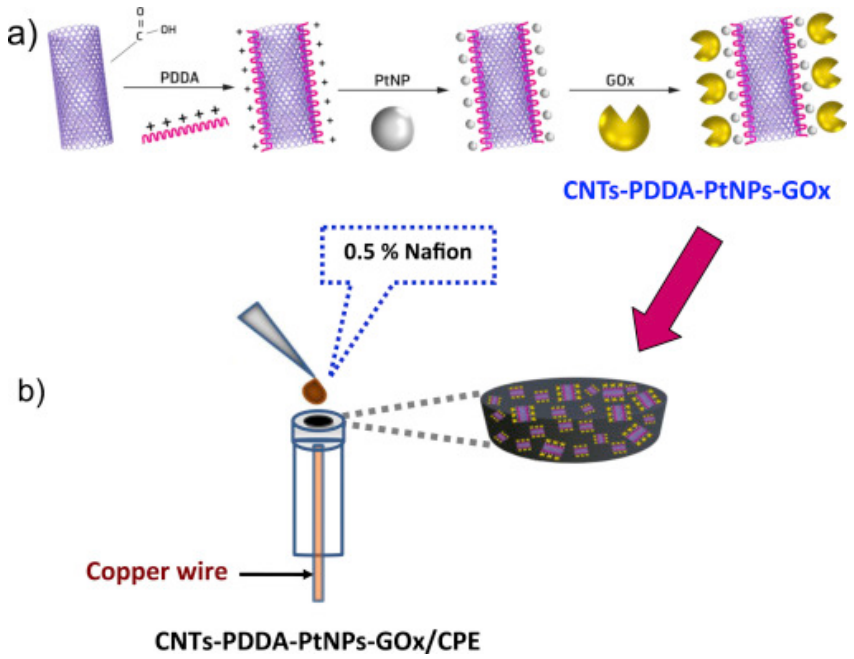


**Figure 2.14 Preparation of glucose biosensors based on (a) CNTs–PDDA–PtNPs–GOx nanocomposites, and (b) CNTs–PDDA–PtNPs–GOx/CPE** [63]

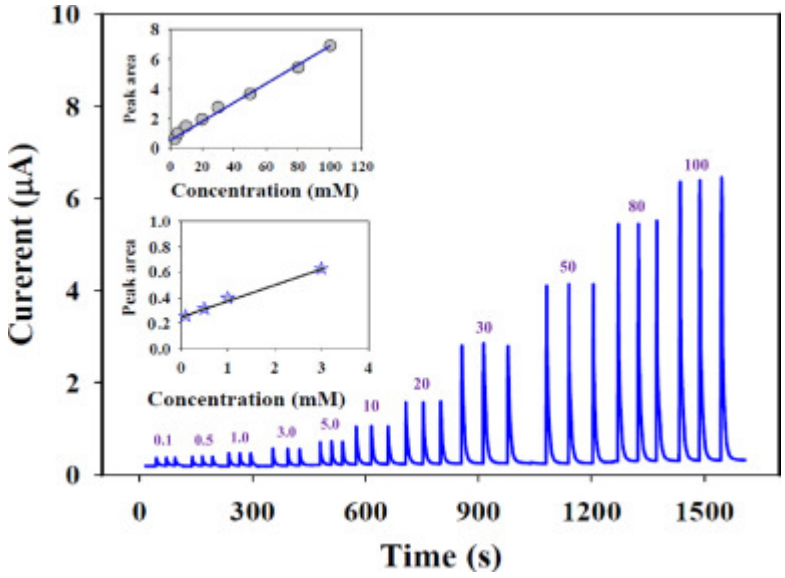


**Figure 2.15 FIA gram obtained from injected glucose standards. The inset shows a linear relationship between the signal current and glucose concentration** [63]

## 2.2 MIP modified QCM sensor for pesticides detection

In 2012, Findeisen, A. et al [64] reported artificial receptor layers for detecting chemical and biological agent mimics. The authors detected dimethyl methyl phosphate (DMMP) and *E.coil* by MIP-QCM. For DMMP sensor, the MIP was synthesized by dissolving 59 mg of PVP, 41 mg of diphenylmethane-4,4'-diisocyanate (DPDI), 8 mg phloroglucinol (PG) as a cross linker, 10 mg of diphenylmethane (DPM) as porogen and 10 mg of DMMP as template in 600 µL THF. Then, the mixture solution was pre-polymerized at 75°C for 30 min. The 600 µL THF was added into mixture solution to dissolve the polymergel to the polymer solution. Finally, MIP was coated on QCM electrode by spin coating at 3,000 rpm. The NIP was synthesized at the same condition but without DMMP. The coated QCM was dried in oven at 120°C for 10 min to achieve full polymerization. Then, the DMMP molecules were removed with toluene for 30 min. The DMMP/QCM electrode was connected to a gas mixing apparatus based on Tylan mass-flow controllers. DMMP-QCM sensor showed the linear from 0.1 – 5 ppm. *E.coil*-MIP was prepared by mixing 50 mg PVP, 56 mg DPDI and 4 mg PG in 200 µL of THF. The mixture was pre-polymerized by heated at 70°C for 15 min. The mixture solution was diluted 10 times with THF. Spin coating of

the prepared polymer on QCM electrode was performed at 3000 rpm. Finally, the *E.coil* was covered with glass stamp and allowed for polymerization. The 0.1% sodium dodecyl sulphate (SDS) solution was used for washing *E.coil* from the polymer matrix. The measurement was set up using sampling cell custom-made from PDMS with a volume of 75 µL. The QCM response shown in Figure 2.16. The sensors linear response *E.coil* was 0.1-5 mg $L^{-1}$.

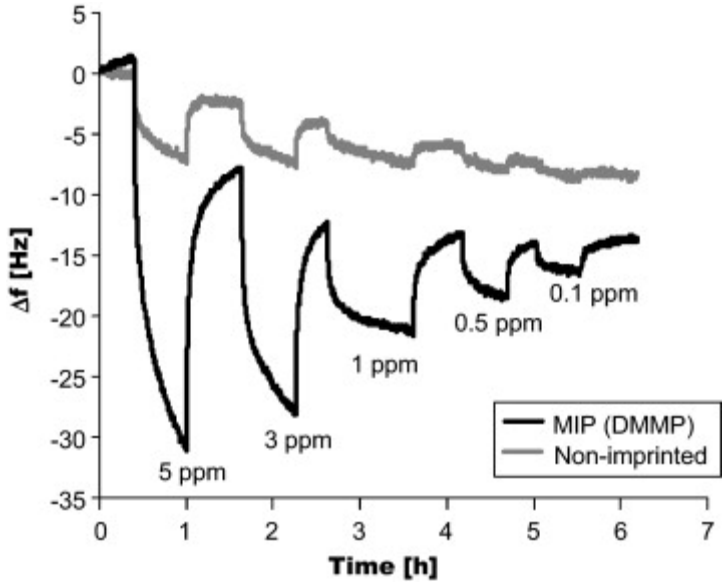


**Figure 2.16 QCM sensor responses of DMMP MIP and reference, respectively, upon exposure to different amounts of DMMP in air** [64]

In 2012, Gao, N. et al [ 65] developed the MIP films for QCM detection of profenofos. The films were prepared by physical entrapment (MIP-A) and *in situ* self-assembly (MIP-B) were tested and compared. MIP-A was prepared by dissolving 1 mmol of profenofos (PFF) and 4 mmol of MAA in 60 mL acetronitrile, and kept at 4°C overnight. Then, 20 mmol of ethylene glycol dimethacrylate (EGDMA) as cross-linker and 10 mg AIBN as initiator were added in the mixture solution. The solution was purged with $N_2$ to remove oxygen for 10 min and kept in thermostatic water bath at 60°C for 24 h. The MIP-A were collected by centrifuging at 4,000 rpm for 10 min. The template was removed by washing with methanol-acetic acid solution (9:1, %v/v). Finally, 10 µL of MIP-A was coated on the surface of sensor by mixing 15 mg of MIP-A in 5 mL THF containing polyvinyl chloride (PVP) and stood at room

temperature. On the other hand, in situ self-assembly (MIP-B) was prepared as following procedure. The clean Au electrode was formed a self-assembled monolayer (SAM) of thiol and activated by 10 mL of mixture solution of 0.2 M EDC and 0.5 M of NHS for 1 h. The electrode was transferred into 200 mM of 2, 2'-azobis(2-amidinopropane) hydrochloride (ABAH) and kept at room temperature for 3 h. The electrode was covered with initiator and immediately dipped in mixture solution containing 27 µL of PFF, 94 µL of MAA, 225 µL of trimethylopropane trimethacrylate (TRIM) and 7 mL of DMSO to pre-polymerization. Then, the electrode was carried out at 60 °C for 18 h in hot-air oven. After that, the template was removed. The synthesis of the MIP-B film on the Au surface of a QCM electrode shown in Figure 2.17. The result indicated that the best sensing signal was through the MIP-B. The response of MIP-B QCM showed two different linears for PFF from 1 x $10^{-8}$ to 1 x $10^{-5}$ mg $mL^{-1}$ and 1x$10^{-5}$ to 1x$10^{-3}$ mg $mL^{-1}$. The LOD was 2 x $10^{-7}$ mg $mL^{-1}$. The obtained sensor was used to detect spiked water sample and showed satisfactory recoveries (94.87 to 97.43%). The developed QCM sensor showed good reproducibility, wide linear range and good selectivity.

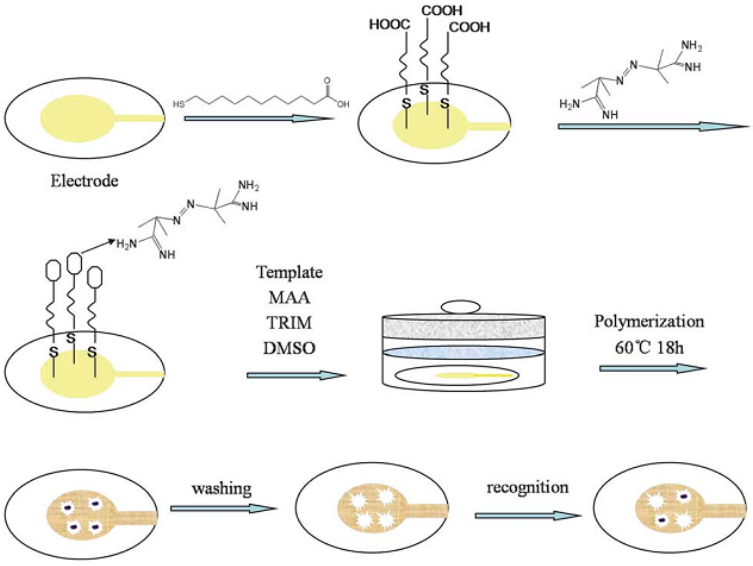


**Figure 2.17 The synthesis of a MIP-B film on the Au surface of a QCM electrode** [65]

In 2013, Kotova, K. et al [43] developed MIP sensor for biological applications. MIP was synthesized usingdifferent acrylate-based systems for the ephedrine, leucovorin and anhydroleucovorin. The ephendrine-MIP was synthesized by adding 5 mg of ephedrine, 10 mg of diphenylmethan (DMF) as porogen and 50 µL of THF in an Eppendorf reaction tube. Then, 20 mg of MAA, 70 mg of EGDMA, 10 mg of MMA and AIBN as initiator were added in the solution. The polymerization by UV was performed for 20 min and then the solution was stirred overnight. The NIP was prepared in exactly the same way but without template addition. Then, 7 µL of the stock solution was spin coated at 3,500 rpm onto the measuring electrode. While the NIP was spin coated on the second electrode. Finally, the devices were kept overnight at room temperature and template was washed out with water overnight. Leucovorin-MIP was synthesized using 32 mg of MAA, 8 mg of N,N' (1,2-dihydorxyethylene) bisacrylamide, 6 mg of sodium peroxidisulphate and 4 mg of leucovorin and 400 µL water. The reaction was allowed to polymerized under UV for 40 min. The QCM were kept overnight and were then heated 100°C in the oven for 2 h. Finally, the template was removed with the warm water at 50°C for 1.5 h. The anhydroleucovorin-MIP was synthesized by dissolving 10 mg of MAA, 10 mg of N-vinyl-pyrrolidone and 30 mg of EGDMA with 200 µL of mixed solvent consisting of 3 part (v/v) of methanol and 2 part (v/v) of DMF containing 4 mg of anhydroleucovorin. The polymerization then was initiated after adding 1 mg of AIBN under UV and pre-polymerized for 3 h. The resulting oligomer solutions were spin-coated onto QCM in the same way as above. The MIP sensor shows dynamic response behavior (Figure 2.18) in the range of 20 - 200, 60-500 and 3-100 mg $L^{-1}$ for ephedrine, leucovorin and anhydroleucovorin, respectively.

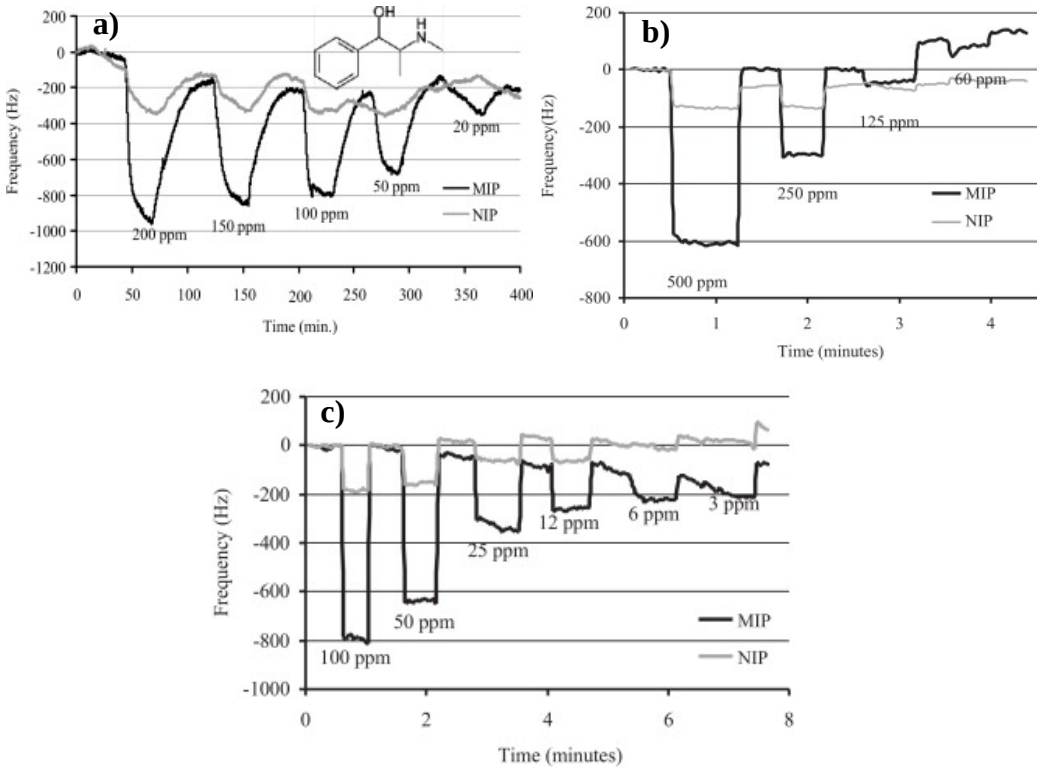


**Figure 2.18 The sensor signal of MIP toward different concentrations of a) ephedrine, b) leucovorin, and c) anhydroleucovorin** [43]

In 2015, Fan, J-P. et al [66] prepared MIP functionalized with core/shell magnetic particles ($Fe_3O_4$@$SiO_2$@MIP) for the simultaneous recognition and enrichment of four toxoids in Taxus x media. Firstly, $Fe_3O_4$@$SiO_2$ was synthesized by dispersing 0.02 mol $FeCl_3 \cdot 6H_2O$ and 0.01 mol $FeCl_2 \cdot 4H_2O$ in water and then solution was gradually heated to 50°C. The $NH_3$ solution was dropped into the solution and followed by the oleic acid was added. The mixture solution was stirred at 50°C for 150 min. The black precipitated was collected by placing external magnet. The $Fe_3O_4$ was re-dispersed in 150 mL of ethanol and ammonium hydroxide was added into the magnetic solution and then 400 µL of tetraethoxysilane (TEOS) was added into the aforementioned solution. The solution was reacted for 3 h at room temperature and collected $Fe_3O_4$@$SiO_2$ with external magnet. Then, the vinyltrimethoxysilane (VTMOS) and ammonium hydroxide was added in $Fe_3O_4$@$SiO_2$ solution with continuous stirring for 8 h. The $Fe_3O_4$@$SiO_2$ was obtained. Then, the $Fe_3O_4$@$SiO_2$@MIP was prepared by dispersing $Fe_3O_4$@$SiO_2$ in chloroform.

0.26 mmol of cephalomannine and 1.2 mmol MAA were added in chloroform and the results mixture was ultrasonicated and stood for 6 h. Then, 1.20 mmol of EGDMA and 0.02 mmol of AIBN were added and sonicated for 30 min. The mixture was pre-polymerized at 70°C for 24 h under $N_2$ atmosphere. The $Fe_3O_4$@$SiO_2$@MIP was separated and the template was removed by washing with mixture solvent (methanol: acetic acid, 9:1 %v/v). The preparation of $Fe_3O_4$@$SiO_2$@MIP was illustrated in Figure 2.19. The NIP was prepared using the same condition except with the absence of template. The as-prepared $Fe_3O_4$@$SiO_2$@MIP particles were characterized by TEM, vibrating sample magnetometer (VSM), and FT-IR. The $Fe_3O_4$@$SiO_2$@MIP were successfully applied to simultaneously enrich and separate of these four toxoids in the extract of Taxus x media.

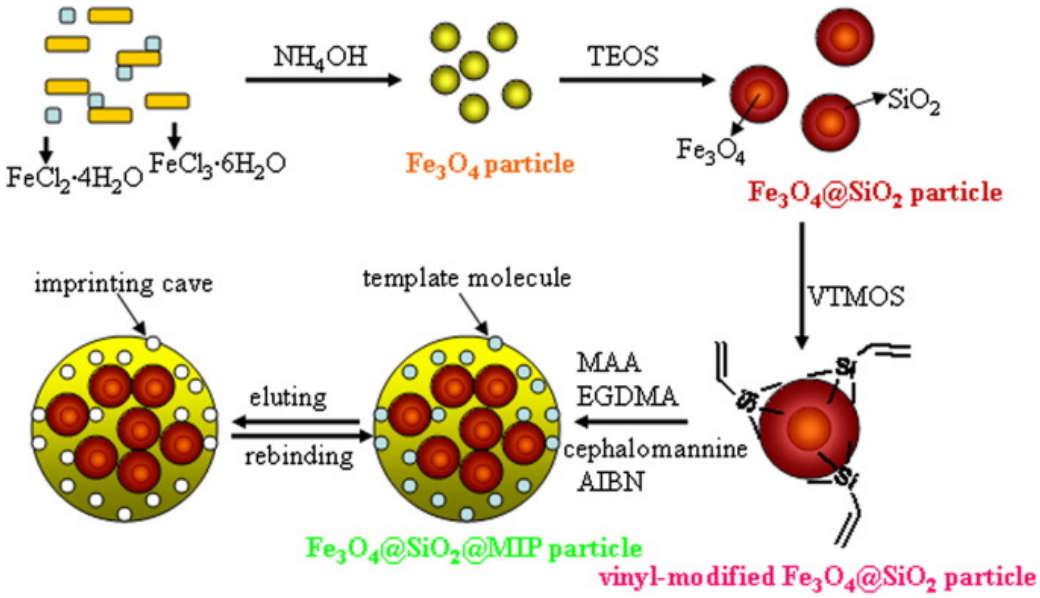


**Figure 2.19 The preparation of $Fe_3O_4$@$SiO_2$@MIP** [66]

# CHAPTER 3
# EXPERIMENTAL

In this section the instrumentation for electrochemical and quartz crystals microbalance (QCM) measurements as well as chemicals and preparation methods are described. The protocol for the different bioassays is also presented.

## 3.1 Instrumentation

Equipment used in this work were listed in table 3.1.

**Table 3.1 Instruments used for nanocomposite characterization, voltammetry, FIA, and QCM measurements**

| Instrument | Model | Company |
|---|---|---|
| ***Nanocomposite characterization*** | | |
| TEM | JEM-1230 | JEOL |
| EDS | INCA x-sight | UK |
| IR | Spectrum 100 | Perkin Elmer |
| SEM | JSM-6460LV | JEOL, Japan |
| AFM | XE-100 | Perkin Elmer |
| ***Voltammetry*** | | |
| Potentiostat | EA 161 | eDAQ, Australia |
| e-Corder | 210 | eDAQ, Australia |
| Data System | e-Chem (v2. 0. 13) | eDAQ, Australia |
| Working electrode | Cylindrical glass tube | In-house developed |
| Auxiliary electrode | stainless steel | CH Instruments, USA |
| Reference electrode | Ag/AgCl electrode (3 M KCl) | CH Instruments, USA |

**Table 3.1 Instruments used for nanocomposite characterization, voltammetry, FIA, and QCM measurements (Continued)**

| Instrument | Model | Company |
|---|---|---|
| ***FIA experiments*** | | |
| Injection | 20 µL injection loop | Rheodyne, USA |
| Pump | LC-10AD | Shimadzu |
| Detector | | |
| Potentiostat | EA 161 | eDAQ, Australia |
| e-Corder | 210 | eDAQ, Australia |
| Data system | e-DAQ-chart (v. 5.5.15) | eDAQ, Autralia |
| Thin layer flow cell | MF-1048 | BASi |
| Working electrode | Teflon block | In-house developed |
| Auxiliary electrode | Stainless steel tube | CH Instruments, USA |
| Reference electrode | Ag/AgCl electrode (3 M KCl) | CH Instruments, USA |
| ***QCM experiments*** | | |
| Frequency counter | Aglilent | Universal |
| Power supply | An input DC voltage source at 12 V and 60 mA | Universal |
| Oscillator circuit | Aglilent | Universal |
| Measuring cell | - | In-house developed |
| Network analyser | E5062A, ENA series | Agilent technology |

## 3.2 Reagents and Chemical

All chemicals used in this work were summarized in Table 3.2.

**Table 3.2 List of reagents, grade and their suppliers**

| Chemical and reagent | Grade | Supplier |
|---|---|---|
| carbon nanotubes (CNTs) | > 95% pure | Nanolab inc.(MA, USA) |
| Uric acid ($C_5H_4N_4O_3$) | Laboratory | Acros Organic |
| Dopamine ($C_8H_{11}NO_2$) | ACS | Sigma-Aldrich |
| Ascorbic acid ($C_6H_8O_6$) | AR | Sigma-Aldrich |
| Graphite powder | AR | Acros Organic |
| Sodium sulfite ($Na_2SO_3$) | Reagent | Sigma-Aldrich |
| Sulfite oxidase (SOx) from chicken liver (30-70 U $mg^{-1}$) | High purity | ProNique Scientifics Inc. (Castle Rock, USA) |
| Cytochrome C (Cyt C) from horse heart | Laboratory | Acros Organic |
| Hydrogen tetrachloroaurate ($HAuCl_4$•3 $H_2O$) | Laboratory | Acros Organic |
| N, N'-dicyclohexylcarbodimide (DCC) | | Acros Organic |
| Folic acid $C_{19}H_{19}N_7O_6$ | 95% pure | Acros Organic |
| L-Cysteine ($C_3H_7NO_2S$) | AR | Acros Organic |
| tri-sodium citrate dihydrate ($C_6H_5Na_3O_7$•$2H_2O$) | AR | Acros Organic |
| ferric nitrate nonahydrate ($Fe(NO_3)_3$•$9H_2O$) | AR | Acros Organic |
| ferrous sulfate heptahydrate ($Fe(SO_4)_2$•$7H_2O$) | AR | Acros Organic |
| Sodium hydrogen phosphate ($NaH_2PO_4$) | Analysis | Carlo Erba |
| di-Sodium hydrogen phosphate anhydrous ($Na_2HPO_4$•$H_2O$) | Analysis | Carlo Erba |
| Carbofuran ($C_{12}H_{15}NO_3$) | 98% | Sigma-Aldrich |
| Profenfos ($C_{11}H_{15}BrClO_3PS$) | 97.6% | Sigma-Aldrich |
| Chlopyrifos ($C_9H_{11}Cl_3NO_3PS$) | ≥98 % | Sigma-Aldrich |

**Table 3.2 List of reagents, grade and their suppliers (Continued)**

| Chemical and reagent | Grade | Supplier |
|---|---|---|
| Sodium chloride (NaCl) | ACS | Carlo Erba |
| Sodium sulfate ($Na_2SO_4$) | ACS | Carlo Erba |
| Sodium acetate ($NaCH_3COO$) | ACS | Carlo Erba |
| Potassium iodide (KI) | ACS | Carlo Erba |
| Sodium nitrate ($NaNO_3$) | AR | Sigma-Aldrich |
| Ethanol ($CH_3CH_2OH$) | ACS | Carlo Erba |
| Glucose ($C_6H_{12}O_6$) | ACS | Sigma-Aldrich |
| Fructose ($C_6H_{12}O_6$) | AR | Sigma-Aldrich |
| Maltose ($C_{12}H_{22}O_{11}$) | AR | Sigma-Aldrich |
| Sucrose ($C_{12}H_{22}O_{11}$) | AR | Sigma-Aldrich |
| Methacrylic acid ($C_4H_6O_2$) | AR | Merck A.G. |
| Ethylene glycol dimethacrylate ($C_{10}H_{14}O_4$) | AR | Merck A.G. |
| 2, 2'-azobisisobutyronitrile ($C_8H_{12}N_4$) | AR | Merck A.G. |
| poly (4-vinylphenol) (PVP) | AR | Sigma-Aldrich |
| diphenyl methane 4, 4'-di-isocyanate ($C_{15}H_{10}N_2O_2$) | AR | Merck A.G. |
| phloroglucinol ($C_6H_6O_3$) | AR | Merck A.G. |
| diphenyl methane ($C_{13}H_{12}$) | AR | Sigma-Aldrich |

## 3.3 Fabrication of new electrochemical sensors using nanomaterials modified carbon-paste electrodes

### 3.3.1 Preparation of chemical sensor for DA and UA detection

3.3.1.1 0.1% Nafion solution (Nf)

0.1% Nf solution was prepared by pipette 500 µL from 1% Nf stock solution then diluted with deionized water to 5 mL in volumetric flask.

3.3.1.2 0.025 M Uric acid (UA)

0.025 M UA solution was prepared by dissolving 0.042 g of UA in 0.1 M NaOH and diluted to 10 mL in volumetric flask.

3.3.1.3 0.1 M Dopamine (DA)

0.153 g of DA solution was dissolved with DI water and diluted to 10 mL in volumetric flask.

3.3.1.4 0.1 M ascorbic acid (AA)

0.176 g of AA solution was dissolved with DI water and diluted to 10 mL in volumetric flask.

3.3.1.5 0.1 M phosphate buffer (PBS) pH 5.0

0.1 M PBS pH 5.0 was prepared by mixing 0.8 mL of 0.1 M $Na_2HPO_4$ and 99.2 mL of 0.1 M $NaH_2PO_4$.

3.3.1.6 *m*-ferrocenylaniline (*m*-FcAni)

The *m*-FcAni (1) was synthesized according to the previous report [54]. In brief, *m*-ferrocenylnitrobenzene was synthesized from the reaction between Fc and *m*-nitroaniline using sodium nitrite/HCl in the presence of diethyl ether, which was then reacted with ferrocene *in situ* to yield the meta-substituted ferrocenylaniline. The product was then reduced to m-ferrocenylaniline using Sn/HCl in an ice bath. The crude product was purified by column chromatography with gradient elution (hexane–ethyl acetate) to afford the Fc derivative. A yellow-orange crystalline solid was obtained after drying under reduced pressure at room temperature. Figure 3.1 illustrates the synthetic procedure used for the preparation of *m*-ferrocenylaniline.

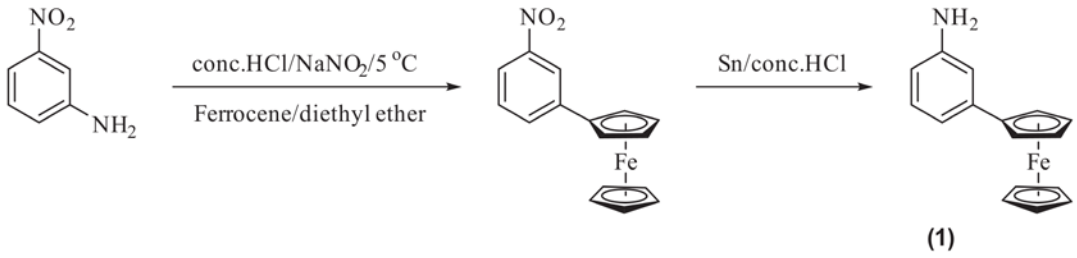


**Figure 3.1 Synthetic procedure for the preparation of *m*-FcAni** [54]

3.3.1.7 poly(*m*-ferrocenylaniline) (p(FcAni))

p(FcAni) ( 2) was prepared by oxidative polymerization of compound (1). The previously reported method according to [55]. The resulting dark brown powder was collected by filtration and then dried in an oven at 80 °C for 24 h. Figure 3.2 illustrates the synthetic procedure used for the preparation of p(FcAni).

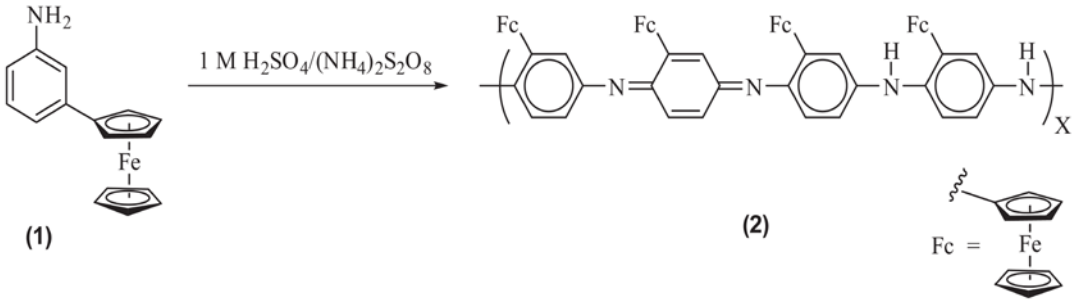


**Figure 3.2 Synthetic procedure for the preparation of p(FcAni)** [55]

3.3.1.8 Electrode preparation of Nf/p(FcAni)-CNTs/CPE

A carbon paste electrode (CPE) was constructed following our previously report with some modifications [67]. Briefly, the copper wire was carefully cut (1.5 mm diameter, 12 cm long) using a sharp scalpel to create electrical contact. Then, 3 mm of the cylindrical glass tube was exposed by inserting of a copper wire into a cylindrical glass tube (2 mm diameter, 10 cm long) from the opposite end, until the end of copper wire was buried into epoxy glue to fix the glass tube with copper wire. Next, a paste ( Nf/p(FcAni)-CNTs) was prepared by hand-mixing 25 mg of p(FcAni), 5 mg of CNTs, 70 mg of graphite powder and 30 μL of mineral oil in a mortar and pestle for 1 h to ensure that the composites were homogeneously amalgamated. Subsequently, this composite paste was packed into a hole of cylindrical glass tube with a depth of approximately 2 mm by pressing the open end of the tube into the paste composite. The surface of the p(FcAni)-CNTs/CPE was manually polished using weighing paper until a flat and smooth surface was obtained. Finally, Nf solution (10 μL, 0.1%) was dropped onto the surface of modified CPE using a micropipette, and the electrode was left to dry at ambient temperature. The method of electrode construction was illustrated in Figure 3.3.

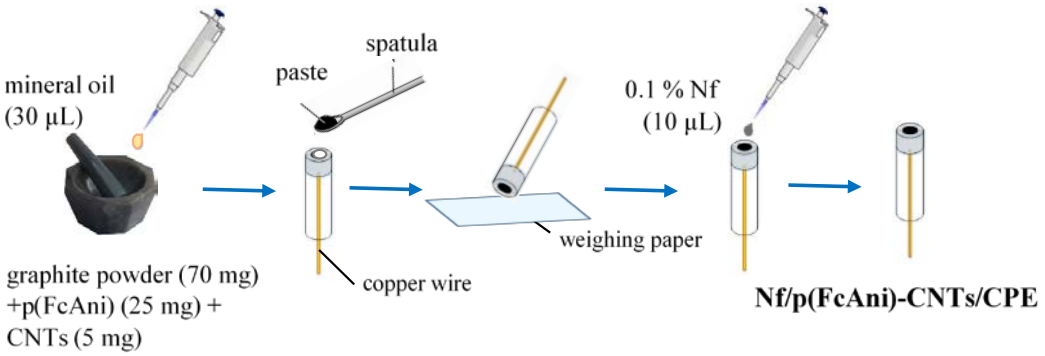


**Figure 3.3 Modification for preparation of the developed Nf/p(FcAni)-CNTs/ CPE**

3.3.1.9 Dopamine hydrochloride solutions and urine samples

The samples for DA determination were hydrochloride solutions (250 mg DA per 10 mL solution) for intravenous infusion, obtained from a local drug store. Urine samples used for UA determination were collected from volunteer students in the lab. All samples were centrifuged, and the supernatants were filtered through a 0.45 µm filters prior to analysis.

### 3.3.2 Preparation of biosensor for sulfite detection

3.3.2.1 0.1 M sulfite solution

Solution of 0.1 M sulfite solution was prepared by dissolving 0.1260±0.0005 g of $Na_2SO_3$ in 0.1 M phosphate buffer pH 7.0 and diluted to 10 mL in volumetric flask with the buffer.

3.3.2.2 0.1 M phosphate buffer (PBS) pH 7.0

0.1 M PBS pH 7.0 was prepared by mixing 58.7 mL of 0.1 M $Na_2HPO_4$ and 41.3 mL of 0.1 M $NaH_2PO_4$.

3.3.2.3 40 mg $mL^{-1}$ Cytochrome c (Cyt c)

Solution of 40 mg $mL^{-1}$ Cyt c was prepared by dissolving 40 mg Cyt c in 1 mL of 0.05 M PBS (pH 7.0).

3.3.2.4 0.1 mg $mL^{-1}$ sulfite oxidase (SOx) enzyme

0.1 mg $mL^{-1}$ SOx enzyme was prepared by diluting 100 µL of 1 mg of 900 µL of 3.2 M of ammonium sulfate ($(NH_4)_2$ $SO_4$) of pH 7.5.

3.3.2.5 Magnetite nanoparticles ($Fe_3O_4$)

$Fe_3O_4$ nanoparticles were prepared by co-precipitation, following a method described by Karamipour, Sh. et al. [62] and Kouassi, KG. et al. [68]. Briefly, 4.83 g of $Fe(NO_3)_3 \cdot 9H_2O$ and 2.78 g of $FeSO_4 \cdot 7H_2O$ were dispersed in 60 mL of 0.2 M HCl. The mixed solution of ferrous and ferric salts was then added dropwise into 100 mL of 1 M NaOH solution with vigorous stirring at 70 °C under $N_2$ atmosphere. The solution was then heated for a further 2 h. The formed black $Fe_3O_4$ precipitates were collected by an external magnetic field, washed with DI water three times by magnetic decantation, and then dried in a desiccator.

3.3.2.6 Fe3O4@Au nanoparticles

$Fe_3O_4$@Au nanoparticles were prepared following literature methods [62, 69], with some modifications. First, 30 mg of $Fe_3O_4$ nanoparticles were dispersed in 10 mL of water in an ultrasonic bath for 30 min. The dispersion was added into a 250 mL round-bottomed flask containing 40 mL of distilled water, and 20 mL of 0.1% $HAuCl_4$ was added while stirring. The reaction was brought to boil under reflux. Upon boiling, 4 mL of 1 wt% tri-sodium citrate was rapidly added to the stirred solution. In this process, $Au^{3+}$ was reduced to Au° on the surface of $Fe_3O_4$ using tri-sodium citrate. The solution color changed from brown to reddish-brown and the stirred mixture was kept at reflux for a further 15 min. The red-brown $Fe_3O_4$@Au nanoparticles were separated using an external magnetic field, washed with DI water three times by magnetic decantation, and then dried in a desiccator.

3.3.2.7 $Fe_3O_4$@Au-Cys-FA nanocomposites

$Fe_3O_4$@Au-Cys-FA nanocomposites was synthesized using L-cysteine (Cys) as a bi-functional linker. The L-cysteine thiol (-SH) group links to the gold surface, and the amino ($-NH_2$) group condenses with the folic acid (FA) carboxylic acid group (–COOH) to form an amide bond [62]. Briefly, the red-brown $Fe_3O_4$@Au solution was adjusted to pH 10 using a 1% aqueous ammonia solution. Then, 5 mL of 1 mM L-cysteine was added to the $Fe_3O_4$@Au solution and the mixture was stirred for 24 h at room temperature. During this phase, the thiol group on L-cysteine displaces the citrate moiety responsible for solvation of the nanoparticles. The obtained $Fe_3O_4$@Au-Cys nanoparticles were separated using an external magnetic field, washed three times with DI water by magnetic decantation, and then dried in a

desiccator. Next, 50 mg of $Fe_3O_4$@Au-Cys was dispersed in 10 mL of $CH_2Cl_2$. 0.1 g of folic acid (FA) was dissolved in 10 mL of DMSO, and 0.06 g of N, N′ dicyclohexylcarbodiimide ( DCC) was added to the solution. The $Fe_3O_4$@Au-Cys dispersion and FA-DMSO solution were mixed together in an ultrasonic bath for 30 min, and the solution then stirred at room temperature for 24 h. The obtained $Fe_3O_4$@Au-Cys-FA nanoparticles were separated using an external magnetic field, then washed three times with $CH_2Cl_2$, deionized water, and ethanol. After drying in a desiccator, $Fe_3O_4$@Au-Cys-FA nanocomposites were obtained as a red-brown powder. Figure 3.4 illustrates the schematic diagram of preparation step of $Fe_3O_4$@Au-Cys-FA nanocomposites.

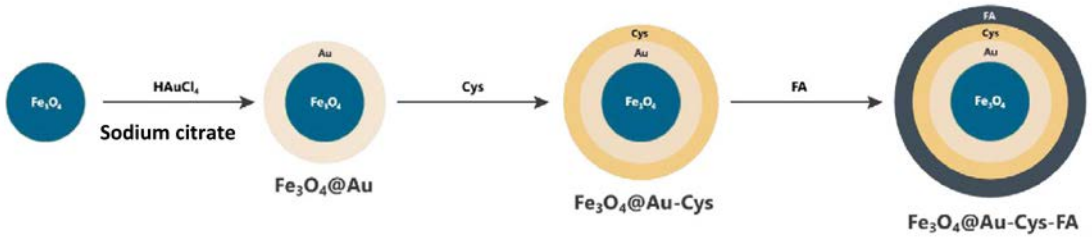


**Figure 3.4 Schematic diagram of preparation step of $Fe_3O_4$@Au-Cys-FA nanocomposites**

3.3.2.8 Electrode preparation of the $Fe_3O_4$@Au-Cys-FA/CPE

The $Fe_3O_4$@Au-Cys-FA/CPE was prepared by thoroughly mixing 0.950 g of graphite powder, 0.035 g of $Fe_3O_4$@Au-Cys-FA nanoparticles, and 0.015 g of PDMS to a homogenous using a mortar and pestle. The composite material was then heated to 60 °C for 30 min. Then, SOx enzyme was immobilized by dropping 40 µL of 0.1 mg $mL^{-1}$ SOx solution containing 40 mg $mL^{-1}$ Cyt c to 0.1 g of the composite. Cyt c was using as mediator between SOx and the electrode to enhance electron transfer. Finally, 30 µL of mineral oil was then added and thoroughly mixed. For batch system, this composite paste was packed into a hole of cylindrical glass tube by pressing the open end of the tube into the paste composite to a depth of approximately 2 mm. For FIA system, this composite was packed in the Teflon block as shown in Figure 3.5b. Then, the surface of the $Fe_3O_4$@Au-Cys-FA was manually

polished using weighing paper until a flat and smooth surface was obtained. The preparation of the sulfite biosensor is illustrated in Figure 3.5a.

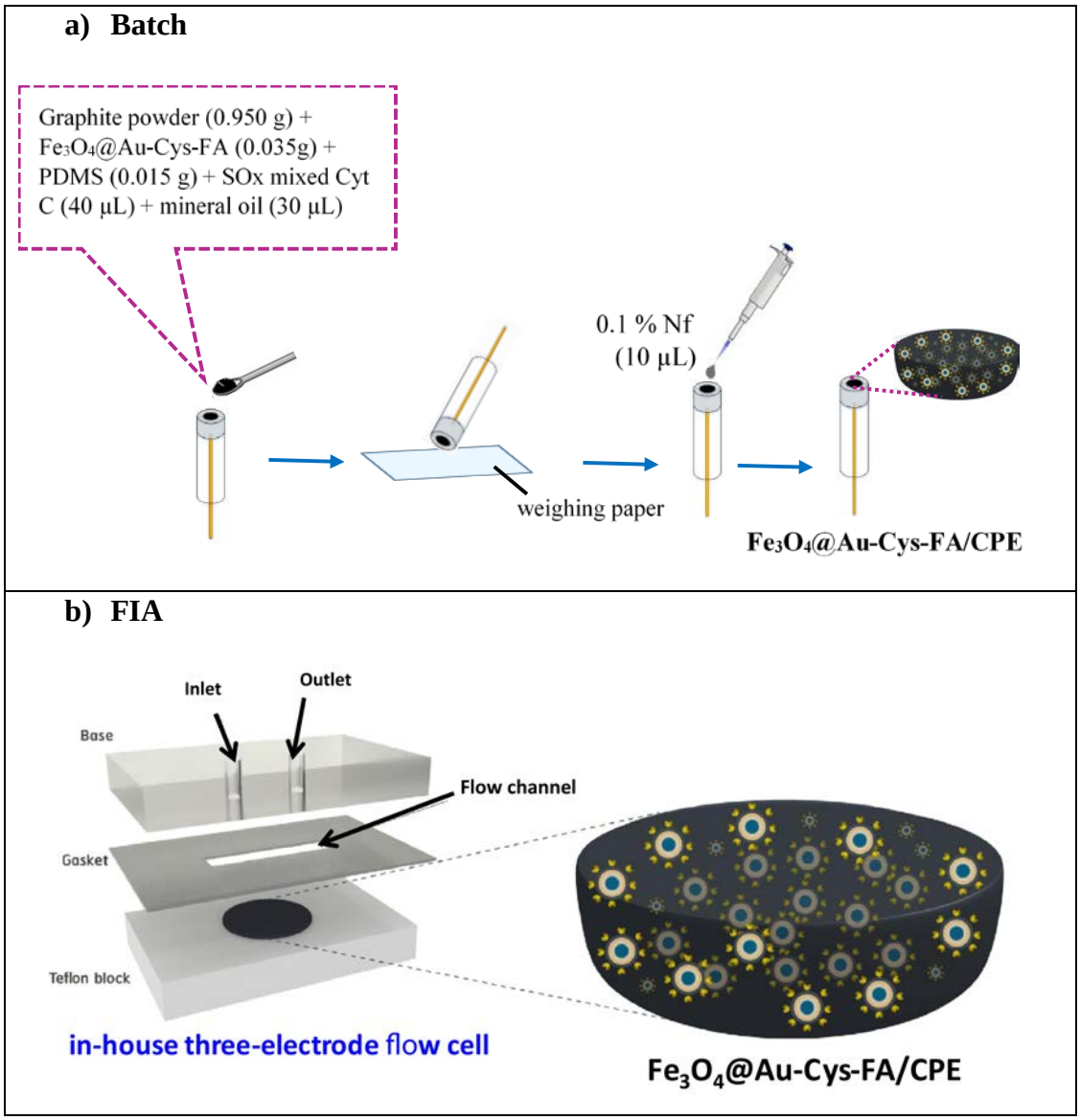


**Figure 3.5 Preparation of $Fe_3O_4$@Au-Cys-FA modified carbon-paste electrode a) batch and b) FIA system**

3.3.2.9 Samples for sulfite determination

Various brands of wines and pickled food samples, including mango, cabbage, and ginger were used for sulfite assay which were purchased from local supermarkets in Ubon Ratchathani province, Thailand. Wine samples were filtered through a 0.25-micron cellulose membrane. For pickled food samples, we used an extraction scheme described by Alamo, LST et al. [70]. Briefly, samples were weighed in 50 g aliquots, and homogenized in 50 mL of phosphate buffer using a blender. The homogenized mixture was collected and filtered through a 0.25-micron cellulose membrane. Sample aliquots were diluted 3 or 6 fold with phosphate buffer prior to analysis. Sulfite content was quantified by the standard addition method.

## 3.4 MIP modified QCM sensor for pesticides detection.

### 3.4.1 Preparation of MIP-QCM sensor

3.4.1.1 1 mM carbofuran (CBF)

2.2000±0.0005 mg of CBF was dissolved and diluted with DI water to 10 mL volumetric flask.

3.4.1.2 1 mM profenofos (PFF)

1 mM PFF solution was prepared by dissolving 3.7000±0.0005 mg and diluted to mark in 10 mL volumetric flask with the DI.

3.4.1.3 1 mM chlopyrifos (CPF)

3.5000 ±0.0005 mg of CPF was dissolved and diluted with deionized water to 10 mL volumetric flask.

3.4.1.4 CBF-MIP

CBF-MIP was prepared in bulk solution method. In the pre-polymerization process, 15 µL of MAA, a functional monomer was dissolved in 600 µL of DMSO in Eppendorf tube and then 25 µL of EGDMA, 2.4 mg of AIBN and 22.2 mg of CBF were added into the tube as a cross-linker, an initiator and a template. The mixture solution was sonicated for 10 min and purged with argon gas before being sealed with a parafilm. Then, the mixture solution was continuously stirred in water bath at 70 °C until the gel point was reached. This solution was coated on the surface of gold QCM electrode. The NIP was prepared in the same way but without addition of CBF.

3.4.1.5 PFF-MIP

PFF-MIP were prepared following a method described by Findeisen, A et al. [64]. 59 mg of PVP, 41 mg of DPDI, 8 mg of PG, 10 mg of DPM and 37.4 mg of profenofos were dissolved in 600 µL of THF in Eppendorf tube and sonicated for 10 min. The mixture solution was pre-polymerized by stirring in water bath at 75 °C for 3 h. Then, the 500 µL of THF was immediately added in pre-polymer solution. Before spin coating, the pre-polymerization was diluted again with THF (1:1). The NIP was synthesized by using the same procedure but without the PFF template. The schematic diagram of synthesis of MIP shows in Figure 3.6.

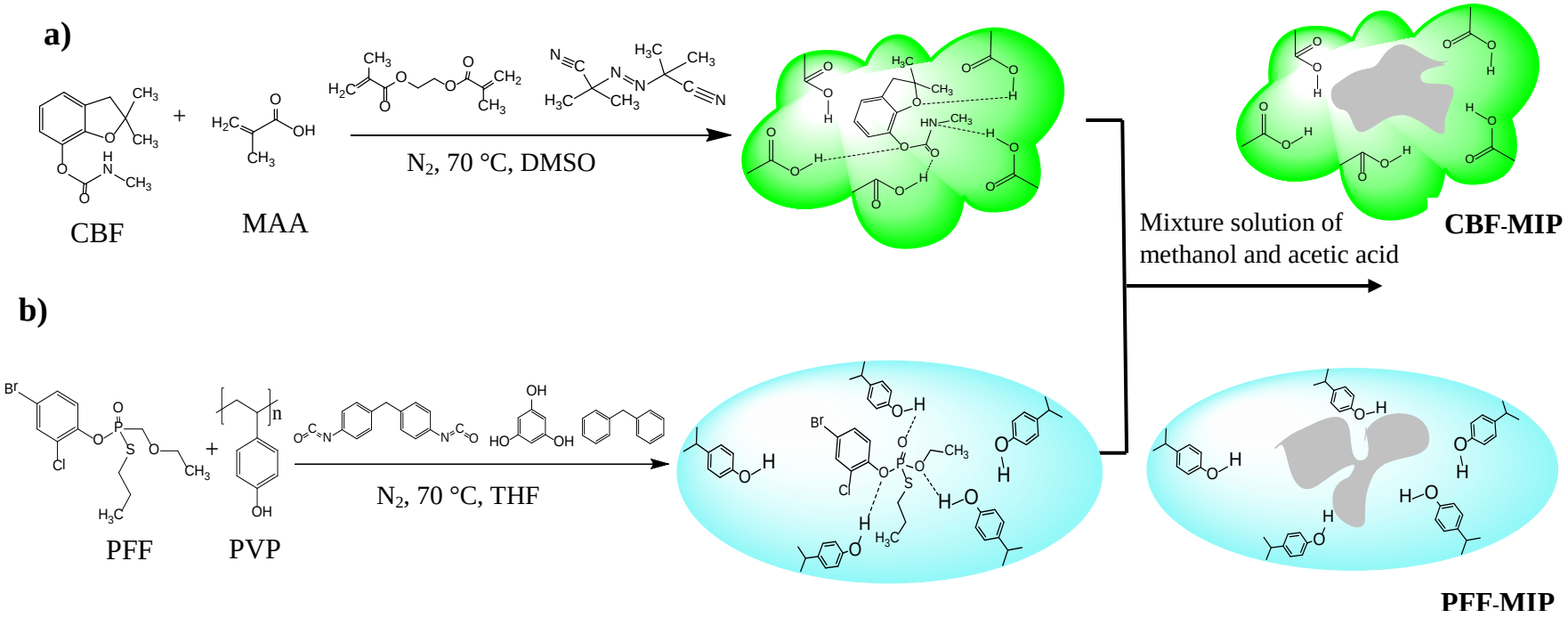


**Figure 3.6 Synthesis approach of a) CBF-MIP and b) PFF-MIP**

3.4.1.6 QCM manufacturing

Electrodes for QCM measurement were screen printed with Brilliant gold paste onto the respective quartz substrate by dual channel geometry. Screen printed QCM were kept at 400 °C for 4 h to remove organic residues. The coated Au electrode is shown in Figure 3.7.

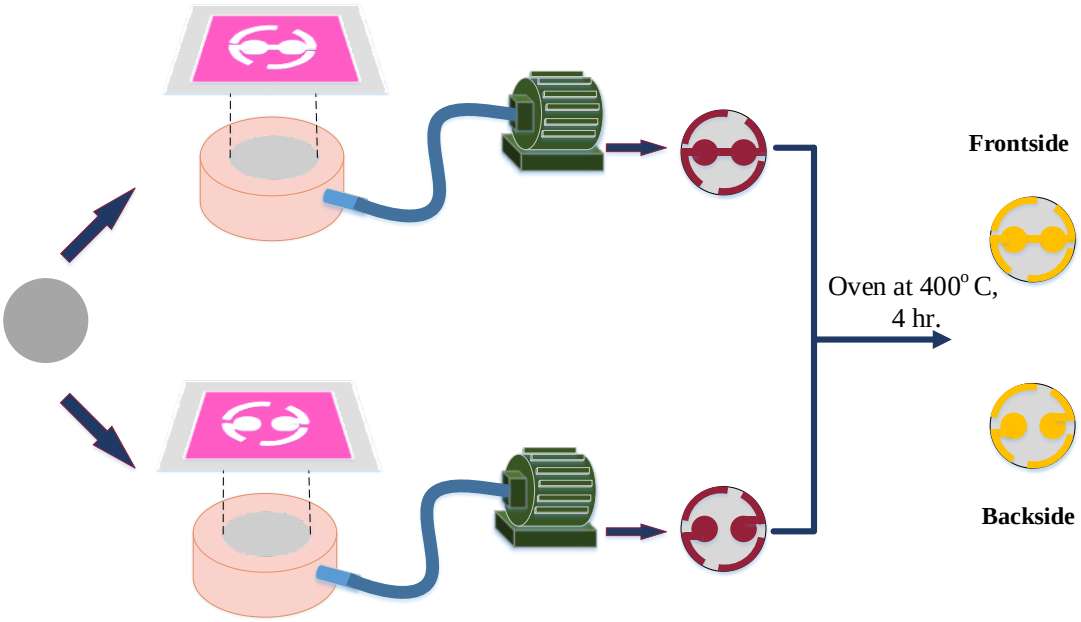


**Figure 3.7 Screen printing step of dual gold quartz crystal microbalance**

3.4.1.7 Screening of CBF-MIP-QCM

4 µL of the obtained MIP-CBF gel solution was dropped onto the surface of gold electrode and then the electrode was spin off at 2,000 rpm for 30 sec. Then, the NIP solution was dropped onto another surface of gold electrode. Finally, the polymerization of QCM with MIP and NIP electrodes was achieved by exposing the electrode under 312 nm UV light for overnight. The CBF were removed from electrode by immersing into using a mixture solution of methanol and acetic acid (9:1 %v/v) and DI water for 30 min, respectively.

3.4.1.8 Screening of PFF-MIP-QCM

The 4 µL of PFF-MIP gel solution was spin-coated onto single side of a QCM electrode at 3,000 rpm for 1 min. PFF-NIP (section 3.3.3) solution was spin-coated onto the another sides. The coated electrode was stored at room temperature overnight and afterwards 10 min in drying oven at 120 °C to achieve complete polymerization. Finally, QCM electrode was immersed into the mixture solution of methanol and acetic acid (9:1 %v/v) to remove PFF and DI water for 30 min, respectively.

## 3.5 Signal measurement

### 3.5.1 Electrochemical measurement

3.5.1.1 Voltammetry

Cyclic voltammetry (CV) and differential pulse voltammetry (DPV) were performed in Voltammetry. The both technique were made on an eDAQ potentiostat (model EA 161) equipped with e-Corder (model 210) interfaced to a computer. The CV measurements was carried out between 0 V and + 1.0 V with the scan rate at 50 mV $s^{-1}$. DPV measurements was performed by from − 0.3 V to + 0.8 V with pulse amplitude of 25 mV and pulse width of 0.05 s, and scan rate of 10 mV $s^{-1}$. A conventional three electrodes system including working electrode, a reference electrode and a counter electrode was employed. Working electrode was CPE modified electrode. Counter electrode was a stainless steel wire and reference electrode was Ag/AgCl. The equipment set up system is shown in Figure 3.8.

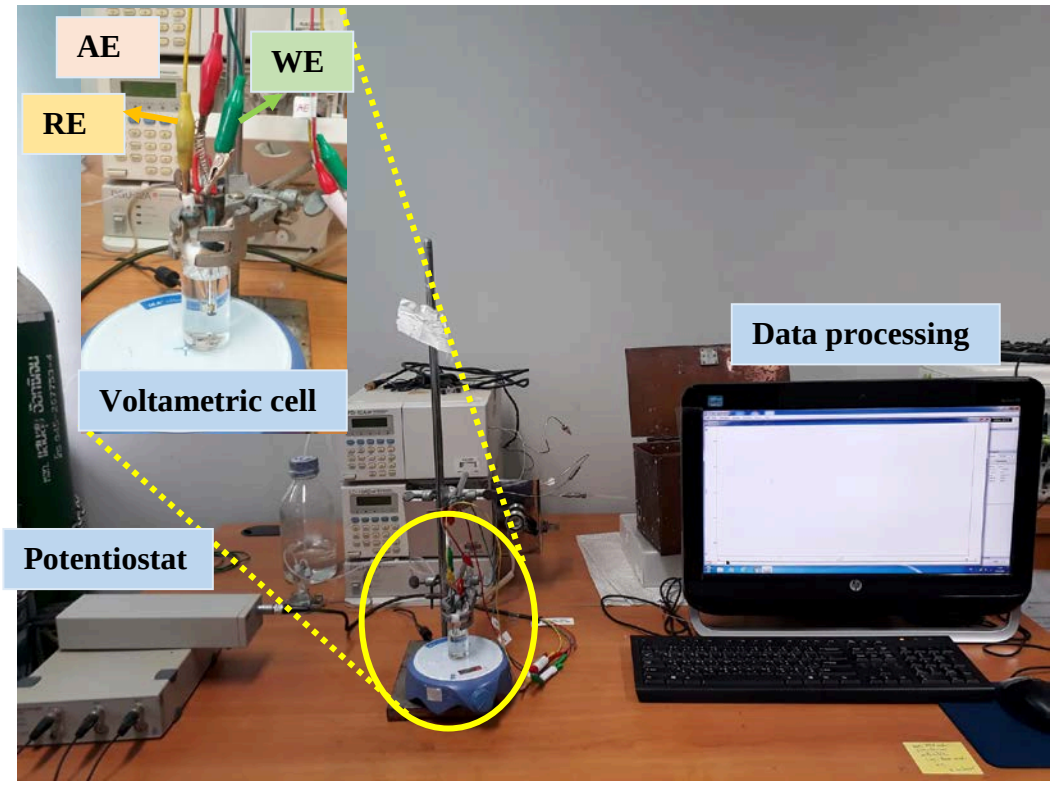


**Figure 3.8 The set up for CV and DPV measurements; potentiostat (e-DAQ) voltammetric cell; (vial 25 mL); working electrode (CPE or modified CPE); reference electrode (Ag/AgCl); auxiliary electrode (stainless steel)**

3.5.1.2 Amperometry based flow injection analysis (FIA) system

The flow injection system used for the amperometric measurements, was comprised of a pump (model LC-10AD), injection valve equipped with 100 µL injection loop. In this study, amperometry was carry out for sulfite determination. Figure 3.9 shows set up of the system used for amperometric detection in flow system.

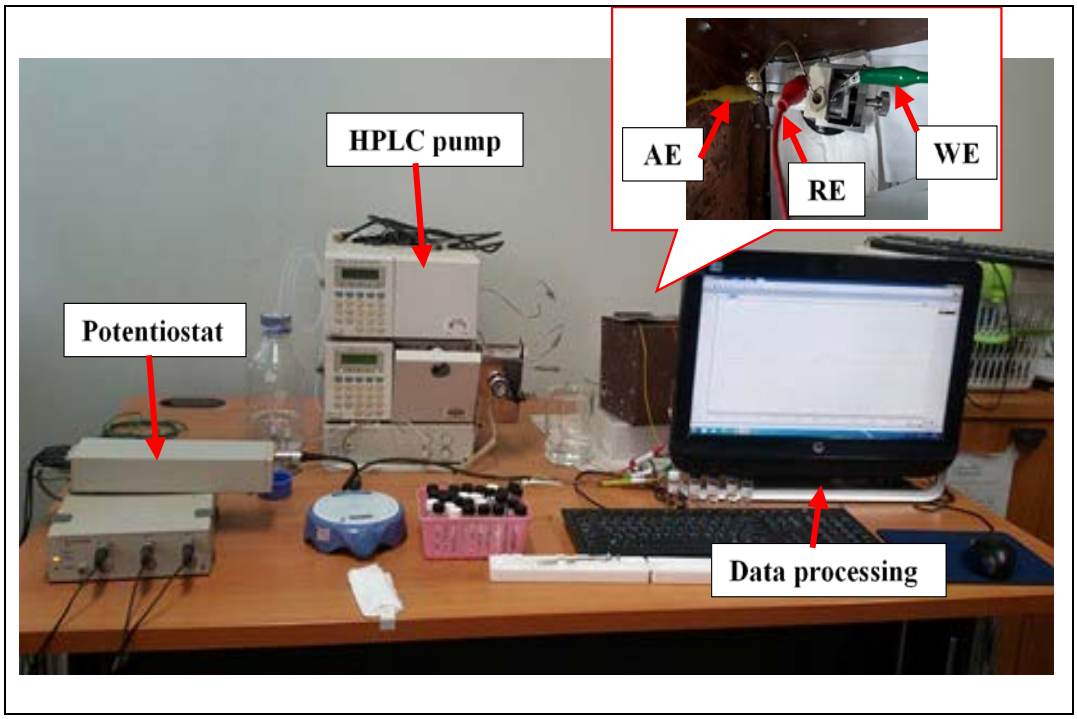


**Figure 3.9 Electrochemical equipment set up for amperometric detection in flow system was used in this work using an e-DAQ potentiostat, Injection valve was equipped with 20 µL loop. Thin layer flow cell is the three electrode type, WE: working electrode, AE: stainless steel tube and RE: Ag/AgCl electrode**.

### 3.5.2 Quartz crystal microbalance (QCM) measurements

QCM measurement were performed by a custom-made cell design and inner case PDMS holding with a dual-channel 10 MHz QCM containing both MIP and NIP. This QCM experiments were conducted at the University of Vienna under the supervision of Prof. Peter Liberzeit. The QCM was connected to an oscillating circuit monitored by means of an Agilent HP5313A frequency counter. The data was read out through Agilent GPIB bus adapter and processed by a custom-made LabView routine. The water was used as a blank solution in all mass sensitive measurements. Figure 3.10 shows the setup of the system used for QCM measurement.

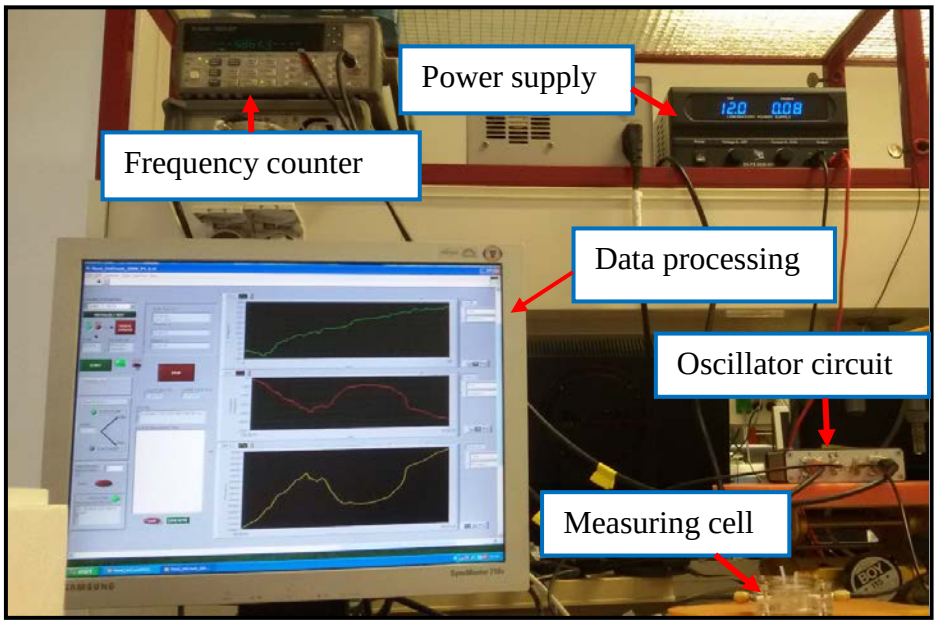


**Figure 3.10 Instrument set up for frequency measurement**

## 3.6 Procedure

### 3.6.1 Characterization of the nanocomposites

3.6.1.1 Scanning electron microscope (SEM)

SEM is widely used for morphological analysis of nanostructured materials. The SEM model: JEOL, JSM-5910 was used to study morphology of the composite material modified electrode for the chemical sensor and biosensor. The SEM sample were prepared by dispersing the nanocomposites in DI water with ultrasonicated for 1 h and then dropped on glass slide. The samples were attached on SEM stubs before investigated by SEM. The results of morphology of p(FcAni) and Nf/p(FcAni)-CNTs/CPE are presented in Section 4.1.1. The results of morphology of the $Fe_3O_4$, $Fe_3O_4$@Au and $Fe_3O_4$@Au-Cys-FA nanoparticles are presented in Section 4.1.2.

3.6.1.2 Transmission electron microscopy (TEM)

TEM imaging was performed on a JEM-1230 TEM. $Fe_3O_4$, and $Fe_3O_4$@Au were prepared for TEM measurement by dispersion the nanocomposites in DI water. The dispersions were dropped cast onto holey carbon TEM grids and dried in the room temperature prior to TEM analysis. Results are discussed in Section 4.1.3.

3.6.1.3 Energy Dispersive X-ray Spectrometer (EDS)

EDS is an analytical technique used for the elemental analysis of a sample. The formation of $Fe_3O_4$@Au-Cys-FA was confirmed with EDS model INCA x-sight. The EDS spectrum are discussed in Section 4.1.4.

3.6.1.4 Atomic force microscopy (AFM)

The surface morphology of the composite material modified electrode ($Fe_3O_4$, $Fe_3O_4$@Au and $Fe_3O_4$@Au-Cys-FA) surface was studied by using AFM model XE-100. Results are discussed in Section 4.1.5.

3.6.1.5 Fourier transform infrared spectroscopy (FT-IR)

FT-IR is an important technique in the functional groups identification in molecules. The spectra were recorded using FT-IR spectrometry (Perkin-Elmer, model: Spectrum 100). The MIP before and after remove template, and NIP were prepared as KBr pellets for FT-IR measurements. The range of measurement was set between 500 to 4000 $cm^{-1}$. Results are discussed in Section 4.1.6.

**Part I: Fabrication of new electrochemical sensors using nanomaterials modified carbon-paste electrodes**

### 3.6.2 Chemical sensor for DA and UA detection

3.6.2.1 Electrochemical characterization of the modified CPE

The electrochemical characterization of the modified CPE (a) Nf/CPE, b) Nf/p(FcAni)/CPE and c) Nf/p(FcAni)-CNTs/CPE) were was further characterized through the CV in 0.1 M PBS (pH 7.0) at a scan rate of 10 mV $s^{-1}$. The results were discussed in Section 4.2.1.

3.6.2.2 Electrocatalytic behaviors of DA, UA, and AA at Nf/p(FcAni)-CNTs/CPE.

The electrochemical behaviors at Nf/p(FcAni)-CNTs/CPE toward DA, UA, and AA were performed by DPV in a PBS (pH 7.0) in a solution with and without DA, UA, and AA at the same concentration (1 mM). The results were illustrated in Section 4.2.2.

3.6.2.3 Effect of buffer pH (0.1 M PBS)

The effect of buffer pH on electrocatalytic oxidation and on the shapes of 0.05 mM DA and 0.1 mM UA waves were investigated over the pH range 4-8 using 0.1 M PBS as supporting electrolyte. The DPV plots were recorded using electrolyte solution of varying pH. The results are presented in Section 4.2.3.

3.6.2.4 Analytical features

1) Linear concentration range

Calibration curve of DA and UA in the presence AA were studied by DPV. The standard DA and UA were spiked onto the 0.1 M PBS pH 5 in the presence AA. DPV were recorded using an applied potential from 0.3 – 0.9 V at scan rate of 10 mV $s^{-1}$. The results are discussed in Section 4.2.4.1.

2) Limit of detection (LOD)

The LOD was calculated from analyte at concentration of 1 and 5 µM for DA and UA, respectively. The signal value of 3-fold signal-to noise (3S/N) was converted to the concentration to give the LOD. Results were presented in Section 4.2.4.2.

3.6.2.5 Interference study

In this study, the effect of foreign ions including glucose, KCl, urea, $CaCl_2$ and $NaNO_3$ which are likely to exist in the sample was investigated. Interfering species were added to the test solution in the range of 10-100 times greater concentration than that of DA and UA. The concentration of the foreign species that provide signal change greater than ±5% was consider as the tolerance limit. Results were discussed in Section 4.2.5.

3.6.2.6 Reproducibility and stability study

The reproducibility and stability of the Nf/p(FcAni)-CNTs/CPE were investigated by DPV. The reproducibility was investigated from the oxidation current of 50 µM of DA and 100 µM of UA in the presence of 1 mM of AA with 0.1 M PBS (pH 5.0) for 15 times. The Nf/p(FcAni)-CNTs/CPE electrode was stored in vial over a 0.1 M PBS (pH 7.0) when not use. The oxidation current of 50 µM of DA and 100 µM of UA in the presence of 1 mM of AA were measured at a Nf/p(FcAni)-CNTs/CPE electrode when stored for 0 to 7 days. The results are discussed in Section 4.2.6.

3.6.2.7 Real samples analysis

All samples were diluted with buffer solution (pH 5.0) prior to analysis. Determinations were performed by the standard addition method. Results are presented in Section 4.2.7.

### 3.6.3 Biosensor for sulfite detection

3.6.3.1 Cyclic voltammetric study of nanomaterials-modified electrode

The electrocatalytic behavior of $Fe_3O_4$@Au/CPE, $Fe_3O_4$@Au-Cys/CPE and $Fe_3O_4$@Au-Cys-FA/CPE were investigated using CV in 0.1 M PBS (pH 7.0). Then, the $Fe_3O_4$@Au-Cys-FA/CPE was measured by CV in 0.1 M PBS (pH 7.0) with various sulfite concentration. The results discussed in Section 4.3.1.

3.6.3.2 Hydrogen peroxide ($H_2O_2$) detection

The unique electrochemical behavior of $H_2O_2$ was studied at different modified electrode materials. The cyclic voltammograms at the bare CPE, $Fe_3O_4$/CPE, $Fe_3O_4$@Au/CPE and $Fe_3O_4$@Au-Cys-FA/CPE without immobilized SOx enzyme were measured using cyclic voltammetry in the absence and presence of $H_2O_2$. The results are discussed in Section 4.3.2.

3.6.3.3 Effect of 0.1 M buffer pHs

The effect of 0.1 M buffer pH as supporting electrolyte on electrocatalytic oxidation of sulfite was investigated over the range 5-9. The response current was recorded using electrolyte solution of varying pH. The results are presented in Section 4.3.3.

3.6.3.4 The apparent Michaelis-Menten constant ($K_m^{app}$)

The apparent Michaelis–Menten constant ($K_m^{app}$), can be calculated by the Lineweaver–Burk equation follow by equation 3.1.

$$\frac{1}{I_{ss}} = \frac{1}{I_{\max}} + \frac{K_m^{app}}{I_{\max} c} \tag{3.1}$$

Where c is a substrate concentration in a bulk solution, $I_{ss}$ the steady-state current after the addition of substrate and Imax is the maximum current measured under saturated substrate conditions. The Michaelis–Menten equation is used to determine the kinetic properties of isolated enzymes. It is also used in

modeling the dynamics of enzyme systems and displayed oscillatory behavior. If low oscillatory reactions were shown the many biochemical processes catalyzed by enzymes. $K_m^{app}$ was studied in the range 0.5–10 mg $L^{-1}$ using CV in phosphate buffer pH 7.0. The results are presented in Section 4.3.4.

3.6.3.5 Scan rate dependence study

The cyclic voltammograms of sulfite on the sulfite biosensor were examined in 0.1 M PBS (pH 7.0) using various scan rate. The peak currents of sulfites oxidation at various scan rates (0.01, 0.02, 0.03, 0.05, 0.06, 0.10, 0.20 and 0.40 V $s^{-1}$) were investigated. The results are discussed in Section 4.3.5.

3.6.3.6 Stability study

The stability of the $Fe_3O_4$@Au-Cys-FA/CPE biosensor for detection of sulfite oxidation was studied. The $Fe_3O_4$@Au-Cys-FA/CPE electrode was stored in vial over a 0.1 M phosphate buffer (pH 7.0) and kept at 4 °C when not use. The sulfite oxidation currents were measured at a $Fe_3O_4$@Au-Cys-FA/CPE electrode when stored for 0, 1, 2, 3, 4, 5, 7, and 14 days. Results are presented in Section 4.3.6.

3.6.3.7 Amperometric determination of sulfite in the developed FIA system

1) Effect of PDMS

The effect of PDMS was studied by 10 mg $L^{-1}$ of sulfite injected into the FIA system using electrode with and without PDMS. The results are discussed in Section 4.3.7.1.

2) Optimum potential for amperometric detection

The influence of potential for amperometric detection was studied in the range -0.1 -1 V. The peaks area was plotted versus at various potential. Results are discussed in Section 4.3.7.2.

3) Optimum flow rate

Optimization of flow rate for sulfite detection was evaluated by injections of 100 µL of 10 mg $L^{-1}$ sulfite at the flow rate between 0.5 to 1.8 mL $min^{-1}$. The peak current and sample throughput versus different values of flow rate was plotted. Results are presented in Section 4.3.7.3.

4) Analytical features

4.1) Linear concentration range

Standard calibration of sulfite was prepared by diluting the appropriate amount in 0.1 M phosphate buffer pH 7.0 to give working solution. 100 µL of each standard was injected into the FIA system using flow rate of 0.8 mL $min^{-1}$ and 0.1 M phosphate buffer pH 7.0 as a carrier solution. Amperometric responses were recorded using the applied potential of +0.35 V. Results are shown in Section 4.3.7.4, 1).

4.2) Limit of detection (LOD) and limit of quantification (LOQ)

In this study, the LOD and LOQ were calculated by injecting 0.1 mg $L^{-1}$ of standard sulfite solution (n=7). The signal value of 3 times standard deviation (3SD) and 10 times standard deviation (10SD) was calculated for LOD and LOQ, respectively. Results are presented in Section 4.3.7.4, 2).

5) Interference study

In this study, the effect of foreign ions, including compounds that are likely to exist in wine and food samples were investigated. The concentration of the foreign species that provide signal change greater than 5% was considered as the tolerance limit. The foreign ions used in this study were sugar (glucose, fructose, sucrose, maltose), ions ($NaNO_3$, $NaCH_3COO$, KI, NaCl, KI and $Na_2SO_4$) and others (ascorbic acid, ethanol). The results are discussed in Section 4.3.6.5.

6) Method validation

The developed method was applied with wine and food samples. The sulfite concentration between developed method and Standard method (Iodometric method) was compared. The results are discussed in Section 4.3.7.6.

6.1) Standard method (Iodometric method)

The iodometric titration of sulfite was performed according to the official method. A back titration mode was used to avoid sulfite loss in the form of $SO_2$ in acidic environment. 5 mL of standard 0.20 mM of potassium iodate ($KIO_3$) was added in the 250.0 mL of conical flask followed by 2.5 mL of 3 M sulfuric acid ($H_2SO_4$). Then 2.5 mL 0.15 M of potassium iodide (KI) was pipetted into the conical flask and 5.0 mL of sample was added. After that, this mixture solution was immediately titrated with 2.50 mM of sodium thiosulfate ($Na_2S_2O_3$) to a light

yellow color. Then 0.5 mL of starch indicator was added and continued the titration until the iodine-starch complex become colorless.

**Part II: MIP modified QCM sensor for pesticides detection**.

### 3.6.4 MIP-QCM sensor

#### 3.6.4.1 Measurement of binding interaction of MIP-QCM sensor

A typical measurement comprised of several steps: first, 200 μL of DI water was injected into the measuring cell to obtain baseline signal. Afterward, the cell was injected with 200 μL of standard CBF solutions for CBF detection or standard PFF solutions for PFF detection at various concentration (1000–10 μM). All measurements were carried out in stopped flow until the signal reached their equilibrium state. Afterward, the cell was washed with 5% mixture solution of methanol and acetic acid (9:1 v/v), followed by DI water. The obtained ΔF value was used to calculate the mass change (Δm) on the QCM electrode surface according to the Sauerbrey equation (1.5). The Equilibrium isotherms parameters and thermodynamic parameters were calculated using QCM signals from binding interaction term of molecularly imprinted QCM sensor. The results are discussed in Section 4.4.1.

#### 3.6.4.2 Specificity and selectivity of QCM sensor

The selectivity of the CBF-MIP film and PFF-MIP film were tested by measuring the signal responses of CBF, PFF and chlopyrifos (CPF) at the same concentration (1000 μM). After obtained ΔF, the imprinting and selecting factors are defined as α and β shown Equation 3.2 and Equation 3.3 [71].

$$\alpha = \frac{\Delta F_{MIP}}{\Delta F_{NIP}} \tag{3.2}$$

$$\beta = \frac{\alpha_{MIP}}{\alpha_{analog}} \tag{3.3}$$

Where the α is imprinting factor (IF) which is defined as the ratio of frequency shift obtained from MIP and NIP, and β is the selectivity coefficient

which was calculated from the ratio of imprinting factor obtained from analyte and analogue. Results is presented in Section 4.4.2.

3.6.4.3 Reproducibility

The reproducibility of CBF-MIP and PFF-MIP were investigated in 1000 µM of CBF and PFF solution for 3 times. Results is presented in Section 4.4.3.

# CHAPTER 4
# RESULTS AND DISCUSSION

## 4.1 Characterization of the nanocomposites

### 4.1.1 Scanning electron microscopy (SEM) of chemical sensor

The morphology of p(FcAni) and composites of Nf/p(FcAni)-CNTs paste was initially characterized with SEM. The SEM images were shown in Figure 4.1. The both morphology of p(FcAni) and Nf/p(FcAni)-CNTs paste composites ( Figure 4.1a and 4.1b, respectively) are spherical in shape. The surface morphology of the Nf/p(FcAni)-CNTs paste composites is smoother than the p(FcAni) composites. Clearly, the thin film is formed for the Nf coating over the Nf/p(FcAni)-CNTs paste surface. SEM images also reveal that the p(FcAni) particles were well dispersed on the electrode surface.

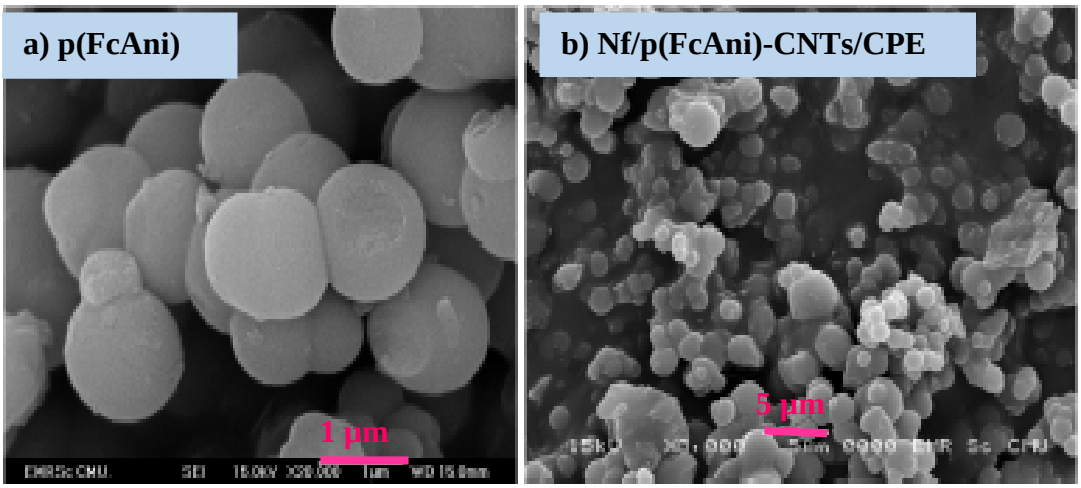


**Figure 4.1 SEM images of a) p(FcAni) and b) Nf/p(FcAni)-CNTs/CPE**

### 4.1.2 Scanning electron microscopy (SEM) of biosensor

SEM was used to observe the changes of the surface morphologies of modified $Fe_3O_4$ nanoparticles. To avoid the influence of extraneous gold during the process of sputter coating, the samples were tested directly without any conductive coating. The SEM results shown in Figure 4.2. As can be seen in Figure 4.2a that as-prepared $Fe_3O_4$ were rough surface morphology. The SEM images of $Fe_3O_4$@Au (Figure 4.2b) and $Fe_3O_4$@Au-Cys-FA (Figure 4.2c) were clearly shown that Au and Cys-FA were attached on the surface of magnetic core because the particle size of $Fe_3O_4$@Au and $Fe_3O_4$@Au-Cys-FA nanoparticles increased as compared with $Fe_3O_4$. Accordingly, it was concluded that the surface modification of $Fe_3O_4$ and $Fe_3O_4$@Au supports were successful. SEM images of $Fe_3O_4$ and $Fe_3O_4$@Au further suggests that the surface modification of $Fe_3O_4$ and $Fe_3O_4$@Au supports were successful.

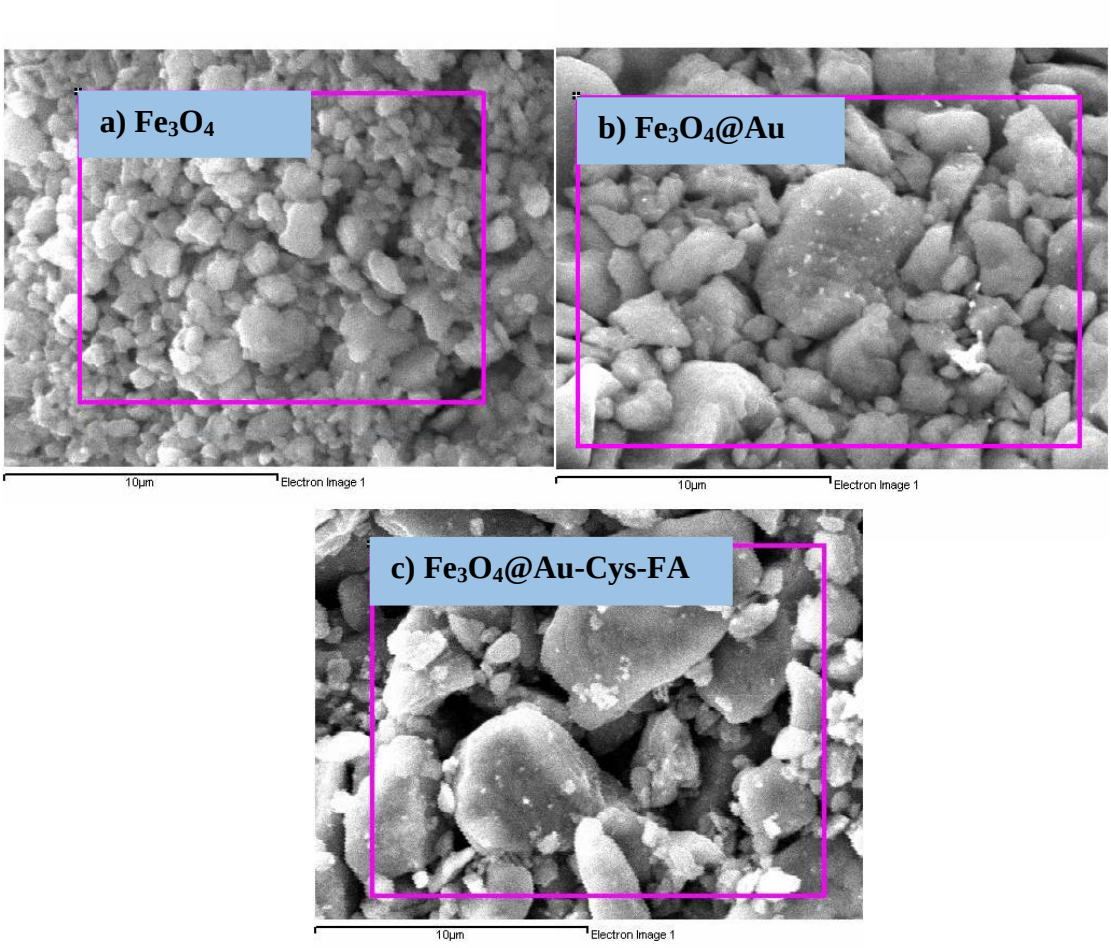


**Figure 4.2 SEM images of a) $Fe_3O_4$, b) $Fe_3O_4$@Au and c) $Fe_3O_4$@Au-Cys-FA**

### 4.1.3 Transmission electron microscopy (TEM)

The morphology of as-prepared $Fe_3O_4$ nanoparticles and $Fe_3O_4$@Au nano-composite was investigated using TEM. It could be seen in Figure 4.3 that $Fe_3O_4$ nanoparticles (Figure 4.3a) were of good spherical dots with very narrow size average diameter of 11.57±2.1 nm. After reduction of $Au^{3+}$ to $Au^0$ on the $Fe_3O_4$ nanoparticle surface, the diameters of this sphere became densely packed ( Figure 4.3b). The average $Fe_3O_4$@Au nanocomposite diameters are 14.17±3.3 nm. The figure shows that the nanocomposite materials aggregate when dried. This results accorded to the previous report [62]. The $Fe_3O_4$ core was well wrapped by the coating layer with the thickness of the coating shell from 2 to 3 nm.

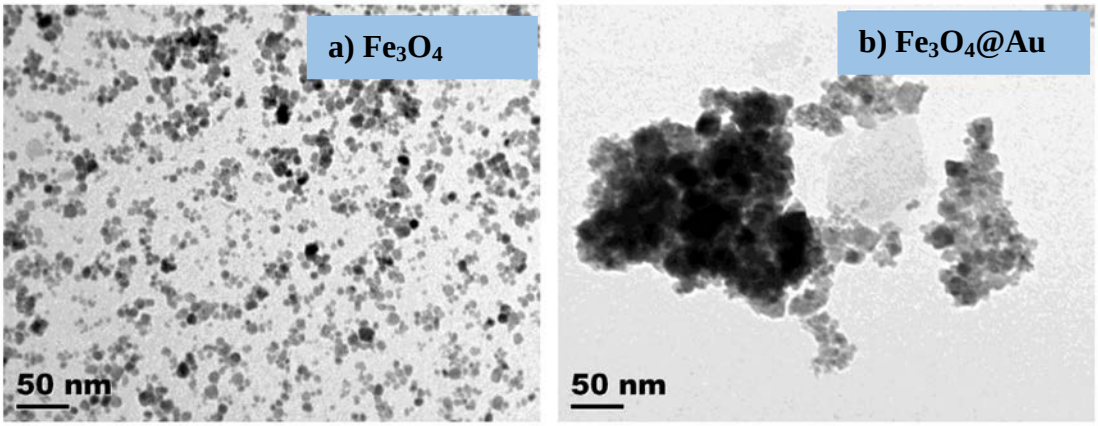


**Figure 4.3 TEM images of a) $Fe_3O_4$ and b) $Fe_3O_4$@Au**

### 4.1.4 Energy dispersion X-ray spectroscopy (EDS)

To further determine the composition of the samples, EDS was performed on an individual particle of $Fe_3O_4$@Au-Cys-FA. The EDS spectrum in Figure 4.4 indicates the presence of Fe, O, Au and S elements in the obtained nanocomposite, demonstrating that the formation of Au-S covalent bond between the shell and core and provides evidence for an attachment between $Fe_3O_4$@Au and folic acid via the thiol group on cysteine, confirming the formation of $Fe_3O_4$@Au-Cys-FA. This reason was similar to previous work reported by Karamipour, Sh et al [62]. These results clearly confirm a success in synthesized $Fe_3O_4$@Au–Cys-FA nano-composites.

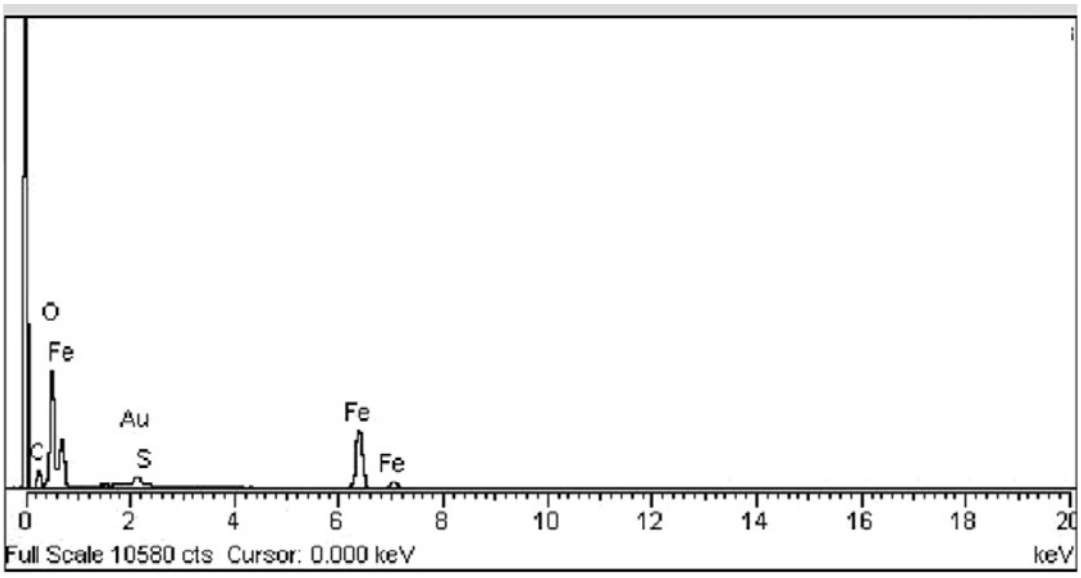


**Figure 4.4 The EDS spectrum of $Fe_3O_4$@Au-Cys-FA nanoparticles**

### 4.1.5 Atomic force microscopy (AFM)

AFM is one of the most widely used instruments for morphological study. Figure 4.5 shows the representative AFM images (5 µm x 5 µm scan size) of the composites used in the modified electrode. As shown in Figure 4.5a, the $Fe_3O_4$ shows an extremely smooth and flat surface featuring gently-domed nodes. As seen clearly, the AFM image for $Fe_3O_4$@Au is very similar to that of $Fe_3O_4$, but shows a rougher surface. We ascribe this to gold nanoparticles deposited on the $Fe_3O_4$ substrate, which accorded to the previous report [72]. $Fe_3O_4$@Au-Cys-FA shows the presence of many tiny particles on the surface; some of which were rough-like. The results show that the adsorption process involves van der walls forces, including hydrogen bonding and other electrostatic interactions, which arise from using cysteine as a linker between the gold shell and folic acid. This reason was similar to previous work reported by Jiang, QL et al [73].

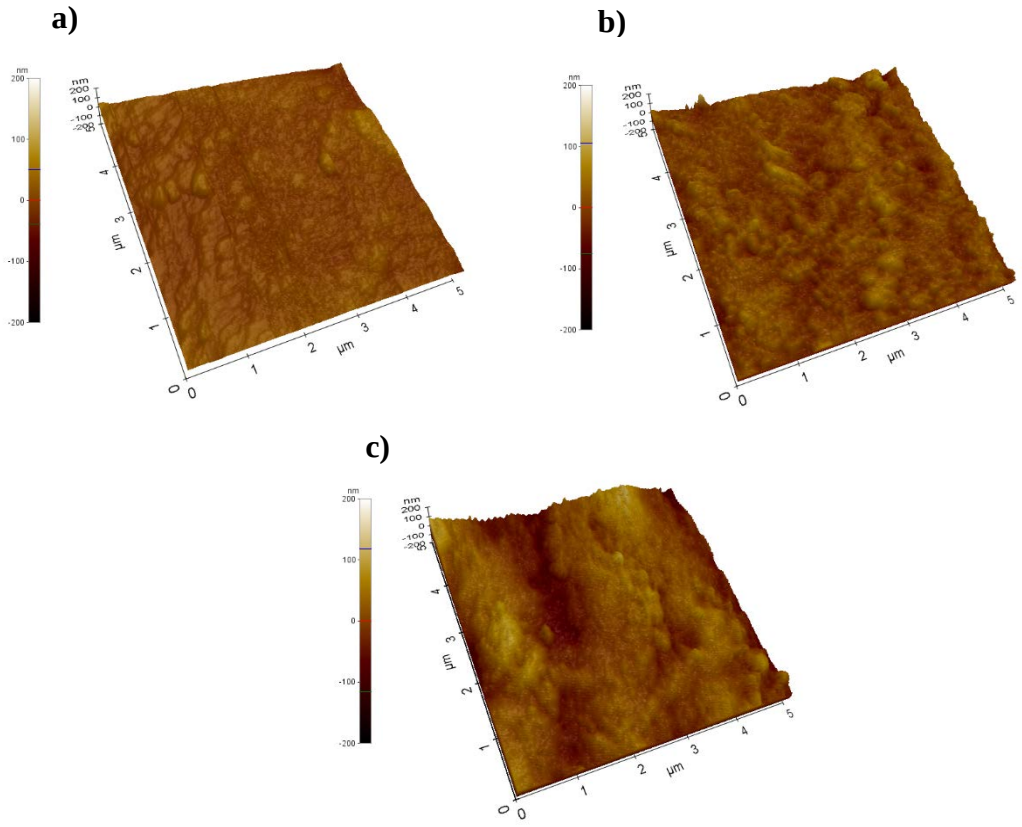


**Figure 4.5 AFM images of a) $Fe_3O_4$, b) $Fe_3O_4$@Au and c) $Fe_3O_4$@Au-Cys-FA**

### 4.1.6 Fourier transform infrared spectroscopy (FT-IR) of MIP and NIP

The FT-IR spectra were recorded to assess the formation of the synthesized materials. Figure 4.6a and Figure 4.6b are the FT-IR spectra concerning the process of the CBF-MIP and PFF-MIP synthesis, respectively. The CBF FT-IR spectra appears peaks at 1528 (C=C), 1374 (C-H), 1296 (C-O), 1236 (C-N) and 871 $cm^{-1}$ (C-H). The FT-IR spectra of CBF-MIP (Fig. 4.6a) before removal of the template show peak at 3355 $cm^{-1}$ which attributed to N-H stretching from CBF molecules that adsorb in the polymer layer synthesized from MAA. Whereas CBF-MIP after the template removal and NIP films did not show the signal peak of N-H while the both spectra show the band around 3425 $cm^{-1}$ of OH stretching. These results demonstrated the successful of CBF removal from the MIP, which accorded to the previous report [74-76]. These result also indicates the successful of CBF removal from the MIP.

The spectra obtained from PFF-MIP is shown in Figure 4.6b. The absorption bands of O-H from PVP at 3329 $cm^{-1}$ were observed for all spectra (MIP before, MIP after remove PFF and NIP). The PFF-MIP before remove the template presents the absorption bands which attributed to PFF molecule at 1464, 1150, 949, 682 and 628 $cm^{-1}$ for C-H, P=O, P-S, C-Cl, and C-Br respectively. The MIP after PFF removal and NIP did not show these adsorption band that contributed to PFF molecules. These result indicates the successful of PFF removal from the MIP and the formation of imprinted sites at the polymer layer. Which are accordance to the previous works [77,78]. In addition, these results also indicate the successful of PFF removal from the MIP and the formation of imprinted sites at the polymer layer.

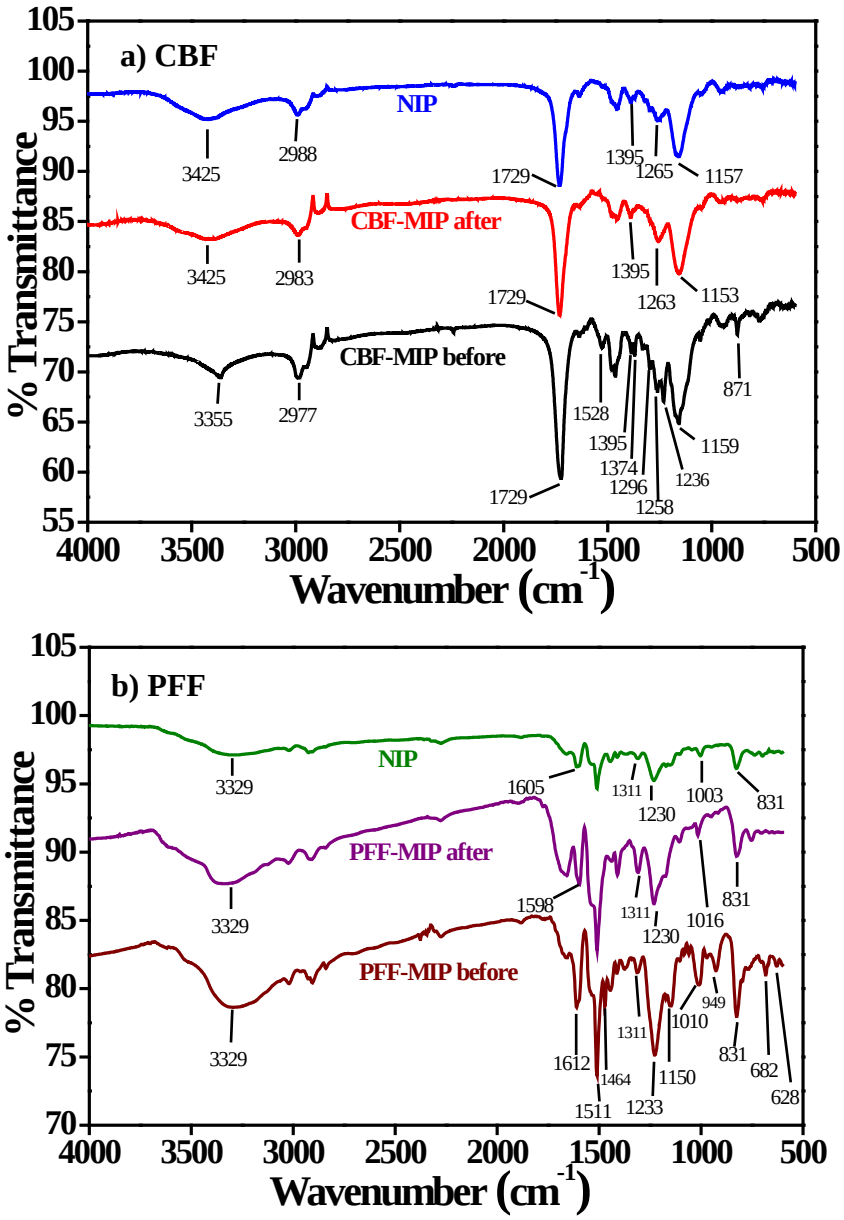


**Figure 4.6 FT-IR spectra of MIP before, MIP after remove template and NIP of a) CBF and b) PFF**

**Part I: Fabrication of new electrochemical sensors using nanomaterials modified carbon-paste electrodes**

## 4.2 Chemical sensor for DA and UA detection

### 4.2.1 Electrochemical characterization of the modified CPE

The electrochemical characterization of the different modified CPE (Nf/CPE, Nf/p(FcAni)/CPE, and Nf/p(FcAni)-CNTs/CPE) were investigated using CV. Figure 4.7 shows the CV responses obtained from (a) bare electrode, (b) Nf/p(FcAni)/CPE, and (c) Nf/p(FcAni)-CNTs/CPE, in a 0.1 M PBS (pH 7.0) at a scan rate of 10 mV $s^{-1}$. There is no redox peak present at a potential window of 0.0 to 1.0 V for the Nf/CPE, and the obtained current is very low (curve a). This result shows that the Nf/CPE has no electrochemical activity over this potential range. The Nf/p(FcAni)/CPE (curve b) and Nf/p(FcAni)-CNTs/CPE (curve c) shows similar two redox peaks at potentials of approximately 0.20 and 0.50 V. The pair of well-defined anodic and cathodic peaks arises from the $Fc|Fc^{+}$ redox system, which exhibits quasi-reversible behavior in aqueous solution. Highest current signal was obtained from the Nf/p(FcAni)-CNTs/CPE because of the excellent electron transfer properties of CNTs [79]. These results indicated that a better conductivity of CNTs combined with p(FcAni) can effectively increase the rate of electron transfer to provide increased current responses. The CV of the Nf/p(FcAni)-CNTs/CPE were investigated to determine the working potential for the electrochemical measurement of AA, DA and UA.

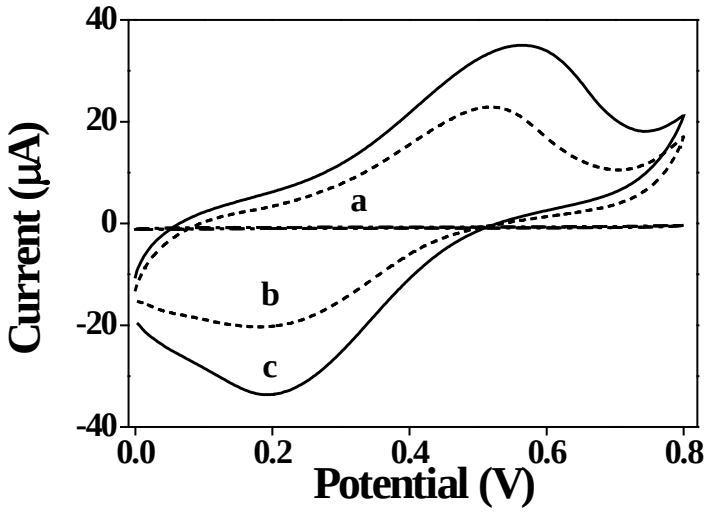


**Figure 4.7 CV plots of a) bare electrode, b) Nf/p(FcAni)/CPE, and c) Nf/ p(FcAni)-CNTs/CPE, in a 0.1 M PBS (pH 7.0) at a scan rate of 10 mV $s^{-1}$**

### 4.2.2 Electrocatalytic behaviors of DA, UA, and AA at Nf/p(FcAni)-CNTs/ CPE.

The electrochemical activity of Nf/p(FcAni)-CNTs/CPE was studied via DPV method in 0.1 M PBS (pH 7.0), with and without the addition of DA, UA, and AA at concentration of 1 mM as shown in Figure 4.8.

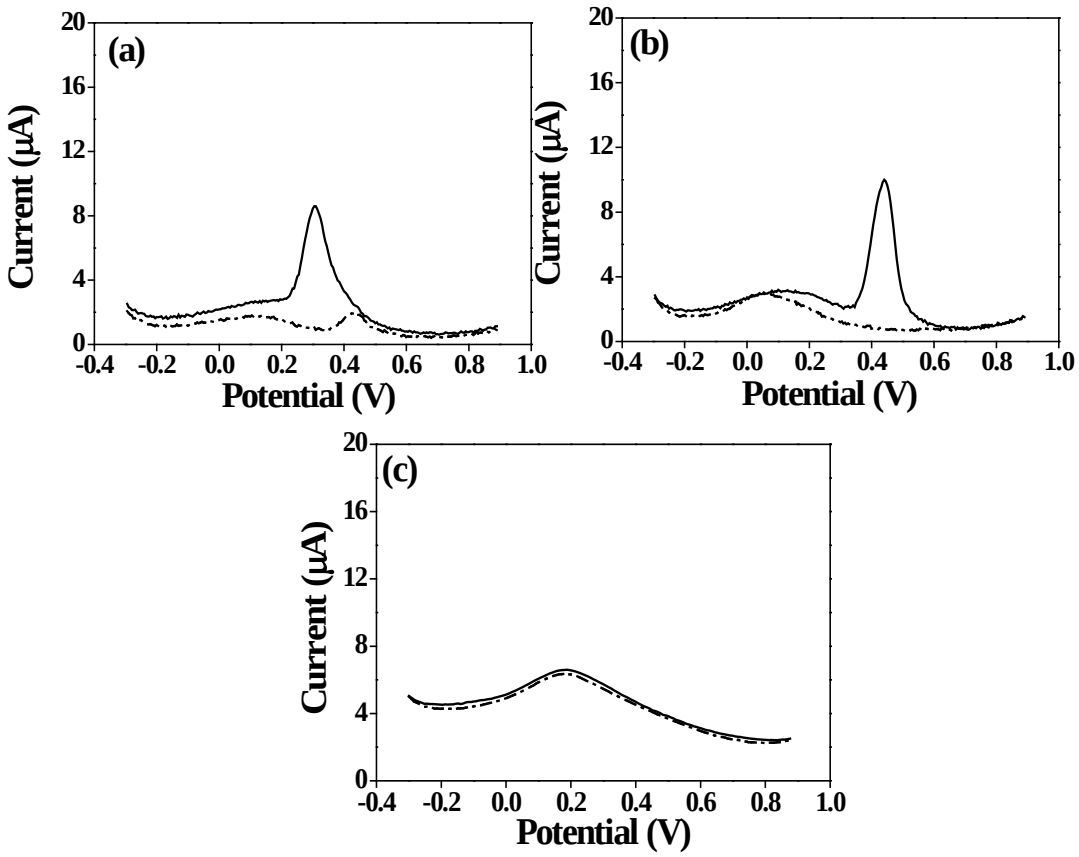


**Figure 4.8 DPV voltammetric plots of Nf/p(FcAni)-CNTs/CPE for a) 1 mM of DA b) 1 mM of UA and c) 1 mM of AA (solid line). Background current 0.1 M (PBS 7.0) also shown as dash line**

From Figure 4.8a and 4.8b, anodic peak at +0.30 and +0.45 V appeared for DA and UA, respectively. On the other hand, anodic peak for AA after the addition into the supporting electrolyte solution disappears (Figure 4.8 c). Thus, the Nf film covering the electrode eliminates the AA signal, and prevents AA interference with the detection of DA and UA. To investigate the effect of Nf, Figure 4.9 shows the effect of coating Nf on the surface of p(FcAni)-CNTs/CPE toward simultaneous AA, DA and UA detection. Anodic peak of DA and UA cannot separate at p(FcAni)-CNTs/CPE (Figure 4.9a) while anodic peak of DA and UA can clearly separate at Nf/p(FcAni)-CNTs/CPE (Figure 4.9b). These results are similar to previous report [80] that Nf film prevents interference by AA because of the hydrophobic backbone ($-CF_2-CF_2-$) and hydrophilic sulfonic acid groups ($-SO_3H$). Nf film exhibits

impermeable of anions, and permeable of cations when coated at the electrode surface. AA (pKa=4.1) exists as the anionic ascorbate ion, so experiences stronger pulsive interactions with Nf [31,32]. While negatively charged Nf-coated electrodes repel negatively charged ascorbate anions, the film allows DA and UA cations to permeate. DA (pKa=8.8) and UA (pKa=5.4) are in their cationic forms, and have strong attractive interactions with the negatively charged, sulfonate groups on Nf. Moreover, the anodized surface has a high affinity towards DA and UA due to hydrogen bonding. These results are accordance to the previous works [81]. Consequently, there is no oxidation current observed from AA at the Nf/p(FcAni)-CNTs/CPE at pH 7.0, and thus, the Fc|Fc+ redox system containing polyaniline at the electrode, allows selective sensing of DA and UA in the presence of AA.

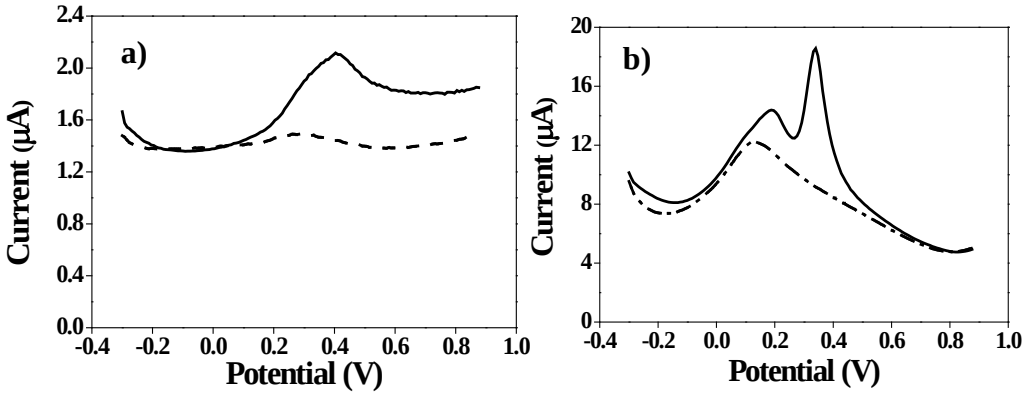


**Figure 4.9 DPV at the a) p(FcAni)-CNTs/CPE and b) Nf/p(FcAni)-CNTs/CPE in mixture solution of DA, UA and AA at 1mM (solid line). Background current 0.1 M PBS (pH 7.0) also shown as dash line**.

### 4.2.3 Effect of buffer pH (0.1 M PBS) study

Electrolyte pH has a significant impact on electrocatalytic oxidation and on the shapes of DA and UA waves. The effect of pH on the electrochemical response of Nf/p(FcAni)-CNTs/CPE was investigated from DA and UA in the presence of 1 mM AA. Voltammetric responses (Figure 4.10 a–b) at Nf/p(FcAni)-CNTs/CPE shows the anodic peak current ($i_{p,a}$) with and without the addition of 0.05 mM of DA and 0.1 mM of UA in PBS at various pH values ( pH 4.0 – 8.0). From Figure 4.10a and b, the

anodic peak potential shift negatively with the increase of electrolyte from pH 4.0 to 8.0. The relationship between pH and anodic peak potential indicated that the electrocatalysis of DA and UA at the Nf/p(FcAni)-CNTs/CPE is a pH dependent reaction. Figure 4.10c shows peak potential responses to pH changes for DA and UA. The peak potentials for DA and UA are a linear function of pH over the range of pH 4.0–8.0. The linear equation for DA and UA are $y = -0.059\ pH + 0.602$ ($r^2 = 0.992$), and $y = -0.065\ pH + 0.782$ ($r^2 = 0.990$), respectively. The slopes of -0.059 V (DA) and -0.065 V ( UA) represented in equations are close to those expected for a monoelectronic/ monoprotonic electrode reaction that is 0.059 mV/pH at 25 ºC, indicating that the number of electron and transferred proton involved in the electrochemical reaction is equal. The oxidation of both DA and UA occurs by a two-electron transfer process, and so two protons are expected to be released at the Nf/p(FcAni)-CNTs/CPE as Equation 1.1 and 1.2. The results obtained here are consistent with previous reports [82, 83]. The anodic peak currents increase as the pH value increased up to 5.0 and then slightly decreased with continuing increasing of pH were observed for both DA and UA. Figure 4.10d shows DA and UA peak current responses to changes in electrolyte pH. The $i_{p,a}$ for DA and UA reached a maximum at pH 5.0, and then decreased with further increases in pH. Consequently, we chose pH 5.0 as the optimal pH value for further electrochemical determination of DA and UA in the presence of AA.

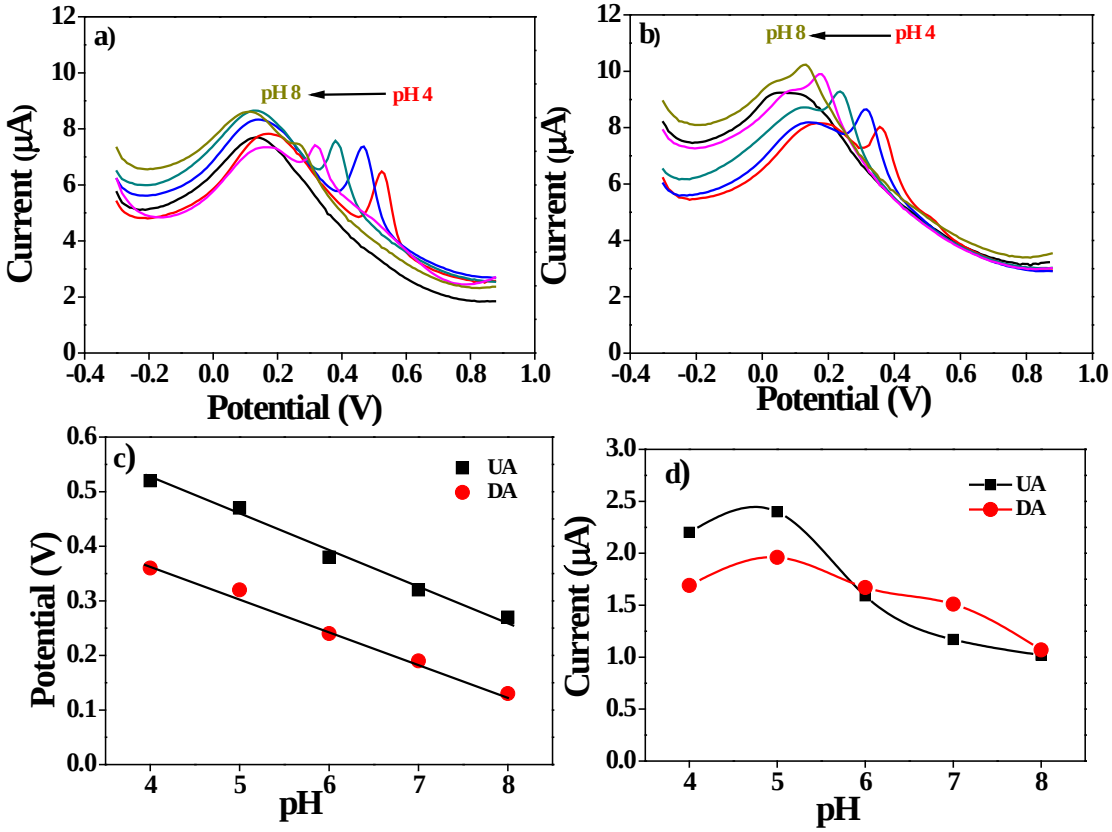


**Figure 4.10 DPV plots of Nf/p(FcAni)-CNTs/CPE in a 0.1 M PBS (pH 4.0-8.0) at a scan rate of 10 mV $s^{-1}$ for a) 0.05 mM DA and b) 0.1 mM UA. Plots of c) anodic peak potential ($E_{p,a}$) vs. pH for DA and UA, d) represents the plot of anodic peak current ($i_{p,a}$) vs. pH for DA and UA.**

### 4.2.4 Analytical features

#### 4.2.4.1 Linear concentration range

The current response of the Nf/p(FcAni)-CNTs/CPE was investigated by DPV method in 0.1 M PBS (pH 5.0) at a scan rate of 10 mV $s^{-1}$. Figure 4.11 shows the peak current increases linearly with increasing the DA (Figure 4.11a) and UA (Figure 4.11b) concentrations. The DA and UA current responses were relatively independent, and the Nf/p(FcAni)-CNTs modified CPE for selective and sensitive determination anodic peak currents ($i_{p,a}$) showed linear responses to changes in concentrations. The calibration curve of sensor shows a linear of DA with the regression equation of y = 0.041x - 0.125 ($r^2$ = 0.992) over the range of 1–150 µM,

while the linear relationship for UA is y = 0.053x - 0.148 ($r^2$ = 0.997) over the range of 5–250 µM.

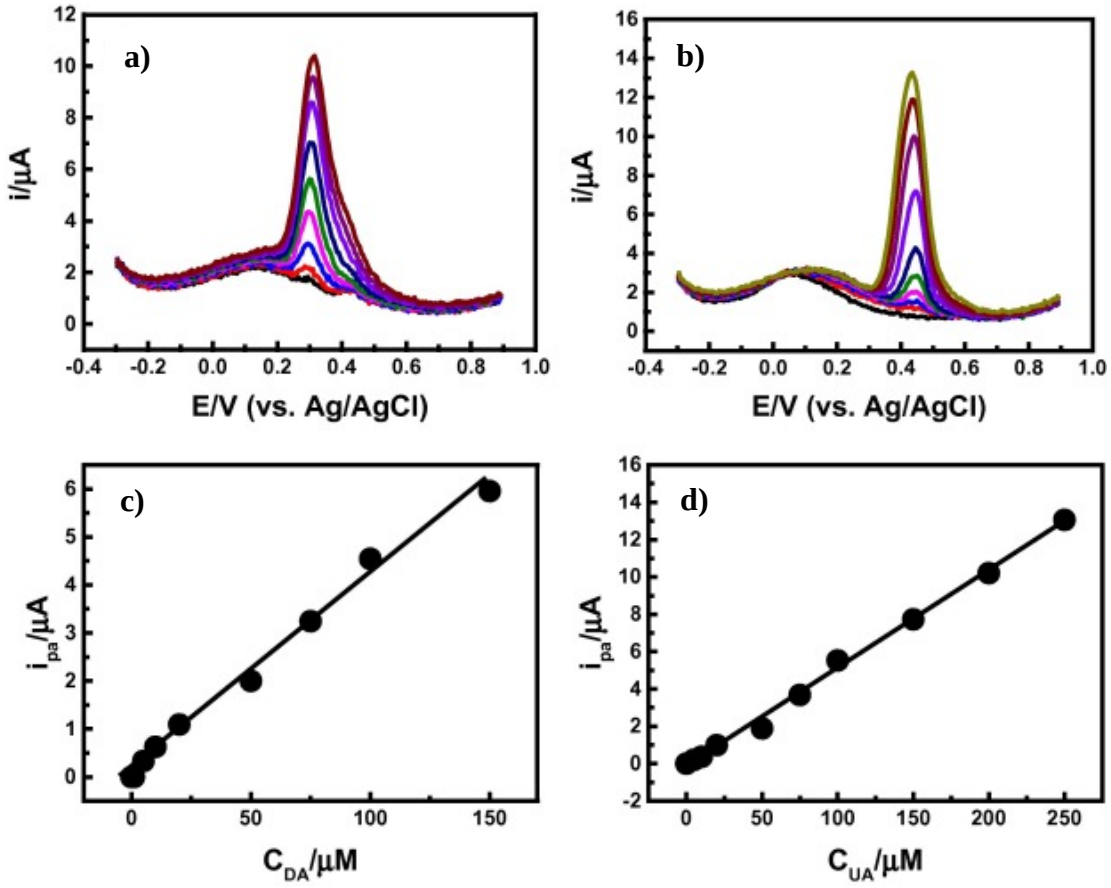


**Figure 4.11 DPV plots of the Nf/p(FcAni)-CNTs/CPE sensor under the optimal condition (pH 5.0) at a scan rate of 10 mV $s^{-1}$ for a) DA (1–150 µM from inner to outer plot) and b) UA (5–250 µM from inner to outer plot). Plots of peak current vs. c) DA and d) UA concentrations**

4.2.4.2 Limit of detection (LOD)

The LOD was investigated by addition of 1 and 5 µM of DA and UA, respectively, into 0.1 M PBS (pH 5.0). The oxidation current of DA and UA (n=3) were used to calculate LOD based on the 3-fold signal-to-noise ratio (S/N = 3). The LODs were 0.21 and 0.58 µM for DA and UA, respectively.

### 4.2.5 Interference study

Interference studies was performed on the determination of DA and UA at the Nf/p(FcAni)-CNTs/CPE sensor using DPV. The DA and UA concentrations were maintained at 0.1 mM in 0.1 M PBS (pH 5.0) containing 1 mM AA. Interfering species were added to the test solution in the range of 10–100 times greater concentration than that of DA and UA. The tolerance limit was taken as the amount of substance needed to cause a signal alteration of greater than ±5%. The results are summarized in Table 4.1. Interferences from this study could be roughly divided in to two groups.

Group I: high interfering potentials. In this group, tolerance limit was in between 2 to 7 mM.

Group II: low interfering potentials. In this group, tolerance limit was up to 10 mM

**Table 4.1 Effect of interference obtained from standard DA and UA**

| **Foreign species/ added as** | **Investigated concentration (mM)** | **Tolerance limit[a] (mM)** | |
|---|---|---|---|
| | | DA | UA |
| 1.glucose/ $C_6H_{12}O_6$ | 0.02-10 | >10 mM | 7 |
| 2. sodium nitrate/ $NaNO_3$ | 0.02-10 | 7 | 5 |
| 4. potassium chloride/ KCl | 0.02-10 | >10 mM | >10 mM |
| 6.urea/$CH_4N_2O$ | 0.02-10 | >10 mM | >10 mM |
| 7.calcium chloride/$CaCl_2$ | 0.02-10 | 2 | 7 |

[a] Greater than ± 5% signal alteration is classified as interfering condition

According to our results, glucose, KCl and urea do not interfere with the DA determination studied up to 10 mM. They provide low interfering effect. While $CaCl_2$ and $NaNO_3$ produce low interference signals at a molar concentration of 2 mM or greater (7 mM) with respect to DA. In addition, KCl also does not interfere with the UA determination studied up to 10 mM. Whereas, glucose, $NaNO_3$ and $CaCl_2$ produce

very low interference signals at a molar concentration of 5 mM or greater (7 mM) with respect to UA. This finding indicates that the Nf/p(FcAni)-CNTs/CPE electrode provides an acceptable selectivity for the determination of DA and UA in real samples.

### 4.2.6 Reproducibility and stability study

The reproducibility of the modified CPE were investigated by DPV responses of 50 µM of DA or 100 µM of UA in the presence of 1 mM AA for 15 measurements. The calculated relative standard deviations (RSD) from oxidation current are 4.3% and 3.2% for DA and UA, respectively. The storage stability of the Nf/p(FcAni)-CNTs/CPE were also studied by measuring its response to DA and UA. The electrode was stored at room temperature for 1 week. The prepared electrochemical sensors exhibit high stability for the detection of DA and UA. Moreover, the response currents of DA and UA also retained 95.68% and 99.9% of its initial measurement values for DA and UA, respectively. These results demonstrate that the Nf/p(FcAni)-CNTs/CPE performs with high stability and good reproducibility for the voltammetric determination of DA and UA.

### 4.2.7 Real samples analysis

To illustrate the applicability of the Nf/p(FcAni)-CNTs/CPE for real samples, measurements of DA or UA in pharmaceutical or biological sample fluids using the standard addition method were carried out. The proposed method was applied for the detection of DA and UA in two different samples including dopamine hydrochloride solutions for intravenous infusion (D-A1 and D-A2) and human urine samples (U-S1 and U-S2). In order to test the reliable of this proposed sensor at a low concentration range, the samples were diluted appropriately with 0.1 M PBS. The precision of the analytical process was evaluated by the repeatability of the process, shown in Table 4.2. The recoveries and RSDs of the presented method for DA and UA samples were found in the range of 90.3–101.0%and 0.3–1.3%, respectively. These results indicated that the fabricated electrochemical sensor (Nf/p(FcAni)-CNTs/CPE) is sufficiently accurate, precise and suitable for the quantification of DA and UA in these samples.

**Table 4.2 DA and UA concentration in different samples (n = 3) obtained from the proposed method and the reference values**

| Sample | Analyte | Detected (μM)[a] | Spiked level (μM) | Found (μM)[b] | Recovery (%) |
|---|---|---|---|---|---|
| D-A1 | DA | 31.3 ± 0.1 | 10.0 | 39.9 ± 0.4 | 96.6 ± 1.0 |
| D-A2 | | 31.6 ± 0.1 | 10.0 | 41.7 ± 0.3 | 101.0 ± 0.6 |
| U-S1 | UA | 41.5 ± 0.6 | 10.0 | 49.5 ± 0.1 | 90.3 ± 0.3 |
| U-S1 | | 59.6 ± 0.3 | 10.0 | 70.1 ± 1.1 | 100.7 ± 1.3 |

[a]Amount found in the samples after dilution, average ± S.D

[b]Amount found after spiked either 10 μM of DA or UA

## 4.3 Biosensor for sulfite detection

### 4.3.1 Cyclic voltammetric study of nanomaterials-modified electrode

To test the electrocatalytic behavior of the modified CPE containing immobilized SOx ( sulfite biosensor), Figure 4.12 shows the comparison of the response obtained from a) $Fe_3O_4$@Au/CPE, b) $Fe_3O_4$@Au-Cys/CPE, and c) $Fe_3O_4$@Au-Cys-FA/CPE toward the electro-oxidation of sulfite in 0.1 M PBS (pH 7.0). $Fe_3O_4$@Au-Cys-FA shows the greatest current response (Figure 4.12, curve c), and exhibits the least negative peak potential when compared to the $Fe_3O_4$@Au (curve a) and $Fe_3O_4$@Au-Cys (curve b) CV plots. Thus, the introduction of $Fe_3O_4$@Au-Cys-FA composite enhanced the redox response and electrocatalytic activity. Therefore, the carbon paste biosensor containing $Fe_3O_4$@Au-Cys-FA was selected for sulfite determination.

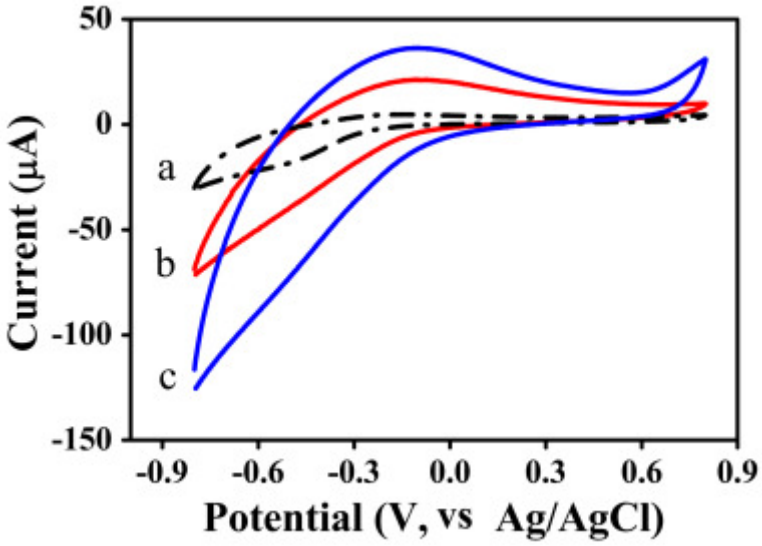


**Figure 4.12 Cyclic voltammograms of a) $Fe_3O_4$@Au/CPE biosensor, b) $Fe_3O_4$@ Au-Cys/CPE biosensor, and c) $Fe_3O_4$@Au-Cys-FA/CPE biosensor, in 0.1 M PBS (pH 7.0) at a scan rate of 50 mV $s^{-1}$**

Figure 4.13 shows voltammograms obtained in the absence of sulfite (dotted line), and in the presence of 2 mM and 4 mM sulfite (solid lines) at the $Fe_3O_4$@Au-Cys-FA/CPE biosensor. $Fe_3O_4$@Au-Cys-FA/CPE biosensor exhibits quasi-reversible oxidation peaks at approximately -0.10 V versus Ag/AgCl. The oxidation peaks at approximately -0.10 V correspond to oxidation of $H_2O_2$ by enzymatic reaction between SOx and sulfite. The increase in the value of the oxidation current with increase in sulfite concentration resulted due to the increased concentration of $H_2O_2$ during enzymatic reaction. These oxidation peaks at approximately -0.10 V clearly demonstrate the $Fe_3O_4$@Au-Cys-FA/CPE catalytic properties.

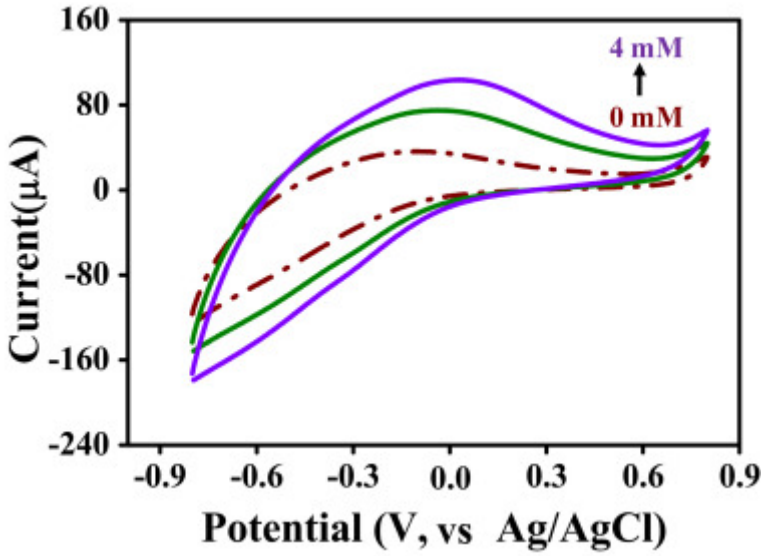


**Figure 4.13 $Fe_3O_4$@Au-Cys-FA/CPE provided an oxidation peak, in response to sulfite addition at a potential of -0.1 V (vs. Ag/AgCl) in PBS (0.1 M, pH 7.0)**

The response measurement of sulfite biosensor was involved these following electrochemical reactions [84-85]:

$$SO_3^{2-} + O_2 + H_2O \xrightarrow{SO^x} SO_4^{2-} + H_2O_2 \quad (4.1)$$

$$H_2O_2 \xrightarrow{CPE} 2H^+ + O_2 + 2e^- \quad (4.2)$$

Sulfite is oxidized to sulfate and hydrogen peroxide ($H_2O_2$) with SOx as catalyst in the presence of oxygen as described in equation 4.1. $H_2O_2$ can be oxidized at a positive applied potential and the carbon paste electrode produced the oxidation current. Thus the amount of $H_2O_2$ produced from sulfite can be used to indirectly determine sulfite level.

### 4.3.2 Hydrogen peroxide ($H_2O_2$) detection

To check whether the detected $H_2O_2$ signal come from sulfite or not, the modified electrode (bare CPE, $Fe_3O_4$/CPE, $Fe_3O_4$@Au/CPE and $Fe_3O_4$@Au-Cys-FA/CPE) without immobilized SOx enzyme was measured in 0.1 M PBS (pH 7.0) in the presence of 2.0 and 4.0 mM $H_2O_2$. As shown in Figure 4.14, the typical CV of a) bare CPE, b) $Fe_3O_4$/CPE and c) $Fe_3O_4$@Au/CPE do not appear oxidation peak of $H_2O_2$ while only the (d) $Fe_3O_4$@Au-Cys-FA/CPE shows the oxidation current from -0.30 to +0.4 V. This is the oxidation peak for $H_2O_2$ which is the product of the enzymatic reaction (sulfite is oxidized by SOx enzyme to sulfate and $H_2O_2$ as proposed in equation 4.1 and 4.2). From these results, it can be concluded that the $Fe_3O_4$@Au-Cys-FA/CPE with immobilized SOx enzyme can be used for the sulfite determination.

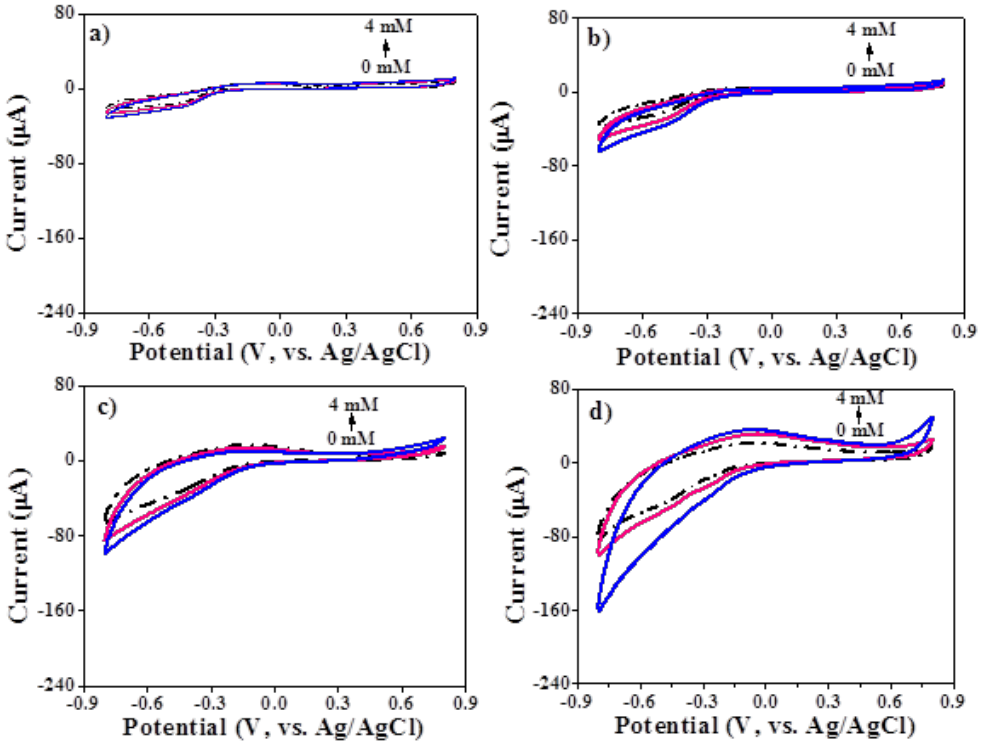


**Figure 4.14 Cyclic voltammograms of 0, 2, and 4 mM of $H_2O_2$ on the non-enzymatic electrodes of a) bare CPE and CPEs modified with b) $Fe_3O_4$; c) $Fe_3O_4$@Au and d) $Fe_3O_4$@Au-Cys-FA. Supporting electrolyte; 0.1 M PBS (pH 7.0) at a scan rate of 50 mV $s^{-1}$**

### 4.3.3 Effect of 0.1 M buffer pHs

The influence of pHs were studied because it is a critical parameter in the determination of enzyme activity. The effects of pHs on the analytical response of modified sulfite biosensor were studied in the range 5.0 to 9.0 in 0.1 M PBS using CV. Figure 4.15 shows that current responses were increased according to pH from 5.0 to 7.0 and reached the maximum at 7.0. Further increasing pH from 7.0 to 9.0 results in the decrease of the current signal. This indicated that pH 7.0 was the optimum pH. This pH, biomolecules retain their originate natural structures and provide the highest efficiency. These results were similar to previous work reported by Dinckaya et al [86]. Therefore, 0.1 M PBS at the pH 7.0 was selected for further study.

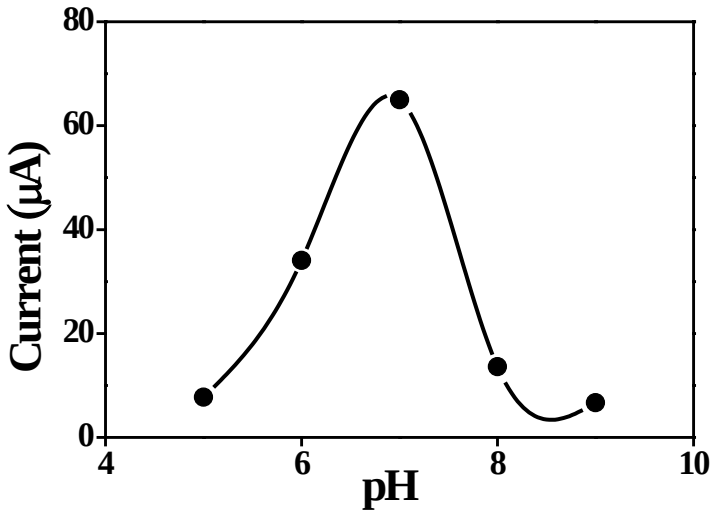


**Figure 4.15 Peak current obtained from the biosensor at scan rate of 50 mV $s^{-1}$**

### 4.3.4 The apparent Michaelis-Menten constant ($K_m^{app}$)

SOx enzyme was immobilized on $Fe_3O_4$@Au-Cys-FA/CPE which catalyze the oxidation of sulfite to sulfate with high selectivity. SOx kinetic parameters was determined within the sulfite concentration over the range of 0.5–10 mg $L^{-1}$. The apparent Michaelis-Menten constant ($K_m^{app}$) was calculated from a Lineweaver-Burk plot equation (3.1). A low $K_m^{app}$ value indicates a strong substrate binding and demonstrates a higher affinity of sulfite for the modified electrode. On the other hand, a high $K_m^{app}$ value means a lot of substrate must be present to saturate the enzyme,

meaning the enzyme has low affinity for the substrate. The current increases when the concentration of sulfite increases, shown in Figure 4.16a. Figure 4.16b shows the Lineweaver-Burk plot of SOx immobilized on the modified electrode in the presence of different concentration of sulfite. The $K_m^{app}$ value for the $Fe_3O_4$@Au-Cys-FA/CPE device is calculated as 2.00 mg $L^{-1}$ (25 μM), indicating that the biosensor has a high affinity for immobilized SOx during $H_2O_2$ determination. This value for $K_m^{app}$ is smaller than the value of 8.08 mg $L^{-1}$, seen for AuNPs-PEI, in which SOx is immobilized onto an Au electrode modified with gold nanoparticles capped with cationic branched poly(ethyleneimine) [87], and is comparable to reported values of 2.05 mg $L^{-1}$ [57], 0.64 mg $L^{-1}$ [60], and 1.60 mg $L^{-1}$ [85] for SOx immobilized onto a gold-nanoparticle/chitosan/carbon nanotube/polyaniline composite modified Au electrode [57], gold-coated magnetic nanoparticles [60], and an ITO electrode modified with a PEI capped CdS quantum-dot [85], respectively. This result indicates that our biosensor provides good SOx electrocatalytic activity.

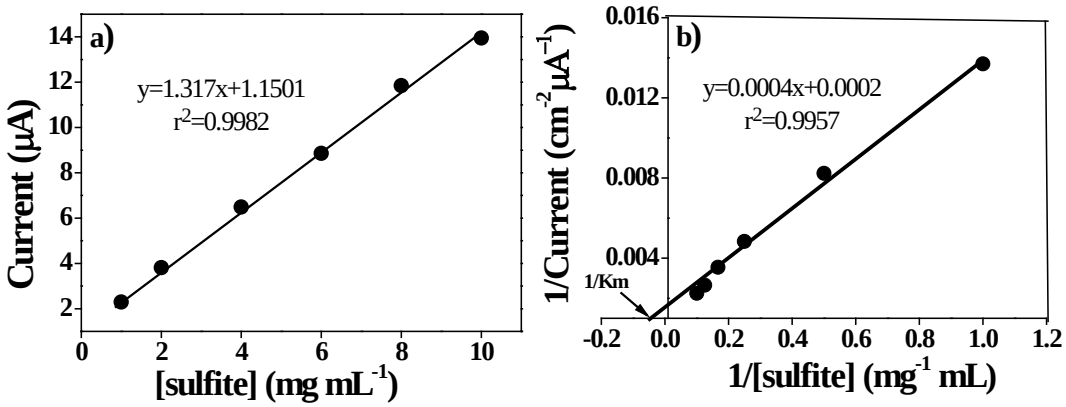


**Figure 4.16 a) Response of modified sulfite biosensor toward sulfite in the concentration range 0.05 – 10 mg $L^{-1}$ and b) Linerweaver-Bulk plot of sulfite immobilized on the sulfite biosensor**

### 4.3.5 Scan rate dependence study

Cyclic voltammograms of sulfite solution at the $Fe_3O_4$@Au-Cys-FA/CPE in 0.1 M PBS (pH 7.0) with the variation of scan rates were investigated, the results are illustrated in Figure 4.17. As shown in the inset of Figure 4.17, the oxidation peaks current (μA) increased linearly with the square root of scan rate ($v^{1/2}$ $s^{1/2}$) within the scan rate of 0.05–0.40 V $s^{-1}$. Linear regression analysis provided y=186.56x+14.157, $r^2$ values of 0.995. These results indicated that the current is limited by diffusion of sulfite to the $Fe_3O_4$@Au-Cys-FA/CPE electrode. It can also be seen in Figure 4.17 that with increasing scan rate, the peak potential for the electro-oxidation of sulfite is shifted to more positive values. This result suggests that the reaction between the oxidation sites of the $Fe_3O_4$@Au-Cys-FA/CPE with sulfite is a diffusion controlled quasi-reversible electrochemical process. These results are similar to previous work [88].

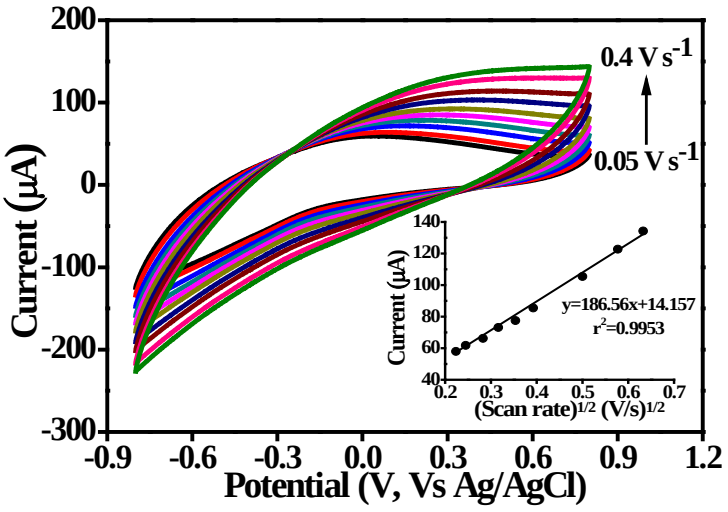


**Figure 4.17 Cyclic voltammograms, obtained at various scan rates for 4 mM sulfite in 0.1 M PBS (pH 7.0) at modified sulfite biosensor and insert linear relationship between oxidation peak currents and square root of the scan rate.**

### 4.3.6 Stability study

The storage stability at the $Fe_3O_4$@Au-Cys-FA/CPE biosensor was studied for sulfite determination in 0.1 M phosphate buffer pH 7.0. The $Fe_3O_4$@Au-Cys-FA/CPE electrode was stored in vial over a 0.1 M phosphate buffer pH 7.0 and kept at 4 °C when not in use. The sulfite oxidation current was measured when stored for 0, 1, 2, 3, 4, 5, 7, and 14 days. The relative oxidation current was calculated and plotted versus storage time. Relationship between percentages of relative oxidation currents and storage time (day) is shown in Figure 4.18. The results indicated that current responses of the novel biosensor remain close to the initial measurements. The current response of the biosensor retains 89% of the initial current response after repeated use for more than one week, and retains approximately 102% after 2 weeks. This indicated high stability of the developed biosensor.

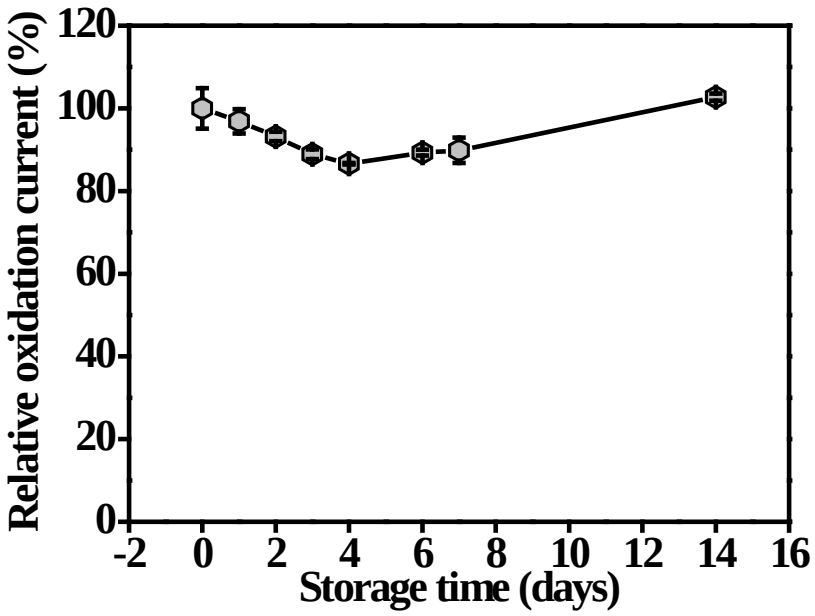


**Figure 4.18 The storage stability of the $Fe_3O_4$@Au-Cys-FA/CPE using 10 $mgL^{-1}$ sulfite in 0.1 M PBS (pH 7.0)**

### 4.3.7 Amperometric detection of sulfite in the developed FIA system

#### 4.3.7.1 Effect of PDMS

The CPE has a porous surface that contains a mixture of conducting graphite, catalyzing materials, and non-conducting mineral oil binder. PDMS oil has attractive properties for constructing carbon paste based chemical sensors [89] and biosensors [63, 90] because its ability to provide an internal source of oxygen for enzymatic reaction. The solubility of oxygen in PDMS is 45–50 fold greater than it is in water [91]. In this work, the use of a PDMS-mineral oil binder to enhance the physical stability of the electrode and facilitate the sealing the CPE to the FIA system was demonstrated. The performances of the $Fe_3O_4$@Au-Cys-FA/CPE electrode using both mineral oil and a mineral oil-PDMS mixture as binder were compared using amperometry, shown in Figure 4.19. This figure compares the amperometric response to 10 mg $L^{-1}$ sulfite at the $Fe_3O_4$@Au-Cys-FA/CPE biosensor using a) mineral and b) mixed mineral oil-PDMS as binder. Sulfite oxidation peaks are clearly visible for the mixed mineral oil-PDMS binder (curve b), while the signal obtained from the mineral oil CPE was barely detectable (curve a). This indicates that using the mixed binder can enhance CPE sensitivity greater than mineral oil alone. The observed improvement in CPE sensitivity and physical stability in the presence of PDMS has been reported for other amperometric biosensors [89-90, 92]. Hence, the mineral oil-PDMS mixture was used to prepare the CPE electrode.

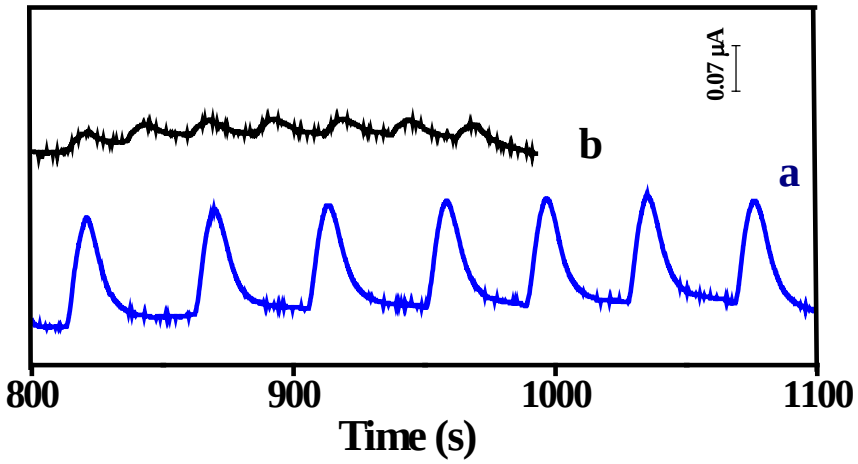


**Figure 4.19 FIA grams comparing sulfite detection performances for CPE with a) mineral oil and b) mixed mineral oil-PDMS binders; sulfite, 10 mg $L^{-1}$; applie potential, +0.35 V; flow rate, 1.0 mL $min^{-1}$, ambient temperature (~25 °C)**

4.3.7.2 Optimum potential for amperometric detection

The detection potential affects the sensitivity of current signal of an analyte. In order to obtain the optimal potential for amperometric detection at the $Fe_3O_4$@Au-Cys-FA/CPE using an FIA manifold, hydrodynamic voltammetric behavior of sulfite was investigated. 10 mg $L^{-1}$ sulfite solution was injected into the flow system with varying detection potential from -0.10 to +0.80 V. Each datum represents the average of 10 mg $L^{-1}$ sulfite injections (n=3) as shown in Figure 4.20. The oxidation current rises from the potential range 0.0 to +0.35 V and remains steady at potentials greater than +0.35 V. Maximum sensitivity occurred at an operating potential of +0.35 V (versus Ag/AgCl), and therefore it was selected as the optimum potential. The results indicated that electrocatalytic activity of enzyme SOx incorporated with the matrix $Fe_3O_4$@Au-Cys-FA/CPE toward the oxidation of sulfite enables the biosensor to effectively detect analyte at low potential. The advantage of detection at low potential is low noise and background current [70]. This potential was similar to previous work reported by Rewal, R et al [84], who studied amperometric sulfite biosensor based on SOx/PBNPs (Prussian blue nanoparticle)/PPY (polypyrrole composite) electrodeposition onto the surface of indium tin oxide (ITO) electrode.

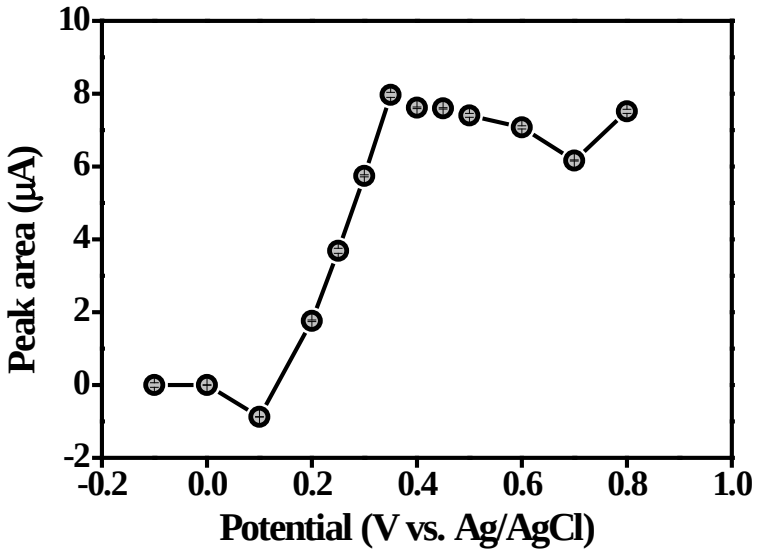


**Figure 4.20 Influence of applied potential on the biosensor response; 10 mg $L^{-1}$ sulfite, flow rate, 1.0 mL $min^{-1}$**

4.3.7.3 Optimum flow rate

In order to achieve the sample throughput with satisfactory sensitivity, the effect of flow rate on the modified sulfite biosensor response was optimized by injection of 10 mg $L^{-1}$ sulfite into the carrier stream (0.1 M phosphate buffer pH 7.0). The flow rate was studied between 0.2 to 1.8 mL $min^{-1}$, shown in Figure 4.21. The signal responses decrease with increasing flow rate. High flow rates normally result in a reduced response because of the shorter contact time between enzyme and analyte, as reported for other enzyme-based amperometric detection FIA systems [63]. On the other hand, sample throughput rapidly increases with increasing flow rate over the range 0.2–1.4 mL $min^{-1}$ and remains constant over the range of 1.4–1.8 mL $min^{-1}$. This behavior is in agreement with theoretical expectations based on laminar flow assumptions under conditions of mass transport control [74]. To provide a balance between sensitivity and sample throughput, the flow rate of 0.8 mL $min^{-1}$ was selected as the optimum for future experimental.

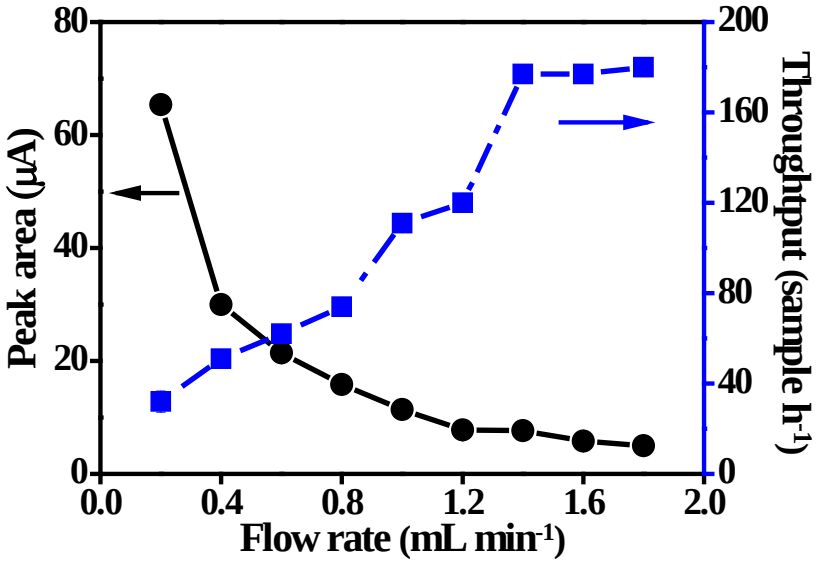


**Figure 4.21 Effect of flow rate at $Fe_3O_4$@Au-Cys-FA/CPE on sulfite response and sample throughput; sulfite, 20 mg $L^{-1}$ at +0.35 V**

4.3.7.4 Analytical features

1) Linear concentration range

The analytical performance of the FIA method with amperometric detection at the developed sulfite biosensor was examined. Under the optimal conditions (operational potential, +0.35 V; carrier solution, 0.1 M PBS, pH 7.0; flow rate, 0.8 mL $min^{-1}$), the relationship between peak area and sulfite concentration was study. FIA gram of sulfite concentration on current signal with different concentration between 0.1-200 mg $L^{-1}$ (n=3) shown in Figure 4.22. The regression equation is given by y=1.086x+1.147 ($r^2$=0.998), where y and x are the height of peak current (μA) and sulfite concentration (mg $L^{-1}$), respectively. The slope of the equation is corresponding to linear sensitivity of 1.086 μA $(mg)^{-1}$ L.

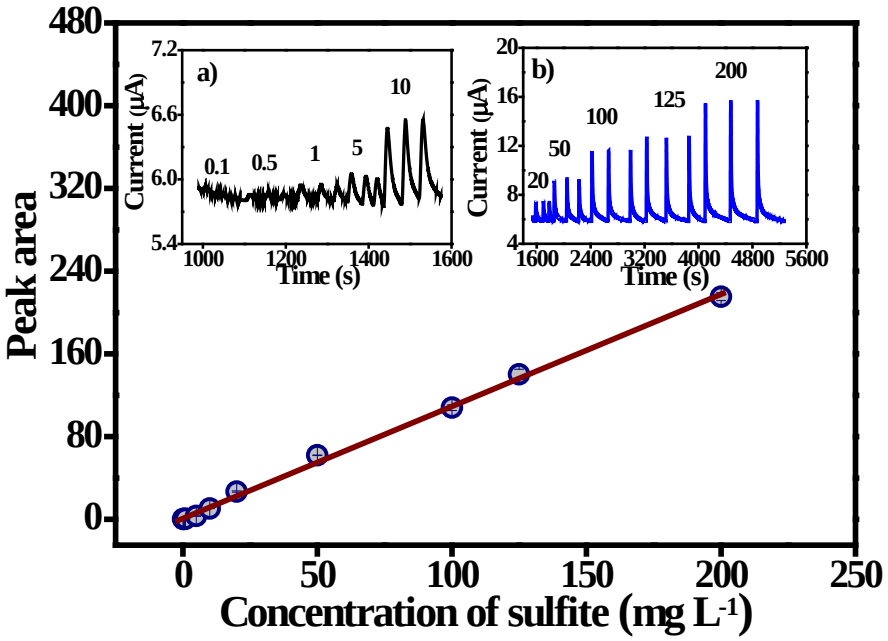


**Figure 4.22 Calibration plot of peak area of current signals versus concentration of sulfite as obtained from the FIA grams. The inset shows FIA grams for sulfite standards (a) 0.1–10 mg $L^{-1}$ and (b) 20–200 mg $L^{-1}$, obtained as the averages of triplet injections.**

2) Limit of detection (LOD) and limit of quantification (LOQ)

The LOD was performed by repeat injection of 10 µg $L^{-1}$ sulfite with the twenty replicate injections into a carrier solution of 0.1 M phosphate buffer pH 7.0 to estimate the standard deviation ($S_b$). The detection limit, determined by three times of the standard deviation of the blank ($3S_b$), is 10 µg $L^{-1}$ of sulfite. The limit of quantification, estimated by ten times of the standard deviation of the blank ($10S_b$) according to ISO11843 [93, 94] is 34 µg $L^{-1}$. The system provides an impressively good precision (%R.S.D = 3.1, n=20) and rapid sample throughput (109 samples $h^{-1}$).

4.3.7.5 Interference study

To evaluate the selectivity of the proposed sensor, we examined the effects of interference, from selected inorganic ions and organic compounds, which are commonly present in sulfite samples. These compounds including sugar (glucose, sucrose, fructose and maltose), various ions ($NO_3^-$, $Cl^-$, $I^-$, $CH_3COO^-$ and $SO_4^{2-}$) and other (ethanol and ascorbic acid) on the alteration of amperometric signal obtained

from 15 mg $L^{-1}$ sulfite was investigated. The results from this study shows in table 4.3. The tolerance was defined as the maximum concentration of the interfering substance required to cause a signal alteration greater than ±5%. Tolerances toward these compounds are 75 mg $L^{-1}$ or greater, and negligible interference was observed during testing. These results conclude that the developed method provides good selectivity for the amperometric determination of sulfite.

**Table 4.3 Effect of foreign ions on the alteration of FIA amperometric signal obtained from triplicate injections (n=3) of 10 mg $L^{-1}$ sulfite.**

| **Foreign species/ added as** | **Investigated concentration (mg $L^{-1}$)** | **Tolerance limit[a] (mg $L^{-1}$)** |
|---|---|---|
| **Sugars** | | |
| - fructose/ $C_6H_{12}O_6$ | 0-3,750 | 1,500 |
| - sucrose/ $C_{12}H_{22}O_{11}$ | | 1,500 |
| - glucose/ $C_6H_{12}O_6$ | | 750 |
| - maltose/ $C_{12}H_{22}O_{11}$ | | 750 |
| **Ions** | | |
| - $NaNO_3$/ $NO_3^-$ | | 1,500 |
| - NaCl/ $Cl^-$ | | 1,500 |
| - $CH_3COONa$/ $CH_3COO^-$ | | 1,500 |
| - $Na_2SO_4$/ $SO_4^{2-}$ | | 1,500 |
| - KI/ $I^-$ | 0-500 | 150 |
| **Other** | | |
| - ethanol/ ($CH_3CH_2OH$) | 0-3,750 | 750 |
| - ascorbic acid/ ($C_8H_8O_6$) | 0-150 | 75 |

[a] Greater than ±5% signal alteration is classified as interfering condition

4.3.7.6 Method validation

The possibility for the use of the developed system in real sample analysis was investigated. The system was applied to the determination of the sulfite content in five wines (W1-W5) and pickled food extracts of mango sheet (M1-M3), ginger (G1-G3) and cabbage (C1-C3). Sulfite determinations were performed by the developed biosensor in FIA with amperometric measurements under optimized conditions, using the standard addition method. The results were compared with measurements obtained from the reference iodometric method as shown in Figure 4.23. Statistical analysis (paired t-test [95]) reveals that data from our developed biosensor are not significantly different to that from the reference method ($t_{observed}$=0.996, $t_{critical}$=2.161, 95% confidence).

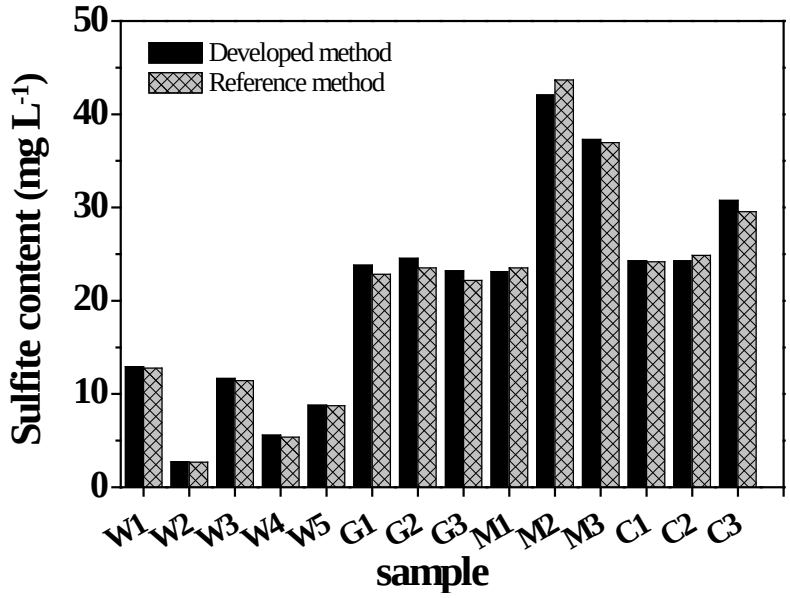


**Figure 4.23 Comparison of sulfite content found in wine and pickled food extracts samples, which were analyzed by the developed method (sulfite biosensor) and iodometric method. Determination by each method was carried out in triplicate runs per sample.**

To clarify observation, the results were summarized in Table 4.4. The relative differences between data obtained from the $Fe_3O_4$@Au-Cys-FA/CPE biosensor and the iodometric method were ranged from 0.4–4.7%. The results obtained from these two method are in good agreement. The results indicate that our sulfite biosensor is sufficiently accurate, and is suitable for the quantification of sulfite in the study samples.

**Table 4.4 Comparison of sulfite determinations in wines (W1-W5) and picked food extracts (ginger; G1-G3, mango; M1-M3 and cabbage; C1-C3), between the developed $Fe_3O_4$@Au-Cys-FA/CPE biosensor and the reference iodometric method.**

| Sample | Sulfite (mg $L^{-1}$ or mg $kg^{-1}$) | | | |
|---|---|---|---|---|
| | Developed biosensor[a] | Reference method[a] | % Relative diference | |
| W1 | 12.94±0.05 | 12.77±0.01 | -1.35 | wine |
| W2 | 2.74±0.01 | 2.69±0.01 | -1.78 | |
| W3 | 11.67±0.02 | 11.42±0.01 | -2.14 | |
| W4 | 5.59±0.09 | 5.38±0.03 | -4.05 | |
| W5 | 8.79±0.04 | 8.74±0.02 | -0.63 | |
| G1 | 23.81±0.04 | 22.85±0.01 | -4.21 | ginger |
| G2 | 24.55±0.03 | 23.52±0.01 | -4.38 | |
| G3 | 23.21±0.02 | 22.18±0.01 | -4.67 | |
| M1 | 23.12±0.04 | 23.52±0.01 | +1.72 | mango |
| M2 | 42.06±0.02 | 43.68±0.01 | +3.71 | |
| M3 | 37.29±0.03 | 36.96±0.07 | -0.90 | |
| C1 | 24.29±0.05 | 24.19±0.01 | -0.40 | cabbage |
| C2 | 24.29±0.10 | 24.86±0.01 | +2.29 | |
| C3 | 30.77±0.02 | 29.57±0.01 | -4.06 | |

[a]Average ± standard deviation of 3 measurements.

## Part II: MIP modified QCM sensor for pesticides detection

### 4.4 MIP-QCM sensor

#### 4.4.1 Measurement of binding interaction of MIP- QCM sensor

A QCM is one of the potential useful quantitative techniques to detect pesticides. The QCM apparatus showed frequency change due to changes in mass on the electrode. This technique can be applied as convenient transducer of recognition of molecular imprinting polymers to provide sensor signal. Figure 4.24 shows the QCM sensor responses of CBF-MIP in comparison with CBF-NIP. CBF-MIP leads to substantial frequency signals in a range of 0.050-1.857 KHz. On the other hand, the NIP-coated electrode yields slightly positive frequency shift in the range of 0.013-0.134 KHz. MIP signals are thus substantially larger, namely around 10 times, than those for the NIP. The reason is that the –NH group of CBF can be expected to interact with the –COOH functionality of the polymer backbone. This result is in agreement with previous report by Kotova, K et al [ 43]. The inset of Figure 4.24 shows the corresponding sensor characteristics. CBF-MIP contains two linear concentration ranges of 5-10 µM and 10-1000 µM, respectively.

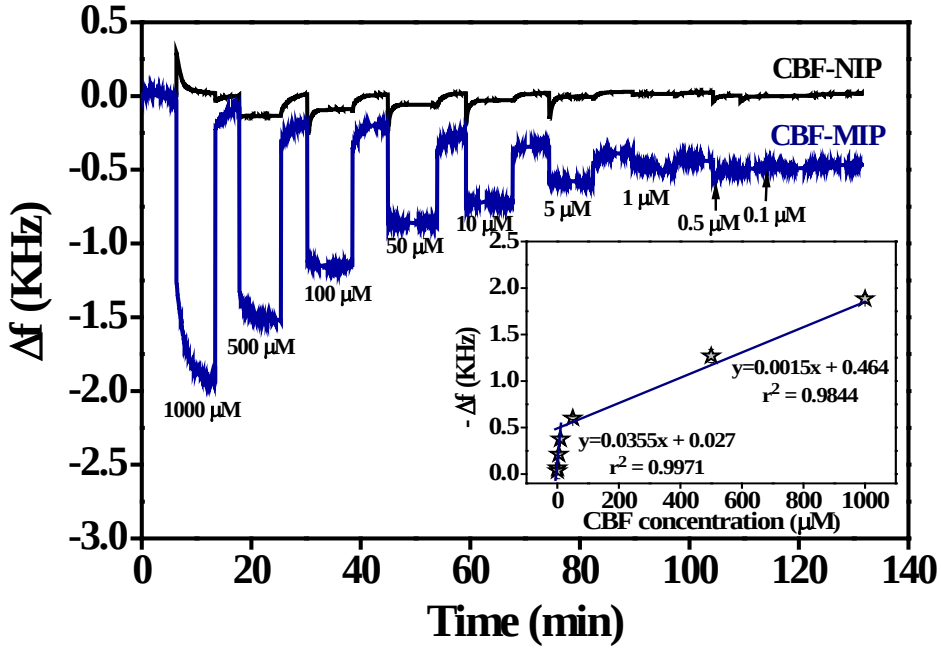


**Figure 4.24 QCM sensor responses toward CBF at various concentrations; the inset shows bi-linear sensor characteristic in the concentration range of 0.5 to 1000 µM**

Figure 4.25 shows typical frequency responses of PFF-MIP and PFF-NIP toward solutions containing different concentrations of this analyte. As can be seen, it is evident that at 1,000 µM of PFF yielded a net sensor signal as high as -0.644 KHz and -0.074 KHz for MIP and NIP, respectively. The frequency shift of the MIP was seven times higher than NIP. The PFF-MIP displays a linear working range from 5 - 1,000 µM. The LOD was found to be about 0.21 µM and 0.38 µM (S/N=3) for CBF-MIP and PFF-MIP, respectively.

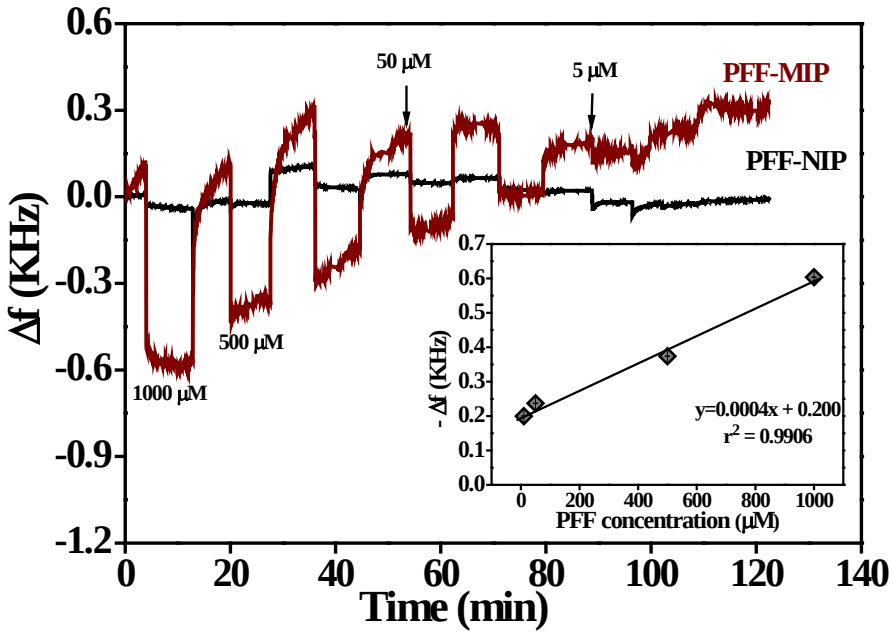


**Figure 4.25 QCM responses toward different concentration of PFF; The insert shows linear sensor characteristic in the concentration range of 5 to 1000 µM.**

QCM sensor data from Figure 4.24 and 4.25 were analyzed for the determination of equilibrium isotherm parameters such as forward and reverse binding constants, $K_a$ ($M^{-1}$) and $K_d$ (M) and thermordymamic parameter. The equilibrium parameters, including the association constant ($K_a$) and maximum saturation binding value ($\Delta m_{max}$), were calculated by fitting the Langmuir adsorption isotherm using the obtained Δf value and the calculated mass change (Δm) on the surface of the QCM Au at each tested CBF and PFF concentration.

In order to analyze $K_d$ and $K_a$ constant of pesticides onto MIP, isotherm adsorption as Langmuir model depicted in Equation 4.3: [96, 97].

$$\Delta m = (\Delta m_{max}\, C)/K_d + C) \qquad (4.3)$$

Where Δm is amount of increased mass on unit area of QCM sensor ($g/cm^2$); $\Delta m_{max}$ is maximum saturation binding value; C is concentration of CBF or PFF solution (µM) for CBF-MIP or PFF-MIP, respectively; $K_d$ is reverse binding

constant and it is equal reverse of the equilibrium association constant ($1/K_a$), can be given as Equation 4.4:

$$\Delta m = (\Delta m_{max} K_a C)/(1+K_a C) \quad (4.4)$$

Equation 4.4 can be rearranged as Equation 4.5. So, Δm versus Δm/C was plotted which gave a slope of $1/K_a$ and Y-intercept of $\Delta m_{max}$.

$$\Delta m = -(1/K_a)(\Delta m/C) + \Delta m_{max} \quad (4.5)$$

The results are summarized in Table 4.5. CBF-MIP contains two $K_a$ of 0.1 and 0.01 $\mu M^{-1}$ for the low and high concentration of CBF, respectively. The rapid increasing of slope at the beginning may be correlated to the presence of large number of vacant imprinted cavities of MIP. Subsequently, these site will be occupied by template molecules causing the decreasing of adsorption rate in the later period. In case of PFF-MIP, the $K_a$ and $\Delta m_{max}$ were 0.12 $\mu M^{-1}$ and 3.03 g, respectively. This revealing that the PFF-MIP immobilized on the QCM electrode surface had strong affinity toward the analyte PFF.

By applying of binding constant ($K_a$), the free energy change (ΔG) value for CBF and PFF adsorbed on the MIP-CBF and PFF-MIP immobilized QCM were calculated according to the Equation 4.6 [98].

$$\Delta G = RT \ln K_a \quad (4.6)$$

Where R is gas constant (8.314 J $mol^{-1}$ $K^{-1}$), T is the temperature (298 K). The results are listed in Table 4.5. The negative values of obtained ΔG were -5.7 and -11.42 for CBF-MIP and -5.51 for PFF-MIP. These results suggest that the sorption process occurs spontaneous at 25 °C.

**Table 4.5 Langmuir constants of CBF-MIP and PFF-MIP**

| substrate | $K_a$ ($\mu M^{-1}$) | $\Delta m_{max}$ (µg) | $\Delta G$ (KJ $mol^{-1}$) at 25 °C |
|---|---|---|---|
| CBF-MIP | 0.10 | 0.65 | -5.7 |
| | 0.01 | 1.27 | -11.42 |
| PFF-MIP | 0.13 | 306.91 | -5.51 |

### 4.4.2 Specificity and selectivity of QCM sensor

The selectivity of the developed MIP-QCM sensor for CBF and PFF was evaluated using their analogues molecules to investigate the effect. PFF and chlopyrifos (CPF) were selected to study the selectivity of CBF-MIP whereas CBF and CPF were selected for PFF-MIP. The obtained frequency response was compared and shown in Figure 4.26. Figure 4.26 shows responses of insecticides binding response of CBF-MIP (a) and MIP-PFF (b), the signals were obtained using the concentration of 1000 µM. It was found that the frequency shift of CBF-MIP and PFF-MIP were higher than that obtained from to CBF-NIP and PFF-NIP, respectively.

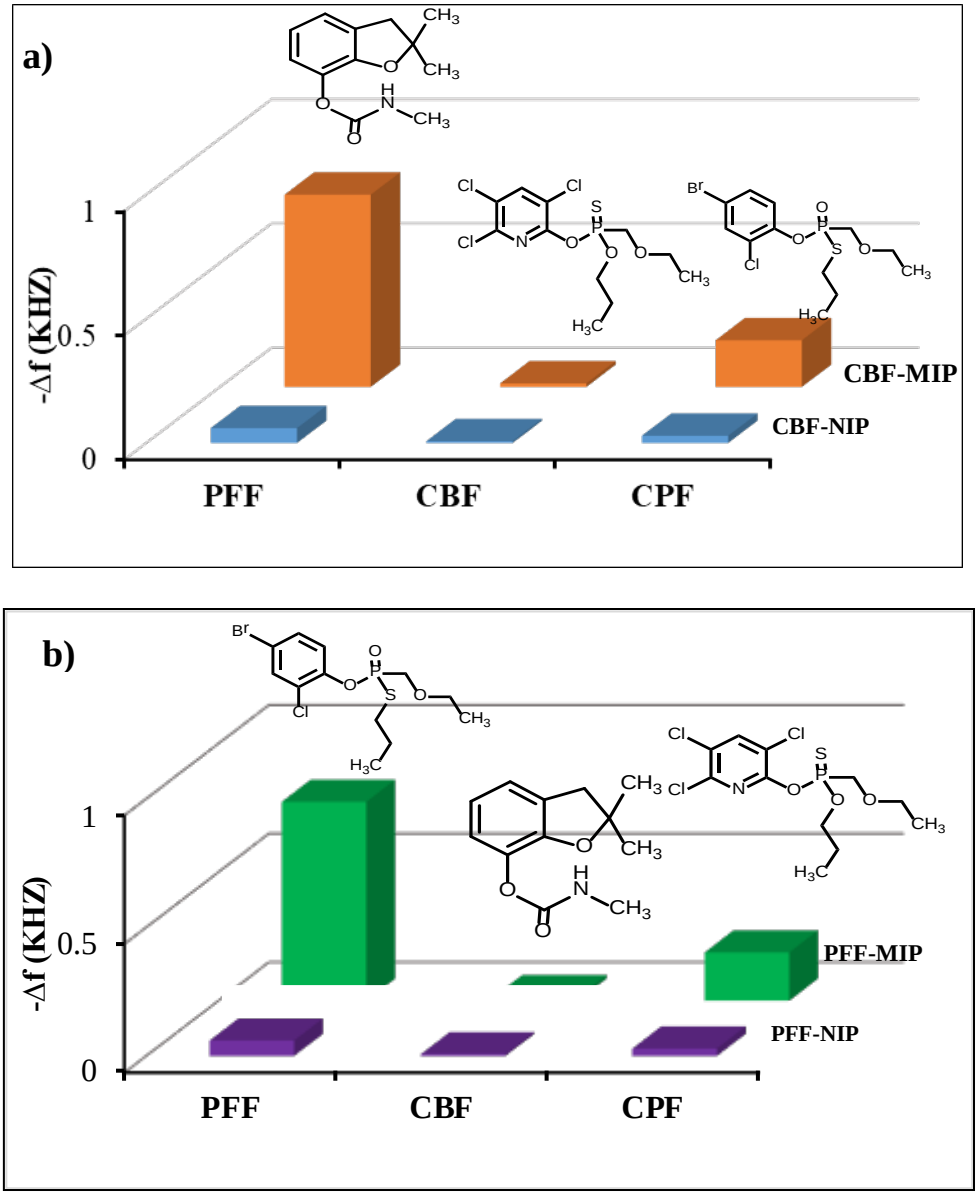


**Figure 4.26 Selectivity pattern of a) CBF-MIP and b) PFF-MIP, respectively, toward CBF, PFF and CPF at a concentration of 1000 µM**

Furthermore, the imprinting and selecting factors are defined as α and β shown Equation 3.2 and Equation 3.3. The results shown in Table 4.6. The calculated α of analyte (CBF for CBF-MIP and PFF for PFF-MIP) were in the range of 0.20 – 2.15. Obviously, α values obtained from CBF-MIP and PFF-MIP higher than that obtained from analogues. The calculated β values were 10.42 (CPF) and 6.78 (PFF) for CBF-MIP and 1.99 (CPF) and 6.50 (CBF) for PFF-MIP. These results

indicate that the QCM sensor using CBF-MIP and PFF-MIP as recognition elements have good and stable selectivity recognition to the target CBF and PFF, respectively. These behaviors explain that the specific complementary shape and size of binding sites in MIP layer were formed during the preparation process.

**Table 4.6 Selectivity of MIP sensor at 1000 µM of analyte and interferents.**

| substrate | ΔF MIP (%) | ΔF NIP (%) | α | β |
|---|---|---|---|---|
| **CBF-MIP** | | | | |
| CBF | 83.89 | 38.88 | 2.15 | 1 |
| CPF | 6.22 | 30.03 | 0.21 | 10.42 |
| PFF | 9.89 | 31.09 | 0.32 | 6.78 |
| **PFF-MIP** | | | | |
| PFF | 79.23 | 62.37 | 1.27 | 1 |
| CPF | 19.26 | 30.15 | 0.64 | 1.99 |
| CBF | 1.46 | 7.48 | 0.20 | 6.50 |

### 4.4.3 Reproducibility

The reproducibility of measurements for the CBF-MIP and PFF-MIP were evaluated by measuring of the frequency shift from CBF and PFF standards at the same concentration for 3 times. The calculated relative standard deviations (RSD) are 4.15% and 5.32 % for CBF-MIP and PFF-MIP, respectively. These results point out that our method provides satisfactorily reproducible signal.

# CHAPTER 5
# CONCLUSIONS

This work presented new electrochemical sensors based on nanocomposite and quartz crystal microbalance (QCM) using molecular imprinted polymer (MIP) modified electrode for diagonostic and food safety monitoring. These sensors were contained 2 parts including electrochemical sensor part and QCM part. Electrochemical sensor parts were based on chemical sensor and biosensor. Chemical sensor was developed for sensitive and selective dopamine (DA) and uric acid (UA) detection in the presence ascorbic acid (AA). Biosensor used sulfite oxidase enzyme (SOx) and nanocomposites was developed for the selective and effective determination of sulfite. The MIP-QCM part was developed using MIP for determination of carbofuran (CBF) and profenofos (PFF).

The chemical sensor with a new redox active ferrocence-based polyaniline and carbon nanotubes modified CPE covered with nafion (Nf/p(Fc-Ani)-CNTs/CPE) was presented for the determination of DA and UA in the presence AA. The nanocomposites were synthesized and characterized by scanning electron microscopy (SEM). The Nf/p(Fc-Ani)-CNTs/CPE was investigated using cyclic voltammetry (CV) and differenctial pulse voltammetry (DPV) in a 0.1 M of phosphate buffer (PBS). The oxidation peak of UA and DA was observed at +0.3 and +0.45 V, respectively. While the oxidation peak of AA does not appear. Therefore, this sensor can achieve quantitatively DA and UA determination in the presence of AA. Under the optimal condition (pH 5.0), peak currents of DA and UA obtained from DPV were increased relatively with increasing the concentrations of DA and UA. The linear relationship for DA is given over the range of 1-150 µM with slope of 0.041 $\mu M^{-1}$, while UA is exhibited linear calibration over the range of 5-250 µM with slope of 0.053 $\mu M^{-1}$. The limit of detection (LOD) were 0.21 and 0.58 (S/N=3) for DA and UA, respectively. The developed method was successfully applied to evaluate DA and UA content in pharmaceutical and urine samples. The Nf/p(Fc-Ani)-CNTs/CPE provides an acceptable selectivity, good reproducibility and high stability.

Biosensor was developed for amperometric determination of sulfite using a simple flow injection analysis (FIA) system. The developed electrode was constructed by immobilizing sulfite oxidase (SOx) onto $Fe_3O_4$@Au-Cys-FA surface using cysteine as a bi-functional linker for attachment to the gold surface via thiol group. Then, the amino-terminated from cysteine was conjugated to folic acid (FA) with an amide-linkage formation. The biosensor was prepared by thoroughly mixing 0.950 g of graphite powder, 0.035 g of $Fe_3O_4$@Au-Cys-FA and 0.015 g of PDMS in mortar and pestle. After that, these materials were heated at 60 ºC for 30 min. Then, SOx enzyme was immobilized by dropping 40 µL of SOx, containing cytochrome C as a mediator, onto the nanocomposite. Finally, 30 µL of mineral oil was added and mixed in mortar and pestle until homogeneous. These composite was packed into the end of glass tube and Teflon block for batch system and FIA system, respectively. The as-prepared $Fe_3O_4$@Au-Cys-FA nanocomposites were characterized by various techniques including transmission electron microscopy (TEM), scanning electron microscopy (SEM), energy Dispersive X-ray Spectrometer (EDS) and atomic force microscopy (AFM). The estimated apparent Michaelis–Menten constant ($K_m^{app}$) for SOx was 2.0 mg $L^{-1}$. The developed biosensor was applied in the FIA system for amperometric detection of sulfite using solution of 0.1 M phosphate buffer (pH 7.0) as a carrier and applied a potential of +0.35 V. The propsed biosensor exhibits linear calibration over the range of 0.1-200 mg $L^{-1}$ of sulfite with correlation coefficient of 0.998. The LOD ($3\sigma$) was 10 µg $L^{-1}$ and limit of quantification was 34 µg $L^{-1}$. The developed biosensor also provides good precision (RSD=3.1%) for sulfite signal (15 mg $L^{-1}$, n=20) with a rapid sample throughput (109 samples $h^{-1}$). Results from the storage stability of $Fe_3O_4$@Au-Cys-FA/CPE indicated the relative current response of 102% after stored for 2 weeks. This implied to stability of the developed biosensor. The method was successfully applied to evaluate sulfite content in wine and pickled food extracts with a good result.

The QCM sensor based MIP to enhance the selectivity of sensor was developed for CBF and PFF detection. The CBF-MIP and PFF-MIP were fabricated using MAA and PVP as the functional monomer, respectively. CBF-MIP was synthesized by dissolving of 15 µL of MAA, a functional monomer in 600 µL of DMSO in Eppendorf

tube. Then 25 µL of EGDMA, 2.4 mg of AIBN and 22.2 mg of CBF were added into the tube as a cross-linker, an initiator and a template, respectively. The mixture solution was continuously stirred in water bath at 70 °C until the gel point was reached. The NIP was prepared in the same way but without addition of CBF. After that, the 4 µL of the obtained CBF-MIP and NIP gel solution were dropped onto the surface of gold electrode and then the electrode was spin off at 2,000 rpm for 30 sec. Finally, the polymerization of QCM with MIP and NIP electrode was achieved by further exposing the electrode under 312 nm UV light for overnight. PFF-MIP was synthesized by adding of 59 mg of PVP and 41 mg of DPDI as a monomer, 8 mg of PG as a cross-linker, 10 mg of DPM as an initiator and 37.4 mg of profenofos as a template in 600 µL of THF in Eppendorf tube. The mixture solution was pre-polymerized by stirring in water bath at 75°C for 3 h. Then, the 500 µL of THF was immediately added in pre-polymer solution. The NIP was synthesized by using the same procedure but without the PFF template. The PFF-MIP and NIP solution were spin-coated onto each of a QCM electrode pair at 3,000 rpm for 1 min. The coated electrode was completely polymerized by drying in oven at 120 ºC for 10 min. Finally, the template (CBF and PFF) was removed by immersing the respective QCM into a mixture solution of methanol and acetic acid (9:1 %v/v) for 30 min followed by DI water for 30 min, respectively. FT-IR was used to confirm structure of MIP before and after remove template and NIP. The developed QCM sensor shows a linear range of 0.5-1,000 and 5-1,000 µM for CBF-MIP and PFF-MIP, respectively. The CBF-MIP and PFF-MIP detection limits are estimated to be 0.21 µM and 0.38 µM (S/N=3), respectively. The results from selectivity studies demonstrated that the CBF-MIP and PFF-MIP provides an acceptable selectivity for the determination of CBF and PFF, respectively.

# REFERENCES

# REFERENCES

[1] Sekhar, PK. and et al. "Chemical sensor for environmental monitoring and homeland security", **The Electrochemical Society Interface.** 19(4): 35-40; winter, 2010.

[2] Koyun, A, Ahlatcioglu, E, and Ipek, YK. (2012). "biosensors and their principles", **Biosensors.** https://pdfs.semanticscholar.org/f661/70f74da25527ba8ea91319b98913738f4a72.pdf. September 1, 2017.

[3] Paddle, BM. "Biosensors for chemical and biological agents of defense interest", **Biosensors and Bioelectronics**. 11(11): 1079-1113; 13 February, 1996.

[4] Adams, RN. "Carbon paste electrode", **Scientific Communications.** 30(9): 1576-1596; September, 1958.

[5] Foroughi, MM. and et al. "Electrochemical Determination of N-acetylcysteine and Folic Acid in Pharmaceutical and Biological Samples Using a Modified Carbon Nanotube Paste Electrode", **International Journal of electrochemical science.** 9(12): 8407-8421; 28 October, 2014.

[6] Adams, R. N. **Electrochemistry at Solid Electrodes.** New York: MARCEL DEKKER, INC, 1969.

[7] Peng, TZ, Li, HP, and Wang, SW. "Selective extraction and voltammetric determination of gold at a chemically modified carbon paste electrode", A**nalyst.** 118(10): 1321-1324; December, 1993.

[8] Pei, JH, Jin, Q, and Zhong, JY. "Potentiometric determination of trace silver based on the use of a carbon paste electrode", **Talanta.** 38(10): 1185-1189; October, 1991.

[9] Kalcher, K. "Sensors based on carbon paste in electrochemical analysis: a review with particular emphasis on the period 1990-1993", **Electroanalysis.** 7(1): 5-22; March, 1994.

[10] Sanghavi, B. J. and et al. "Nanomaterial-based electrochemical sensing of neurological drugs and neurotransmitters", **Microchimica Acta.** 182(1-2):1–41; 8 July, 2014.

# REFERENCES (CONTINUED)

[11] Sajid, M. and et al. "Chemically modified electrodes for electrochemical detection of dopamine in the presence of uric acid and ascorbic acid: A review", **Trends in Analytical Chemistry.** 76: 15-29; October, 2016.

[12] Janáky, C. and Visy, C. "Conducting polymer-based hybrid assemblies for electrochemical sensing: a materials science perspective", **Analytical and Bioanalytical Chemistry.** 405(11): 3489–3511; 23 January, 2013.

[13] Han H.S. and et al. "Electrochemical oxidation and determination of dopamine in the presence of AA using ferulic acid functionalized electrochemically reduced grapheme", **Sensors and Actuators B: chemical.** 204: 289-296; 1 December, 2014.

[14] Liu, A, Honma, I, and Zhou H. "Amperometric biosensor based on tyrosinase-conjugated polysaccharide hybrid film: Selective determination of nanomolar neurotransmitters metabolite of 3,4-dihydroxyphenylacetic acid (DOPAC) in biological fluid", **Biosensors and Bioelectronics.** 21(5): 809–816; 5 November, 2005.

[15] Mo, JW. and Ogorevc, B. "Simultaneous measurement of dopamine and ascorbate at their physiological levels using voltammetric microprobe based on overoxidized poly(1,2-phenylenediamine)-coated carbon fiber", **Analytical Chemistry Laboratory.** 73(6): 1196-1202; 15 March, 2001.

[16] Ardakani, MM. and et al. "Electrochemical and catalytic investigations of dopamine and uric acid by modified carbon nanotube paste electrode", **Bioelectrochemistry.** 75(1): 1-8; November, 2008.

[17] Lijima, S. "Helical microtubules of graphitic carbon", **Letter of Nature.** 354: 56; 7 November, 1991.

[18] Merkoci, A. and et al. "New materials for electrochemical sensing VI: Carbon nanotubes", **Trends in Analytical Chemistry.** 24(9): 826-838; October, 2005.

# REFERENCES (CONTINUED)

[19] Nessim, GD. "Properties, synthesis, and growth mechanisms of carbon nanotubes with special focus on thermal chemical vapor deposition", **Nanoscale.** 2(8): 1306-1323; March, 2010.

[20] Salimi, A. and et al. "Modification of glassy carbon electrode with multi-walled carbon nanotubes and iron(III)-porphyrin film: Application to chlorate, bromate and iodate detection", **Electrochimica Acta.** 52(20): 6097–6105; 10 June, 2007.

[21] Manjunatha, JG. And et al. "Sodium dodecyl sulfate modified carbon nanotubes paste electrode as a novel sensor for the simultaneous determination of dopamine, ascorbic acid, and uric acid", **Comptes Rendus Chimie.** 17(5): 465-476; May, 2014.

[22] Jacobs, CB, Peairs, MJ, and Venton, BJ. "Review: Carbon nanotube based electrochemical sensors for biomolecules", **Analytica Chimica Acta.** 662(2): 105-127; 10 March, 2010.

[23] Ren, X. and et al. "Carbon nanotubes as adsorbents in environmental pollution management: A review", **Chemical Engineering Journal.** 170(2-3): 395-410, 1 June, 2011.

[24] Gopalan, AI. and et al. "A novel multi component redox polymer nanobead based high performance non-enzymatic glucose sensor", **Biosensors and Bioelectronics.** 84: 53-63; 15 October, 2015.

[25] Raoof, JB, Ojani, R, abd Baghayeri, M. "Simultaneous electrochemical determination of glutathione and tryptophan on a nano-$TiO_2$/ferrocene carboxylic acid modified carbon paste electrode", **Sensors and Actuators B: Chemical.** 143(1): 261-269; 4 December, 2009.

[26] Cheng, H. and et al. "Investigation of the electrochemical behavior of dopamine at electrodes modified with ferrocene-filled double-walled carbon nanotubes", **Electrochimica Acta.** 63: 83-88; 29 February, 2012.

# REFERENCES (CONTINUED)

[27] Raoof, J-B., Ojani, R. and Kiani, A. "Carbon paste electrode spiked with ferrocene carboxylic acid and its application to the electrocatalytic determination of ascorbic acid", **Journal of Electroanalytical Chemistry.** 515(1-2): 45-51; 30 November, 2001.

[28] Neuse, E.W. "Synthetic polymers as drug-delivery vehicles in medicine", **Metal-based Drugs.** 2008: 1-19; October, 2007.

[29] Satienperakul, S, Phongdong, P, and Liawruangrath, S. "Pervaporation flow injection analysis for the determination of sulphite in food samples utilising potassium permanganate–rhodamine B chemiluminescence detection**", Food Chemistry.** 121(3): 893–898; 1 August, 2010.

[30] Ummihan, T, and Somer, G. "Determination of trace sulfite by direct and indirect methods using differential pulse polarography", **Analytica Chimica Acta.** 603(1): 30-35; 5 November, 2007.

[31] Dadamos, TRL, and Teixeira, MFS. "Electrochemical sensor for sulfite determination based on a nanostructured copper-salen film modified electrode", **Electrochimica Acta.** 54(19): 4552-4558; 30 July, 2009.

[32] Hassan, SSM, Hamza, MSA, and Mohamed, AHK. "A novel spectrophotometric method for batch and flow injection determination of sulfite in beverages", **Analytica Chimica Acta.** 570(2): 232-239; 16 June, 2006.

[33] Salihov, SV. and et al. "Recent advances in the synthesis of $Fe_3O_4$@AU core/shell nanoparticles", **Journal of Magnetism and Magnetic Materials.** 394: 173-178; 15 November, 2015.

[34] Wu, W., He, Q., and Jiang, C. "Magnetic iron oxide nanoparticles: Synthesis and surface functionalization strategies", **Nanoscale Research Letters.** 3(11): 397-415; 2 October, 2008.

[35] Spricigo, R. and et al. "Electrocatalytic sulfite biosensor with human sulfite oxidase co-immobilized with cytochrome c in a polyelectrolyte-containing multilayer", **Analytical and Bioanalytical Chemistry.** 393(1): 225–233; 21 October, 2008.

# REFERENCES (CONTINUED)

[36] Abass, AK, Hart, JP, and Cowell, D. "Development of an amperometric sulfite biosensor based on sulfite oxidase with cytochrome c, as electron acceptor, and a screen-printed transducer", **Sensors and Actuators B: Chemical.** 62(2): 148–153; 25 February, 2000.

[37] Tian, X. and et al. "Simultaneous determination of l-ascorbic acid, dopamine and uric acid with gold nanoparticles-β-cyclodextrin–graphene-modified electrode by square wave voltammetry", **Talanta.** 93: 79–85; 15 May, 2012.

[38] Andrade, CAS. and et al. "Biosensors for Detection of Low-Density Lipoprotein and its Modified Forms Biosensors for Health", **Environment and Biosecurity.** 9: 215-240; 19 July, 2011.

[39] Robles, I. and et al. "Electrochemical Detection of Mercury Removal from Polluted Bentonite and Quartz using Different Removing Agents", **International Journal of Electrochemistry.** 13: 379-396; 26 March, 2014.

[40] Theveno, DR. and et al. "Electrochemical biosensors: recommended definitions and classification", **Biosensors and Bioelectronics.** 16(1-2): 121–131; January, 2001.

[41] Cardosi, MF. "Glucose Measurement", **Encyclopedia of Analytical Chemistry.** 10(1): 1-12; 15 September, 2006.

[42] Siangproh, W. and et al. "Electrochemical Detection for Flow-based System: A Review", **Journal of Flow Injection Analysis.** 26(1): 5–25; 15 August, 2009.

[43] Kotova, K. and et al. "MIP sensors on the way to biotech applications: Targeting selectivity", **Sensors and Actuator B.** 189: 199-202; December, 2013.

[44] Diltemiz, SE. and et al. "Designing of MIP based QCM sensor having thymine recognition sites based on biomimicking DNA approach", **Biosensors and Bioelectronics.** 25(3): 599-603; 15 November, 2009.

# REFERENCES (CONTINUED)

[45] Figueiredo, L. and et al. "Applications of molecularly imprinted polymers to the analysis and removal of personal care products: A review", **Talanta.** 146: 754-765; 1 January, 2016.

[46] Vasapollo, G and et al. "Molecularly Imprinted Polymers: Present and Future Prospective", **International Journal of Molecular Sciences.** 12(2): 5908-5945; 14 September, 2011.

[47] Özkütük, E.B. and et al. "Paraoxon imprinted biopolymer based QCM sensor", **Materials Chemistry and Physics.** 139(1): 107-112; 15 April, 2013.

[48] Gamry instrument. <www.gamry.com/application-notes/physechem/basics-of-a-quartz-crystal-microbalance/> **Basics of a quartz crystal microbalance.** 2018.

[49] Johannsmann, D. "Viscoelastic, mechanical, and dielectric measurements on complex samples with the quartz crystal microbalance", **Physical Chemistry Chemical Physics.** 10: 4516-4534; 7 June, 2008.

[50] March, C. and et al. "High-frequency phase shift measurement greatly enhances the sensitivity of QCM immunosensors", **Biosensors and Bioelectronics.** 65: 1-8; 15 March, 2015.

[51] Britto, PJ, Santhanam, KSV, and Ajayan, PM. "Carbon nanotube electrode for oxidation of dopamine", **Bioelectrochemistry and Bioenergetics.** 41(1): 121-125; October, 1996.

[52] Wang, HS. and et al. "Highly selective and sensitive determination of dopamine using a Nafion/carbon nanotubes coated poly (3-methylthiophene) modified electrode", **Biosensors and Bioelectronics.** 22(5): 664-669; 15 December, 2006.

[53] Beitollahi, H. and et al. "Novel 2,2-[1,2-ethanediylbis (nitriloethylidyne)]-bis-hydroquinone double-wall carbon nanotube paste electrode for simultaneous determination of epinephrine, uric acid and folic acid", **Biosensors and Bioelectronics.** 24(3): 362-368; 15 November, 2008.

# REFERENCES (CONTINUED)

[54] Savage, D. and et al. "The synthesis and structural characterization of novel N-meta-ferrocenyl benzoyl dipeptide esters", **Inorganic Chemistry Communications.** 9(12): 152-155; December, 2005.

[55] Chaicharoenwimolkul, L. and et al. "Effect of Ferrocene Substituents and Ferricinium Additive on the Properties of Polyaniline Derivatives and Catalytic Activities of Palladium-Doped Poly(m-ferrocenylaniline)-Catalyzed Suzuki–Miyaura Cross-Coupling Reactions", **Journals of Applied Polymer Science.** 130(3): 1489-1497; 29 April, 2013.

[56] Amatatongchai, M. and et al. "Simple flow injection for determination of sulfite by amperometric detection using glassy carbon electrode modified with carbon nanotube-PDDA-gold nanoparticles", **Talanta.** 133: 134-141; July, 2015.

[57] Rawal, R. and et al. "Development of an amperometric sulfite biosensor based on a gold nanoparticles/chitosan/multiwalled carbon nanotubes/polyaniline-modified gold electrode", **Analytical and Bioanalytical Chemistry.** 401(8): 196–204; November, 2011.

[58] Kim, DK. and et al. "Synthesis and characterization of surfactant-coated superparamagnetic monodispersed iron oxide nanoparticles", **Journal of Magnetism and Magnetic Materials.** 225(1-2): 30-36; January, 2001.

[59] Wei, X. and et al. "A magnetic-controlled amperometric biosensor based on composite bio-particulates $Fe_3O_4$ and nano-Au with the signal enhancement by increasing loading of horseradish peroxidase", **International Journal of Electrochemical Science.** 6(10): 4653-4966; October, 2011.

[60] Rawal, R, Chawla, S, and Pundir, CS. "An electrochemical sulfite biosensor based on gold coated magnetic nanoparticles modified gold electrode", **Biosensors and Bioelectronics.** 31(1): 144–150; 15 June, 2012.

[61] Qiu, J-Q. and et al. "Synthesis and characterization of ferrocene modified $Fe_3O_4$@Au magnetic nanoparticles and its application", **Biosensors and Bioelectronics.** 24(8): 2649–2653; 15 April, 2009.

# REFERENCES (CONTINUED)

[62] Karamipour, Sh, Sadjadi, MS, and Farhadyar, N. "Fabrication and spectroscopic studies of folic acid-conjugated $Fe_3O_4$@Au core-shell for targeted drug delivery application", **Spectrochimica Acta Part A: Molecular and Biomolecular Spectroscopy.** 148: 146-155; 5 September, 2015.

[63] Amatatongchai, M. and et al. "Amperometric flow injection analysis of glucose using immobilized glucose oxidase on nano-composite carbon nanotubes-platinum nanoparticles carbon paste electrode", **Talanta.** 166: 420-427; 1 May, 2017.

[64] Findeisen, A. and et al. "Artificial receptor layer for detecting chemical and biological agent mimics", **Sensors and Actuators B: Chemical.** 170: 196-200; 31 July, 2012.

[65] Gao, N. and et al. "Delvelopment of molecularly imprinted polymer films used for detection of profenofos based on a quartz crystal microbalance sensor", **Analyts.** 137(5): 1252-1258; 7 March, 2012.

[66] Fan, J-P. and et al. "Preparation and characterization of molecular imprinted polymer functionalized with core/shell magnetic particles ($Fe_3O_4$@$SiO_2$@MIP) for the simultaneous recognition and enrichment to four toxoids in Taxus x media", **Chemical Engineering Journal.** 279: 567-577; May, 2015.

[67] Chairam, S. and et al. "Nonenzymatic sensor for hydrogen peroxide using a carbon paste electrode modified with a composite consisting of silver nanoparticles, poly(o-aminobenzoic acid) and magnetite", **International Journal of Electrochemical Science.** 10(6): 4611-4625; 28 April, 2015.

[68] Kouassi, KG, Irudayaraj, J, and McCarthy, G. "Examination of cholesterol oxidase attachment to magnetic nanoparticles", **Journal of Nanobiotechnology.** 3(1): 1-9; 20 January, 2005.

[69] Tamer, U. and et al. "Synthesis of magnetic core-shell $Fe_3O_4$@Au nanoparticles for biomolecules immobilization and detection", **Journal of Nanoparticle Research.** 12(4): 1187-1196; 17 September, 2009.

# REFERENCES (CONTINUED)

[70] Alamo, LST, Tangkuaram, T, and Satienperakul, S. "Determination of sulfite by pervaporation-flow injection with amperometric detection using copper haxacyanoferrate-carbon nanotube modified carbon paste electrode", **Talanta.** 81(4-5): 1793–1799; June, 2010.

[71] Tan, X. and et al. "Electrochemical sensor based on molecularly imprinted polymer reduced graphene oxide and gold nanoparticles modified electrode for detection of carbofuran", **Sensor and Actuators, B.** 220: 216-221; 1 December, 2015.

[72] Bini, RA. and et al. "Synthesis and functionalization of magnetite nanoparticles with different amino-functional alkoxysilanes", **Journal of Magnetism and Magnetic Materials.** 324(4): 534–539; February, 2012.

[73] Jiang, QL. and et al. "Folic acidconjugated $Fe_3O_4$ magnetic nanoparticles for hyperthermia and MRI in vitro and in vivo", **Applied Surface Science.** 307: 224-233; 15 July, 2014.

[74] Casella, IG. and Marchese, R. "Sulfite oxidation at a platinum glassy carbon electrode. Determination of sulfite by ion exclusion chromatography with amperometric detection", **Analytical Chimica Acta.** 311(2): 199-210, 31 July, 1995.

[75] Phan, NVH, Sussitz, HF, and Liberzeite, PA. "Polymerization Parameters Influencing the QCM Response Characteristics of BSA MIP", **Biosensors.** 4(2): 161-171; 16 January, 2014.

[76] Hussain, M, Iqbal, N and Lieberzeit, PA. "Acidic and basic polymers for molecularly imprinted folic acid sensors-QCM studies with thin films and nanoparticles", **Sensors and Actuators B: Chemical.** 176: 1090-1095; January, 2013.

[77] Barbara H. Stuart. **Infrared Spectroscopy: Fundamentals and Applications.** Australia: John Wiley & Sons, Ltd, 2004.

# REFERENCES (CONTINUED)

[78] Khalifa, ME. and et al. "Extractive separation of profenofos as an organophosphorous insecticide from wastewater and plant samples using molecular imprinted cellulose", **Journal of Environmental Chemical Engineering.** 5(4): 3447–3454; August, 2017.

[79] Barsan, MM. and et al. "Electrochemical sensors and biosensors based on redox polymer/carbon nanotube modified electrodes: a review", **Analytica Chimica Acta.** 881: 1–23; 30 June, 2015.

[80] Zen, J–M and Hsu, C-T. "A selective voltammetric method for uric acid detection at Nafon®-coated carbon paste electrode", **Talanta.** 46(6): 1363-1369; August, 1998.

[81] Chen, M and et al. "Fabrication of GNPs/CDSH-Fc/nafion modified electrode for the detection of dopamine in the presence of ascorbic acid", Materials **Science and Engineering: C.** 31(7): 1271-1277; 10 October, 2011.

[82] Quan, DP. and et al. "Electrochemically selective determination of dopamine in the presence of ascorbic and uric acids on the surface of the modified Nafion/single wall carbon nanotube/poly(3-methylthiophene) glassy carbon electrodes", **Colloids and Surfaces B: Biointerfaces.** 88: 764–770; 1 December, 2011.

[83] Jiao, S and et al. "Fabrication of Fc–SWNTs modified glassy carbon electrode for selective and sensitive determination of dopamine in the presence of AA and UA", **Electrochimica Acta.** 52(19): 5939–5944; 25 May, 2007.

[84] Rawal, R. and Pundir, CS. "Development of an amperometric sulfite biosensor based on SOx/PBNPs/PPY modified ITO electrode", **International Journal of Biological Macromolecules.** 51(4): 449–455; November, 2012.

[85] Zeng, T. and et al. "Effective Electrochemistry of Human Sulfite Oxidase Immobilized on Quantum-Dots-Modified Indium Tin Oxide Electrode", **Applied Materials & Interfaces.** 7: 21487−21494; September, 2015.

# REFERENCES (CONTINUED)

[86] Dinckaya, E. and et al. "Sulfite determination using sulfite oxidase biosensor based glassy carbon electrode coated with thin mercury film", **Food Chemistry.** 101(4): 1540–1544; 3 April, 2006.

[87] Frasca, S. and et al. "Human sulfite oxidase electrochemistry on gold nanoparticles modified electrode", **Bioelectrochemistry.** 87: 33–41; December, 2011.

[88] Sartori, ER, Vicentini, FC. and Fatibello-Filho, O. "Indirect determination of sulfite using a polyphenol oxidase biosensor based on a glassy carbon electrode modified with multi-walled carbon nanotubes and gold nanoparticles within a poly(allylaminehydrochloride) film", **Talanta.** 87: 235-242; 15 December, 2011.

[89] Sameenoi, Y. and et al. "Poly(dimethylsiloxane) cross-linked carbon paste electrodes for microfluidic electrochemical sensing", **Analyst.** 136: 3177-3184; August, 2011.

[90] Wang, J. and et al. "Oxygen-independent poly(dimethylsiloxane)-based carbon-paste glucose biosensors", **Biosensors and Bioelectronics.** 17(11-12): 999-1003; March, 2002.

[91] Robb, WL. "Thin silicone membranes-their permeation properties and some applications", **Annals of the New York Academy of Sciences.** 146: 119-137; January, 1968.

[92] Rattanarat, P. and et al. "An electrochemical compact disk-type-microfluidics platform for use as an enzymatic biosensor", **Electroanalysis.** 27(3): 703-712; March, 2015.

[93] Molinero-Abad, B. and et al. "Sulfite oxidase biosensor based on tetrathiafulva-lene modified screen-printed electrode for sulfite determination in wine", **Analytica Chimica Acta.** 812: 41-44; 17 February, 2014.

[94] BRITISH STANDARD ISo 11843. **Capability of Detection, PartI/II.** United Kingdom: British Standards Institution, 2000.

# REFERENCES (CONTINUED)

[95] Miller, J.N. and Miller, J.C. **Statistics and Chemometrics for Analytical Chemistry.** England: Pearson/Prentice Hall, 2005.

[96] Pan, M. and et al. "Reproducible molecularly imprinted QCM sensor for accurate, stable, and sensitive detection of enrofloxacin residue in animal-derived foods", **Food Analytical Methods.** 11(2): 495–503; February, 2018.

[97] Bayramoglu, G. and Arica, MY. "Development of a sensitive method for selection of affinity ligan for typsin using quartz crystal microbalance sensor", **Bioprocess and Biosystems Engineering.** 35(3): 423-431; March, 2012.

[98] Wang, Z. and et al. "Investigation of the factors affecting the carbohydrate-lectin interaction by ITC and QCM-D", **Colloid and Polymer Science.** 292: 391-398; February, 2014.

# APPENDICES

# APPENDIX A

## Chemical sensor for DA and UA detection

**Effect of inference (raw data for Table 4.1)**

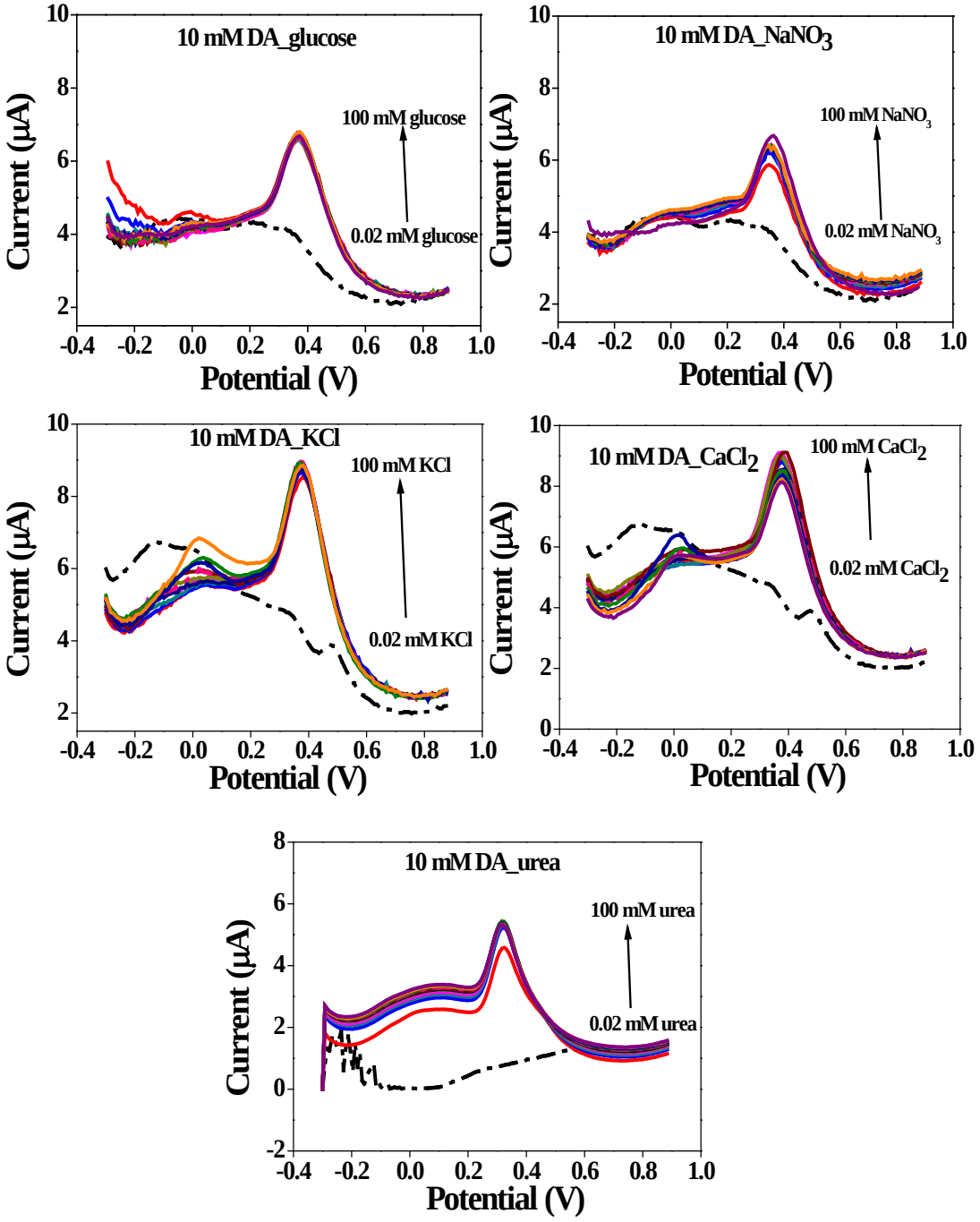


**Figure A.1 Difference pulse voltamogram of the interference on the Nf/p(AniFc)-CNTs/CPE**

**Effect of inference (raw data for Table 4.1) (Continuted)**

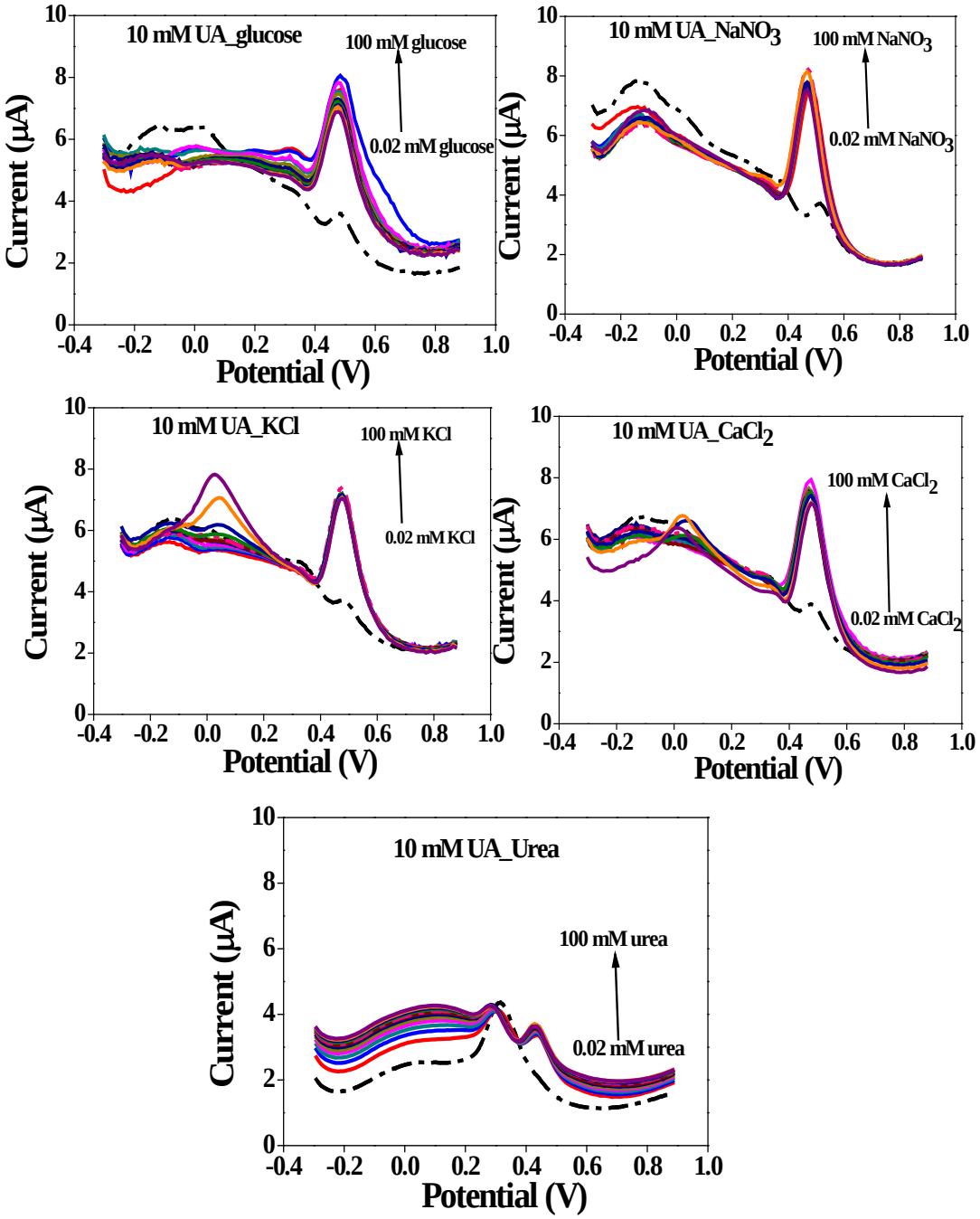


**Figure A.1 Difference pulse voltamogram of the interference on the Nf/p(AniFc)-CNTs/CPE**

**Example of signal obtained from dopamine determination (raw data for Table 4.2)**

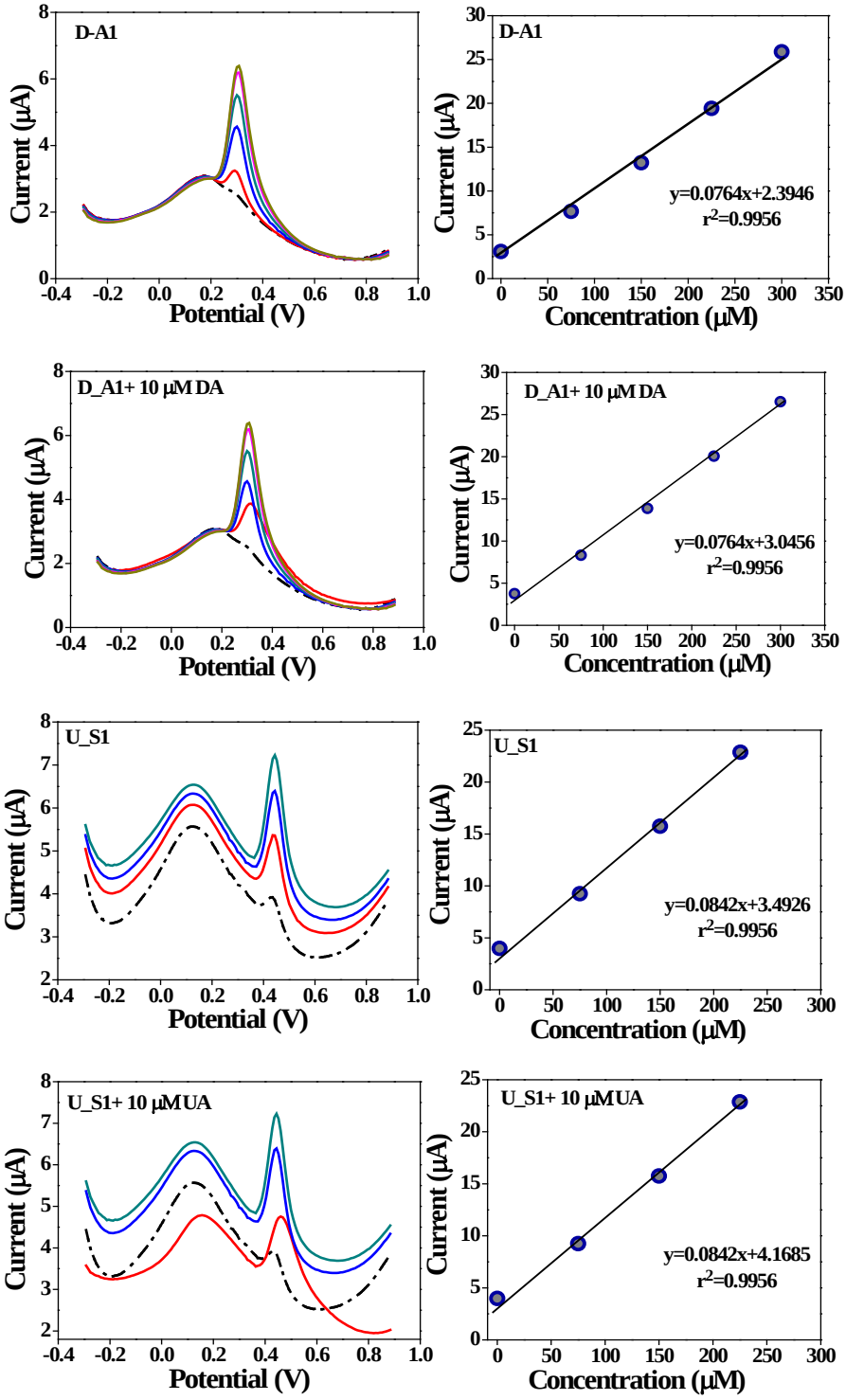


**Figure A.2 Difference pulse voltammogram and linear calibration plot of anodic current versus dopamine concentration**

# APPENDICES B

## Biosensor for sulfite detection

**Stability study of sulfite detection (raw data for Figure 4.18)**

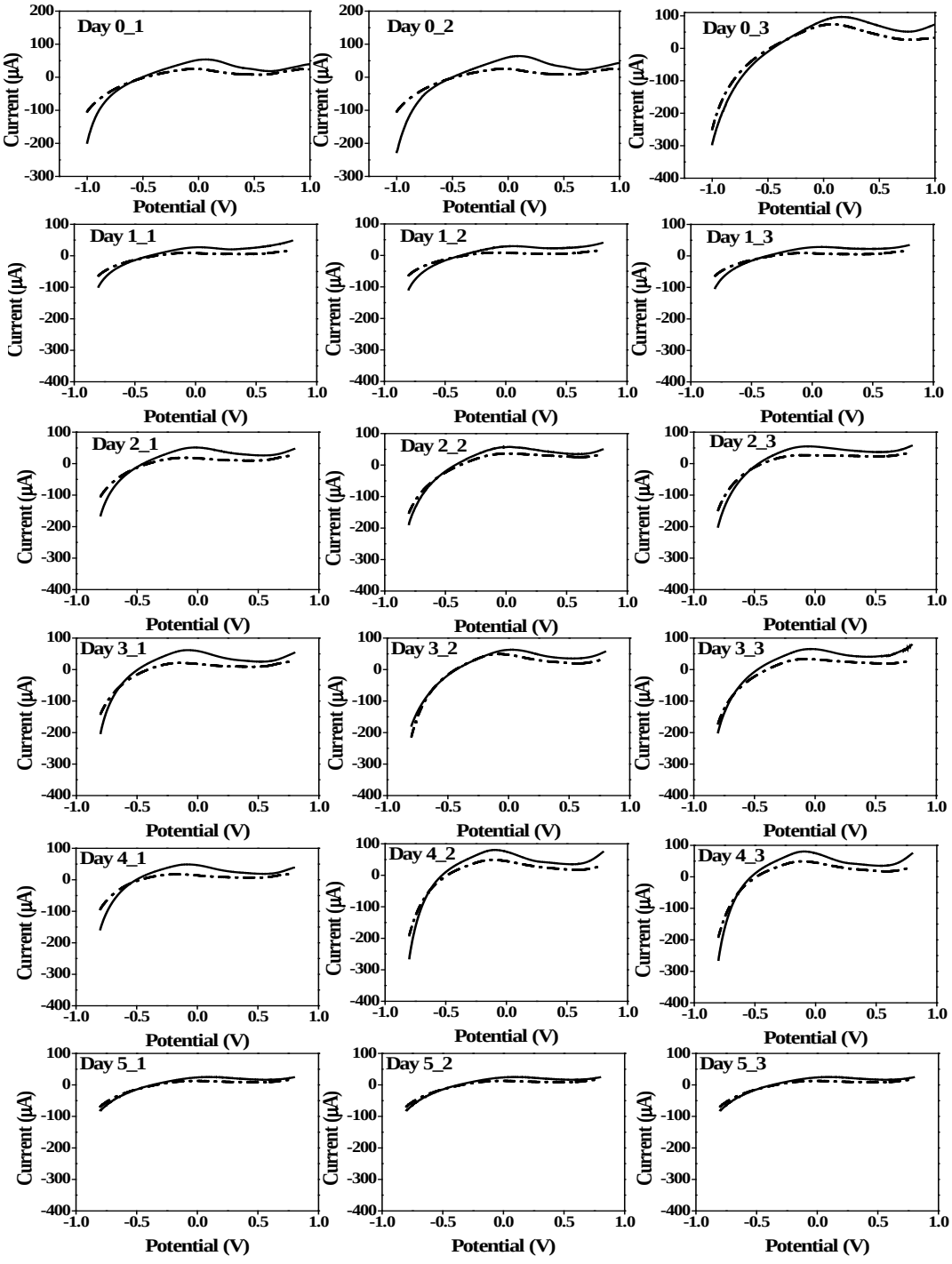


**Figure B.1 The storage stability of the developed sulfite detection calculated from response 10 mg $L^{-1}$ sulfite in 0.1 M PBS (pH 7.0)**

**Stability study of sulfite detection (raw data for Figure 4.18) (continued)**

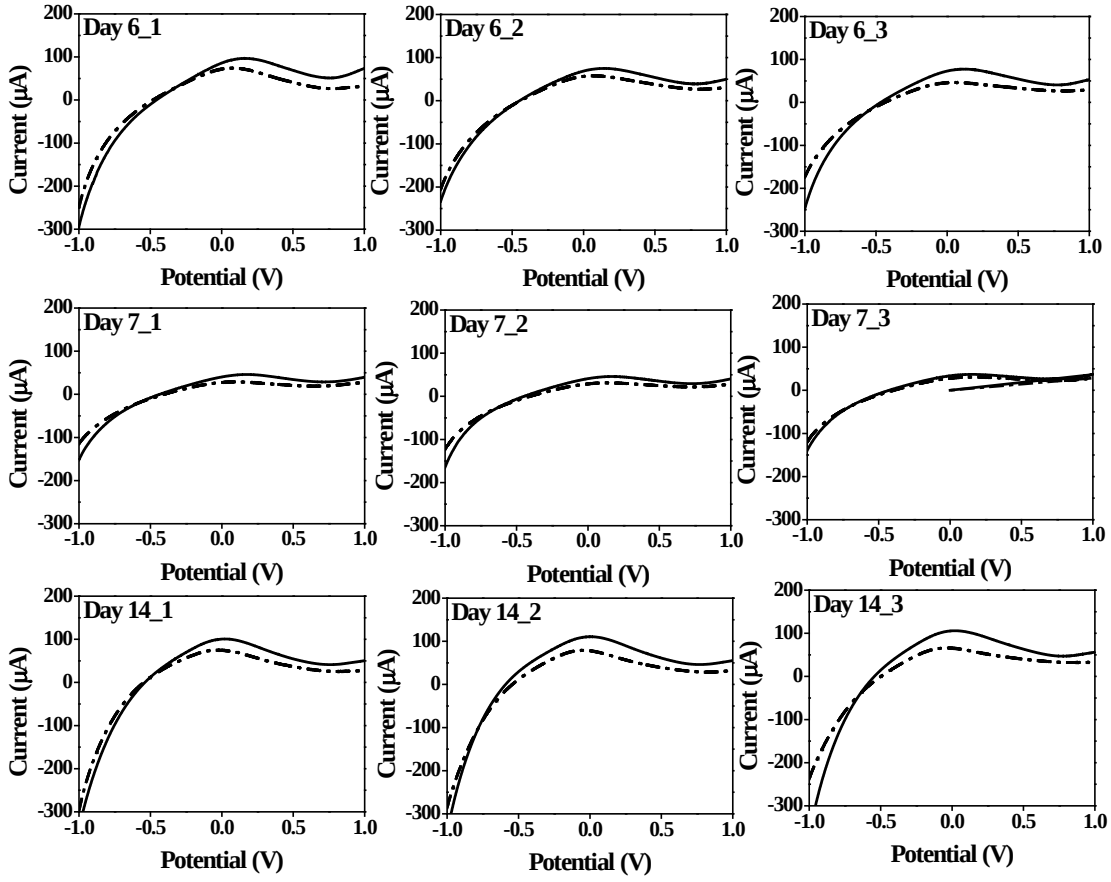


**Figure B.1 The storage stability of the developed sulfite detection calculated from response 10 mg $L^{-1}$ sulfite in 0.1 M PBS (pH 7.0)**

**Optimum potential (raw data for Figure 4.20)**

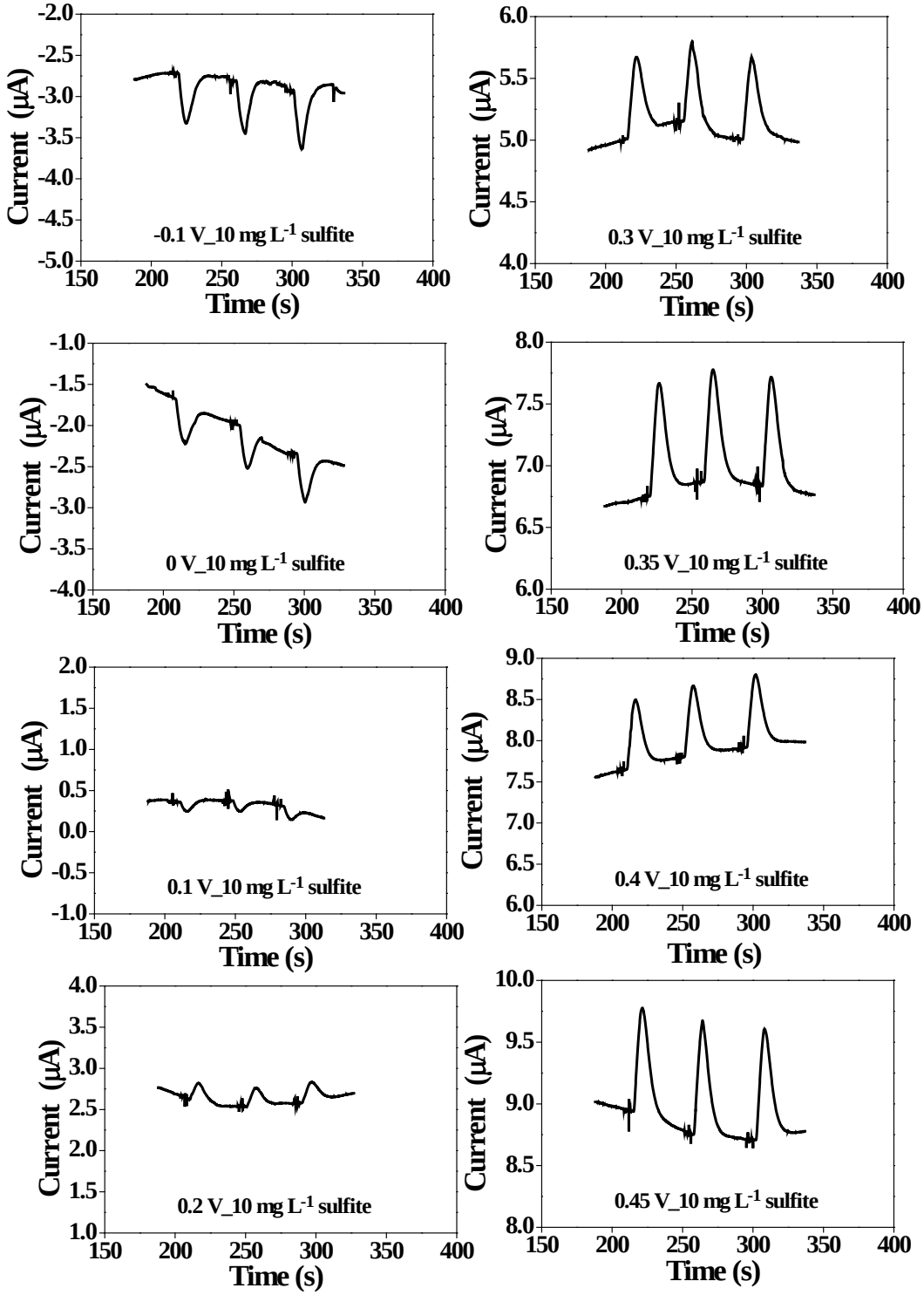


**Figure B.2 FIA gram of the applied potential on the biosensor response; 10 mg $L^{-1}$ sulfite, flow rate 1.0 mL $min^{-1}$**

**Optimum potential (raw data for Figure 4.20) (continued)**

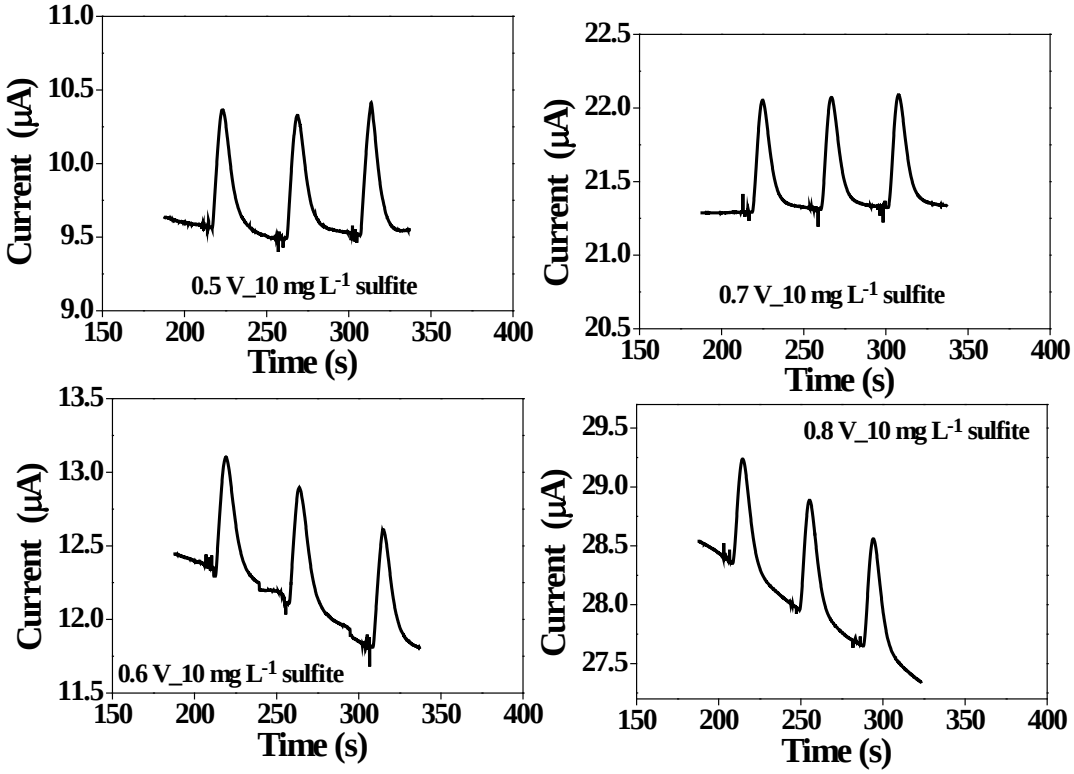


**Figure B.2 FIA gram of the applied potential on the biosensor response; 10 mg $L^{-1}$ sulfite, flow rate 1.0 mL $min^{-1}$**

**Optimum flow rate (raw data for Figure 4.21)**

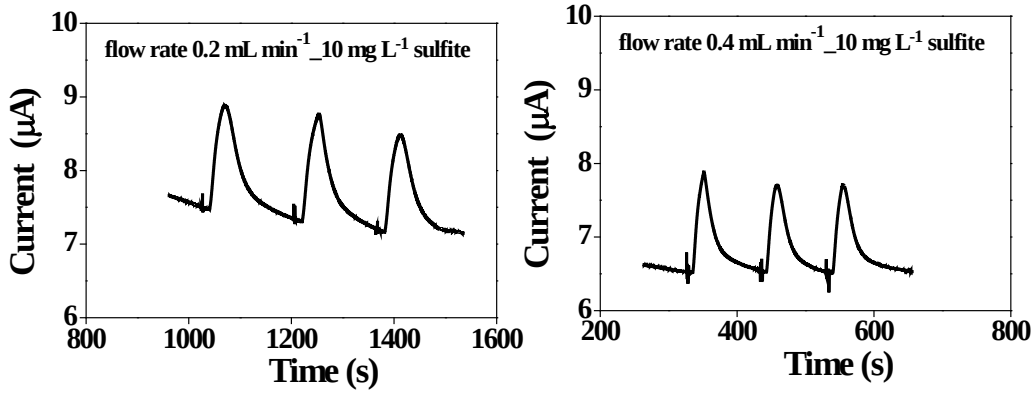


**Figure B.3 FIA gram of the applied potential on the biosensor response; 10 mg $L^{-1}$ sulfite at +0.35 V**

**Optimum flow rate (raw data for Figure 4.21) (continued)**

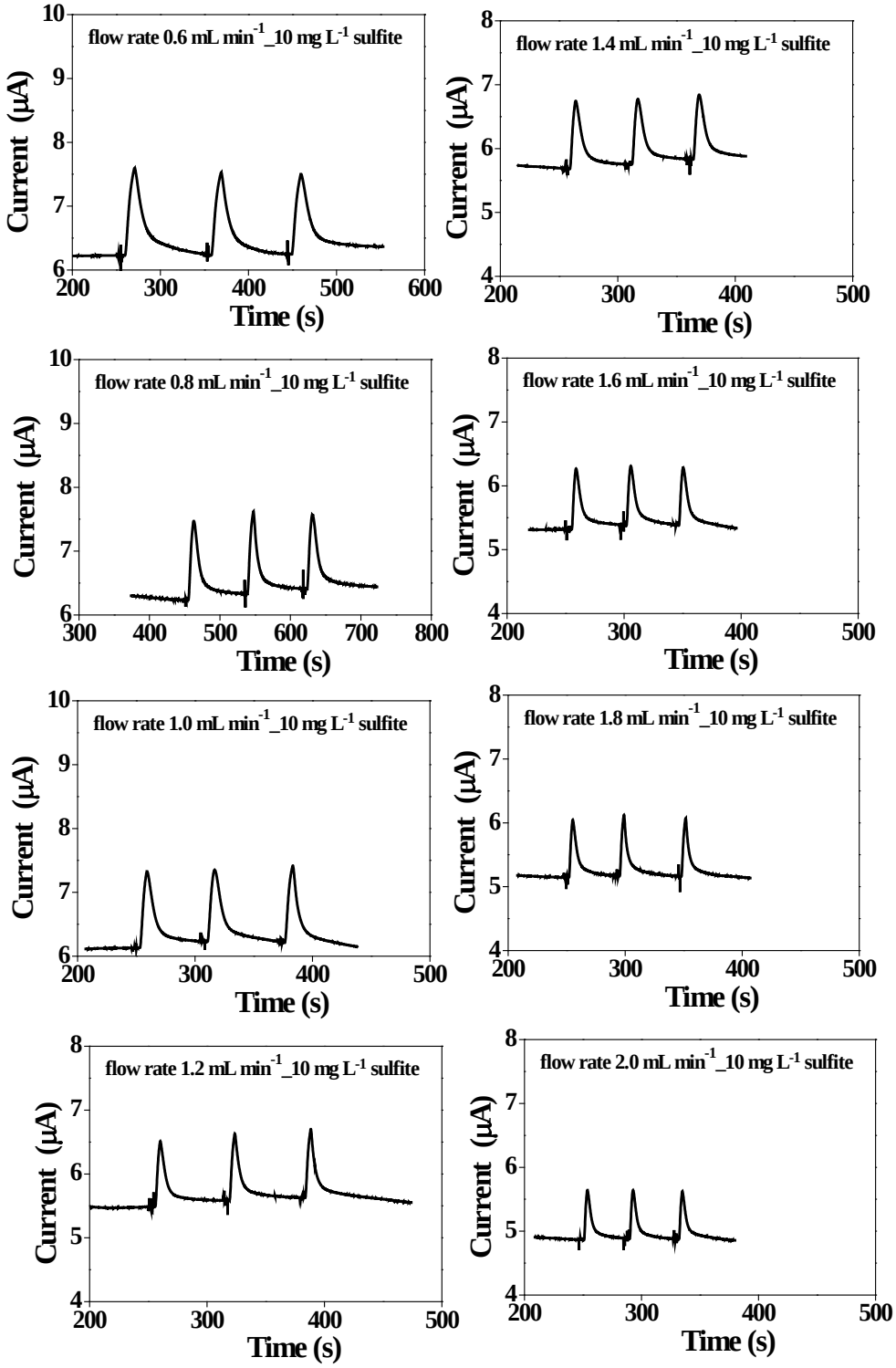


**Figure B.3 FIA gram of the applied potential on the biosensor response; 10 mg $L^{-1}$ sulfite at +0.35 V**

**Example of FIA grams obtained from sulfite determination with the developed biosensor (raw data for Table 4.4)**

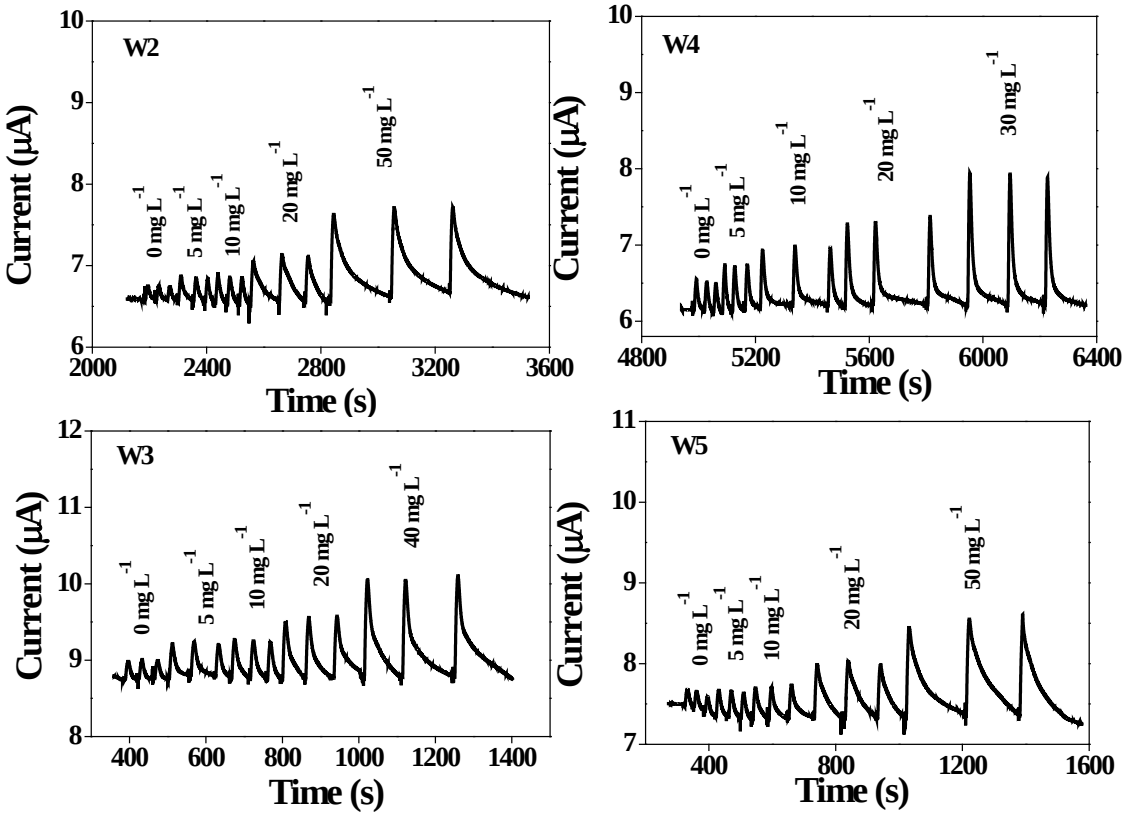


**Figure B.4 FIA gram of sample on the developed biosensor at +0.35 V, flow rate 0.8 mL min$^{-1}$**

# APPENDICES C
# CONFERENCES

# CONFERENCES

**Poster presentation**

1. Wongduan Sroysee, Sanoe Chairam, Maliwan Amatatongchai, Purim Jarujamrus, Suparb Tamuang. Poly(m-ferrocenylaniline)-multiwalled carbon nanotubes modified carbon paste electrode covered with nafion film for selective and sensitive determination of dopamine and uric acid in the presence of ascorbic acid, PURE AND APPLIED CHEMISTRY INTERNATIONAL CONFERENCE, 9-11 February 2016, Bangkok International Trade and Exhibition Centre, Bangkok, Thailand.

2. Wongduan Sroysee, Nongyao Nontavong, Sanoe Chairam, Purim Jarujamrus, Suparb Tamuang, Maliwan Amatatongchai. Sensitive and selective colorimetric assay of sulfite in food using sulfite oxidase immobilized on magnetite-gold-folate nanoparticles, The 3rd International Congress on Advanced Materials (AM2016), 27-30 November 2016, Chulalongkorn University, Thailand.

3. Wongduan Sroysee, Suticha Chanta, Maliwan Amatatongchai, Peter A. Liberzeit. Molecular imprinted polymer for carbofuran detection. PURE AND APPLIED CHEMISTRY INTERNATIONAL CONFERENCE, 7-9 February, 2018, Hai Yai, Songkhla, Thailand

**Publications**

1. Wongduan Sroysee, Sanoe Chairam, Maliwan Amatatongchai, Purim Jarujamrus, Suparb Tamuang, Saichol Pimmongkol, Laksamee Chaicharoenwimolkul, Ekasith Somsook. Poly(m-ferrocenylaniline) modified carbon nanotubes-paste electrode encapsulated in nafion film for selective and sensitive determination of dopamine and uric acid in the presence of ascorbic acid. Journal of Saudi Chemical Society, Volume 22, Issue 2, February 2018, Pages 173-182.

2. Wongduan Sroysee, Kitayanan Ponlakhet, Sanoe Chairam, Purim Jarujamrus, Maliwan Amatatongchai. A sensitive and selective on-line amperometric sulfite biosensor using sulfite oxidase immobilized on a magnetite-gold-folate nanocomposite modified carbon-paste electrode, Talanta, Volumes 156–157, 15 August 2016, Pages 154-162.

PACCON 2016
Pure and Applied Chemistry International Conference

'THAILAND: One Hundred Years of Advancement in Chemistry' 100 Years

9 - 11 February 2016
BITEC, Bangkok, Thailand

# Poly(*m*-ferrocenylaniline)-MWCNTs modified carbon paste electrode covered with nafion film for selective and sensitive determination of dopamine and uric acid in the presence of ascorbic acid

Wongduan Sroysee, Sanoe Chairam*, Maliwan Amatatongchai, Purim **Jarujamrus**, Suparb Tamuang

*Dept of Chemistry and Center of Excellence for Innovation in Chemistry, Fac. of Science, Ubon Ratchathani Univ., Ubon Ratchathani 34190. Thailand.*
*e-mail: sanoe.c@ubu.ac.th

## ABSTRACT

Nafion covered poly(*m*-ferrocenylaniline)-MWCNTs modified carbon paste electrode (Nf/p(FcAni)-MWCNTs/CPE) was fabricated as a novel voltammetric sensor for the selective determination of dopamine (DA) and uric acid (UA) in the presence of ascorbic acid (AA). The electrochemical activity of Nf/p(FcAni)-MWCNTs/CPE towards DA, UA and AA was studied by differential pulse voltammetry (DPV). The anodic peaks of DA and UA were observed at 0.3 and 0.45 V (vs Ag/AgCl), respectively. On the other hand, the anodic peak of AA was not observed. When the Nf/p(FcAni)-MWCNTs/CPE was applied to determine DA and UA in the presence of AA, the DPV oxidation peaks were linearly dependent on the DA and UA concentrations in the range of 1-150 and 5-250 µM with $r^2$= 0.9918 and 0.9968, respectively. The detection limit of DA and UA were 0.21 and 0.58 µM (S/N = 3), respectively. In addition, the Nf/p(FcAni)-MWCNTs/CPE showed a well reproducibility and good stability. The interferences of some common inorganic ions and organic compounds did not significantly affect the determination of DA and UA. Therefore, the Nf/p(FcAni)-MWCNTs/CPE is a promising sensor for the selective determination of DA and UA in real samples.

## Objective

- To develop the Nf/p(FcAni)-MWCNTs/CPE and applied in the determination of DA and UA in real samples.

## Experimental

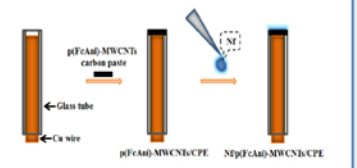


**Scheme 1.** Schematic illustration of the preparation of Nf/p(FcAni)-MWCNTs/CPE.

### Reaction

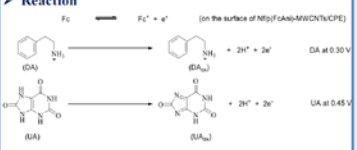


**Scheme 2.** Electrochemical reaction process on the surface of Nf/p(FcAni)-MWCNTs/CPE.

## RESULTS

### i) Electrochemical behaviors of modified CPEs

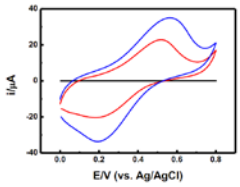


**Fig. 1.** CVs of (a) NfCPE, (b) Nf/p(FcAni)/CPE, and (c) Nf/p(FcAni)-MWCNTs/CPE in 0.1 M PBS (pH 5) at scan rate of 10 mV $s^{-1}$.

### ii) Electrochemical behaviors of DA, UA and AA at Nf/p(FcAni)-MWCNTs/CPE

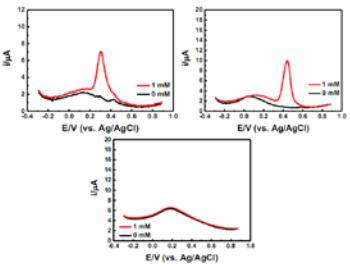


**Fig.2 .** (A) DPV of Nf/p(FcAni)-MWCNTs/CPE in PBS with the addition of 1 mM DA and without DA. (B) DPV in PBS with the addition of 1 mM UA and without UA. (C) DPV in PBS with the addition of 1 mM AA and without AA. Supporting electrolyte; 0.1 M PBS (pH 5), scan rate; of 10 mV $s^{-1}$.

### iii) pH for the determination of DA and UA in the presence of AA

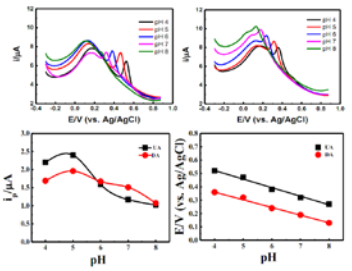


**Fig. 3** A) DPV of 0.05 mM DA in various pHs of 0.1 M PBS containing 1.0 mM AA. (B) DPV of 0.1 mM UA in various pHs of 0.1 M PBS containing 1 mM AA. (C) Relationship between $i_{p,a}$ and pH for DA and UA. (D). Relationship $E_{p,a}$ and pH for DA and UA.

### iv)Calibration plot and detection limit of DA and UA in the presence of AA

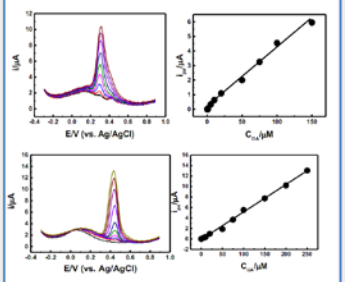


**Fig. 4.** (A) DPV of DA at Nf/p(FcAni)-MWCNTs/CPE in 0.1 M PBS containing 1 mM AA. (B) Plot of peak current vs. concentration of DA. (C) DPV of UA in 0.1 M PBS containing 1 mM AA at scan. (D) Plot of $i_{pa}$ vs. concentration of UA. Supporting electrolyte; 0.1 M PBS (pH 5), scan rate of 10 mV $s^{-1}$.

### v) Real sample analysis

**Table 1** Determination of DA and UA in real samples.

| Sample | Detected (mM)[b] | Added (mM) | Founded (mM) [a] | Recovery (%) | RSD. (%) |
|---|---|---|---|---|---|
| **DA 1** | 31.34 | 10 | 39.92 | 96.56 | 1.06 |
| **DA 2** | 42.14 | 10 | 52.61 | 100.90 | 0.62 |
| **Urine 1** | 59.56 | 10 | 70.07 | 105.10 | 1.59 |

## CONCLUSIONS

- The catalytic detection of the Nf/p(FcAni)-MWCNTs/CPE towards DA and UA.
- The developed CPE exhibited high selectivity, reproducibility, and stability in DPV measurements of DA and UA in the presence of AA.
- The developed CPE was also successfully applied for the determination of DA and UA in pharmaceutical and urine samples.

## REFERENCES

1. Chen, Q., Ai, S., Ma, Q., Yin, H. J Appl Electrochem 40 (2010) 1379-1385.
2. Jiao, S., Li, M., Wang, C., Chen, D., Fang, B. Electrochim. Acta. 52 (2007) 5939-5944.
3. Chairam, S., Sriraksa, W., Amatatongchai, M., Somsook, E. Sensors 11 (2011) 10166.

**Acknowledgments**

PERCH-CIC PERDO
NRCT


# SENSITIVE AND SELECTIVE COLORIMETRIC ASSAY OF SULFITE IN FOOD USING SULFITE OXIDASE IMMOBILIZED ON MAGNETITE-GOLD-FOLATE NANOPARTICLES

Wongduan Sroysee, Nongyao Nantawong, Sanoe Chairam, Purim Jarujamrus, Suparb Tamuang and Maliwan Amatatongchai*

*Department of Chemistry and Center of Excellent for Innovation in Chemistry, Faculty of Science, Ubon Ratchathani University, Ubon Ratchathani , 34190, Thailand.*

**E-mail: amaliwan@gmail.com*

## Abstract

We report a new colorimetric method for sulfite detection, using sulfite oxidase (SOx) immobilized on a gold-coated magnetite nanoparticle core and encased within a conjugated folic acid (FA) cysteine (Cys) shell. The as-prepared $Fe_3O_4$@Au-Cys-FA performs as an efficient peroxidase mimetic catalyst and exhibits good biocompatibility and affinity, making it suitable for SOx immobilization for sulfite detection. We used $Fe_3O_4$@Au-Cys-FA-SOx nanocomposites to catalyze the oxidation of sulfite, generating $H_2O_2$, and to act as a peroxidase-like enzyme in the presence of the newly-formed peroxide to catalyze the oxidation of ABTS *in situ*, generating a green colored product. The absorbance of the reaction products ($ABTS^{\bullet+}$) at 420 nm is proportional to the concentration of sulfite in the range of 0.1 to 100 mg $L^{-1}$. Parameters affecting the sensitivity for evaluation of sulfite were studied. Potential use of this method for sulfite determination in foods and the agreement with the standard method will be discussed.

## Experimental

### Synthesis of $Fe_3O_4$@Au-Cys-FA-SOx

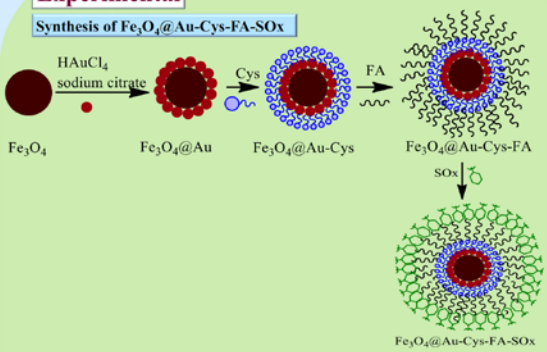


### Colorimetric sensing of sulfite

Mixing 72 µL of 60 mM of ABTS + 600 µL of 4 mg $mL^{-1}$ of $Fe_3O_4$@Au-Cys-FA-SOx + sulfite+ 2400 µL of 0.2 M of acetate buffer pH 4

Incubated at 40 °C, 15 min

measurement

Changing color from colorless to green color

UV-Vis spectrophotometer

### Reaction

$SO_3^{2-} + O_2 \xrightarrow{Fe_3O_4@Au\text{-}cys\text{-}FA\text{-}SOx} SO_4^{2-} + H_2O_2$ (1)

$H_2O_2 \xrightarrow{Fe_3O_4@Au\text{-}cys\text{-}FA\text{-}SOx} 2OH^{\bullet}$ (2)

$OH^{-} \xrightarrow{Fe_3O_4@Au\text{-}cys\text{-}FA\text{-}SOx} 2H_2O + \text{oxidized ABTS}$ (3)

## Results

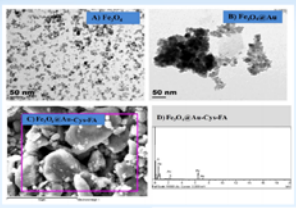

Fig. 1. TEM images of (A) $Fe_3O_4$ and (B) $Fe_3O_4$@Au. (C) SEM image of $Fe_3O_4$@Au-Cys-FA nanoparticles, and (D) the EDS spectrum of $Fe_3O_4$@Au-Cys-FA nanoparticles.

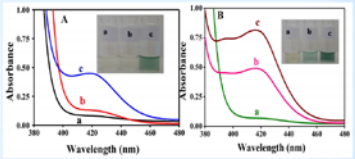


Fig. 2 UV-Vis spectra of (A): a) ABTS-$Fe_3O_4$@Au-Cys-FA-SOx, b) ABTS- sulfite and c) ABTS-$Fe_3O_4$@Au-Cys-FA-SOx-sulfite, and (B): a) ABTS- $Fe_3O_4$@Au-Cys-FA b) ABTS- $H_2O_2$ and c) ABTS- $Fe_3O_4$@Au-Cys-FA- $H_2O_2$

## Analytical feature

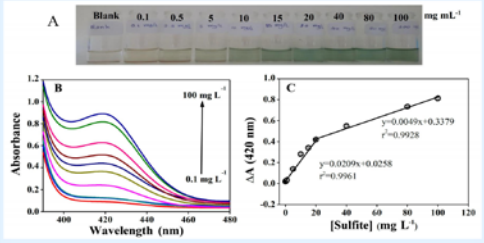


Fig. 3 Changing of visible color of solution from light green to deep green color (A), UV spectrum at various concentration of sulfite (B) and linear calibration plot of sulfite in the range 0.1 to 100 mg $L^{-1}$ (C).

Table 1 Comparison of sulfite contents analyzed from the colorimetric method and standard method (iodometric method)

| Sample | Content of sulfite (mg $mL^{-1}$) Propose method | Iodometric method | % relative error |
|---|---|---|---|
|  Garlic | 118.80 ± 0.002 | 116.98 ± 0.24 | 1.55 |
|  Mango sheet | 84.00 ± 0.082 | 87.60 ± 0.002 | 4.29 |
|  Rice stick | 39.14 ± 0.047 | 40.40 ± 0.08 | 3.21 |

## Conclusions

-A new colorimetric method, using sulfite oxidase (SOx) immobilized on a gold-coated magnetite nanoparticle core and encased within a conjugated folic acid (FA) cysteine (Cys) shell was reported for sulfite detection.

-The method is inherently simple and rapid, with excellent analytical performance in terms of sensitivity, dynamic range and precision with RSD values typically below 3.4 %.

## Acknowledgements

PERCH-CIC PERDO NRCT

## References

1. W. Sroysee, K. Ponlakhet, S. Chairam, P. Jarujamrus and M. Amatatongchai, Talanta 156-157 (2016) 154–162.
2. W. Qin, L. Su, C. Yang, Y. Ma, H. Zhang, and X. Chen, J. Agric. Food Chem. 62 (2014) 5827−5834.


# Molecular imprinted polymer for carbofuran detection

Wongduan Sroysee [1], Suticha Chanta [2], Maliwan Amatatongchai [1]
and Peter A. Liberzeit [2*]

[1] Department of Chemistry and Center of Excellence for Innovation in Chemistry, Faculty of Science, Ubon Ratchathani University, Ubon Ratchathani 34190, Thailand.
[2] University of Vienna, Faculty for Chemistry, Department of Physical Chemistry, 1090 Vienna, Austria.
*E-mail: peter.lieberzeit@univie.ac.at

**Molecularly imprinted polymer (MIP) were designed for selective recognition of carbofuran (CBF). The CBF-MIP were prepared using a methacrylic acid (MAA) as a functional monomer, ethylene glycol dimethacrylate (EGDMA) as a crosslinker, and the azodiisobutyronitrile (AIBN) as an initiator. Fourier transform infrared spectroscopy (FT-IR) was employed to characterize the non-covalent interactions between CBF template and the polymer. The MIP was coated on the surface of quartz Au electrode to develop a novel molecularly imprinted QCM sensor. The molecular recognition characteristics of CBF-MIP sensor for the respective CBF molecules exhibits the dynamic detection range of 0.5 -10 µM with good reproducibility (RSD) of 4.15% (n=3). The MIP exhibits significantly higher binding response than the non-imprinted polymer (NIP).**

## Experimental

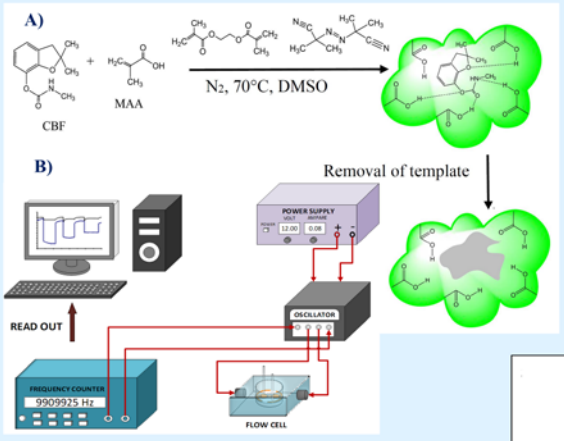


Fig. 1 (A) Synthesis approach to CBF-MIP, (B) setup of MIP-QCM detection system.

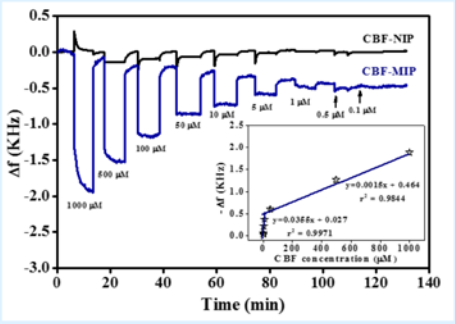


Fig. 3 QCM sensor responses toward CBF at various concentrations; The inset shows linear sensor characteristics in the concentration range of 0.5 to 1,000 µM.

## Results and discussion

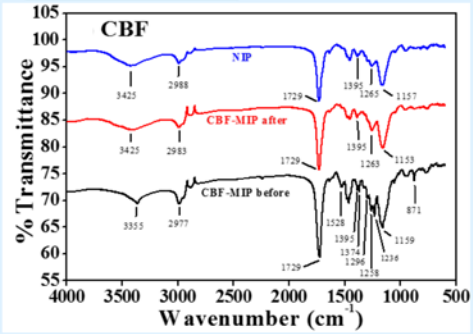


Fig. 2 FT-IR spectra of CBF-MIP

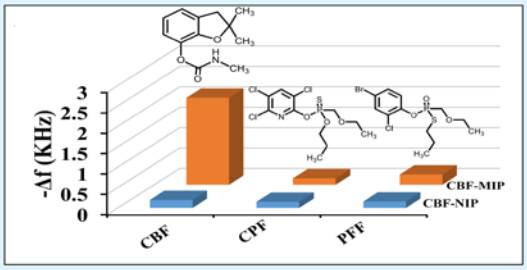


Fig.4 Selectivity pattern of CBF-MIP toward profenofos (PFF) and chlopyrifos (CPF) at a concentration of 1,000 µM.

## Conclusions

We design a MIP sensor for selective carbofuran (CBF) detection. FT-IR was used to confirm structure of CBF- MIP. The MIP coated QCM sensor shows a widely linear range 0.5-1000 µM with the LOD of 0.21 µM . The CBF-MIP provides an acceptable selectivity for the determination of CBF.

**References**

1. S. Yan and et. al., Biosens. Bioelectron. 22 (2007) 1087-1091.
2. A. Findeisen and et. al., Sens. Actuators, B 170 (2012) 196-200.
3. M. Hussain and et. al., Sens. Actuators, B. 176 (2013) 1090-1095.

**Acknowledgments**

PERCH-CIC PERDO NRCT

PACCON
Pure and Applied Chemistry International Conference 2018

# CERTIFICATE OF ATTENDANCE

to certify that

participated in

**Pure and Applied Chemistry International Conference**

## PACCON 2018

**CHEMISTRY TOWARD A SUSTAINABLE FUTURE**

**7-9 February 2018**

Hat Yai, Songkhla, Thailand

**Associate Professor Dr. Suchada Chantrapromma**
Head of Department of Chemistry
Faculty of Science, Prince of Songkla University

**Professor Dr. Supa Hannongbua**
President of the Chemistry Society of Thailand

Journal of Saudi Chemical Society (2018) **22**, 173–182

King Saud University

**Journal of Saudi Chemical Society**

www.ksu.edu.sa
www.sciencedirect.com

ORIGINAL ARTICLE

# Poly(*m*-ferrocenylaniline) modified carbon nanotubes-paste electrode encapsulated in nafion film for selective and sensitive determination of dopamine and uric acid in the presence of ascorbic acid

**Wongduan Sroysee [a], Sanoe Chairam [a,*], Maliwan Amatatongchai [a], Purim Jarujamrus [a], Suparb Tamuang [a], Saichol Pimmongkol [b], Laksamee Chaicharoenwimolkul [c], Ekasith Somsook [d]**

[a] *Department of Chemistry and Center of Excellence for Innovation in Chemistry, Faculty of Science, Ubon Ratchathani University, Warin Chamrap, Ubon Ratchathani 34190, Thailand*
[b] *Department of Physics, Faculty of Science, Ubon Ratchathani University, Warin Chamrap, Ubon Ratchathani 34190, Thailand*
[c] *School of Chemistry, Faculty of Science and Technology, Suratthani Rajabhat University, 272 Moo 9, Surat-Nasan Rd., Khuntale, Muang, Surat Thani 84100, Thailand*
[d] *NANOCAST Laboratory, Center for Catalysis, Department of Chemistry and Center of Excellence for Innovation in Chemistry, Faculty of Science, Mahidol University, 272 Rama VI Rd. Rachathewi, Bangkok 10400, Thailand*

Received 3 December 2015; revised 17 February 2016; accepted 20 February 2016
Available online 2 March 2016

**KEYWORDS**

Poly(*m*-ferrocenylaniline);
Carbon nanotubes-paste electrode;
Nafion;
Electrochemical sensor;
Dopamine;
Uric acid

**Abstract** A nafion covered carbon nanotubes-paste electrode modified with poly(*m*-ferrocenylaniline), (Nf/p(FcAni)-CNTsPE), provides a novel voltammetric sensor for the selective determination of dopamine (DA) and uric acid (UA) in the presence of ascorbic acid (AA). We studied the electrochemical activity of Nf/p(FcAni)-CNTsPE toward DA, UA, and AA by differential pulse voltammetry (DPV). DA and UA anodic peaks appear at 0.30 and 0.45 V, respectively while an anodic peak for AA was not observed. DPV oxidation peak values are linearly dependent on DA concentration over the range 1–150 μM ($r^2$ = 0.992), and on UA concentration over the range 5–250 μM ($r^2$ = 0.997). DA and UA detection limits are estimated to be 0.21 and 0.58 μM, respectively. The modified electrode shows both good selectivity and reproducibility for

* Corresponding author. Tel.: +66 45 353 400x4137; fax: +66 45 288 379.
E-mail address: sanoe.c@ubu.ac.th (S. Chairam).
Peer review under responsibility of King Saud University.

Production and hosting by Elsevier

http://dx.doi.org/10.1016/j.jscs.2016.02.003

the selective determination of DA and UA in real samples. Finally, the modified electrode was successfully applied for the determination of DA and UA in pharmaceutical or biological sample fluids.



## 1. Introduction

Dopamine (DA), uric acid (UA), and ascorbic acid (AA) normally coexist in human biological fluids, mainly in serum, blood, and urine. These compounds play important roles in renal, hormonal, cardiovascular, and central nervous systems, and are essential for correct function of the metabolism. The neurotransmitter DA is a precursor for catecholamine synthesis, for example, of epinephrine and norepinephrine; disorders in DA synthesis can lead to Parkinson's disease [1]. UA is the major final product of purine metabolism in humans. UA is weakly soluble in aqueous media, and this can lead to problems in humans when UA levels are pathologically elevated [2]. AA (vitamin C) is a powerful reducing agent, and is an essential nutrient for humans [3]. As an antioxidant, AA provides nonspecific protection against oxidative damage, and it is an essential cofactor for monooxygenases and dioxygenases in various metabolic pathways [4]. Therefore, the determination of these compounds is very important in pharmaceutical or biological sample fluids. There are several analytical methods for the determination of DA, UA, and AA, such as chemiluminescence and fluorescence spectroscopy, spectrophotometry, and high-performance liquid chromatography (HPLC). However, these methods usually require expensive laboratory facilities, are time-consuming, and can be complex to perform. As an electroactive substance, they can be also determined via electrochemical techniques.

Electrochemical methods for DA, UA, and AA sensing can be performed using common electrodes. These methods generally offer greater sensitivity, and are simpler and less time-consuming than other methods available. The major obstacle to selective electrochemical determination of DA, UA, and AA is that their oxidation potentials are similar. This results in overlapping of voltammetric responses and therefore provides poor selectivity and inaccurate quantitative analysis. Most studies report a lower electrochemical oxidation potential for AA compared to DA and UA [5,6]. Thus, interference caused by AA presents a challenge for the determination of DA and UA. Attempts to overcome this problem have used various materials to modify the electrode surface, such as polymers, metal complexes, metal or metal-oxide nanoparticles, and nanocomposites [7,8].

There is great interest in the development of inexpensive, simple, and rapid methods for routine analysis of DA, UA in the presence of AA. In a recent review, Erden and Kiliç [9] identified several electrochemical approaches, including the use of modified electrodes, to separate the oxidation peaks of DA, UA, and AA, and to reduce interference by AA. As a polymeric film, nafion (Nf) exhibits good selectivity against anions and can pre-concentrate cations at the electrode surface, creating a protective coating for the electrode surface [10]. Nafion-modified electrodes can be easily prepared by drop casting or by spin coating the polymer solution directly onto the electrode surface. There are many reports of the successful application of nafion-coated chemically-modified electrodes for voltammetric determination of DA and UA in the presence of ascorbic acid [11,12].

In the field of analytical and bioanalytical electrochemistry, carbon paste electrodes (CPE) are one of the most common self-made electrodes because of their facile construction from a mixture of graphite powder and a pasting liquid [12]. The conductive graphite serves as the conducting electrode material. The pasting material is of insulating character and acts as an inert medium, binding individual particles into a compact mixture [13]. CPEs modified with various materials are termed "chemically modified electrodes". These modified CPEs possess several advantages over other electrode materials, including low cost, ease of fabrication, low ohmic resistance, low background current, renew ability, and stable responses. Nanomaterials have received a great deal of attention and have a wide range of applications that exploit their unique properties. Among these materials, carbon nanotubes (CNTs), with their advantageous electrical and chemical properties, are promising materials for enhancing electrode electrocatalytic activity. CNTs have many applications in the fabrication of electrochemical sensors and biosensors [14]. Recently, CNTs-paste electrode (CNTsPE) were successfully applied to voltammetric measurements of various biological species, including dopamine, uric acid, ascorbic acid, epinephrine, benserazide, glutathione, acetaminophen, cysteamine, NAD, folic acid, glutathione and piroxicam [15,16].

Redox mediators are widely used to improve sensitivity, selectivity, and detection limits of electrochemical sensors and biosensors. Among these, ferrocene (Fc) is well suited to modify the electrode surface due to its excellent electron transfer properties during redox reactions [17,18]. Fc and its derivatives are effective in catalyzing both the oxidation and reduction of various electroactive compounds [19–21]. However, Fc leakage is a major problem for the modified electrode; Fc adsorbs weakly to the electrode surface due in part to its neutral charge. Substituting the Fc rings with high molecular weight compounds or polymers can resolve this problem.

We propose a new redox active ferrocene-based polyaniline chemically modified paste electrode for the detection of DA and UA. The fabrication of a poly(*m*-ferrocenylaniline)-carbon nanotubes-paste electrode covered with nafion film (Nf/p(FcAni)-CNTsPE) as a novel voltammetric sensor for the selective determination of DA and UA in the presence of ascorbic acid was reported. To our knowledge, this is the first report of using p(FcAni)-CNTs to improve the electrochemical activity of DA and UA sensors. The Nf/p(FcAni)-CNTsPE exhibits significant enhancement in sensor performance. The electroactive surface area and unique nanostructure of p(FcAni)-CNTs provide good conductivity and enhance electron transfer. The Nf/p(FcAni)-CNTsPE was successfully applied for the determination of DA and UA.

## 2. Experimental details

### 2.1. Materials and solutions

All reagents were used as received without further purification. Multiwalled carbon nanotubes (CNTs), diameters 30 ± 15 nm, length 1–5 μm and purity greater than 95% were purchased from Nanolab Inc. (MA, USA). Uric acid (UA) and graphite powder were purchased from Acros Organic (Geel, Belgium). Nafion (Nf), dopamine hydrochloride (DA) and ascorbic acid (AA) were purchased from Sigma–Aldrich (St. Louis, USA). All aqueous solutions were freshly prepared using de-ionized water (resistance ⩾18.2 MΩ cm, purified by a Nanopore Ultrapure Water System).

### 2.2. Synthesis of m-ferrocenylaniline

The *m*-ferrocenylaniline (FcAni) (**1**) was synthesized according to the reported method [22]. In brief, *m*-ferrocenylnitrobenzene was synthesized from the reaction between ferrocene and *m*-nitroaniline using sodium nitrite/hydrochloric acid in the presence of diethyl ether. The product was then reduced to *m*-ferrocenylaniline using Sn/HCl in an ice bath. The crude product was purified by column chromatography with gradient elution (hexane–ethyl acetate) to afford the ferrocene derivative. A yellow-orange crystalline solid was obtained after drying under reduced pressure at room temperature. Scheme 1 illustrates the synthetic procedure used for the preparation of *m*-ferrocenylaniline. $^{1}$H NMR (500 MHz, $CDCl_3$, 298 K): $\delta$ (ppm) = 3.53 (*br s*, NH, 2H), 3.97 (*s*, $C_5H_4$, 5H), 4.20 (*s*, $C_5H_4$, 2H), 4.51 (*s*, $C_5H_4$, 2H), 6.45 (*d*, $C_6H_4$, 1H), 6.73 (*s*, $C_6H_4$, 1H), 6.83 (*d*, $C_6H_4$, 1H), 7.01 (*t*, $C_6H_4$, 1H). $^{13}$C NMR (300 MHz, $CDCl_3$, 298 K): $\delta$ (ppm) = 66.5, 68.7, 69.5, 76.6, 77.0, 77.4, 85.6, 112.9, 113.1, 117.1, 129.1, 140.2, 146.1. EIMS Exact Mass: Calculated for $C_{16}H_{15}NFe$ $[M]^+$ = 277.05, Found $[M+H]^+$ = 278.06. FTIR (KBr): $\nu_{max}$ ($cm^{-1}$) = 3437, 3365, 3103, 1617, 1602, 1582, 1509, 1469, 1388, 1308, 1235, 1169, 1102, 1028, 999, 863, 820, 806, 782, 693, 519, 504, 485, 453. Elemental C:H:N Analysis (%): Calculated for $C_{16}H_{15}Nfe$: C = 69.34, H = 5.46, N = 5.05, Found: C = 69.52, H = 5.22, N = 5.06.

### 2.3. Synthesis of poly(m-ferrocenylaniline)

Poly(*m*-ferrocenylaniline) (p(FcAni)) (**2**) was prepared by oxidative polymerization of compound (**1**), following the previously reported method [23]. The resulting dark brown powder was collected by filtration and then dried in an oven at 80 °C for 24 h. Scheme 2 illustrates the synthetic procedure used for the preparation of poly(*m*-ferrocenylaniline).

### 2.4. Preparation of working electrodes

A carbon paste electrode (PE) was constructed following our previously reported method with some modifications [24]. Graphite powder (100 mg) and paraffin oil (30 μL) were hand-mixed in a mortar to form a homogeneous paste. Subsequently, the graphite and mineral oil composite was packed into a cylindrical glass tube (2 mm diameter, 10 cm long) by pressing the open end of the tube into the paste composite to a depth of approximately 2 mm. Next, a copper wire (1.5 mm diameter, 12 cm long) was inserted into the tube from the opposite end, until the end of copper wire was buried into the graphite/mineral oil composite, forming an electrical contact between the paste and wire.

The Nf/p(FcAni)-CNTsPE was prepared by hand-mixing of 25 mg p(FcAni), 5 mg CNTs, 70 mg graphite powder and 30 μL mineral oil in a mortar and pestle. The homogeneous paste was then packed into the end of a glass tube. The surface of the p(FcAni)–CNTsPE was manually polished using weighing paper until a flat and smooth surface was obtained. Next, Nf solution (10 μL, 0.1%) was dropped onto the modified CNTsPE using a micropipette, and the electrode was left to dry at ambient temperature. The fabricated CNTsPE used for electrochemical studies were kept in a desiccator at room temperature when not in use.

For comparison purposes, the Nf/PE, Nf/p(FcAni)/PE and p(FcAni)/PE were also prepared following the same procedure.

### 2.5. Voltammetric procedures

All electrochemical measurements were carried out using an eDAQ potentiostat (EA161) equipped with an e-corder (210), and using e-Chem v2.0.13 software. A Metrohm 713 pH meter was used to monitor the phosphate buffer pH. Cyclic voltammetry (CV) and differential pulse voltammetry (DPV) were used for the analysis of DA, UA, and AA. CV and DPV measurements were performed in a buffer solution over a running potential range from −0.3 to 0.9 V. A conventional three-electrode cell assembly, consisting of a platinum wire counter electrode and an Ag/AgCl (sat. 3.0 M KCl) reference electrode was used. The working electrode was either the PE or the modified-carbon nanotubes paste (CNTsPE). All solutions were purged with nitrogen gas for 5 min prior to use. DPV measurements were used for the simultaneous determination of DA and UA in the presence of AA. The electrochemical parameters for DPV measurements were: pulse amplitude = 50 mV, modulation time = 0.2 s, interval time = 0.5 s, and scan rate = 10 mV $s^{-1}$.

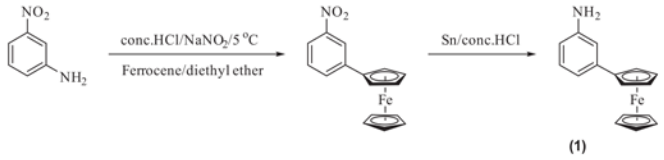


(1)

**Scheme 1** Synthetic procedure for the preparation of *m*-ferrocenylaniline.

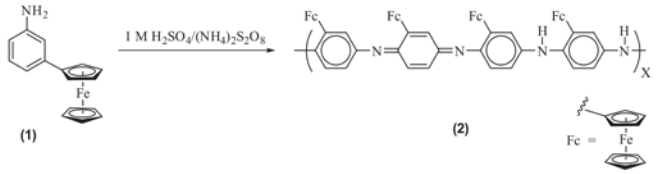


**Scheme 2** Synthetic procedure for the preparation of poly(*m*-ferrocenylaniline).

*2.6. Samples*

The samples to be determined were dopamine hydrochloride solutions (250 mg DA per 10 mL solution) for intravenous infusion, obtained from a local pharmacy. Urine samples used for UA determination were collected from students. All samples were centrifuged, and the supernatants filtered through a 0.45 μm filter prior to analysis. All samples were diluted with buffer solution (pH 5) prior to analysis. Determinations were performed by the standard addition method.

## 3. Results and discussion

*3.1. Characterization*

The *m*-ferrocenylaniline (FcAni) (**1**) was synthesized from the reaction between ferrocene and *m*-nitroaniline using sodium nitrite/hydrochloric acid in the presence of diethyl ether to produce nitro-substituted ferrocene, which then was reduced to the amine using Sn/HCl. Then, poly(*m*-ferrocenylaniline) (p(FcAni)) (**2**) was prepared by the oxidative polymerization of compound **(1)** using ammonium persulfate, and then used in the fabrication of the modified PE. The morphology of p(FcAni) and Nf/p(FcAni)-CNTsPE was characterized using a JEOL, JSM-5910 field emission scanning electron microscope (SEM) by accelerating at a voltage of 15 kV. Fig. 1 shows SEM images of p(FcAni) and composites of Nf/p(FcAni)-CNTs paste. As shown in Fig. 1A, the synthesized p(FcAni) is spherical in shape with the average diameter of *ca.* 1 μm. The morphological structure of the Nf/p(FcAni)-CNTs paste composites (Fig. 1B) is quite similar to the p(FcAni), but the composites has a smoother surface. Clearly, the thin film is formed for the Nf coating over the Nf/p(FcAni)-CNTs paste surface. The p(FcAni) particles were well dispersed on the electrode surface.

*3.2. Electrochemical behaviors of modified CNTsPE*

The electrochemical behaviors of the modified PEs were investigated using cyclic voltammetry (CV). Fig. 2 shows the CV responses obtained from (a) Nf/PE, (b) Nf/p(FcAni)PE, and (c) Nf/p(FcAni)-CNTsPE, in a 0.1 M phosphate buffer solution (pH 7) at a scan rate of 10 mV $s^{-1}$. There is no redox peak present for the Nf/PE, and the obtained current is very low (Fig. 2, curve a), indicating that the Nf/PE has no electrochemical activity over this potential range. For the plot in Fig. 2, curve b shows two redox peaks for Nf/p(FcAni)PE, at potentials of approximately 0.20 and 0.50 V. The pair of well-defined anodic and cathodic peaks arises from the $Fc|Fc^{+}$ redox system, which exhibits quasi-reversible behavior in aqueous solution. To investigate the effect of CNTs, Nf/p(FcAni)-CNTsPE (Fig. 2, curve c) and Nf/p(FcAni)PE (Fig. 2b) exhibit similar electrochemical characteristics, although the peak current is greater for Nf/p(FcAni)-CNTsPE because of the excellent electron transfer properties of CNTs. Barsan et al. [25] proposed that the synergistic amplification effect seen for electrochemical sensors based on redox polymer/carbon nanotubes modified electrodes such as Nf/p(FcAni)-CNTsPE, generally have very good electron transfer rates. Nishihara and Murata [26] noted that such materials enhance sensitivity by promoting electron-transfer reactions between molecules and the electrode substrate. In our case, ferrocene-containing polyaniline provides a high electrical conductivity with convenient doping|de-doping characteristics, and offers good environmental stability. Ferrocene is an excellent electron mediator, and can increase the rate of electron transfer to provide increased current responses.

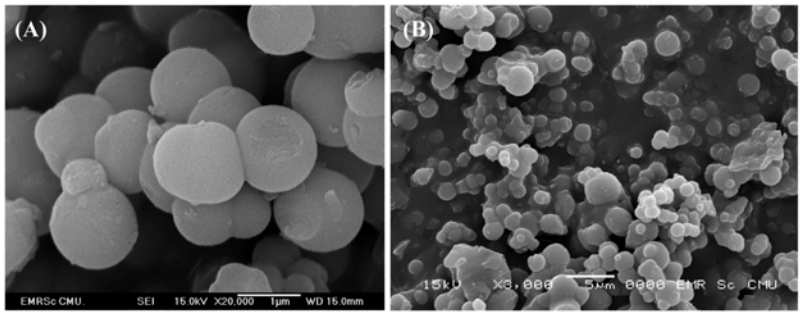


**Figure 1** SEM images of (A) p(FcAni) and (B) Nf/p(FcAni)-CNTsPE.

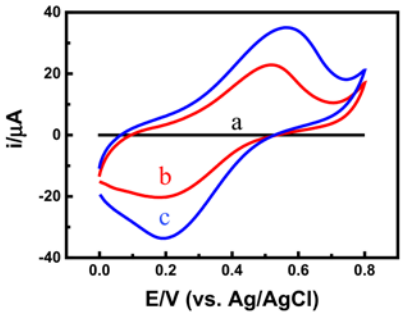


**Figure 2** CV plots of (a) Nf/PE, (b) Nf/p(FcAni)PE, and (c) Nf/p(FcAni)-CNTsPE, in a 0.1 M PBS (pH 7) at a scan rate of 10 mV $s^{-1}$.

### *3.3. Electrochemical behaviors of DA, UA, and AA at the Nf/p (FcAni)-CNTsPE*

Yang et al. [27] demonstrated that the AA oxidation potential is very similar to those of DA and UA, and that AA coexists with DA and UA in reduced graphene oxide modified electrodes. To study the electrochemical activity of Nf/p(FcAni)-CNTsPE toward DA, UA, and AA, DPV method was performed in a PBS (pH 7), with and without the addition of 1.0 mM DA, 1.0 mM UA, and 1.0 mM AA at a scan rate of 10 mV $s^{-1}$ as shown in Fig. 3. Chen et al. [28] reported that DPV offers greater sensitivity and selectivity than CV for electrocatalytic oxidation of DA, UA, and AA.

After the addition of the analyte to the supporting electrolyte solution, DA and UA anodic peaks appear at 0.30 and 0.45 V, respectively (Figs. 3A and 4B). However, no anionic peak is seen for the AA sample (Fig. 3C). Thus, the Nf film covering the electrode eliminates the AA signal, and prevents AA interference with the detection of DA and UA. This behavior suggests that the Nf/p(FcAni)-CNTsPE might electrochemically catalyze the DA and UA oxidation in the presence of AA. Previous reports [29,30] provide explanations for the beneficial effects of integrating an Nf film coating. The Nf film prevents interference by AA because of its polymeric structure, which contains a hydrophobic backbone ($-CF_2-CF_2-$) and hydrophilic sulfonic acid groups ($-SO_3H$). Nf exhibits selectivity against anions, and can pre-concentrate cations at the electrode surface. AA (pKa = 4.1) exists as the anionic ascorbate ion, so experiences strong repulsive interactions with Nf [31,32]. While negatively charged Nf-coated electrodes repel negatively charged ascorbate anions, the film allows DA and UA cations to permeate. DA (pKa = 8.8) and UA (pKa = 5.4) are in their cationic forms, and have strong attractive interactions with the negatively charged, sulfonate groups on Nf. Moreover, the anodized surface has a high affinity toward DA and UA due to hydrogen

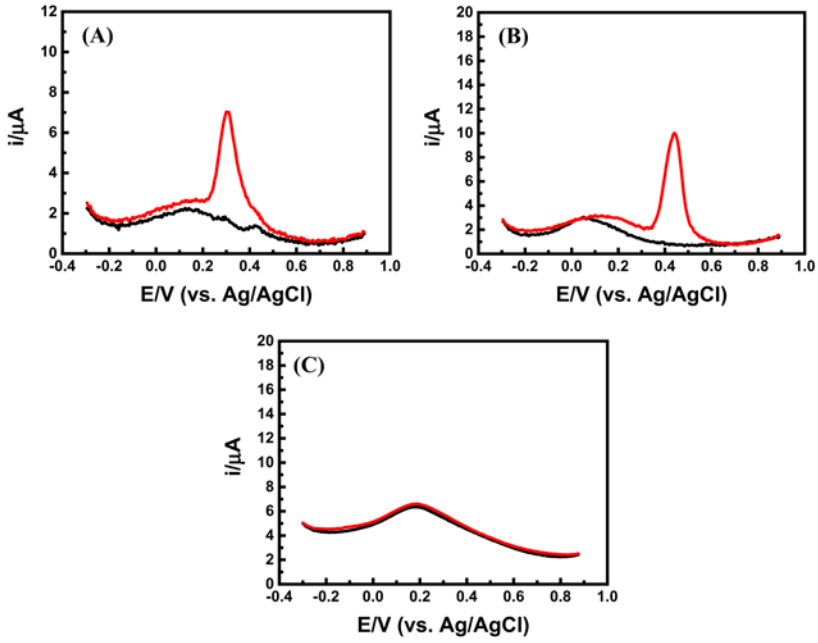


**Figure 3** DPV voltammetric plots of Nf/p(FcAni)-CNTsPE in a 0.1 M PBS (pH 7) at a scan rate of 10 mV $s^{-1}$ for (A) with and without 1 mM DA, (B) with and without 1 mM UA, and (C) background voltammograms (0.1 M PBS, pH 7) and 1 mM of AA.

bonding [28]. Consequently, there is no observed oxidation current from AA at the Nf/p(FcAni)-CNTsPE at pH 5, and thus, the $Fc|Fc^{+}$ redox system containing polyaniline at the electrode, allows selective sensing of DA and UA in the presence of AA.

### *3.4. pH for the determination of DA and UA in the presence of AA*

Electrolyte pH has a significant impact on electrocatalytic oxidation and on the shapes of DA and UA waves. We investigated the relationship between supporting electrolyte pH and the current response obtained from DA and UA at the Nf/p(FcAni)-CNTsPE in the presence of AA. Differential pulse voltammetry (DPV), using buffer solutions containing 1 mM of AA at various pH values from pH 4 to 8 was performed. Fig. 4A–B shows Nf/p(FcAni)-CNTsPE voltammetric responses with and without the addition of 0.05 mM DA and 0.1 mM UA, and also shows the anodic peak current ($i_{p,a}$), anodic peak potential ($E_{p,a}$), and pH for DA and UA in buffer solutions at various pH values (see Fig. 4A–B). The increasing of pH from 4 to 8 results in a negative shift of the anodic peak potential for both DA and UA. The result indicated that the electrocatalysis of DA and UA at the Nf/p(FcAni)-CNTsPE is a pH dependent reaction.

Fig. 4C shows peak potential responses to pH changes for DA and UA. The peak potentials for DA and UA are a linear function of pH over the range of pH 4–8. The linear equation for DA is $y = -0.059x + 0.602$, with $r^2 = 0.992$, while the linear equation for UA is $y = -0.065x + 0.782$ with $r^2 = 0.990$. The slopes of $-0.059$ V $pH^{-1}$ and $-0.065$ V $pH^{-1}$ for DA and UA respectively, are close to those expected for a monoelectronic/monoprotonic electrode reaction that is $-0.059$ mV/pH at 25 °C, confirming that the total number of electrons and protons transferred during the DA and UA oxidation mechanisms are the same. The oxidation of both DA and UA occurs by a two-electron transfer process, and so two protons are expected to be released at the Nf/p(FcAni)-CNTsPE. The results obtained here are consistent with previous reports [33,34]. Fig. 4D shows DA and UA peak current responses to changes in electrolyte pH. The $i_{p,a}$ for DA and UA reached a maximum at pH 5, and then decreased with further increases in pH. Consequently, we chose pH 5 as the optimal pH value for further electrochemical determination of DA and UA in the presence of AA.

### *3.5. Calibration plot and detection limit for DA and UA in the presence of AA*

We used DPV to enhance sensitivity toward the detection of DA and UA by the Nf/p(FcAni)-CNTsPE sensor electrode under the optimal condition (pH 5) at a scan rate of 10 mV $s^{-1}$. Fig. 5 shows the peak currents for DA and UA, at 0.30 and 0.45 V, respectively. Peak current increases linearly with increasing the DA and UA concentrations. The DA and UA current responses were relatively independent, and the

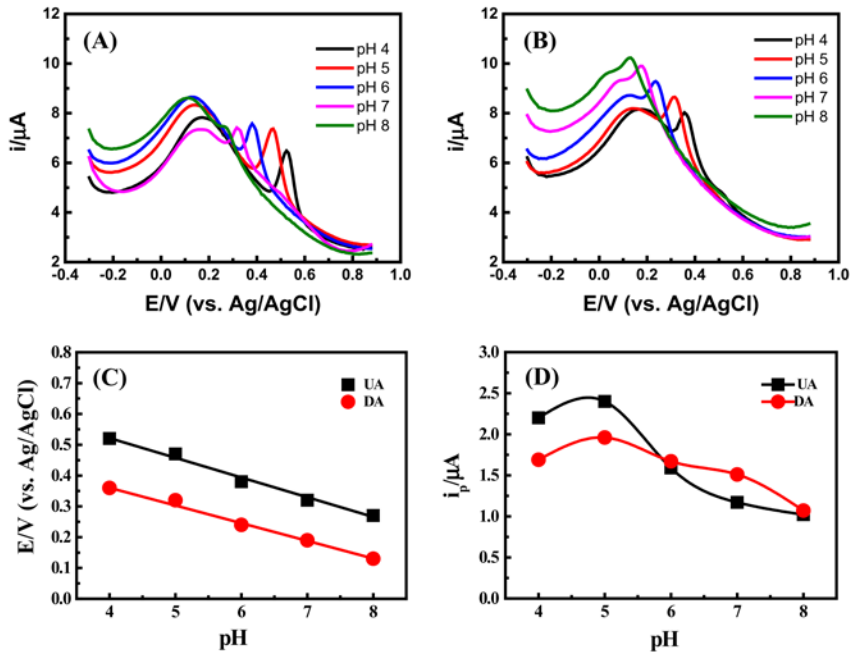


**Figure 4** (A) DPV plots of Nf/p(FcAni)-CNTsPE in a 0.1 M buffer solution (pH 4–8) at a scan rate of 10 mV $s^{-1}$ for (A) 0.05 mM DA and (B) 0.1 mM UA. (C) Anodic peak potential ($E_{p,a}$) vs. pH for DA and UA. (D) Anodic peak current ($i_{p,a}$) vs. pH for DA and UA.

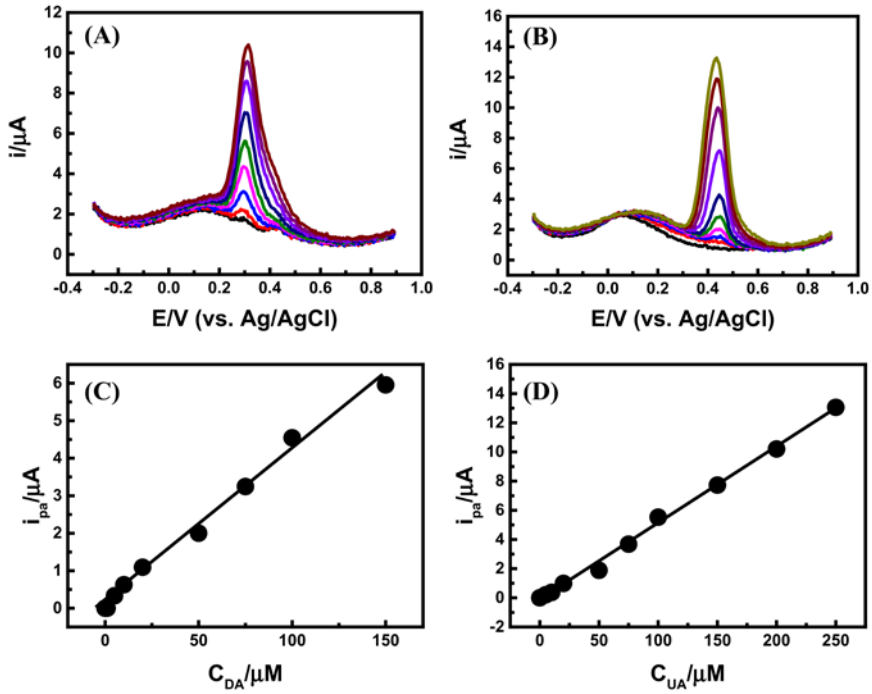


**Figure 5** (A) DPV plots of the Nf/p(FcAni)-CNTsPE sensor under the optimal condition (pH 5) at a scan rate of 10 mV $s^{-1}$ for (A) DA (1–150 μM from inner to outer plot) and (B) UA (5–250 μM from inner to outer plot). Plots of peak current vs. (C) DA and (D) UA concentrations.

**Table 1** Comparison of analytical performance of the Nf/p(FcAni)-CNTsPE sensor for determination of DA and UA, with literature reports of differently modified electrodes.

| Electrode | Modifier | pH | Linear range (μM) | | Detection limit (μM) | | Method | References |
|---|---|---|---|---|---|---|---|---|
| | | | DA | UA | DA | UA | | |
| GCE | Fc@DWNTs | 7.0 | 0.5–20 | – | 0.30 | – | Amper-ometry | [19] |
| GCE | Fc–SWNTs | 7.0 | 5.0–30 | – | 0.05 | – | DPV | [33] |
| GCE | DNA/Pp-ABSA bi-layer | 7.0 | 0.2–13 | 0.4–23 | 0.09 | 0.19 | DPV | [35] |
| GCE | Nf-Fc | 7.0 | – | 250–5000 | – | 22.7 | Amper-ometry | [36] |
| PE | Pyrogallol red | 7.0 | 1–700 | 50–1000 | 0.78 | 35 | DPV | [37] |
| Pt | GNPs/CDSH–Fc/Nf | 6.5 | 2–50.0 | – | 0.09 | – | DPV | [28] |
| GCE | GN | 7.0 | 3.3–249.1 | 6.7–386.3 | 1.50 | 2.70 | LPV | [38] |
| ITO | Nf-CNT-ABTS | 7.0 | 2.2–240 | 3.1–400 | 0.84 | 1.75 | DPV | [39] |
| PGE | – | 5.0 | 0.2–15 | 0.3–150 | 0.03 | 0.12 | DPV | [40] |
| GCE | NCHSs | 7.0 | 1–400 | 5–350 | 0.30 | 1 | DPV | [41] |
| CNTsPE | Fc | 7.0 | – | 15–1000 | – | 10 | SWV | [42] |
| GCE | Pt/RGO | 7.0 | 10–170 | 10–130 | 0.25 | 0.45 | DPV | [43] |
| GCE | Fc@β-CD | 4.0 | – | 5–120 | – | 0.08 | DPV | [44] |
| CNTsPE | Nf/p(FcAni) | 5.0 | 1–150 | 5–250 | 0.21 | 0.58 | DPV | This work |

Fc–SWNTs = ferrocene and single wall carbon nanotube, Pp-ABSA = poly(*p*-aminobenzenesulfonic acid), Nf-Fc = ferrocene bound nafion, GNPs = gold nanoparticles, CDSH–Fc = mono-6-thio-β-cyclodextrin and ferrocene, GN = graphene nanopowder, ABTS = 2,2′-Azino-bis (3-ethylbenzthiazoline-6-sulfonic acid), CNT = carbon nanotube, NCHSs = nitrogen-doped carbon hollow spheres, Pt/RGO = platinum/reduced graphene oxide, N-CDs/Fc@β-CD = nitrogen-doped carbon dot/ferrocene@β-cyclodextrin, *N*-(4-hydroxyphenyl)-3,5-dinitrobenzamide = NHPDA.

GCE = glassy carbon electrode, Pt = platinum electrode, ITO = indium tin oxide, PGE = pencil graphite electrode, PE = carbon paste electrode, CNTsPE = carbon nanotubes-paste electrode, DPV = differential pulse voltammetry, LPV = linear polarization voltammetry, SWV = square wave voltammetry.

**Table 2** DA and UA concentration in different samples ($n$ = 3) obtained from the proposed method and the reference values.

| Sample | Analyte | Detected (μM)[a] | Spiked level (μM) | Found (μM)[b] | Recovery (%) |
|---|---|---|---|---|---|
| D-A1 | DA | 31.3 ± 0.1 | 10.0 | 39.9 ± 0.4 | 96.6 ± 1.0 |
| D-A2 | | 31.6 ± 0.1 | 10.0 | 41.7 ± 0.3 | 101.0 ± 0.6 |
| U-S1 | UA | 41.5 ± 0.6 | 10.0 | 49.5 ± 0.1 | 90.3 ± 0.3 |
| U-S2 | | 59.6 ± 0.3 | 10.0 | 70.1 ± 1.1 | 100.7 ± 1.3 |

[a] Amount found in the samples after dilution, X ± S.D.
[b] Amount found after spiked either 10 μM of DA or UA.

anodic peak currents ($i_{p,a}$) showed linear responses to changes in concentrations. For DA, the linear relationship is given by $y = 0.041x - 0.125$ ($r^2 = 0.992$) over the range of 1–150 μM, while the linear relationship for UA is $y = 0.053x - 0.148$ ($r^2 = 0.997$) over the range of 5–250 μM. The DA and UA detection limits, calculated from the 3-fold signal-to-noise ratio ($S/N$ = 3) were 0.21 and 0.58 μM, respectively.

Table 1 provides a comparison of analytical performances obtained from our developed sensor with differently modified electrodes. The analytical characteristics of our sensor are comparable to, or better than, those reported for other DA and UA designs. Additionally, the detection limit for our sensor is lower, or comparable to, those in previous reports, providing the sensitive detection. The use of Nf/p(FcAni)-CNTsPE also offers a wider range of linearity compared with previously reported modified electrodes [19,33–35,38–40]. Moreover, the Nf/p(FcAni)-CNTsPE offers a simple preparation procedure and handling and storage of the sensor is uncomplicated. Clearly, the Nf/p(FcAni)-CNTsPE sensor exhibits the simplicity and high selectivity for DA and UA quantitation in the presence of AA. The oxidation peak potentials of our sensor for DA and UA are lower than [35,44], or comparable [33,37,43] to those of electrochemical sensors described in literature. In addition, the major advantages of the Nf/p(FcAni)-CNTsPE over previously reported devices are ease and fast preparation, high stability and good reproducibility for the determination of DA and UA.

### 3.6. Interference studies

We performed interference studies on the determination of DA and UA at the Nf/p(FcAni)-CNTsPE sensor using DPV. The DA and UA concentrations were maintained at 0.1 mM in 0.1 M buffer (pH 5) containing 1 mM AA. Interfering species were added to the test solution in the range of 10–100 times greater concentration than that of DA and UA. The tolerance limit was taken as the amount of substance needed to cause a signal alteration of greater than ±5%. According to our results, glucose, KCl and urea do not interfere with the DA determination studied up to 10 mM. While $CaCl_2$ and $NaNO_3$ produce very low interference signals at a molar concentration of 2 mM or greater (7 mM) with respect to DA. In addition, KCl also does not interfere with the UA determination studied up to 10 mM. Whereas, glucose, $NaNO_3$ and $CaCl_2$ produce very low interference signals at a molar concentration of 5 mM or greater (7 mM) with respect to UA. This finding indicates that the Nf/p(FcAni)-CNTsPE electrode provides an acceptable selectivity for the determination of DA and UA in real samples.

### 3.7. Reproducibility and stability

The reproducibility and stability of the modified PE were investigated by DPV. We used the Nf/p(FcAni)-CNTsPE in a 0.1 M buffer solution (pH 5) to determine 50 μM of DA or 100 μM of UA in the presence of 1 mM AA for 15 measurements. The calculated relative standard deviations (RSD) are 4.3% and 3.2% for DA and UA, respectively. Results from our stability study reveal that after storage for 1 week at room temperature, the Nf/p(FcAni)-CNTsPE performs well, providing 95.68% and 99.9% of its initial measurement values for DA and UA, respectively. These results demonstrate that the Nf/p(FcAni)-CNTsPE performs with high stability and good reproducibility for the voltammetric determination of DA and UA.

### 3.8. Real sample analysis

To evaluate the analytical applicability of the Nf/p(FcAni)-CNTsPE sensor, we performed the determination of DA or UA in pharmaceutical or biological sample fluids using the standard addition method. The proposed method was applied for the detection of DA and UA in two different samples, including dopamine hydrochloride solutions for intravenous infusion (D-A1 and D-A2) and human urine samples (U-S1 and U-S2). In order to test the reliable of this proposed sensor at a low concentration range, the samples were diluted appropriately with 0.1 M PBS. The precision of the analytical process was evaluated by the repeatability of the process. The spiked concentration of 10 μM was performed to investigate the accuracy of the method. Table 2 summarizes the analytical results. The RSDs and recoveries of the proposed method were found in the range of 0.3–1.3% and 90.3–101.0%, respectively. These results indicated that there are no significant matrix interferences in the analyzes samples as well as that this presented method is sufficiently accurate and precision and suitable for the quantification of DA and UA in the mentioned samples.

## 4. Conclusions

The Nf/p(FcAni)-CNTsPE provides a simple and easy approach to selectively detect DA and UA in the presence of AA. The results show that the oxidation of DA and UA is electrochemically catalyzed at 0.3 and 0.45-V, respectively, whereas the peak potential of AA does not appear by DPV method. The Nf/p(FcAni)-CNTsPE exhibits high selectivity and good reproducibility in measurements of DA and UA in the presence of AA. DPV oxidation peak values are linearly

dependent on DA concentration over the range 1–150 μM ($r^2$ = 0.992), and on UA concentration over the range 5–250 μM ($r^2$ = 0.997). DA and UA detection limits are estimated to be 0.21 and 0.58 μM, respectively. The results from interference, reproducibility and stability studies demonstrate that the Nf/p(FcAni)-CNTsPE electrode provides an acceptable selectivity for the determination of DA and UA and performs with high stability and good reproducibility for the voltammetric determination of DA and UA. Finally, the Nf/p(FcAni)-CNTsPE was successfully applied for the determination of DA and UA in pharmaceutical or biological sample fluids with good results. This work offers a novel sensor for the voltammetric determination of DA and UA with a great promise toward pharmaceutical and clinical applications.

**Acknowledgements**

This work was supported by grants from the Thailand Research Fund (TRF; TRG5680049), the Center of Excellence for Innovation in Chemistry (PERCH-CIC), the Office of the Higher Education Commission, the Ministry of Education, and the National Research Council of Thailand (NRCT, 2558A11703003). Scholarship from The Scholarship from the Science Achievement Scholarship of Thailand (SAST) given to W. Sroysee is gratefully acknowledged. We gratefully acknowledge the help and facilities provided by the Faculty of Science, Ubon Ratchathani University (UBU).

**References**

[1] E. Hirsch, A.M. Graybiel, Y.A. Agid, Melanized dopaminergic neurons are differentially susceptible to degeneration in Parkinson's disease, Nature 334 (1988) 345–348.
[2] K.L. Rock, H. Kataoka, J.-J. Lai, Uric acid as a danger signal in gout and its comorbidities, Nat. Rev. Rheumatol. 9 (2013) 13–23.
[3] J. Du, J.J. Cullen, G.R. Buettner, Ascorbic acid: chemistry, biology and the treatment of cancer, Biochim. Biophys. Acta, Rev. Cancer 1826 (2012) 443–457.
[4] M.G. Traber, J.F. Stevens, Vitamins C and E: beneficial effects from a mechanistic perspective, Free Radical Biol. Med. 51 (2011) 1000–1013.
[5] C.-L. Sun, C.-T. Chang, H.-H. Lee, J. Zhou, J. Wang, T.-K. Sham, W.-F. Pong, Microwave-assisted synthesis of a core–shell MWCNT/GONR heterostructure for the electrochemical detection of ascorbic acid, dopamine, and uric acid, ACS Nano 5 (2011) 7788–7795.
[6] M. Hadi, A. Rouhollahi, Simultaneous electrochemical sensing of ascorbic acid, dopamine and uric acid at anodized nanocrystalline graphite-like pyrolytic carbon film electrode, Anal. Chim. Acta 721 (2012) 55–60.
[7] K. Deng, J. Zhou, X. Li, Noncovalent nanohybrid of cobalt tetraphenylporphyrin with graphene for simultaneous detection of ascorbic acid, dopamine, and uric acid, Electrochim. Acta 114 (2013) 341–346.
[8] J. Jiang, X. Du, Sensitive electrochemical sensors for simultaneous determination of ascorbic acid, dopamine, and uric acid based on Au@Pd-reduced graphene oxide nanocomposites, Nanoscale 6 (2014) 11303–11309.
[9] P.E. Erden, E. Kiliç, A review of enzymatic uric acid biosensors based on amperometric detection, Talanta 107 (2013) 312–323.
[10] M.N. Szentirmay, C.R. Martin, Ion-exchange selectivity of Nafion films on electrode surfaces, Anal. Chem. 56 (1984) 1898–1902.
[11] H.-S. Wang, T.-H. Li, W.-L. Jia, H.-Y. Xu, Highly selective and sensitive determination of dopamine using a Nafion/carbon nanotubes coated poly(3-methylthiophene) modified electrode, Biosens. Bioelectron. 22 (2006) 664–669.
[12] D. Bellido-Milla, L. Cubillana-Aguilera, M. El Kaoutit, M. Hernández-Artiga, J. Hidalgo-Hidalgo de Cisneros, I. Naranjo-Rodríguez, J. Palacios-Santander, Recent advances in graphite powder-based electrodes, Anal. Bioanal. Chem. 405 (2013) 3525–3539.
[13] I. Švancara, A. Walcarius, K. Kalcher, K. Vytřas, Carbon paste electrodes in the new millennium, Cent. Eur. J. Chem. 7 (2009) 598–656.
[14] C. Oueiny, S. Berlioz, F.-X. Perrin, Carbon nanotube–polyaniline composites, Prog. Polym. Sci. 39 (2014) 707–748.
[15] H. Beitollahi, M.M. Ardakani, B. Ganjipour, H. Naeimi, Novel 2,2′-[1,2-ethanediylbis(nitriloethylidyne)]-bis-hydroquinone double-wall carbon nanotube paste electrode for simultaneous determination of epinephrine, uric acid and folic acid, Biosens. Bioelectron. 24 (2008) 362–368.
[16] H. Karimi-Maleh, F. Tahernejad-Javazmi, A.A. Ensafi, R. Moradi, S. Mallakpour, H. Beitollahi, A high sensitive biosensor based on FePt/CNTs nanocomposite/N-(4-hydroxyphenyl)-3,5-dinitrobenzamide modified carbon paste electrode for simultaneous determination of glutathione and piroxicam, Biosens. Bioelectron. 60 (2014) 1–7.
[17] L. Peng, A. Feng, M. Huo, J. Yuan, Ferrocene-based supramolecular structures and their applications in electrochemical responsive systems, Chem. Commun. 50 (2014) 13005–13014.
[18] Y. Lu, Y. Jiang, H. Wu, W. Chen, Ferrocene-functionalized graphene oxide nanosheets: efficient electronic communication between ferrocene centers across graphene nanosheets, Electrochim. Acta 156 (2015) 267–273.
[19] H. Cheng, H. Qiu, Z. Zhu, M. Li, Z. Shi, Investigation of the electrochemical behavior of dopamine at electrodes modified with ferrocene-filled double-walled carbon nanotubes, Electrochim. Acta 63 (2012) 83–88.
[20] J.-B. Raoof, R. Ojani, A. Kiani, Carbon paste electrode spiked with ferrocene carboxylic acid and its application to the electrocatalytic determination of ascorbic acid, J. Electroanal. Chem. 515 (2001) 45–51.
[21] J.-B. Raoof, R. Ojani, M. Baghayeri, Simultaneous electrochemical determination of glutathione and tryptophan on a nano-TiO2/ferrocene carboxylic acid modified carbon paste electrode, Sens. Actuators B 143 (2009) 261–269.
[22] D. Savage, S.R. Alley, J.F. Gallagher, A. Goel, P.N. Kelly, P.T. M. Kenny, The synthesis and structural characterization of novel *N*-meta-ferrocenyl benzoyl dipeptide esters, Inorg. Chem. Commun. 9 (2006) 152–155.
[23] L. Chaicharoenwimolkul, S. Chairam, M. Namkajorn, A. Khamthip, C. Kamonsatikul, U. Tewasekson, S. Jindabot, W. Pon-On, E. Somsook, Effect of ferrocene substituents and ferricinium additive on the properties of polyaniline derivatives and catalytic activities of palladium-doped poly(*m*-ferrocenylaniline)-catalyzed Suzuki–Miyaura cross-coupling reactions, J. Appl. Polym. Sci. 130 (2013) 1489–1497.
[24] S. Chairam, W. Sroysee, C. Boonchit, C. Kaewprom, T.G.N. Wangnoi, M. Amatatongchai, P. Jarujamrus, S. Tamaung, E. Somsook, Nonenzymatic sensor for hydrogen peroxide using a carbon paste electrode modified with a composite consisting of silver nanoparticles, poly(*o*-aminobenzoic acid) and magnetite, Int. J. Electrochem. Sci. 10 (2015) 4611–4625.
[25] M.M. Barsan, M.E. Ghica, C.M.A. Brett, Electrochemical sensors and biosensors based on redox polymer/carbon nanotube modified electrodes: a review, Anal. Chim. Acta 881 (2015) 1–23.

[26] H. Nishihara, M. Murata, Electron transfer in ferrocene-containing π-conjugated polymers, J. Inorg. Organomet. Polym Mater. 15 (2005) 147–156.
[27] L. Yang, D. Liu, J. Huang, T. You, Simultaneous determination of dopamine, ascorbic acid and uric acid at electrochemically reduced graphene oxide modified electrode, Sens. Actuators B 193 (2014) 166–172.
[28] M. Chen, X. Wei, H. Qian, G. Diao, Fabrication of GNPs/CDSH–Fc/nafion modified electrode for the detection of dopamine in the presence of ascorbic acid, Mater. Sci. Eng. C 31 (2011) 1271–1277.
[29] L.S. Rocha, H.M. Carapuça, Ion-exchange voltammetry of dopamine at Nafion-coated glassy carbon electrodes: quantitative features of ion-exchange partition and reassessment on the oxidation mechanism of dopamine in the presence of excess ascorbic acid, Bioelectrochemistry 69 (2006) 258–266.
[30] J.-M. Zen, C.-T. Hsu, A selective voltammetric method for uric acid detection at Nafion®-coated carbon paste electrodes, Talanta 46 (1998) 1363–1369.
[31] Y.-T. Shieh, Y.-T. Lu, T.-L. Wang, C.-H. Yang, R.-H. Lin, Electrocatalytic activities of Nafion/CdSe/Self-doped polyaniline composites to dopamine, uric acid, and ascorbic acid, J. Solid State Electrochem. 18 (2014) 975–984.
[32] D.P. Quan, D.P. Tuyen, T.D. Lam, P.T.N. Tram, N.H. Binh, P. H. Viet, Electrochemically selective determination of dopamine in the presence of ascorbic and uric acids on the surface of the modified Nafion/single wall carbon nanotube/poly(3-methylthiophene) glassy carbon electrodes, Colloids Surf. B 88 (2011) 764–770.
[33] S. Jiao, M. Li, C. Wang, D. Chen, B. Fang, Fabrication of Fc–SWNTs modified glassy carbon electrode for selective and sensitive determination of dopamine in the presence of AA and UA, Electrochim. Acta 52 (2007) 5939–5944.
[34] Q. Chen, S. Ai, Q. Ma, H. Yin, Selective determination of dopamine in the presence of ascorbic acid using ferrocenyl-tethered PAMAM dendrimers modified glassy carbon electrode, J. Appl. Electrochem. 40 (2010) 1379–1385.
[35] X. Lin, G. Kang, L. Lu, DNA/Poly(*p*-aminobenzenesulfonic acid) composite bi-layer modified glassy carbon electrode for determination of dopamine and uric acid under coexistence of ascorbic acid, Bioelectrochemistry 70 (2007) 235–244.
[36] A.S. Kumar, P. Swetha, K.C. Pillai, Enzyme-less and selective electrochemical sensing of catechol and dopamine using ferrocene bound Nafion membrane modified electrode, Anal. Methods 2 (2010) 1962–1968.
[37] A.A. Ensafi, A. Arabzadeh, H. Karimi-Maleh, Simultaneous determination of dopamine and uric acid by electrocatalytic oxidation on a carbon paste electrode using pyrogallol red as a mediator, Anal. Lett. 43 (2010) 1976–1988.
[38] Y. Bu, W. Dai, N. Li, X. Zhao, X. Zuo, The graphene nanopowder for electro-catalytic oxidation of dopamine and uric acid in the presence of ascorbic acid, J. Energy Chem. 22 (2013) 685–689.
[39] Y.-K. Chih, M.-C. Yang, An 2,2′-azino-bis(3-ethylbenzthiazoline-6-sulfonic acid)-immobilized electrode for the simultaneous detection of dopamine and uric acid in the presence of ascorbic acid, Bioelectrochemistry 91 (2013) 44–51.
[40] E. Alipour, M.R. Majidi, A. Saadatirad, S.M. Golabi, A.M. Alizadeh, Simultaneous determination of dopamine and uric acid in biological samples on the pretreated pencil graphite electrode, Electrochim. Acta 91 (2013) 36–42.
[41] Y. Li, M. Yao, T.-T. Li, Y.-Y. Song, Y.-J. Zhang, S.-Q. Liu, Simultaneous electrochemical determination of uric acid and dopamine in the presence of ascorbic acid using nitrogen-doped carbon hollow spheres, Anal. Methods 5 (2013) 3635–3638.
[42] S.E. Baghbamidi, H. Beitollahi, S.Z. Mohammadi, S. Tajik, S. Soltani-Nejad, V. Soltani-Nejad, Nanostructure-based electrochemical sensor for the voltammetric determination of benserazide, uric acid, and folic acid, Chin. J. Catal. 34 (2013) 1869–1875.
[43] T.-Q. Xu, Q.-L. Zhang, J.-N. Zheng, Z.-Y. Lv, J. Wei, A.-J. Wang, J.-J. Feng, Simultaneous determination of dopamine and uric acid in the presence of ascorbic acid using Pt nanoparticles supported on reduced graphene oxide, Electrochim. Acta 115 (2014) 109–115.
[44] H. Zhang, P. Dai, L. Huang, Y. Huang, Q. Huang, W. Zhang, C. Wei, S. Hu, A nitrogen-doped carbon dot/ferrocene@[small beta]-cyclodextrin composite as an enhanced material for sensitive and selective determination of uric acid, Anal. Methods 6 (2014) 2687–2691.

Talanta 156-157 (2016) 154–162

Contents lists available at ScienceDirect

Talanta

journal homepage: www.elsevier.com/locate/talanta

# A sensitive and selective on-line amperometric sulfite biosensor using sulfite oxidase immobilized on a magnetite-gold-folate nanocomposite modified carbon-paste electrode

Wongduan Sroysee, Kitayanan Ponlakhet, Sanoe Chairam, Purim Jarujamrus, Maliwan Amatatongchai *

*Department of Chemistry and Center of Excellence for Innovation in Chemistry, Faculty of Science, Ubon Ratchathani University, Ubon Ratchathani 34190, Thailand*

ARTICLE INFO

*Article history:*
Received 6 March 2016
Received in revised form
27 April 2016
Accepted 28 April 2016
Available online 7 May 2016

*Keywords:*
Sulfite
Biosensor
Amperometry
$Fe_3O_4$@Au
Folic acid
Carbon paste electrode

ABSTRACT

We describe a novel amperometric sulfite biosensor, comprising a carbon-paste electrode ($Fe_3O_4$@Au-Cys-FA/CPE) modified with immobilized sulfite oxidase (SOx) on a gold-coated magnetite nanoparticle core, encased within a conjugated folic acid (FA) cysteine (Cys) shell. The biosensor electrode was fabricated using a polydimethylsiloxane (PDMS) and mineral oil mixture as binder, which also enhances the physical stability and sensitivity of the electrode. The developed biosensor displays good electrocatalytic activity toward oxidation of $H_2O_2$, which occurs by an enzymatic reaction between SOx and sulfite. The $Fe_3O_4$@Au-Cys-FA electrode exhibits good electrocatalytic activity, and has good retention of chemisorbed SOx on the electrode because of its large surface area. Sulfite was quantified using amperometric measurements from the $Fe_3O_4$@Au-Cys-FA/CPE biosensor, and using an in-house assembled flow cell at +0.35 V (vs. Ag/AgCl), with a phosphate buffer carrier (0.10 M, pH 7.0) at a flow rate of 0.8 mL $min^{-1}$. The system detects sulfite over the range 0.1–200 mg $L^{-1}$ ($r^2$=0.998), with a detection limit of 10 μg $L^{-1}$ (3σ of blank). The system exhibits acceptable precision (%R.S.D.=3.1%), rapid sample throughput (109 samples $h^{-1}$), and good stability (2 w). The developed biosensor shows satisfactory tolerance to potential interferences, such as sugars, anions, ascorbic acid, and ethanol. We applied the developed method to the determination of sulfite content in wines and pickled food extracts, and our results are in good agreement with those obtained by the standard iodometric method.



## 1. Introduction

Sulfite ion ($SO_3^{2-}$) has wide application as a food preservative and as an antioxidant in food and beverages to inhibit enzymatic and non-enzymatic activities that cause browning, and to suppress the growth of microorganisms during storage [1–4]. However, sulfite is potentially toxic and may cause adverse reactions in sulfite-sensitive, asthmatic individuals [1–3]. The US Food and Drug Administration (FDA), recommends warning labels on any food that contains sulfite at concentrations greater than 10 mg $kg^{-1}$, and on beverage and wine products containing in excess of 10 mg $L^{-1}$ sulfite [1–5]. To accurately control the quality of manufactured products, a simple, sensitive, and accurate analytical method for the determination of sulfite is required.

Various techniques for quantitative analysis of sulfite are available, including fluorescence spectroscopy [6], high-performance liquid chromatography in combination with ultraviolet spectrophotometry [7], and chemiluminescence spectroscopy [1,8]. However, these techniques are time-consuming, need sample pre-treatment and reagent preparation, and may suffer from lack of sensitivity or precision, and so, the development of more sensitive and selective methods is crucially important for routine monitoring. Electrochemical measurements, using enzymatic modification at metallic electrodes, carbon/graphite electrodes, or chemically modified electrodes, offer several benefits over traditional methods, including greater selectivity, sensitivity, and reliability, and offer the possibility of on-line applications [9]. Fabrication of ch7emically modified electrodes allows electrocatalysis of sulfite oxidation reactions and reduction of the sulfite oxidation potential [10–12], although the reported selectivity, sensitivity, and reliability are poor. Thus, it is of considerable interest to develop an enzyme-based biosensor for the detection of sulfite ion; this would provide high selectivity, sensitivity, and accuracy in the

* Corresponding author.
*E-mail address:* maliwan.a@ubu.ac.th (M. Amatatongchai).

http://dx.doi.org/10.1016/j.talanta.2016.04.066
0039-9140/

quantification of sulfite, without interference from sample constituents or fouling of the electrode. A high degree of selectivity toward sulfite is achievable by using sulfite oxidase (SOx) enzyme to convert sulfite to sulfate and $H_2O_2$ [9, 13–15]. There are several recent reports of amperometric sulfite-biosensors using SOx immobilized on various electrodes [13–15]. These biosensors use a SOx catalyzed reaction for sulfite detection; molybdenum active sites in SOx undergo both oxidation and reduction during oxidation of sulfite to sulfate [15]. Sulfite determination can be performed by detecting the SOx-electrode signal directly, or indirectly by monitoring the depletion of oxygen or formation of $H_2O_2$ [9,14,15]. The simplest approach might be to measure the generation of peroxide. However, the high operating potential of such a biosensor, can result in oxidation of other components within the sample matrix, which will generate nonspecific signals. Electron-transfer mediators such as tetrathiafulvalene (TTF) [15], cytochrome c (Cyt c) [13,14], and ferro/ferricyanide [16] provide greater selectivity for sulfite determination by $H_2O_2$ detection. Minimization of the biosensor operating potential is based on either regeneration of the mediator, or on catalysis of $H_2O_2$ formation, or both [9,15].

Magnetite ($Fe_3O_4$) nanoparticles have useful physical and chemical properties including being superparamagnetic, having a large surface area, strong adsorption characteristics, good mechanical stability and electrical conductivity, and superb electrocatalytic activity [17–19]. There are many approaches available for the functionalization or modification of $Fe_3O_4$ surfaces for biomedical applications. Methods include using metals, oxides, organic monolayers, and polymers [17]. One of the most promising modifications is to use gold-coated magnetite ($Fe_3O_4$@Au). This material is simple to prepare, offers the possibility of bioconjugation, and has good biocompatibility for drug delivery applications [17,18]. Samphao et al.[20] and Li et al. [21] reported the application of $Fe_3O_4$@Au to improve electrocatalytic activity in enzyme-based sensors for the analysis of glucose [20] and *Escherichia coli* [21]. $Fe_3O_4$@Au nanoparticles were integrated into composite materials to immobilize glucose oxidase [20] and horseradish peroxidase [21] via chemisorption or physisorption, and then used to modify screen printed electrodes [20] and glassy carbon electrodes [21]. Recently, Karamipour et al. [22] reported the synthesis of folic acid (FA)-cysteine (Cys)-conjugated gold-coated magnetite nanoparticles ($Fe_3O_4$@Au-Cys-FA) using L-cysteine as a bi-functional linker for attachment to the gold surface via its thiol group. The nanomaterial was characterized and designed its utilization to drug delivery applications. However, there are no reports of catalyst or biosensor applications using $Fe_3O_4$@Au-Cys-FA nanocomposite materials.

In this work, we report the synthesis of $Fe_3O_4$@Au-Cys-FA nanoparticles and fabrication of a sensitive and selective sulfite biosensor. The biosensor was constructed by immobilizing sulfite oxidase on a $Fe_3O_4$@Au-Cys-FA nanocomposite-modified carbon paste electrode via direct chemisorption. To our knowledge, this is the first report of using $Fe_3O_4$@Au-Cys-FA to enhance the electrocatalytic activity and enzyme immobilizing performance of a sulfite biosensor. The $Fe_3O_4$@Au-Cys-FA/CPE provides significant improvement in biosensor performance. The large surface area and unique nanostructure of $Fe_3O_4$@Au-Cys-FA provide good electrocatalytic activity and facilitate retention of SOx on the electrode, resulting in high sensitivity and selectivity by the biosensor. When applied to on-line amperometric detection of sulfite in a flow injection (FI) system, the sensor successfully quantified sulfite in pickled food extracts and wine samples. The biosensor exhibits excellent sensitivity, selectivity, and stability with a sample throughput of 109 samples per hour.

## 2. Experimental

### 2.1. Chemicals and reagents

All chemicals used were of analytical reagent grade. Deionized-distilled water (Water Pro-PS, USA) was used for preparation of standards and reagents. Chicken liver sulfite oxidase (SOx, 30–70 U $mg^{-1}$) was purchased from ProNique Scientific, Inc. (Castle Rock, USA). Sodium sulfite ($Na_2SO_3$) and horse heart cytochrome c (Cyt c, 90%) were purchased from Sigma-Aldrich (St. Louis, USA). Hydrogen tetrachloroaurate (III) hydrate ($HAuCl_4 \cdot 3H_2O$), 99.99%), N, N′-dicyclohexylcarbodimide (DCC), folic acid ($C_{19}H_{19}N_7O_6$, 97% purity), L-Cysteine ($C_3H_7NO_2S$), tri-sodium citrate dihydrate ($C_6H_5Na_3O_7 \cdot 2H_2O$), $NaH_2PO_4 \cdot H_2O$, $Na_2HPO_4$, ferric nitrate nonahydrate ($Fe(NO_3)_3 \cdot 9H_2O$), ferrous sulfate heptahydrate ($Fe(SO_4)_2 \cdot 7H_2O$), and graphite powder were purchased from Acros Organic (Geel, Belgium). Poly(dimethylsiloxane) (Sylgard® 184) were purchased from Dow Corning (Wiesbaden, Germany).

### 2.2. Apparatus

#### 2.2.1. Cyclic voltammetry

Cyclic voltammetry (CV) was performed in batches using an eDAQ potentiostat (model EA161, Australia) equipped with e-corder (model 210), and e-Chem software v2.0.13. For CV measurements, we used a self-assembled three-electrode cell, comprising a $Fe_3O_4$@Au-Cys-FA-SOx carbon-paste working electrode, an Ag/AgCl (sat.) reference electrode, and a platinum wire counter electrode. The carbon paste electrode (CPE) active surface area was approximately 0.031 $cm^2$ (inner diameter 0.2 cm). Electrochemical measurements were performed in phosphate buffered solution (PBS) (0.1 M, pH 7).

For the cyclic voltammetry study, we assembled electrodes by packing $Fe_3O_4$@Au-Cys-FA-SOx paste inside a glass tube (inner diameter 0.2 cm, length 7.5 cm) and fixing a copper wire in place using epoxy resin. The $Fe_3O_4$@Au-Cys-FA electrode surface was polished to a smooth surface with weighing paper. The electrode was encapsulated by drop casting 0.01% Nafion® solution in water (10 μL) onto the polished electrode surface. Finally, the electrode was dried at room temperature, and then stored at 4 °C in a refrigerator until required for use.

#### 2.2.2. On-line amperometric detection using a simple flow injection system

The flow injection system used for amperometric detection of sulfite [23] comprised a Shimadzu pump (model LC-10CE, Japan), a Rheodyne injector (model 7725, USA) fitted with a 20 μL sample loop, and an electrochemical detector (ECD). For the measurements, we used an eDAQ potentiostat (EA161), equipped with an e-corder 210, Chart software v5.5.11, and our in-house three-electrode flow cell. The $Fe_3O_4$@Au-Cys-FA carbon-paste biosensor served as the working electrode, Ag/AgCl as the reference electrode, and a stainless steel tube as the counter electrode. The electrode area in the flow cell was approximately 0.060 $cm^2$.

The $Fe_3O_4$@Au-Cys-FA/CPE electrodes were assembled by packing composite paste inside the working electrode block of the thin-layer flow cell (Fig. 1B). The surface of the electrode was covered with a 0.01% Nafion® film (40 μL), formed by drop casting and drying at room temperature. In the ECD, a silicone rubber gasket (flow channel = $0.1 \times 0.6$ $cm^2$) provided a spacer between the base of the cell and the working electrode. The analyte solution passes through an inlet passage in the base, and along a channel in the gasket contacting the biosensor, then to the outlet.

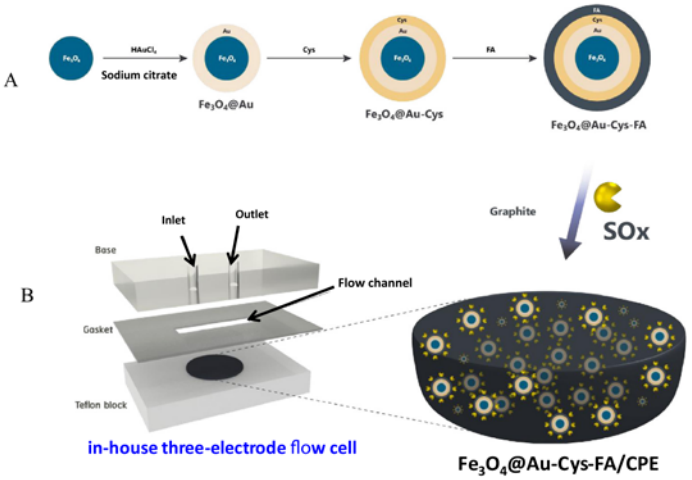


**Fig. 1.** Preparation of sulfite biosensors (A) $Fe_3O_4$@Au-Cys-FA nanocomposites with immobilized Sox, and (B) $Fe_3O_4$@Au-Cys-FA modified carbon-paste electrode.

*2.2.3. Characterization*

A JEM-1230 transmission electron microscope (TEM; JEOL, Japan) was used to observe the size and morphology of $Fe_3O_4$ and $Fe_3O_4$@Au nanoparticles. Elemental analysis data for $Fe_3O_4$ and $Fe_3O_4$@Au, and EDS spectra for $Fe_3O_4$@Au-Cys-FA nanoparticles were collected using energy dispersive X-ray spectroscopy (INCAx-sight, UK) coupled to a scanning electron microscope (SEM, JEOL, JSM-6460LV, Japan) operated under vacuum at an accelerating voltage of 20 kV.

*2.3. Preparation of the sulfite biosensor*

*2.3.1. Preparation of magnetite nanoparticles ($Fe_3O_4$)*

Magnetite nanoparticles were prepared by co-precipitation, following a method described by Karamipour et al. [22] and Kouassi et al. [24]. Briefly, $Fe(NO_3)_3 \cdot 9H_2O$ (0.02 mol) and $FeSO_4 \cdot 7H_2O$ (0.01 mol) were dissolved in HCl (60 mL, 0.2 M). The mixed solution of ferrous and ferric salts was then added dropwise into aqueous NaOH solution (100 mL, 1 M, purged with nitrogen gas) with vigorous stirring at 70 °C under nitrogen. Stirring was continued for a further 2 h. The formed black $Fe_3O_4$ precipitates were collected by an external magnetic field, washed with water three times by magnetic decantation, and then dried in a desiccator.

*2.3.2. Preparation of $Fe_3O_4$@Au*

$Fe_3O_4$@Au nanoparticles were prepared following literature methods [22,25], with some modifications. First, $Fe_3O_4$ nanoparticles (30 mg) were dispersed in 10 mL of water in an ultrasonic bath for 30 min Next, $Au^{3+}$ was reduced to $Au^{\circ}$ on the surface of $Fe_3O_4$ using tri-sodium citrate. The dispersion was added into a 250 mL round-bottom flask containing 40 mL of distilled water, and 20 mL of 0.1% $HAuCl_4$ was added while stirring. The reaction was bought to a boil under reflux. Upon boiling, 4 mL of 1 wt% tri-sodium citrate was rapidly added to the stirred solution. The solution color changed from brown to reddish brown and the stirred mixture was kept at reflux for a further 15 min The red-brown $Fe_3O_4$@Au nanoparticles were separated using an external magnetic field, washed with water three times by magnetic decantation, and then dried in a desiccator.

*2.3.3. Preparation of $Fe_3O_4$@Au-Cys-FA*

Fig. 1A illustrates the preparation of $Fe_3O_4$@Au-Cys-FA nanocomposite. $Fe_3O_4$@Au-Cys-FA nanoparticles was synthesized using L-cysteine as a bi-functional linker The L-cysteine thiol (-SH) group links to the gold surface, and the amino (-$NH_2$) group condenses with the folic acid (FA) carboxylic acid group (–COOH) to form an amide bond [22]. Briefly, the red-brown $Fe_3O_4$@Au solution was adjusted to pH 10 using a 1% aqueous ammonia solution. L-cysteine (5 mL, 1 mM) was added to the $Fe_3O_4$@Au solution and the mixture stirred for 24 h at room temperature. During this phase, the thiol group on L-cysteine displaces the citrate moiety responsible for solvation of the nanoparticles. The $Fe_3O_4$@Au-Cys nanoparticles were separated using an external magnetic field, washed three times with water by magnetic decantation, and then dried in a desiccator.

Next, $Fe_3O_4$@Au-Cys (50 mg) was dispersed in 10 mL of $CH_2Cl_2$. Folic acid (0.1 g) was dissolved in 10 mL of DMSO, and N, N′ dicyclohexylcarbodiimide (DCC) (0.06 g) was added to the solution. The $Fe_3O_4$@Au-Cys dispersion and folic acid-DMSO solution were sonicated together in an ultrasonic bath for 30 min, and the solution then stirred at room temperature for 24 h. $Fe_3O_4$@Au-Cys-FA nanoparticles were separated using an external magnetic field, then washed three times with $CH_2Cl_2$, deionized water, and ethanol. After drying in a desiccator, $Fe_3O_4$@Au-Cys-FA nanoparticles were obtained as a red-brown powder.

*2.3.4. Fabrication of the $Fe_3O_4$@Au-Cys-FA carbon-paste electrode*

Fig. 1 illustrates the preparation of the sulfite biosensor. The $Fe_3O_4$@Au-Cys-FA/CPE device was prepared by thoroughly mixing graphite powder (0.950 g), $Fe_3O_4$@Au-Cys-FA nanoparticles (0.035 g), and PDMS (0.015 g) to a homogenous consistency using a mortar and pestle. The composite material was then heated to 60 °C for 30 min Immobilization of SOx was performed by dropping SOx solution (40 μL, 0.1 mg $mL^{-1}$), containing Cyt c (40 mg $mL^{-1}$), onto the composite. Cyt c was using as mediator between SOx and the electrode to obtain selectivity for sulfite determination. Mineral oil (30 μL) was then added and thoroughly mixed. The electrodes were fabricated in-house as described in the cyclic voltammetry section below.

### 2.4. Sample preparation for sulfite determination

Various brands of wines and pickled food samples, including mango, cabbage, and ginger were used for sulfite assay. Wine samples were filtered through a 0.25-micron cellulose membrane and diluted appropriately with phosphate buffer prior to sulfite determination. For pickled food samples, we used an extraction scheme described by Alamo et al. [26]. Briefly, samples were weighed in 50 g aliquots, and homogenized in phosphate buffer (50 mL) using a blender. The homogenized mixture was collected and filtered through a 0.25-micron cellulose membrane. Sulfite content was quantified by the standard addition method.

### 2.5. Method validation

Sulfite determination results obtained using the proposed FI-sulfite biosensor were compared to those obtained from a standard iodometric method [27,28]. An accurately measured sample volume (5.00 mL) was transferred into a 125 mL conical flask, and 5.00 mL of standard iodine solution was added. Excess iodine was titrated with standard sodium thiosulfate solution using starch as indicator. Titrations were carried out as quickly as possible, with the end point indicated by the formation of a light blue color.

Wine and pickled food samples were purchased from local supermarkets in Ubon Ratchathani province, Thailand. Five brands of wines (W1-W5) and three brands each of picked cabbage (C1-C3), pickled mango (M1-M3), and picked ginger (G1-G3) were used for sulfite assay using the developed amperometric biosensor. Sample aliquots were diluted 3 or 6 fold with phosphate buffer prior to analysis.

## 3. Results and discussion

### 3.1. Characterization of $Fe_3O_4$@Au-Cys-FA nanocomposites

Nanocomposite morphology was studied by TEM, SEM, and EDS. TEM samples were prepared by ultrasonic dispersion of the product in deionized water, and drying a drop of the resulting suspension on a copper grid. Fig. 2 shows TEM images of (A) synthesized $Fe_3O_4$ nanoparticles, and (B) $Fe_3O_4$@Au nanocomposites. $Fe_3O_4$ nanoparticles appear approximately spherical in shape with an average diameter of $11.5 \pm 2.1$ nm. After reduction of $Au^{3+}$ to $Au^0$ on the $Fe_3O_4$ nanoparticle surface, the obtained nanocomposites appear much darker than the uncoated $Fe_3O_4$ nanoparticles (Fig. 2B) because of heavy atom effects [22,29]. The figure shows that the nanocomposite materials aggregate when dried [23,29,30]. The average $Fe_3O_4$@Au nanocomposite diameter is $14.1 \pm 3.3$ nm. The formation of $Fe_3O_4$@Au-Cys-FA was confirmed by SEM and EDS (Fig. 2C and D). Fig. 2C shows the micro-morphologies of the synthesized $Fe_3O_4$@Au-Cys-FA. SEM images of $Fe_3O_4$ and $Fe_3O_4$@Au (Supplementary Fig. S1) further suggests that the surface modification of $Fe_3O_4$ and $Fe_3O_4$@Au supports were successful. We used EDS to characterize the composition of the synthesized $Fe_3O_4$@Au–Cys-FA nanocomposites (Fig. 2D). The EDS spectrum reveals the presence of Fe, O, Au, and S atoms, and provides evidence for an attachment between $Fe_3O_4$@Au and folic acid via the thiol group on L-cysteine,

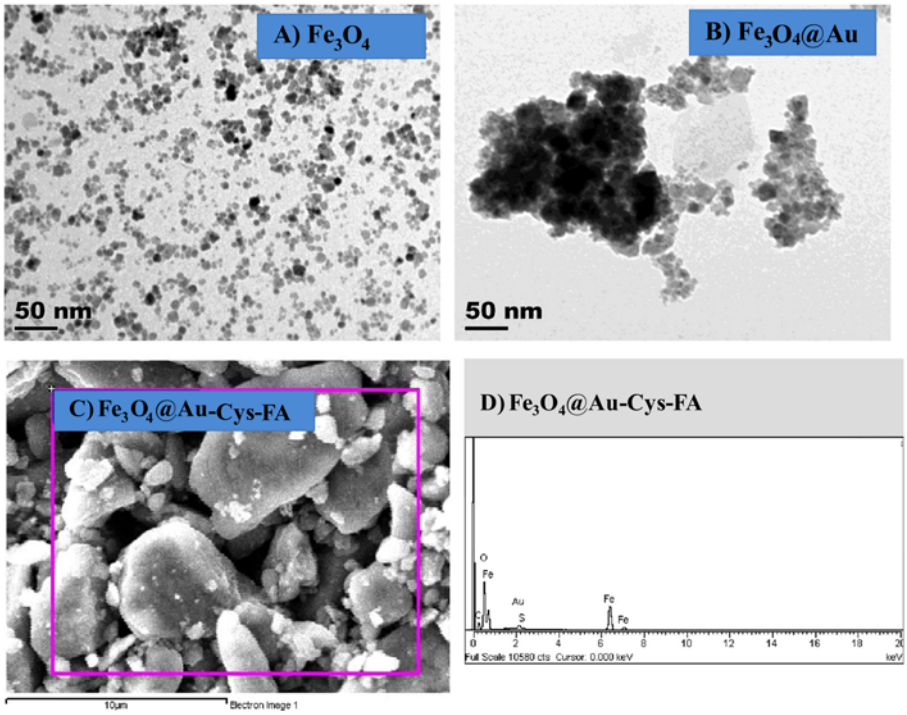


**Fig. 2.** TEM images of (A) $Fe_3O_4$ and (B) $Fe_3O_4$@Au. (C) SEM image of $Fe_3O_4$@Au-Cys-FA nanoparticles, and (D) the EDS spectrum of $Fe_3O_4$@Au-Cys-FA nanoparticles.

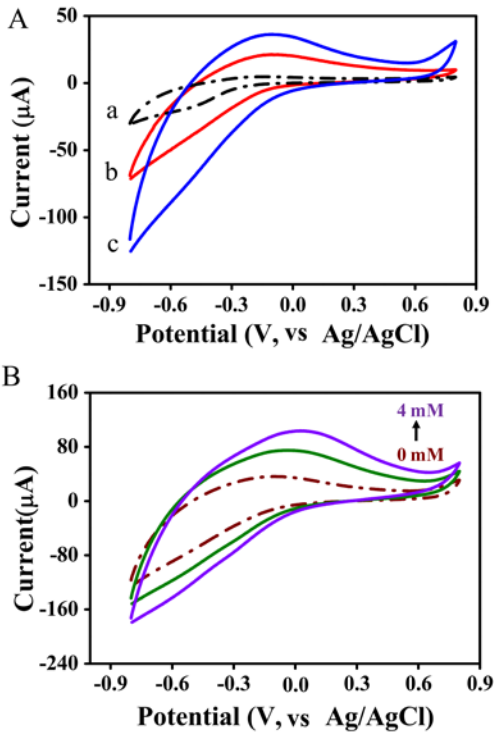


**Fig. 3.** (A) Cyclic voltammograms of (a) $Fe_3O_4$@Au/CPE biosensor, (b) $Fe_3O_4$@Au-Cys/CPE biosensor, and (c) $Fe_3O_4$@Au-Cys-FA/CPE biosensor, in 0.1 M PBS (pH 7) at a scan rate of 50 mV $s^{-1}$. (B) CVs of 0, 2, and 4 mM of sulfite on the $Fe_3O_4$@Au-Cys-FA/CPE biosensor, at a scan rate of 50 mV $s^{-1}$.

confirming the formation of $Fe_3O_4$@Au-Cys-FA [22].

### 3.2. Electrocatalytic behavior of the $Fe_3O_4$@Au-Cys-FA carbon paste electrode

Cyclic voltammetry (CV) is a useful technique to study the electrocatalytic behavior of nanomaterial-modified electrodes. The electrochemical behaviors of the carbon paste electrodes containing immobilized SOx were investigated using 0.1 M PBS as the supporting electrolyte. Fig. 3A shows cyclic voltammograms for (a) $Fe_3O_4$@Au/CPE, (b) $Fe_3O_4$@Au-Cys/CPE, and (c) $Fe_3O_4$@Au-Cys-FA/CPE. The $Fe_3O_4$@Au, $Fe_3O_4$@Au-Cys, and $Fe_3O_4$@Au-Cys-FA carbon-paste biosensors produce characteristic responses. The cyclic voltammogram for the $Fe_3O_4$@Au-Cys-FA modified carbon paste (Fig. 3A, curve c) shows the greatest current response, and exhibits the least negative peak potential when compared to the $Fe_3O_4$@Au and $Fe_3O_4$@Au-Cys CV plots. Therefore, we conclude that $Fe_3O_4$@Au-Cys-FA will provide the greatest enhancement in redox response and electrocatalytic activity.

Fig. 3B shows voltammograms obtained in the absence of sulfite (dotted line), and in the presence of 2 mM and 4 mM sulfite (solid lines) for the $Fe_3O_4$@Au-Cys-FA/CPE biosensor. $Fe_3O_4$@Au-Cys-FA/CPE biosensor exhibits quasi-reversible oxidation peaks at approximately −0.10 V versus Ag/AgCl. The oxidation peaks at approximately −0.10 V correspond to oxidation of $H_2O_2$ by enzymatic reaction between SOx and sulfite. The figure shows that increased sulfite concentrations induce apparent enhancements in the oxidation-reduction peak currents, because of increased $H_2O_2$ concentrations during enzymatic reaction. These oxidation peaks at approximately −0.10 V clearly demonstrate the $Fe_3O_4$@Au-Cys-FA/CPE catalytic properties. The electrochemical reactions associated with this amperometric biosensor may be a two-step process [31–33]:

$$SO_3^{2-} + O_2 + H_2O \xrightarrow{\text{sulfite oxidase}} SO_4^{2-} + H_2O_2 \quad (1)$$

$$H_2O_2 \xrightarrow{\text{CPE}} O_2 + 2H^+ + 2e^- \quad (2)$$

$H_2O_2$, the product from Eq. (1) was electrochemically measured at the sulfite biosensor ($Fe_3O_4$@Au-Cys-FA/CPE). Thus the amount of $H_2O_2$ produced in the SOx reaction can be used to indirectly determine sulfite level. To clarify that the observed catalytic oxidation current was due to the generated $H_2O_2$ by SOx, the effects of $H_2O_2$ on the non-enzymatic electrode based on CPE modified with $Fe_3O_4$@Au-Cys-FA were investigated. Cyclic voltammograms (Fig. S2d) show that the oxidation current based on $H_2O_2$from +0.35 V was observed at the non-enzymatic electrode. Furthermore, FIA grams obtained from amperometric measurement of the non-enzymatic electrode at +0.35 V (vs. Ag/AgCl), (Fig. S5) revealed that the oxidation peak currents increase linearly with increasing the concentration of $H_2O_2$.

In this work, a Nafion® film formed by drop casting provides a stable support to the $Fe_3O_4$@Au-Cys-FA/CPE biosensor. It is known that chemically inert ionomeric membrane of Nafion® can be mainly used to avoid influence negatively charged interferents such as ascorbate [34,35] in real samples. On the other hand, to clarify the acceptable permeable of the negatively charged of sulfite analyte to the Nafion® covered electrode surface is caused. Linear correlation between oxidation currents and the concentration of analyte obtained from CV and FIA experiments (Fig. 3B and Fig. S5) demonstrated that there are efficient diffusion shuttle between the Nafion® film and electrode surface. These results are in good accordance with the reports for the application of Nafion® coated electrode surfaces for determination of some anions including nitrite [36], sulfite [37] and the reduction of dioxygen to $H_2O_2$ [38].

The relationship between peak current and scan rate was examined at the $Fe_3O_4$@Au-Cys-FA/CPE. The results reveals that anodic and cathodic peak currents (μA) increase linearly with the square root of the scan rate ($\nu^{1/2}$ $s^{-1/2}$) over the scan range 0.05–0.40 V $s^{-1}$. Linear regression analysis provides $r^2$ values of 0.995, indicating a diffusion controlled quasi-reversible electrochemical process.

To investigate the effect of sulfite concentration over the range 0.5–10 mg $L^{-1}$, we calculated the apparent Michaelis-Menten constant ( $K_M^{app}$) from a Lineweaver-Burk plot (data not shown) [23,39,40]:

$$\frac{1}{I_{ss}} = \frac{1}{I_{max}} + \frac{K_M^{app}}{I_{max}C} \quad (3)$$

where $I_{ss}$ is the steady-state current after addition of the substrate; $I_{max}$ is the maximum current measured under saturated substrate conditions, and C is the bulk concentration of the substrate. The $K_M^{app}$value for the $Fe_3O_4$@Au-Cys-FA/CPE device is calculated as 2.00 mg $L^{-1}$ (25 μM), indicating that our biosensor has a high affinity for immobilized SOx immobilization during $H_2O_2$ determination. This value for $K_M^{app}$ is smaller than the value of 8.08 mg $L^{-1}$, seen for AuNPs-PEI, in which SOx is immobilized onto an Au electrode modified with gold nanoparticles capped with cationic branched poly(ethyleneimine) [41], and is comparable to reported values of 2.05 mg $L^{-1}$ [40], 0.64 mg $L^{-1}$ [42], and

1.60 mg $L^{-1}$ [32] for SOx immobilized onto a gold-nanoparticle/chitosan/carbon nanotube/polyaniline composite modified Au electrode [40], gold-coated magnetic nanoparticles [42], and an ITO electrode modified with a PEI capped CdS quantum-dot [32], respectively. This result indicates that our biosensor provides good SOx electrocatalytic activity.

### 3.3. Amperometric detection in the FI system

#### 3.3.1. Optimization

We investigated how the carbon-paste binder, applied potential, and flow rate, affect the sensitivity and stability of the sulfite determination in a FIA system. The CPE has a porous surface that contains a mixture of conducting graphite, catalyzing materials, and non-conducting mineral oil binder. PDMS oil has attractive properties for constructing carbon paste based chemical sensors [43] and biosensors [23,44,45]. Used in a glucose biosensor application, the oil provides an internal source of oxygen for enzymatic reaction [23,44,45]; the solubility of oxygen in PDMS is 45–50 fold greater than it is in water [46]. In the construction of a CPE for chemical sensing applications [43], use of a PDMS-mineral oil binder has been demonstrated to enhance the physical stability of the electrode, and facilitate the sealing the CPE to microfluidic devices [43].

The performances of the $Fe_3O_4$@Au-Cys-FA/CPE electrode using both mineral oil and a mineral oil-PDMS mixture as binder were compared using amperometry. Fig. 4A shows the amperometric responses to standard sulfite (20 μL, 10 mg $L^{-1}$) by the $Fe_3O_4$@Au-Cys-FA/CPE biosensor using (a) mineral and (b) mixed mineral oil-PDMS as binder. Sulfite oxidation peaks are clearly visible for the mixed mineral oil-PDMS binder (curve b), while the signal obtained from the mineral oil CPE was barely detectable (curve a). CPE sensitivity is much greater using the mixed binder than it is with mineral oil alone. The observed improvement in CPE sensitivity and physical stability in the presence of PDMS has been reported for other amperometric biosensors [43–45].

We investigated the optimal potential for amperometric detection at the $Fe_3O_4$@Au-Cys-FA/CPE device over a potential range from −0.10 to +0.80 V (Fig. 4B). Each datum represents the average of triplicate standard sulfite injections (20 μL, 10 mg $L^{-1}$). The modified CPE produces strong current responses at potentials between +0.20 and +0.35 V. The signal remains steady at potentials greater than +0.35 V. Maximum sensitivity occurred at an operating potential of +0.35 V (versus Ag/AgCl), and thus, we used this optimal voltage for amperometric detection.

To maximize sample throughput with satisfactory sensitivity, we varied flow rate over the range 0.2–1.8 mL $min^{-1}$ (Fig. 4C). The signal response decreases with increasing flow rate. High flow rates normally result in a reduced response because of the shorter contact time between enzyme and analyte, as reported for other enzyme-based amperometric detection FIA systems [23,47,48]. However, sample throughput rapidly increases with increasing flow rate over the range 0.2–1.4 mL $min^{-1}$and remains constant over the range 1.4–1.8 mL $min^{-1}$. To provide a balance between sensitivity and sample throughput, we selected an optimal flow rate of 0.8 mL $min^{-1}$.

#### 3.3.2. Analytical features

We investigated the analytical performance of the FI amperometric detection method with the developed sulfite biosensor. Under optimal conditions (operational potential, +0.35 V; carrier solution, 0.1 M PBS, pH 7; flow rate, 0.8 mL $min^{-1}$), FIA traces were obtained (Fig. 5A), and these were used to prepare a calibration curve. The figure illustrates a satisfactorily linear correlation from 0.1 to 200 mg $L^{-1}$. The regression equation is given by $y = 1.086x + 1.147$ ($r^2 = 0.998$), where y and x are the height of peak

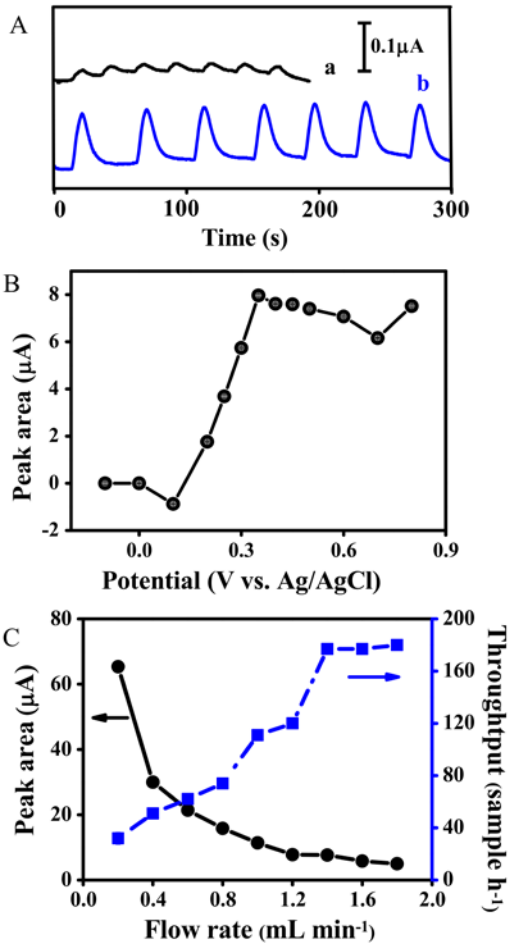


**Fig. 4.** (A) FIA grams comparing sulfite detection performances for mineral oil and mixed mineral oil-PDMS binders; sulfite, 10 mg $L^{-1}$; applied potential, +0.35 V; flow rate, 1.0 mL $min^{-1}$, ambient temperature (~25 °C). (B) Influence of applied potential on the biosensor response; sulfite, 10 mg $L^{-1}$; flow rate, 1.0 mL $min^{-1}$. (B) Effect of flow rate at $Fe_3O_4$@Au-Cys-FA/CPE on sulfite response and sample throughput; sulfite, 20 mg $L^{-1}$; applied potential, +0.35 V.

current (μA) and sulfite concentration (mg $L^{-1}$), respectively. The slope of the equation is corresponding to linear sensitivity of 1.086 μA $(mg)^{-1}$ L. The relative standard deviation (%R.S.D.) calculated from the current response among the sulfite concentrations in the calibration curve are ranged from 0.4–5.1% (Table S1) indicates good precision of developed technique. The calculated detection limit for the biosensor is 10 μg $L^{-1}$ (3σ of blank). The limit of quantification is 34 μg $L^{-1}$ estimated according to ISO11843 [15,49]. Sample throughput is 109 samples $h^{-1}$. Our $Fe_3O_4$@Au-Cys-FA/CPE shows good linearity over the concentration range, and a low limit of detection compared with previously reported amperometric sulfite biosensors (Table 1). The linear range of our biosensor is comparable with [14,51] or better than [15,31,40–42,50] other biosensors using immobilized SOx electrode. The developed biosensor offers a comparable [31,42,50] or

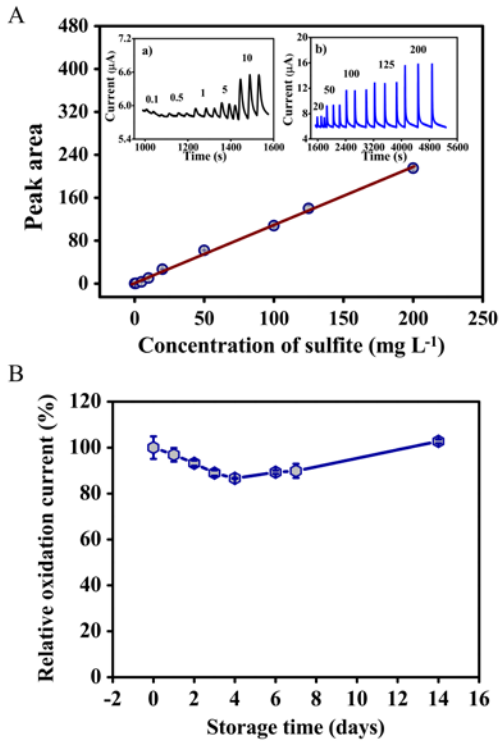


**Fig. 5.** Calibration plot of peak area of current signals versus concentration of sulfite as obtained from the FIA grams. The inset shows FIA grams for sulfite standards (a) 0.1–10 mg $L^{-1}$ and (b) 20–200 mg $L^{-1}$, obtained as the averages of triplet injections.

lower [14,15,40] detection limit compared to other sensors of similar design. Moreover, the operating potential for our biosensor is lower than [40,50] or comparable to previous reports [14,15,31,42]. A low operating potential minimizes interferences from sample constituents. Major advantages of the $Fe_3O_4$@Au-Cys-FA/CPE over previously reported devices are ease of preparation and high stability. Our approach, immobilize SOx on the $Fe_3O_4$@Au-Cys-FA modified carbon-paste electrode provides in high electrode stability and improves biosensor performance toward sulfite detection.

Reproducibility and stability are important features for the practical use of the biosensors. In this report, we have demonstrated that the CPE provides good precision (%R.S.D.=3.1) for 20 μL injections (n=20) of 15 mg $L^{-1}$ sulfite. Repeatability between successive tests was investigated using the same biosensor, and monitoring the current response of sulfite at an applied potential of +0.35 V (vs. Ag/AgCl). As shown in Fig. 5B, current responses of the novel biosensor remain close to the initial measurements. The current response of the biosensor retains 89% of the initial current response after repeated use for more than one week, and retains approximately 102% after 2 weeks when it was stored at 4 °C. These results suggest that the novel biosensor performs with satisfactory stability.

### 3.4. Interference study and application to real samples

To evaluate the selectivity of the proposed sensor, we examined the effects of interference, from selected inorganic ions and organic compounds, which are commonly present in sulfite samples. These compounds include sugar (glucose, sucrose, fructose, and maltose), ethanol, ascorbic acid, and various ions ($NO_3^-$, $Cl^-$, $I^-$, $CH_3COO^-$, and $SO_4^{2-}$). We studied the interference effects of foreign species on the FI signals obtained from standard 15 mg $L^{-1}$ sulfite (Table 2). The tolerance was defined as the maximum concentration of the interfering substance required to cause a signal alteration greater than ±5%. Tolerances toward these compounds are 75 mg $L^{-1}$ or greater, and negligible interference was observed during testing. We conclude that our proposed device provides good selectivity for the amperometric determination of sulfite.

The system was applied to the determination of the sulfite content of five wines (W1-W5) and pickled food extracts (G1-G3, M1-M3 and C1-C3) (Table 3). Sulfite determinations were performed by FIA with amperometric measurements under optimized conditions, using the standard addition method. Our results compare well with measurements obtained from the reference

**Table 1**
Comparison of analytical characteristics of the proposed sulfite biosensor with previously reported SOx-based biosensors.

| Electrode type | material | $K_M^{app}$ (mg $L^{-1}$) | Potential (V) | Linearity range (mg $L^{-1}$) | LOD (μg $L^{-1}$) | Ref. |
|---|---|---|---|---|---|---|
| Au | AuNPs/CHIT/CNTs/PANI | 2.05 | +0.47 | 0.06–32 | 40 | [40], batch |
| Au | PBNPs/PPY | – | +0.40 | 0.04–80 | 8 | [50], batch |
| Au | $Fe_3O_4$@Au | 0.64 | +0.20 | 0.04–80 | 12 | [42], batch |
| Au[a] | AuNPs-PEI | 8.08 | −0.10 | 0.04–0.43 | – | [41], batch |
| ITO | PBNPs/PPY | – | +0.30 | 0.04–80 | 9.6 | [31], batch |
| ITO[a] | PEI-CdS-QDs | 1.60 | −0.16 | – | – | [32], batch |
| GC | MTF | – | −0.24 | 16–224 | – | [51], batch |
| SPE | Cyt c | – | +0.30 | 4.1–750 | 4000 | [14], batch |
| SPE | TTF | – | +0.20 | 0.79–6.61 | 480 | [15], batch |
| CPE | $Fe_3O_4$@Au-Cys-FA | 2.00 | +0.35 | 0.1–200 | 10 | This work, FIA |

Au=gold electrode.
ITO=Indium tin oxide.
GC=glassy carbon.
SPE=screen printed electrode.
CPE=screen-printed electrode.
AuNPs=gold nanoparticles, CHIT=chitosan, CNTs=carbon nanotubes, PANI=polyaniline, PBNPs=Prussian blue nanoparticles, PPY=polypyrrole, MTF=Mercury thin film, Cyt c=Cytochrome C, TTF=tetrathiafulvalene, $Fe_3O_4$@Au=gold coated magnetic nanoparticles, PEI-CdS-QDs=polyethylenimine capped CdS quantum-dots, $Fe_3O_4$@Au-Cys-FA=folic acid-cysteine-conjugated gold-coated magnetite core shell.
[a] Using human sulfite oxidase (hSOx).

**Table 2**
Effects of foreign substances on the FIA signal, obtained from triplicate injections of sulfite standard (15 mg $L^{-1}$).

| Foreign species | Results[a] (mg $L^{-1}$) |
|---|---|
| **Sugars** | |
| Sucrose /$C_{12}H_{22}O_{11}$, fructose /$C_6H_{12}O_6$ | 1500 |
| Glucose /$C_6H_{12}O_6$, maltose/$C_{12}H_{22}O_{11}$ | 750 |
| **Ions** | |
| $SO_4^{2-}$/$Na_2SO_4$, $Cl^-$/NaCl, $NO_3^-$N/$NaNO_3$, $CH_3COO^-$/$NaCH_3COO$ | 1500 |
| $I^-$/KI | 150 |
| **Others** | |
| Ethanol ($CH_3CH_2OH$) | 750 |
| Ascorbic acid ($C_8H_8O_6$) | 75 |

[a] Greater than ±5% signal alteration is classified as an interfering condition.

**Table 3**
Comparison of sulfite determinations of wines (W1-W5) and picked food extracts (ginger; G1-G3, mango; M1-M3 and cabbage; C1-C3), between the developed $Fe_3O_4$@Au-Cys-FA/CPE biosensor and the reference iodometric method.

| Samples | Sulfite (mg $L^{-1}$ or mg $kg^{-1}$) | | %Relative difference |
|---|---|---|---|
| | Developed biosensor[a] | Reference method[a] | |
| W1 | 12.94 ± 0.05 | 12.77 ± 0.01 | −1.35 |
| W2 | 2.74 ± 0.01 | 2.69 ± 0.01 | −1.78 |
| W3 | 11.67 ± 0.02 | 11.42 ± 0.01 | −2.14 |
| W4 | 5.59 ± 0.09 | 5.38 ± 0.03 | −4.05 |
| W5 | 8.79 ± 0.04 | 8.74 ± 0.02 | −0.63 |
| G1 | 23.81 ± 0.04 | 22.85 ± 0.01 | −4.21 |
| G2 | 24.55 ± 0.03 | 23.52 ± 0.01 | −4.38 |
| G3 | 23.21 ± 0.02 | 22.18 ± 0.01 | −4.67 |
| M1 | 23.12 ± 0.04 | 23.52 ± 0.01 | +1.72 |
| M2 | 42.06 ± 0.02 | 43.68 ± 0.01 | +3.71 |
| M3 | 37.29 ± 0.03 | 36.96 ± 0.07 | −0.90 |
| C1 | 24.29 ± 0.05 | 24.19 ± 0.01 | −0.40 |
| C2 | 24.29 ± 0.10 | 24.86 ± 0.01 | +2.29 |
| C3 | 30.77 ± 0.02 | 29.57 ± 0.01 | −4.06 |

[a] Average ± standard deviation of 3 measurements.

iodometric method. The relative differences between data obtained from the $Fe_3O_4$@Au-Cys-FA/CPE biosensor and the iodometric method range from 0.4–4.7%, and are in good agreement. Statistical analysis (paired *t*-test [52]) reveals that data from our developed biosensor are not significantly different to that from the reference method ($t_{observed}$ = 0.996, $t_{critical}$ = 2.161, 95% confidence). The results indicate that our sulfite biosensor is sufficiently accurate, and is suitable for the quantification of sulfite in the study samples.

## 4. Conclusion

In this work, we described a novel sulfite biosensor fabricated by immobilizing sulfite oxidase by chemisorption on the $Fe_3O_4$@Au-Cys-FA nanocomposite-modified carbon-paste electrode. The $Fe_3O_4$@Au-Cys-FA/CPE shows a significant improvement in biosensor performance when compared to the $Fe_3O_4$@Au/CPE and $Fe_3O_4$@Au-Cys/CPE devices. The biosensor produces oxidation peaks that correspond to oxidation of $H_2O_2$ by an enzymatic reaction between SOx and sulfite ion. Thus, we quantified sulfite by taking amperometric measurements at the $Fe_3O_4$@Au-Cys-FA/CPE biosensor using an in-house assembled flow injection system at +0.35 V. Enhancement of the electrode physical stability and sensitivity of the response was achieved using mixed PDMS-mineral oil as binder for electrode fabrication. Under optimal conditions, the proposed biosensor exhibits rapid sample throughput, with excellent sensitivity and selectivity toward sulfite quantitation. Moreover, the $Fe_3O_4$@Au-Cys-FA/CPE biosensor exhibits good stability in our flow system, and presents fair reproducibility for amperometric detection. The method was successfully applied to sulfite determination in wines and pickled food extracts.

## Acknowledgments

Financial support from the National Research Council of Thailand (NRCT), the Center of Excellence for Innovation in Chemistry (PERCH-CIC), the Commission on Higher Education, the Ministry of Education, and the Faculty of Science at Ubon Ratchathani University (UBU) are all gratefully acknowledged. The Scholarship from the Science Achievement Scholarship of Thailand (SAST) given to W. Sroysee is also gratefully acknowledged.

## Appendix A. Supplementary material

Supplementary data associated with this article can be found in the online version at http://dx.doi.org/10.1016/j.talanta.2016.04.066.

## References

[1] S. Satienperakul, P. Phongdong, S. Liawruangrath, Pervaporation flow injection analysis for the determination of sulphite in food samples utilizing potassium permanganate-rhodamine B chemiluminescence detection, Food Chem. 212 (2010) 893–898.
[2] S.S.M. Hassan, M.S.A. Hamza, A.H.K. Mohamed, A novel spectrophotometric method for batch and flow injection determination of sulfite in beverages, Anal. Chim. Acta 570 (2006) 232–239.
[3] U.T. Yilmaz, G. Somer, Determination of trace sulfite by direct and indirect methods using differential pulse polarography, Anal. Chim. Acta 603 (2007) 30–35.
[4] C.S. Pundir, R. Rawal, Determination of sulfite with emphasis on biosensing methods: a review, Anal. Biochem. 405 (2013) 3049–3062.
[5] O. Fatibello-Filho, I. da Cruz Vieira, Flow injection spectrophotometric determination of sulfite using a crude extract of sweet potato root (Ipomoea-batatas (L.) Lam.) as a source of polyphenol oxidase, Anal. Chim. Acta 354 (1997) 51–57.
[6] C. Wang, S. Feng, L. Wu, S. Yan, C. Zhong, P. Guo, R. Huang, X. Weng, X. Zhou, A new fluorescent turn-on probe for highly sensitive and selective detection of sulfite and bisulfite, Sens. Actuators, B 190 (2014) 792–799.
[7] R.F. Mcfeeters, A.O. Barish, Sulfite analysis of fruits and vegetables by high-performance liquid chromatography (HPLC) with ultraviolet spectrophotometric detection, J. Agric. Food Chem. 51 (2003) 1513–1517.
[8] X. Zhang, S. He, Z. Chen, Y. Huang, $CoFe_2O_4$ nanoparticles as oxidase mimic-mediated chemiluminescence of aqueous luminol for sulfite in white wine, J. Agric. Food Chem. 61 (2013) 840–847.
[9] A. Isaac, C. Livingstone, A.J. Wain, R.G. Compton, J. Davis, Electroanalytical methods for the determination of sulfite in food and beverages, Trac. Trends Anal. Chem. 25 (2006) 589–598.
[10] A.A. Ensafi, H. Karimi-Maleh, Ferrocenedicarboxylic acid modified multiwall carbon nanotubes paste electrode for voltammetric determination of sulfite, Int. J. Electrochem. Sci. 5 (2010) 392–406.
[11] M.M. Ardakani, F. Habibollahi, H.R. Zare, H. Naeimi, Electrocatalytic oxidation of sulfite by quinizarine at carbon paste electrode, Int. J. Electrochem. Sci. 3 (2008) 1236–1247.
[12] H.M. Moghaddam, M. Malakootian, H. Beitollah, P. Biparva, Nanostructured based electrochemical sensor for determination of sulfite, Int. J. Electrochem. Sci. 9 (2014) 327–341.
[13] R. Spricigo, R. Dronov, F. Lisdat, S. Leimkuhler, F.W. Scheller, U. Wollenberger, Electrocatalytic sulfite biosensor with human sulfite oxidation co-immobilized with cytochrome c in a polyelectrolyte-containing multilayer, Anal. Bioanal. Chem. 393 (2009) 225–233.
[14] A.K. Abass, J.P. Hart, D. Cowell, Development of an amperometric sulfite biosensor based on sulfite oxidase with cytochrome c, as electron acceptor, and a screen-printed transducer, Sens. Actuators, B 62 (2000) 148–153.
[15] B. Molinero-Abad, M.A. Alonso-Lomillo, O. Dominguez-Renedo, M.J. Arcos-Martinez, Sulfite oxidase biosensors based on tetrathiafulvalene modified

screen-printed carbon electrodes for sulfite determination in wine, Anal. Chim. Acta 812 (2014) 41–44.
[16] J. Svitel, M. Stredansky, M. Pizzariello, A. Miertus, Composite biosensor for sulfite assay-use of water insoluble hexacyanoferrate (III) salts as electron-transfer mediators, Electroanalysis 10 (1998) 591–596.
[17] S.V. Salihov, Y.A. Ivanenkov, S.P. Krechetov, M.S. Veselov, N.V. Sviridenkova, A. G. Savchenko, N.L. Klyachko, Y.I. Golovin, N.V. Chufarova, E.K. Beloglazkina, A. G. Majouga, Recent advances in the synthesis of $Fe_3O_4$@Au core/shell nanoparticles, J. Magn. Magn. Mater. 394 (2015) 173–178.
[18] L. Vayssieres, C. Chaneac, E. Tronc, J.P. Jolivat, Size tailoring of magnetite particles formed by aqueous precipitation: an example of thermodynamic stability of nanometric oxide particles, J. Colloid Interface Sci. 205 (1998) 205–212.
[19] E. Umut, E. Pineider, P. Arosio, C. Sangregorio, M. Corti, F. Tabak, F. Lascialfari, P. Ghigna, Magnetic, optical and relaxometric properties of organically coated gold-magnetite (Au-$Fe_3O_4$) hybrid nanoparticles for potential use in biomedical applications, J. Magn. Magn. Mater. 324 (2012) 2373–2379.
[20] A. Samphao, P. Butmee, J. Jitcharoen, L. Svorc, G. Raber, K. Kalcher, Flow-injection amperometric determination of glucose using a biosensor based on immobilization of glucose oxidase onto Au seeds decorated on core $Fe_3O_4$ nanoparticles, Talanta 142 (2015) 35–42.
[21] K. Li, Y. Lai, W. Zhang, L. Jin, Fe2O3@Au core/shell nanoparticle-based electrochemical DNA biosensor for *Escherichia coli* detection, Talanta 84 (2011) 607–613.
[22] Sh Karamipour, M.S. Sadjadi, N. Farhadyar, Fabrication and spectroscopic studies of folic acid-conjugated $Fe_3O_4$@Au core-shell for targeted drug delivery application, Spectrochim. Acta, Part A 148 (2015) 146–155.
[23] **M. Amatatongchai, W. Sroysee, S. Chairam, D. Nacapricha, Amperometric flow injection analysis of glucose using immobilized glucose oxidase on nanocomposite carbon paste electrode, Talanta. in press,** http://dx.doi.org/10.1016/j.talanta.2016.04.066.
[24] K.G. Kouassi, J. Irudayaraj, G. McCarthy, Examination of cholesterol oxidase attachment to magnetic nanoparticles, J. Nanobiotechnol. 3 (2005) 1–9.
[25] U. Tamer, Y. Gundogdu, I.H. Boyaci, K. Pekmez, Synthesis of magnetic core-shell $Fe_3O_4$-Au nanoparticle for biomolecule immobilization and detection, J. Nanopart. Res. 12 (2010) 1187–1196.
[26] L.S.T. Alamo, T. Tangkuaram, S. Satienperakul, Determination of sulfite by pervaporation-flow injection with amperometric detection using copper haxacyanoferrate-carbon nanotube modified carbon paste electrode, Talanta 81 (2010) 1793–1799.
[27] AOAC, Official Methods of Analysis of AOAC International, sixteenth ed., AOAC International, USA, 1995.
[28] M. Amatatongchai, W. Sroysee, S. Chairam, D. Nacapricha, Simple flow injection for determination of sulfite by amperometric detection using glassy carbon carbon electrode modified with carbon nanotubes-PDDA-gold nanoparticles, Talanta 133 (2015) 134–141.
[29] L. Wang, J. Luo, Q. Fan, M. Suzuki, I.S. Suzuki, M.H. Engelhard, Y. Lin, N. Kim, J. Q. Wang, C.J. Zhong, Monodispersed Core-Shell $Fe_3O_4$@Au Nanoparticles, J. Phys. Chem. B 109 (2005) 21593–21601.
[30] X. Wei, T. Liu, J. Li, A magnetic-controlled amperometric biosensor based on composite bio-particulates $Fe_3O_4$ and nano-Au with the signal enhancement by increasing loading of horseradish peroxidase, Int. J. Electrochem. Sci. 6 (2011) 4953–4966.
[31] R. Rawal, C.S. Pundir, Development of an amperometric sulfite biosensor based on SOx/PBNPs/PPY modified ITO electrode, Int. J. Biol. Macromol. 51 (2012) 449–455.
[32] T. Zeng, S. Leimkuhler, J. Koetz, U. Wollenberger, Effective electrochemistry of human sufite oxidase immobilized on quantum-dots-modified indium tin oxide electrode, ACS Appl. Mater. Interfaces 7 (2015) 21487–21494.
[33] S.J. Elliott, A.E. McElhaney, C. Feng, J.H. Enemark, F.A. Armstrong, A voltammetric study of interdomain electron transfer within sulfite oxidase, J. Am. Chem. Soc. 124 (2002) 11612–11613.
[34] A.C. Torres, M.M. Barsan, C.M.A. Brett, Simple electrochemical sensor for caffeine based on carbon and nafion-modified carbon electrode, Food Chem. 149 (2014) 215–220.
[35] **W. Sroysee., S. Chairam., M. Amatatongchai., P. Jarujamrus., S. Tamuang., S. Pimmongkol., L. Chaicharoenwimolkul., E. Somsook., Poly(*m*-ferrocenylaniline) modified Carbon nanotubes-paste electrode encapsulated in nafion film for selective and sensitive determination of dopamine and uric in the presence of ascorbic acid, J. Saudi Chemical Society. in press,** http://dx.doi.org/10.1016/j.jscs.2016.02.003.
[36] M.G. Almeida, C.M. Silveira, J.J.G. Moura, Biosensing nitrite using the system nitrite redutase/Nafion/methyl viologen-A votammetric study, Biosens. Bioelectron. 22 (2007) 2485–2492.
[37] K. Calfuman, M.J. Aguirre, D. Villagra, C. Yanez, C. Arevalo, B. Matsuhiro, L. Mendoza, M. Isaacs, Nafion/tetraruthenated porphyrin glassy carbon-modified electrode: characterization and voltammetric studies of sulfite oxidation in water-ethanol solutions, J. Solid State Electrochem. 14 (2010) 1065–1072.
[38] J. Premkumar, R. Ramaraj, Photoreduction of dioxygen to hydrogen peroxide at propyrins and phthalocyanines adsorbed Nafion membrane, J. Mol. Catal. A: Chem. 142 (1999) 153–162.
[39] **A. Lehninger, D. Nelson, M. Cox, Lehninger Principles of Biochemistry, fourth ed., W.H. Freeman, New York, 2008.**
[40] R. Rawal, S. Chawal, T. Dahiya, C.S. Pundir, Development of an amperometric sulfite biosensor based on a gold nanoparticles/chitosan/multiwalled carbon nanotubes/ polyaniline-modified gold electrode, Anal. Bioanal. Chem. 401 (2011) 2599–2608.
[41] S. Frasca, O. Rojas, J. Salewski, B. Neumann, K. Stiba, I.M. Weidinger, B. Tiersch, S. Leimkuhler, J. Koetz, U. Wollenberger, Human sulfite oxidase electrochemistry on gold nanoparticles modified electrode, Bioelectrochemistry 87 (2012) 33–41.
[42] R. Rawal, S. Chawla, C.S. Pundir, An electrochemical sulfite biosensor based on gold coated magnetic nanoparticles modified gold electrode, Biosens. Bioelectron. 31 (2012) 144–150.
[43] Y. Sameenoi, M.M. Mensack, K. Boonsong, R. Ewing, W. Dungchai, O. Chailapakul, D.M. Cropeke, C.S. Henry, Poly(dimethylsiloxane) cross-linked carbon paste electrodes for microfluidic electrochemical sensing, Analyst 136 (2011) 3177–3184.
[44] J. Wang, S. Li, J.W. Mo, J. Porter, M.M. Musameh, P.K. Dasgupta, Oxygen-independent poly(dimethylsiloxane)-based carbon-paste glucose biosensors, Biosens. Bioelectron. 17 (2002) 999–1003.
[45] P. Rattanarat, P. Teengam, W. Siangproh, R. Ishimatsu, K. Nakano, O. Chailapakul, T. Imato, An electrochemical compact disk-type-microfluidics platform for use as an enzymatic biosensor, Electroanalysis 27 (2015) 703–712.
[46] W.L. Robb, Thin silicone membranes-their permeation properties and some applications, Ann. N. Y. Acad. Sci. 146 (1968) 119–137.
[47] M. Amatatongchai, W. Sroysee, S. Laosing, S. Chairam, Rapid screening method for assessing total phenolic content using simple flow injection system with laccase based-biosensor, Int. J. Electrochem. Sci. 8 (2013) 10526–10539.
[48] F. Sánchez, T. Tzanov, G.M. Gübitz, A. Cavaco-Paulo, Voltammetric monitoring of laccase-catalysed mediated reactions, Bioelectrochemistry 58 (2002) 149–156.
[49] **ISO 11843, Capability of Detection, Part I/II, Geneve, 1997/2000.**
[50] R. Rawal, C.S. Pundir, development of electrochemical sulfite biosensor basensor based on SOx/PBNPs/PPY modified Au electrode, Biochem. Eng. J. 71 (2013) 30–37.
[51] E. Dinckaya, M.K. Sezginturk, E. Akyilmaz, F.N. Ertas, Sulfite determination using sulfite oxidase biosensor based glassy carbon electrode coated with thin mercury film, Food Chem. 101 (2007) 1540–1544.
[52] J.N. Miller, J.C. Miller,, Statistics and Chemometrics for Analytical Chemistry, Fifth ed., Essex, England, 2005.

# CURRICULUM VITAE

| | |
|---|---|
| **NAME** | MissWongduan Sroysee |
| **EDUCATION** | B.Sc. (chemistry), Ubon Ratchathani University, Ubon Ratchathani, Thailand (2011) |
| | M. Sc. (chemistry), Ubon Ratchathani University, Ubon Ratchathani, Thailand (2014) |
| **SCHOLARSHIP** | The Science Achievement Scholarship of Thailand (SAST) in the Academic Years of 2012-2013 |